

STUDIA  
UNIVERSITATIS BABEŞ-BOLYAI

CHEMIA

1-2

1993

CLUJ-NAPOCA

REDACTOR ȘEF: Prof. A. MARGA

REDACTORI ȘEFI ADJUNȚI: Prof. N. COMAN, prof. A. MAGYARI, prof. I. A. RUS, prof. C. TULAI

COMITETUL DE REDACȚIE AL SERIEI CHIMIE: Prof. S. GOCAN, prof. L. LITERAT, prof. S. MAGER (redac. or. coordonator), prof. L. ONICIU, prof. I. SILBERG, conf. N. DULĂMIȚĂ, conf. I. SILAGHI - DUMITRESCU, lector C. SĂRBU (secretar de redacție)

# STUDIA

## UNIVERSITATIS BABEȘ-BOLYAI

### CHEMIA

1-2

---

 Redacția: 3400 CLUJ-NAPOCA, str. M. Kogălniceanu, 1 • Telefon 11 61 01
 

---

#### SUMAR — CONTENTS — INHALT

M. V. DIUDEA, Molecular Topology. 20. The Matriceal Description of Molecular Graphs . . . . .	3
I. BĂLDEA, ALEXANDRA RUSTOIU—CSAVDARI, Reactor Analysis for Some Consecutive and Competitive-Consecutive Irreversible Reactions . . . . .	29
C. SĂRBU, IOVANCA HAIDUC, Optimal Choice of Solvent Systems in Bidimensional Thin Layer Chromatography . . . . .	49
MARIA OLEA, L. ONICIU, Z. KUBASZEK, Monte-Carlo Simulation in the Reaction of p, p'-Dinitrodibenzyl Electroreduction to p, p'-Diaminodibenzyl. I. The mathematical Model . . . . .	57
MARIA OLEA, L. ONICIU, ȘT. OIȚĂ, The Sensitivity of Ethyl-Acetate Synthesis Reactor. (I) . . . . .	63
ELENA HOPÎRTEAN, MONICA HORN, A Potentiometric Method for Lead Determination in Alkaline Zinc-Plating Electrolyte . . . . .	71
ELENA M. PICĂ, ILEANA TRUCA, Oxygen Electroreduction by Cyclic Voltammetry and Chronopotentiometry . . . . .	75
MARIA TOMOAIĂ—COTIȘEL, E. CHIFU, J. ZSAKÓ, P. T. FRANGOPOL, P. J. QUINN, AURORA MOCANU, Interaction of Some Drugs with Monomolecular Membranes at the Fluid Interfaces . . . . .	81
LUMINIȚA SILAGHI—DUMITRESCU, R. SEMENIUC, RODICA MICU—SEMENIUC, Metal Complexes with Hidrazone Type Ligands. III. Synthesis and ESR Spectra of Cu(II) Compounds with Sulfonamidobenzhidrazones . . . . .	87
CRISTINA RAȚIU, MARIANA RUSU, A. BOTAR, Study of the Formation of Heteropolymolybdotungstates of Dawson-Type with La(III), Ce(III) and Ce(IV) as Central Ions . . . . .	93

F. MAKKAY, CS. VÁRHELYI, J. ZSAKÓ, ZSUZSANNA SZÁSZ, On the Dioximine Complexes of Transition Metals. Part XCII. Spectrophotometric Study of the Formation of Copper (II) Chelates with Some $\alpha$ -Substituted Alicyclic Oximes . . . . .	99
F. MAKKAY, CS. VÁRHELYI, ENIKŐ SZAKÁCS, E. GRÜNWARD, On the Dioximine Complexes of Transition Metals. XCIII. Alicyclic $\alpha$ -Substituted Oximes as Chelating Agents for the Determination of Cobalt . . . . .	107
F. JUGRESTAN, V. MICLĂUŞ, MONICA TOŞA, GABRIELA CÎMPAN, DANIELA HOMORODEAN, Preparation and Characterization of Some New Nitrofuranydrazometlines . . . . .	115
I. CRISTEA, CARMEN SUCIU, New Bis-(-L-Glutamyl)-Diamide Derivatives. Part II . . . . .	121
I. BATIU, I. CRISTEA, V. FĂRCĂŞAN, Some New Hydrazones and Hydrazido-Hydrazones of Terpenoids and Related Compounds . . . . .	125
I. HOPÂRTEAN, A. LUPU, IRINA TARSICHE, IOANA HOPÎRTEAN, Optimization of Hippuric Acid Synthesis . . . . .	131
I. HOPÂRTEAN, M. VLASSA, IOANA HOPÎRTEAN, The Mass Spectrum of 3-Phenyl-2,1-Benzisoxazole . . . . .	137
A. BENKŐ, ILDIKÓ SZÁTMÁRI, Thiazol XIII. Nitrierungsreaktion in der Phenylthiazolreihe • The Nitration Reaction in the Phenylthiazole Series . . . . .	141
N. DULĂMIŢĂ, MARIA STANCA, FLORINA BUCIUMAN, Ethylbenzene Dehydrogenation on Fe-Cr-K Catalist. I. The Influence of the Addition of Several Materials with Vanadium on the Catalytic Performances and Mechanical Strength of the Catalist . . . . .	147
MARIA STANCA, N. DULĂMIŢĂ, FLORINA BUCIUMAN, The Study of Hydrogen Adsorption on the Surface of Pd/Al <sub>2</sub> O <sub>3</sub> Catalyst Using the Gas-Chromatography Method . . . . .	153
GEORGETA ȚARĂLUNGĂ, L. ONICIU, CS. BÖLLA, L. D. BOBOŞ, Intercalation Compounds. II. Physical Investigation Methods of the Intercalation Compounds . . . . .	159
C. ANGHEL, VIOLETA ANGHEL, Considérations Concernant L'écoulement des Phases dans le Rotor des Centrifuges de Sédimentation. Implications Fonctionnelles . . . . .	173
Note de cercetare — Research Notes	
I. SFLAGHI—DUMITRESCU, I. HAIDUC, On the Ring Angles in the Four-Membered Cyclodiphosphazanes . . . . .	183
Cronică — Chronicle — Chronik	
The 4th International EAST-Conference (LIVIU ONICIU) . . . . .	187
Recenzii — Book Reviews — Buchbesprechungen	
Oxford Chemistry Primers, Series editor Stephen G. Davies, Oxford Science Publications, (VASILE MICLĂUŞ) . . . . .	191
David T. Davies, Aromatic Heterocyclic Chemistry (VASILE MICLĂUŞ) . . . . .	191
Malcom Sainsbury, Aromatic Chemistry (VASILE MICLĂUŞ) . . . . .	191
MICHAEL LEDERER, ALFRED O. KUHN, Adsorption on Cellulose, Collected Data on Chromatography on Cellulose with Aqueous Solvents (CONSTANTIN MĂRUŢOIU) . . . . .	192

MOLECULAR TOPOLOGY. 20. THE MATRICEAL  
DESCRIPTION OF MOLECULAR GRAPHS

MIRCEA V. DIUDEA\*

## Contents :

1. Introduction 2. Symmetric matrices. 2.1. Adjacency matrix. 2.2. Distance matrix. 3. Layer matrices 3.1. Sequence matrices 3.2. Layer matrices 3.3. Line form of layer matrices. 3.4. Discussion on layer matrices 4. Applications. 4.1. Spectrum of a graph and Huckel theory 4.2. Conjugation detection. 4.3. SP matrices and the ordering of alkanes 4.4. Structural similarity testing. 5. Conclusions

## List of symbols.

**A** — adjacency matrix  
 $a_{ij}$  — elements of adjacency matrix  
 $\alpha; \beta$  — Huckel parameters (Coulomb and resonance energy, respectively)  
 $b_{ij}$  — conventional bond order  
**C** — coconnectivity matrix  
 $c_{ij}$  — elements of connectivity matrix  
 $c(\mathbf{L.M.})_i$  — centrality index (of vertex  $i$ )  
**D** — distance matrix  
 $d_{ij}$  — elements of distance matrix  
 $d(G)$  — diameter of graph  
 $d_{sp}$  — specified distance  
 $D_M$  — generalized Minkowski distance  
 $D_{Mh}$  — Manhattan distance  
 $DM^h$  — Balaban et al. superindex  
**E** — set of edges in graph  
**E** — energy matrix  
**EA** — edge adjacency matrix  
 $E_{\pi}$  — total  $\pi$  electron energy of a molecule  
 $e$  — elongation of a walk  
 $ecc_i$  — eccentricity of a vertex  $i$   
 $f_i$  — multigraph factor  
 $\Phi_p$  — a  $p$  atomic orbital  
**G** — graph  
 $g_i$  — occupation number  
**H** — Hamiltonian matrix  
**H** — ES — Huckel matrix  
**J** — Balaban index  
 $h_i$  — vertex degree  
 $l_i$  — local parameter for multiple bond  
**L.M.** — layer matrices of:  
     **L.C.** — cardinality  
     **L.E.** — electronegativity  
     **L. $\chi$**  — Randić' index  
     **L.J.** — Balaban index  
     **L.K.** — degree

\* Department of Chemistry, „Babeș-Bolyai” University, 3400 Cluj, Romania.

- DM** -- distance sum  
**DMD** -- (3I) distance sum  
**MP** -- path sum  
**MRW<sup>e</sup>** -- returning walk sum  
**MW<sup>e</sup>** -- walk sum  
**LRW<sup>e</sup>** -- returning walk degree  
**LW<sup>e</sup>** -- walk degree  
**V** -- potential  
**LOVI** -- Local Vertex Invariant  
**MB** -- multiple bond adjacency matrix  
 $p$  -- number of vertices in graph  
 $P(G; x)$  -- characteristic polynomial  
 $P^{\otimes}$  -- logical product of matrices **SB** and **MB**  
 $\Psi_i$  -- a  $\pi$  Huckel-molecular orbital (HMO)  
 $q$  -- number of edges in graph  
**QSPR** -- Quantitative Structure Property Relationship  
**QSAR** -- Quantitative Structure Activity Relationship  
**R** -- eigenvector matrix  
 $r(G)$  -- radius of graph  
**S** -- overlap matrix  
**SB** -- single bond adjacency matrix  
**SM** -- sequence matrices of:  
     **SD** -- distance  
     **SP** -- path  
     **SRW<sup>e</sup>** -- returning walk  
     **SW<sup>e</sup>** -- walk  
**TI** -- topological index  
**U** -- unity matrix  
**V** -- set of vertices in graph  
 $\lambda$  -- eigenvalue matrix  
 $x(\mathbf{M})_i$  -- centrocomplexity index (of vertex  $i$ )  
 $w_i^e$  -- walk degree of vertex  $i$   
**WM<sup>e</sup>** -- extended Wiener index

**1. Introduction.** Before detailing the matricial description of molecular graphs, some ground definitions are needed.

A graph  $G = (V, E)$  is defined as an ordered pair of two sets:  $V$ , a finite nonempty set and  $E$ , a binary relation defined on the set  $V$ . The elements of  $V$  are called vertices and those of  $E$  are called edges. A graph is visualized by representing the elements of  $V$  as points and by joining each pair  $(v_i, v_j)$  of points with a line if and only if  $(v_i, v_j) \in E$ . The number of vertices in  $G$  is denoted by  $p$  (the cardinality of the set  $V$ ) while that of edges by  $q$  (the cardinality of the set  $E$ ). A graph one says of the order  $p$  and dimension  $q$ .

Two vertices in  $G$  are called adjacent if they are connected by a line. The degree of a vertex,  $k_i$ , is equal to the number of lines incident in  $v_i$ . A graph  $G$  is a multigraph if it contains more than one edge between at least one pair of adjacent vertices.

A walk [1] in  $G$  is a sequence of vertices,  $v_0, v_1, \dots, v_e$ , (starting in  $v_0$  and ending in  $v_e$ ) with the condition that any two consecutive vertices to be adjacent, that is  $(v_i, v_{i+1}) \in E$ . The length (elongation) of a walk,  $e$ , is the number of edges occurring in it. A walk is closed if  $v_0 = v_e$  (self returning

walk), otherwise it is open. A *path* (or *self avoiding walk*) is a walk in which vertices involved are visited but once (and no branching and no repetition is allowed [2]). In other words, in a path all vertices are distinct. A *cycle* is a walk which is both self returning and self avoiding.

A graph  $G$  is connected if any pair of its vertices are joined by a path. The topological distance between  $v_i$  and  $v_j$ ,  $d(v_i, v_j)$ , or simply  $d_{ij}$ , represents the number of edges along the shortest path connecting the two vertices. For any vertex,  $v_i$ , the maximal distance to any other vertex  $v_j$  is called the vertex eccentricity,  $ecc_i = \max_{j \in V} d_{ij}$ . The radius of a graph,  $r(G)$ , represents the minimal eccentricity among the vertex eccentricities,  $r(G) = \min_{i \in V} ecc_i$ , while the diameter of a graph is given by  $d(G) = \max_{i \in V} ecc_i$ . The sum of all distances of vertex  $i$  to all other vertices in  $G$ ,  $D_i = \sum_j d_{ij}$  is called the vertex distance sum. A set of vertices  $i \in V(G)$  which obey  $ecc_i = r(G)$ , is called the center of the graph [3].

In a molecular graph, the vertices represent the set of atoms and the edges are the covalent bonds between the adjacent atoms. Usually in the molecular graph only nonhydrogen atoms are represented (hydrogen depleted graphs)

A graph can be represented either by a number, a sequence, a polynomial or a matrix [2]. These representations are aimed to be unique for a given graph. The present review try to give a synopsis of the matricial representation of molecular graphs and some of the most important applications of matrices and matricial calculations.

**2. Symmetric matrices.** This class of matrices  $\mathbf{M}(G)$  include quadratic arrays of dimensions  $p * p$ , such as the adjacency and the distance matrices, which are symmetrical *vs.* their principal diagonal, *i.e.* their transpose,  $\mathbf{M}^T$ , leaves the corresponding matrices unchanged.

**2.1. Adjacency matrix.** In 1874 Sylvester [4] first represented an organic molecule by the adjacency matrix,  $\mathbf{A}(G)$ , of the corresponding molecular graph. Its elements  $a_{ij}$  are defined [5] as follows:

$$a_{ij} = 0 \quad (1)$$

$$a_{ij} = 1, \text{ if } (i, j) \in E(G) \quad (2)$$

$$a_{ij} = 0, \text{ if } (i, j) \notin E(G) \quad (3)$$

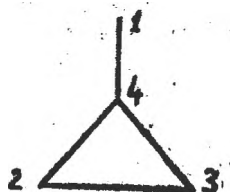
and the matrix  $\mathbf{A}(G)$ :

$$\mathbf{A}(G) = \{a_{ij}; i, j \in V(G)\} \quad (4)$$

$\mathbf{A}(G)$  characterizes the graph until the isomorphism [5]; from it the original graph can be reconstituted. Fig. 1 presents the adjacency matrix of the graph  $G_1$  and its powers until the exponent  $e = 3$ . Notice that the elements  $a_{ij}^e$  (not to be confused with  $a_{ij}$  raised at power  $e$ ) of the matrices  $\mathbf{A}^e$  represent walks of elongation  $e$  while their diagonal elements,  $a_{ii}^e$ , count the self returning walks (*i.e.* cycles of  $e$  edges). The sum of all entries in a row equals the number of walks of elongation  $e$  emerging from the given vertex:

$$\sum_j a_{ij}^e = w_i^e \quad (5)$$

For  $w_i^1$  the classical vertex degree,  $k_i$ , is found.

Fig. 1. Adjacency matrices for the graph  $G_1$ .

A	$w_i^1 = k_i$	$A^2$	$w_i^2$	$A^3$	$w_i^3$
0 0 0 1	1	1 1 1 0	3	0 1 1 3	5
0 0 1 1	2	1 2 1 1	5	1 2 3 4	10
0 1 0 1	2	1 1 2 1	5	1 3 2 4	10
1 1 1 0	3	0 1 1 3	5	3 4 4 2	13

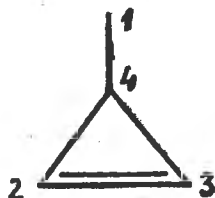
The matrix  $A$  does not consider the multigraph character (i.e. the multiple bonds) but it is made by the connectivity matrix,  $C(G)$ , a variant of the matrix  $A$ :

$$c_{ii} = 0 \quad (6)$$

$$c_{ij} = b_{ij} \quad (7)$$

$$C(G) = \{c_{ij}; i, j \in V(G)\} \quad (8)$$

where  $b_{ij}$  is the conventional bond order: 0; 1; 2; 3; 1.5, for nonbond ng, single, double, triple and aromatic bonds, respectively. Fig. 2. presents the connectivity matrices for the graph  $G_2$ .

Fig. 2. Connectivity matrices for the graph  $G_2$ .

C	$w_i^1 = k_i$	$C^2$	$w_i^2$	$C^3$	$w_i^3$
0 0 0 1	1	1 1 1 0	3	0 2 2 3	7
0 0 2 1	3	1 5 1 2	9	2 4 12 7	25
0 2 0 1	3	1 1 5 2	9	2 12 4 7	25
1 1 1 0	3	0 2 2 3	7	3 7 7 4	21

The walk degree,  $w_i^e$ , will be now  $\sum_j c_{ij}^e$ .

The raising of  $A/C$  matrices at the exponent  $e$ , in the calcul of  $w_i^e$  [3], can be eluded by applying the algorithm of Diudea et al [6]. It is iteratively constructed on a matrix  $CM^e$ , which is the sum of matrix  $C$  and the diagonal matrix  $M^e$  (of walk degrees):

$$C + M^e = CM^e \quad (9)$$

which elements are defined as follows:

$$m_{ii}^{e+1} = \sum_j (c_{ij} * m_{jj}^e); \quad m_{jj}^0 = 1 \quad (10)$$

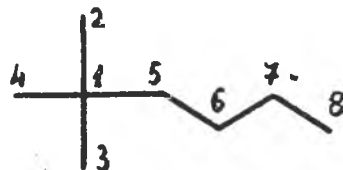
$$m_{ij}^e = c_{ij} \quad (11)$$

The diagonal elements  $m_{ii}^e$  are just the walk degrees,  $w_i^e$ .

The edge adjacency matrix,  $EA(G)$ , determines the adjacency of edges in  $G$  [5]. This matrix also can be constructed ba using the line derivative,  $L_n(G)$ , [5, 7]. (Fig. 3).

Fig. 3. The matrix EA for the graph  $G_3$ :

	12	13	14	15	56	67	78
12	0	1	1	1	0	0	0
13	1	0	1	1	0	0	0
14	1	1	0	1	0	0	0
15	1	1	1	0	1	0	0
56	0	0	0	1	0	1	0
67	0	0	0	0	1	0	1
78	0	0	0	0	0	1	0



2.2. Distance matrix. Distance matrix is a quadratic array (of dimensions  $p \times p$ ) which collects the topological distances between the vertices of graph [3, 5]:

$$D(G) = \{d_{ij}; i, j \in V(G)\} \tag{12}$$

In the followings the matrix  $D$  for the graph  $G_3$  is presented:

$D(G_3)$ :		1	2	3	4	5	6	7	8	$D_i$
	1	0	1	1	1	1	2	3	4	13
	2	1	0	2	2	2	3	4	5	19
	3	1	2	0	2	2	3	4	5	19
	4	1	2	2	0	2	3	4	5	19
	5	1	2	2	2	0	1	2	3	13
	6	2	3	3	3	1	0	1	2	15
	7	3	4	4	4	2	1	0	1	19
	8	4	5	5	5	3	2	1	0	25

Distance matrix  $D(G)$  can be constructed by calculating the powers  $A^e$ , (where  $A = U + \mathbf{A}$  and  $U$  is the unity matrix, i.e. the diagonal matrix which elements are 1);  $e \in [1, d(G)]$ , with  $d(G)$  being the diameter of graph, by using the boolean (logical) operators. Fig. 4 presents the construction of  $D(G)$  for  $G_3$ :

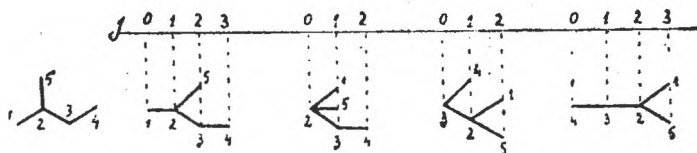


Fig. 4. Construction of the matrix  $\mathbf{D}(G)$  for the graph  $G_3$ 

$A^1(G_3)$	1	2	3	4	5	6	7	8
1	1	1	1	1	1	0	0	0
2	1	1	0	0	0	0	0	0
3	1	0	1	0	0	0	0	0
4	1	0	0	1	0	0	0	0
5	1	0	0	0	1	1	0	0
6	0	0	0	0	1	1	1	0
7	0	0	0	0	0	1	1	1
8	0	0	0	0	0	0	1	1

$A^2(G_3)$	1	2	3	4	5	6	7	8	$A^3(G_3)$	1	2	3	4	5	6	7	8
1	1	1	1	1	1	7	0	0	1	1	1	1	1	1	7	0	0
2	1	1	7	7	7	0	0	0	2	1	1	1	1	1	7	0	0
3	1	7	1	7	7	0	0	0	3	1	1	1	1	1	7	0	0
4	1	7	7	1	7	0	0	0	4	1	1	1	1	1	7	0	0
5	1	7	7	7	1	1	7	0	5	1	1	1	1	1	1	1	7
6	7	0	0	0	1	1	1	7	6	1	7	7	7	1	1	1	1
7	0	0	0	0	7	1	1	1	7	7	0	0	0	1	1	1	1
8	0	0	0	0	0	7	1	1	8	0	0	0	0	7	1	1	1

$A^4(G_3)$	1	2	3	4	5	6	7	8	$A^5(G_3)$	1	2	3	4	5	6	7	8
1	1	1	1	1	1	1	1	7	1	1	1	1	1	1	1	1	1
2	1	1	1	1	1	1	7	0	2	1	1	1	1	1	1	1	7
3	1	1	1	1	1	1	7	0	3	1	1	1	1	1	1	1	7
4	1	1	1	1	1	1	7	0	4	1	1	1	1	1	1	1	7
5	1	1	1	1	1	1	1	1	5	1	1	1	1	1	1	1	1
6	1	1	1	1	1	1	1	1	6	1	1	1	1	1	1	1	1
7	1	7	7	7	1	1	1	1	7	1	1	1	1	1	1	1	1
8	7	0	0	0	1	1	1	1	8	1	7	7	7	1	1	1	1

According to this algorithm, the elements  $d_{ij}$  of  $\mathbf{D}(G)$  will be just the subsequent exponents  $c$  generating new nonzero  $a_{ij}^c$  entries:

$$d_{ij} = c: a_{ij}^c \neq a_{ij}^{c-1}; c = 1, 2, \dots, d(G) \quad (13)$$

or, in other words, the matrix  $\mathbf{D}(G)$  is constructed by introducing the distance „ $e$ ” instead of the marked figures.

**3. Layer matrices.** The layer matrices were proposed [6,8–14] in connection with the sequences of routes: DDS (Distance Degree Sequence), PDS (Path Degree Sequence), [15, 16] and WS (Walk Sequence), [2], and are constructed on the ground of the relative partitions in graph.

A partition  $G(i)$  relative to the vertex  $i$  of the graph  $G$  is defined as [8, 11, 13]:

$$G(i) = \{G(u)_j, j \in [0, ecc_i] \text{ and } u \in G(u)_j \Leftrightarrow d_{iu} = j\} \quad (14)$$

where  $G(u)_j$  are sets of vertices located at distance  $j$  on concentric layers around the vertex  $i$ . Pictorially, the partitions are equivalent to the sequential design of the graph. Fig. 5 presents relative partitions in the graph  $G_4$ .

Fig. 5. Relative partitions in  $G_4$

$G_4$	$G_4(1, 5)$	$G_4(2)$	$G_4(3)$	$G_4(4)$
	$G_4(1) = \{\{1\}, \{2\}, \{3,5\}, \{4\}\}$			
	$G_4(2) = \{\{2\}, \{1,3,5\}, \{4\}\}$			
	$G_4(3) = \{\{3\}, \{2,4\}, \{1,5\}\}$			
	$G_4(4) = \{\{4\}, \{3\}, \{2\}, \{1,5\}\}$			
	$G_4(5) = \{\{5\}, \{2\}, \{1,3\}, \{4\}\}$			

**3.1. Sequence matrices.** A sequence matrix  $\mathbf{SM}^e$  [13] collects routes of various elongations  $e$  which start from the vertex  $i$  to all other  $p - 1$  vertices in  $G$ . Its elements,  $sm_i^e$  (with  $m$  the label of route type:  $d$  — the distance;  $p$  — the path;  $rw$  — the returning walk;  $w$  — the walk) mean the number of routes of elongation  $e$  emerging from the vertex  $i$  (i.e. a walk degree). The matrix  $\mathbf{SM}^e$  can be written as:

$$\mathbf{SM}^e(G) = \{sm_i^e; i \in [1, p(G)]; e \in [1, esp]\} \quad (15)$$

where  $p(G) = |V(G)|$  is the number of points in graph and  $esp$  (the specified elongation) is:  $ecc_i$  (for  $\mathbf{M} = \mathbf{D}$ );  $path-ecc_i$  (for  $\mathbf{M} = \mathbf{P}$ ) and  $esp \in [1, \infty)$ , (for  $\mathbf{M} = \mathbf{RW}^e$  and  $\mathbf{W}^e$ ). Thus, the rows in the matrices  $\mathbf{SM}^e$  represent just the sequences of routes emerging from a given vertex, i.e. DDS, PDS [15–18] or WS [2, 19].

The half sum on columns of  $sm_i^e$  offers the global sequence,  $M^e(G)$ :

$$M^e(G) = 1/2 \sum_i sm_i^e; e \in [1, esp] \quad (16)$$

In the followings sequence matrices  $SM^e$  for the graph  $G_1$ .  
Sequence matrices  $SM^e$  for the graph  $G_1$ :

	SD		SP			SRW <sup>1</sup>		SRW <sup>2</sup>		SRW <sup>3</sup>			SW <sup>1</sup>		SW <sup>2</sup>		SW <sup>3</sup>		
	1	2	1	2	3	1	1	2	1	2	3	1	1	2	1	2	3		
1	1	2	1	2	2	0	0	1	0	1	0	1	1	3	1	3	5		
2	2	1	2	3	1	0	0	2	0	2	2	2	2	5	2	5	10		
3	2	1	2	3	1	0	0	2	0	2	2	2	2	5	2	5	10		
4	3	0	3	2	0	0	0	3	0	3	2	3	3	5	3	5	13		
$W^e(G)$	4	2	4	5	2	0	0	4	0	4	3	4	4	9	4	9	19		
$WD = 8$		$WP = 20$			$WRW^3 = 17$			$WW^3 = 79$											

Notice that the matrix **SD** was symbolized by  $\lambda$  in ref. [8] and **F** in ref. [20] while the matrix **SP** denoted as  $\tau$  in ref. [8].

It is known that the Wiener index,  $W$ , [21] equals the sum of all distances in graph, that is the half sum of the elements of matrix **D**. Since this topological index is **SD**-calculable, by extension, the generalized Wiener index,  $WM^e$ , was introduced (Diudea et al. [13]). It is **SM**<sup>*e*</sup>-calculable, cf. eq. (17):

$$WM^e = 1/2 \sum_i \sum_e (sm_i^e * e) \quad (17)$$

$WM^e$  values were presented within the **SM**<sup>*e*</sup> matrices for the graph  $G_1$  (see above).

**3.2. Layer matrices.** A layer matrix, **LM**<sup>*e*</sup>, [13], collects the properties (topological or chemical) in the relative partitions  $G(i)$ , for all vertices  $u \in V(G)$  located on concentric shells (layers) around the vertex  $i \in V(G)$ , at distance  $j$  ( $j = 0, 1, \dots, ecc_i$ ). The  $j^{\text{th}}$  layer of partition  $G(i)$  may be written as:

$$G(u)_j = \{u : d_{iu} = j\} \quad (18)$$

and the layer matrix:

$$lm_{i,j}^e = \Omega_{u \in G(u)_j} m_u^e \quad (19)$$

$$LM^e(G) = \{lm_{i,j}^e; i \in [1, p(G)]; j \in [0, d(G)]; e \in [1, esp]\} \quad (20)$$

where:  $m$  and  $M$  specifies the property (see Table 1)  
 $e$  is the elongation (i.e. for  $m = \text{walks}$ )  
 $\Omega$  stands for the mathematical operator acting on the properties of vertices  $u \in G(u)_j$ , at the level of each  $j$  layer

Table 1

Types of LM<sup>e</sup> matrices (cf. eq s. 19 and 20) [13]

No.	property m <sub>u</sub> <sup>e</sup>		Ω	LM <sup>e</sup> matrices		Ref.
	name	label		relation	name	
1.	cardinality	1	—	Σ	Cardinality	LC 13
2.	degree	k	$\sum_j a_{ij}$	Σ	Degree	LK/B 10,14
3.	walk degree	w <sup>a</sup>	$\sum_j (a_{ij})^e$	Σ	Walk Degree	LW <sup>a</sup> 13
4.	distance sum <sup>a</sup>	D	$\sum_j d_{ij} = \sum_e (sd^e * e)$	Σ	Distance sum	LMD/R 12
5.	path sum <sup>a</sup>	p	$\sum_e (sp^e * e)$	Σ	Path sum	LMP 13
6.	self returning <sup>a</sup> walk sum	RW <sup>a</sup>	$\sum_e (srw^e * e)$	Σ	Returning Walk sum	LMRW <sup>a</sup> 13
7.	random walk sum <sup>a</sup>	W <sup>a</sup>	$\sum (sw^b * e)$	Σ	Walk sum	LMW <sup>a</sup> 13
8.	Randic' index	χ	$\sum_{all(rs)} (kr * ks)^{-1/2}$	Σ	Randic' index	Lχ 13,22
9.	Balaban index	J	$\sum_{all(rs)} (Dr * Ds)^{-1/2}$	Σ	Balaban index	LJ 12,13,23
10.	electronegativity <sup>b</sup>	E	—	(II) <sup>1/ G(u)_j </sup>	Electronegativity	LE 25
11.	molecular potentials <sup>c</sup>	V	$q_u/(1 + j_u)$	Σ	Potential	LV 25

a) sm<sup>a</sup> — the sequence numbers, in SM<sup>d</sup> matrices

b) |G(u)<sub>j</sub>| — the number of vertices in u the j-th layer

c) q<sub>u</sub> — the residual charge

j<sub>u</sub> — the distance (topological or geometrical one) from the vertex i to all vertices u ∈ G(u);

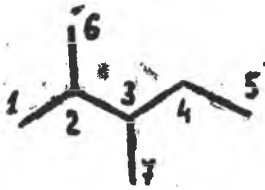
The  $LM^e$  matrices are  $p(G) * d(G)$  in dimensions. Notice that the elongation  $e$  (i.e. in  $m^e = w^e$ ) is formally unlimited. However, usually, a suitable maximal value  $esp$  is taken. Table 1 presents some types of layer matrices, cf. eqs. (19) and (20).

The half sum on rows, of the elements  $lm_{ij}^e$  of matrices  $LM^e$  offers the global property,  $M^e(G)$ :

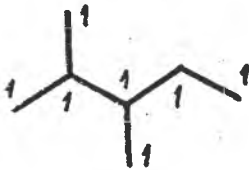
$$M^e(G) = 1/2 \sum_j lm_{ij}^e \tag{21}$$

Fig. 6 presents layer matrices for the graph  $G_5$  by using weighted graphs,  $G\{m_{ij}^e\}$ , (showing a given property instead of vertex labels).

Fig. 6. Layer matrices **SM** and **LM** for the graph  $G_5$

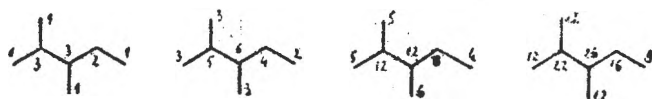


	SD = SP				SRM <sup>4</sup>				SW <sup>4</sup>			
<i>i/e</i>	1	2	3	4	1	2	3	4	1	2	3	4
1	1	2	2	1	0	1	0	3	1	3	5	12
2	3	2	1	0	0	3	0	11	3	5	12	22
3	3	3	0	0	0	3	0	12	3	6	12	26
4	2	2	2	0	0	2	0	6	2	4	8	16
5	1	1	2	2	0	1	0	2	1	2	4	8
6	1	2	2	1	0	1	0	3	1	3	5	12
7	1	2	3	0	0	1	0	3	1	3	6	12
$M^e(G)$	6	7	6	2	0	6	0	20	6	13	26	56
$WD = 46 = WP$				$WRW^4 = 92$				$WVW^4 = 326$				



$G_5\{c_{ic}\}$	<i>i/j</i>	LC					LRM <sup>4</sup>				
	<i>i/j</i>	0	1	2	3	4	0	1	2	3	4
	1	1	1	2	2	1	3	11	15	9	2
	2	1	3	2	1	0	11	18	9	2	0
	3	1	3	3	0	0	12	20	8	0	0
	4	1	2	2	2	0	6	14	14	6	0
	5	1	1	1	2	2	2	6	12	14	6
	6	1	1	2	2	1	3	11	15	9	2
	7	1	1	2	3	0	3	12	17	8	0
$M^e(G)$		20									

Fig. 6 (continued)



$i/j$	$G_5\{w_{10}^1\}$ LW <sup>1</sup> = LK					$G_5\{w_{10}^2\}$ LW <sup>2</sup>					$G_5\{w_{10}^3\}$ LW <sup>3</sup>					$G_5\{w_{10}^4\}$ LW <sup>4</sup>				
	0	1	2	3	4	0	1	2	3	4	0	1	2	3	4	0	1	2	3	4
1	1	3	4	3	1	3	5	9	7	2	5	12	17	14	4	12	22	38	28	8
2	3	5	3	1	0	5	12	7	2	0	12	22	14	4	0	22	50	28	8	0
3	3	6	3	0	0	6	12	8	0	0	12	26	14	0	0	26	50	32	0	0
4	2	4	4	2	0	4	8	8	6	2	8	16	18	10	0	16	34	34	24	0
5	1	2	3	4	2	2	4	6	8	6	4	8	12	18	10	8	16	26	34	24
6	1	3	4	3	1	3	5	9	7	2	5	12	17	14	4	12	22	38	28	8
7	1	3	5	3	0	3	6	9	8	0	6	12	20	14	0	12	26	38	32	0
$M^e(G)$	6					13					26					54				

$i/j$	LMD = LMP					LMD					LMRW <sup>4</sup>				
	0	1	2	3	4	0	1	2	3	4	0	1	2	3	4
1	15	10	24	26	17	18.118	12.869	28.935	32.041	19.279	14	50	68	42	10
2	10	39	26	17	0	12.869	47.053	32.041	19.279	0.000	50	82	42	10	0
3	9	36	47	0	0	12.390	44.910	53.943	0.000	0.000	54	92	38	0	0
4	12	26	24	30	0	15.174	31.669	29.736	34.664	0.000	28	64	64	28	0
5	17	12	9	24	30	19.279	15.174	12.390	29.736	34.664	10	28	54	64	28
6	15	10	24	26	17	16.546	12.869	30.507	32.041	19.279	14	50	68	42	10
7	14	9	22	47	0	16.867	12.390	28.043	53.943	0.000	14	54	78	38	0

$i/j$	LMW <sup>1</sup>					LMW <sup>2</sup>					LMW <sup>3</sup>					LMW <sup>4</sup>				
	0	1	2	3	4	0	1	2	3	4	0	1	2	3	4	0	1	2	3	4
1	1	3	4	3	1	7	13	22	17	5	22	49	73	59	17	70	137	225	171	49
2	3	5	3	1	0	13	29	17	5	0	49	95	59	17	0	137	295	171	49	0
3	3	6	3	0	0	15	30	19	0	0	51	108	61	0	0	155	308	189	0	0
4	2	4	4	2	0	10	20	20	14	0	34	68	74	44	0	98	204	210	140	0
5	1	2	3	4	2	5	10	15	20	14	17	34	51	74	44	49	98	155	210	140
6	1	3	4	3	1	7	13	22	17	5	22	49	73	59	17	70	137	225	171	49
7	1	3	5	3	0	7	15	23	19	0	25	51	83	61	0	73	155	235	189	0

Fig. 6. (continued)

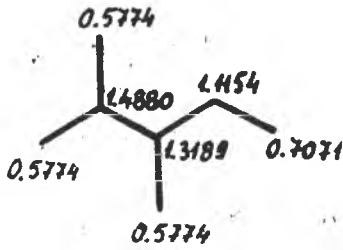


Fig. 8

$G_5\{\chi_{i0}\}$	$L\chi$				
	$i/j$	0	1	2	3
1	0.5774	1.4880	1.8963	1.6928	0.7071
2	1.4880	2.4737	1.6928	0.7071	0.0000
3	1.3189	3.1808	1.8619	0.0000	0.0000
4	1.1154	2.0260	2.0654	1.1548	0.0000
5	0.7071	1.1154	1.3189	2.0654	1.1548
6	0.5774	1.4880	1.8963	1.6928	0.7071
7	0.5774	1.3189	2.6034	1.8619	0.0000

$$\sum_j l \chi_{ij} = 2\chi$$

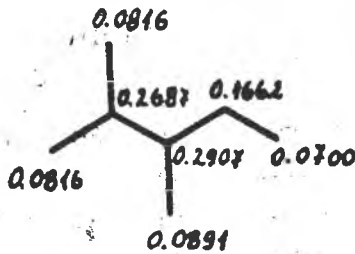


Fig. 9

$G_5\{J_{i0}\}$	$LJ$				
	$i/j$	0	1	2	3
1	0.0816	0.2687	0.3723	0.2553	0.0700
2	0.2687	0.4539	0.2553	0.0700	0.0000
3	0.2907	0.5240	0.2332	0.0000	0.0000
4	0.1662	0.3607	0.3578	0.1632	0.0000
5	0.0700	0.1662	0.2907	0.3578	0.1632
6	0.0816	0.2687	0.3723	0.2553	0.0700
7	0.0891	0.2907	0.4349	0.2332	0.0000

$$\sum_j l J_{i,j} = 2 J/q$$

From the Fig. 6. one can see that the matrices  $\mathbf{LM}$  are built on the ground of the relative partitions in graph (see eq. [14]). The first column ( $j = 0$ ) in  $\mathbf{LM}$  represents just the vertex property,  $m_{i,0}^*$ , specified in the weighted graphs  $G\{m_{i,0}^*\}$ .

The matrices  $\mathbf{LM}$  can be easily constructed by using a distance property matrix,  $\mathbf{DM}$ , defined as:

$$\mathbf{DM}(G) = \mathbf{D}(G) + \mathbf{M}(G) \tag{22}$$

Where  $\mathbf{D}(G)$  is the distance matrix and  $\mathbf{M}(G)$  is the diagonal matrix of properties  $m_i$ ,  $i \in V(G)$  (see also ref. [24]).

In **LM** the elements of column  $j = 0$  will be just the diagonal entries in **DM**( $G$ ). The next layers result by applying the operator  $\Omega$  on the properties  $m_u^e$  of the vertices  $u \in G(u)_j$ , until  $j = ecc_i$ . Most often (but not in general) the operator  $\Omega$  leaves the diagonal elements unchanged because the set  $G(u)_0$  consists of single vertex. The procedure is exemplified for the graph  $G_1$  in the building of the layer matrix of degrees, **LK**, with  $\Omega = \Sigma$ , and  $lm_{ij}^e = \sum_{u \in G(u)_j} m_u^e$

<b>D</b>	<b>M = K</b>	<b>DM</b>	<b>LK</b>	<b>LK</b>
0 2 2 1	1 0 0 0	1 2 2 1	1 3 2+2	1 3 4
2 0 1 1 + 0	2 0 0 = 2	2 1 1 → 2	2+3 1 = 2	5 1
2 1 0 1	0 0 2 0	2 1 2 1	2 2+3 1	2 5 1
1 1 1 0	0 0 0 3	1 1 1 3	3 1+2+2 0	3 5 0

3.3. *Line form of layer matrices.* Layer matrices can be represented in a line form [8], which recall their origin in the sequences of routes. For the graph  $G_1$  the matrices **SD** and **LC** will be :

$$\mathbf{SD}(G_1) = \{1 (1, 2); 2 (2, 1); 3 (2, 1); 4 (3, 0); \} \tag{23}$$

$$\mathbf{LC}(G_1) = \{1 (1, 1, 2); 2 (1, 2, 1); 3(1, 2, 1); 4 (1, 3, 0)\} \tag{24}$$

If the vertex labeling is not important (i.e. in the comparison of matrix invariants within the isomorfism testings), the canonical form is used: the rows are wrtten in decreasing order of their length (as nonzero elements) and lexicografical order (in case of equal length) along with the multiplicity of identical rows. For the graph  $G_1$  the two matrices will be :

$$\mathbf{SD}(G_1) = \{2 * (2, 1); (1, 2); (3, 0)\} \tag{25}$$

$$\mathbf{LC}(G_1) = \{2 * (1, 2, 1); (1, 1, 2); (1, 3, 0)\} \tag{26}$$

Another way to order the rows in a layer matrix is to apply the *centricity criteria* of Bonchev et al. [16, 17], resulting in a centric ordering of the graph [12].

Appendix 1 presents recursive relations for the calcul of walk degrees,  $w_i^e$ , along with the partitions (as **LC** matrices) and the matrices **LM**<sup>e</sup>, in the line form, for some special graphs.

3.4. *Discussion on layer matrices.* A regard upon the layer matrices enables one some remarques :

- 1) **SM**, as sequences of degrees (e.g. DDS [15-18]) count the number of walks (of various type and elongation) emerging from a given vertex ;
- 2) **LM**, as matrices of vertex property, count the value of property at various shells surrounding a given vertex ;

- 3) excepting **SD**, the **SM** matrices do not superimpose over the partitions of graph, and more over, **SRW<sup>e</sup>** and **SW<sup>e</sup>** have formally nonrestricted number of columns (nonlimited  $e$ )
- 4) the **LM** matrices follow the partitions of graph, the number of columns being the graph eccentricity (diameter) plus one ;
- 5) **LM** based on graph theoretical properties can be grouped into layer degree matrices (**LC**, **LK** and **LW<sup>e</sup>**) and layer metric matrices (**LMD**, **LMP**, **LMRW<sup>e</sup>** and **LMW<sup>e</sup>** — where **M** remembers of "metric") ;
- 6) layer degree matrices, as **LW<sup>e</sup>**, can be derived by "exploding" the **SW<sup>e</sup>** matrix (the columns of **SW<sup>e</sup>** beacome the first one in **LW<sup>1</sup>** to **LW<sup>e</sup>** matrices). The same could be done for the other **SM** matrices but the resulting **LD<sup>e</sup>**, **LP<sup>e</sup>**, **LRW<sup>e</sup>** matrices are not suitable for **LOVI** (Local Vertex Invariant) task because of their zero entries. However **LRW<sup>e</sup>** could be of interest for  $e = \text{even}$  (see Fig. 6) or in cyclic graphs ;
- 7) layer metric matrices are **SM** calculable, their first column being  $\Sigma_e(sm_i^e * e)$
- 8) the matrices **SD** and **LC** differ only by  $lc_{i0}$  column, which counts the vertex  $i$ , itself. If one neglect this column the two matrices are identical and represent the joint point between **SM** and **SL** matrices. The **LC** matrices just count the vertices in the partitions of graph. Thus, it is not a surprize that Skorobogatov [8] and Dobrynin [9] called their  $\lambda$  matrix a layer matrix. However, in its line form,  $\lambda/\mathbf{SD}$  matrix coincides with DDS [15—18]. In the followings, some properties of layer matrices are presented :

$$\mathbf{SD} : \quad \Sigma_e sd_i^e = p - 1 \quad (27)$$

$$\Sigma_i sd_i^1 = \Sigma_i k_i = 2q \quad (28)$$

$$\Sigma_i (sd_i^1)^2 - \Sigma_i sd_i^2 = 2q \quad (29)$$

$$\mathbf{LC} : \quad \Sigma_j lc_{ij} = p \quad (30)$$

$$\Sigma_j lc_{i0} = p \quad (31)$$

$$\Sigma_i lc_{i1} = \Sigma_i k_i = 2q \quad (32)$$

$$\mathbf{LK} : \quad \Sigma_i (lk_{i0})^2 = \Sigma_i lk_{i1} \quad (33)$$

$$lc_{i1} = lk_{i0} ;$$

$$lc_{ij} + lc_{i(j+1)} = lk_{ij} ; j \in [1, ecc_i - 1] \quad (34)$$

$$lc_{i, ecc_i} = lk_{i, ecc_i} ;$$

$$\mathbf{LW}^e : \quad \Sigma_i (lw_{i0}^1)^2 = \Sigma_i lw_{i1}^1 = \Sigma_i lw_{i0}^2 \quad (35)$$

$$lw_{i1}^e = lw_{i0}^{e+1} \quad (36)$$

$$\mathbf{LM}^e : \quad \Sigma_j lm_{ij}^e = \Sigma_i lm_{i0}^e = 2 M^e(G) \quad (37)$$

$$M^e(G) = WM^e \quad (38)$$

In the above relations,  $p$  stands for the number of vertices in graph and  $q$  is the number of edges, Eq. (28) holds in graphs without cycles  $C_3$  and  $C_4$  (see<sup>9</sup>) and eq. (34) holds only for trees. In eqs. (37) and (38),  $M^e(G)$  means the global property (involving  $\Omega = \Sigma$ ) which in layer metric matrices equals the corresponding Wiener index  $WM^e$ .

For LC, which local property does not involve edges, and for matrices such as LE and L $\mathcal{L}$ , reported in Table 1 (and [25]) the eq. (37) does not hold. The properties in the last two matrices involve more sophisticated mathematical operations. These matrices are, however, of limited interest. In ref. [26] there is a reference to Balandin's matrices, the entries of which also recorded molecular properties.

Eq. (36) needs a particular attention. It shows that the second column in  $LW^1$  becomes the first one in the higher term matrix  $LW^2$ . This result holds for any two consecutive elongations in  $LW^e$  of a graph (excepting the multi-graphs). We proposed in [6] an iterative procedure for counting walk degrees  $w_i^{e+1}$  from the values  $w_i^e$  of the vertices belonging to the first shell around each vertex  $i$  in  $G$  (see part 2.1., eqs. (9) to (11) and Fig 6). Thus, one reduces the calcul of power matrices  $A^e$  (see [3]) to a simple summation of degrees. Such a procedure involving extended connectivity is encountered within the well-known HOC-algorithm of Balaban et al. [27] (the second ordering of vertices by the sum of degrees of the first neighbours) but they did not iterated this step, for finding higher  $w_i^e$  terms.

The count of  $w_i^e$  and the global number of walks of elongation  $e$ ,  $W^e(G)$  is also important by virtue of their relationship with the largest eigenvalue,  $x_1$ , as shown by Cvetkovic, and Gutman [28].

$$W^e(G) \simeq n(x_1)^e \quad (39)$$

Since  $W^e(G)$  is a measure of molecular branching, eq. (39) proves the topological relation of molecular energy levels, i.e. in Huckel approach (see part 4.1.).

**4. Applications.** Matrices associated with molecular graphs are themselves invariants but they represent an additional source of other invariants [13, 26]. Among such invariants, the topological indices (single numerical values coding a graph theoretical or a chemical property in graph) were widely used in QSPR QSAR (Quantitative Structure Property Relationships/Quantitative Structure Activity Relationships) [10, 26, 29, 30]. They are important tools in vertex and graph ordering [7, 12, 31–33] or also in vertex equivalence perception (topological symmetry) [2, 12, 20, 32]. A synopsis of the main topological indices is given in [34].

We confine here to four direct application of matrices, the first two (*Spectrum of a graph and Huckel theory* and *Conjugation detection*) based on symmetric (quadratic) matrices, and the last two (*SP matrices and the ordering of alkanes* and *Molecular similarity testing*) constructed on layer matrices.

4.1. *Spectrum of a graph and Huckel theory* [35]. In the graph theory, the spectrum of a graph is defined [5] as the set of eigenvalues of the adjacency matrix,  $\mathbf{A}$ :

$\{x_1, x_2, \dots, x_p\}$ , and  $x_1 \geq x_2 \geq \dots \geq x_p$ . The diagonal matrix  $\mathbf{X}$ :

$$\mathbf{X} = \begin{vmatrix} x_1 & & & \\ & x_2 & & 0 \\ & & & \\ 0 & & & \\ & & & x_p \end{vmatrix}$$

is obtained from  $\mathbf{A}$  by the matrix  $\mathbf{R}$ :

$$\mathbf{R} * \mathbf{A} * \mathbf{R}^{-1} = \mathbf{X} \quad (40)$$

where  $\mathbf{R}(G)_{p \times p}$  is the matrix of eigenvectors:

$$\mathbf{R} = \begin{vmatrix} r_{11} & r_{12} & \dots & r_{1p} \\ r_{21} & r_{22} & \dots & r_{2p} \\ \dots & \dots & \dots & \dots \\ r_{p1} & r_{p2} & \dots & r_{pp} \end{vmatrix}$$

Eq. (40) may be written as:

$$\mathbf{R}_i * \mathbf{A} = x_i * \mathbf{R}_i; \quad i = 1, 2 \dots P \quad (41)$$

where  $\mathbf{R}_i$  is the row  $i$  in matrix  $\mathbf{R}$ , and also represents the eigenvector belonging to the eigenvalue  $x_i$ . Eq (41) may be written as:

$$\mathbf{R}_i * [x_i \mathbf{U} - \mathbf{A}] = \mathbf{0} \quad (42)$$

Relation (42) represents a system of homogeneous linear equations, called the *secular equations* [5, 36]. The matrix  $[x_i \mathbf{U} - \mathbf{A}]$  is called the *secular matrix* of a graph. In order that the secular equations (42) have nontrivial solutions, the corresponding *secular determinant* must vanish:

$$\det |\mathbf{XU} - \mathbf{A}| = 0 \quad (43)$$

The polynomial constructed by the expansion of the secular determinant is called the *characteristic polynomial*:

$$P(G; x) = \det |\mathbf{XU} - \mathbf{A}| \quad (44)$$

$$P(G; x) = \sum_{p=0}^P a_p * x^{P-p} \quad (45)$$

where  $a_p$  ( $p = 0, 1, 2, \dots, P$ ) are the coefficients of this polynomial. They may also be generated by the Sachs method [37].

The set of solutions of the polynomial constitutes just the spectrum of the graph. The interval in which the Huckel eigenvalues lie is limited by the maximal degree of vertices in graph (the theorem of Frobenius [38]):

$$-k_{max} \leq x_i \leq k_{max} \quad (46)$$

By introducing the eigenvalues  $x_i$  in relation (42) the corresponding eigenvectors may be derived.

Huckel theory considers a  $\pi$  molecular orbital (MO) as a linear combination of atomic orbitals (LCAO), of the form:

$$\Psi_i = \sum_{p=1}^p c_{i,p} \Phi_p \quad (47)$$

where  $\Phi_p$  is a  $p$  orbital on atom  $p$ , and  $c_{i,p}$  is the contribution of the orbital of atom  $p$  to the construction of the molecular orbital  $\Psi_i$ .

The total  $\pi$  electron energy,  $E_\pi$ , is a function of the occupation number, number,  $g_i$ , of  $\Psi_i$ :

$$E_\pi = \sum_{i=1}^p g_i E_i = E(HMO) \quad (48)$$

where  $E_i$  is the energy associated with  $\Psi_i$ .

Minimization of  $E_\pi$  [36] by means of the variational method leads to a system of homogenous linear equations:

$$\sum_{p=1}^p c_{i,p} (H_{pr} - E_i S_{pr}) = 0; \quad i, r = 1, 2, \dots, P \quad (49)$$

This system has nontrivial solutions if the corresponding Huckel determinant vanishes:

$$\det | H_{pr} - E_i S_{pr} | = 0 \quad (50)$$

where  $H_{pr}$  and  $S_{pr}$  are respectively the resonance and overlap integrals (between the orbitals of atoms  $p$  and  $r$ ). Relation (50) may be written in the matrix form:

$$\det | \mathbf{H} - \mathbf{E} \mathbf{S} | = 0 \quad (51)$$

where  $\mathbf{H}$ ,  $\mathbf{E}$  and  $\mathbf{S}$  are the Hamiltonian, the energy and the overlap matrices respectively. By virtue of the Bloch - Huckel approximations [35, 39] the matrices  $\mathbf{H}$  and  $\mathbf{S}$  have the following structure [40]:

$$\mathbf{H} = \alpha * \mathbf{U} + \beta * \mathbf{A} \quad (52)$$

$$\mathbf{S} = \mathbf{U} \quad (53)$$

where  $\mathbf{A}$  is the adjacency matrix of a Huckel graph (a conjugated molecule),  $\alpha$  is the Coulomb energy of the atomic orbitals  $\Phi_p$ , while  $\beta$  is the resonance energy corresponding to the bond ( $p, r$ );  $\beta < 0$ .

The matrix  $[\mathbf{H} - \mathbf{E} \mathbf{S}]$  is called the Huckel matrix. Fig. 7 presents the Huckel matrix for butadiene.

Fig. 7. Huckel approach for butadiene



Fig. 10

$$[\mathbf{H} - E\mathbf{S}] = \begin{array}{cccc} \alpha - E & \beta & 0 & 0 \\ \beta & \alpha - E & \beta & 0 \\ 0 & \beta & \alpha - E & \beta \\ 0 & 0 & \beta & \alpha - E \end{array} \quad \det |\mathbf{XU} - \mathbf{A}| = \begin{array}{cccc} x & -1 & 0 & 0 \\ -1 & x & -1 & 0 \\ 0 & -1 & x & -1 \\ 0 & 0 & -1 & x \end{array}$$

$$P(G; x) = x^4 - 3x^2 + 1$$

$$\text{Eigenvalues: } \{1.618034; 0.618034; -0.618034; -1.618034\}$$

$$\text{Energy levels: } E_1 = \alpha + 1.618034 * \beta \quad E_3 = \alpha - 0.618034 * \beta$$

$$E_2 = \alpha + 0.618034 * \beta \quad E_4 = \alpha - 1.618034 * \beta$$

Eigenvectors:

$$\mathbf{R}_i * [\mathbf{x}_i \mathbf{U} - \mathbf{A}] = 0; \quad \begin{array}{l} r_{11}x_i - r_{12} + 0 + 0 = 0 \\ -r_{11} + r_{12}x_i - r_{13} + 0 = 0 \\ 0 - r_{12} + r_{13}x_i - r_{14} = 0 \\ 0 + 0 - r_{13} + r_{14}x_i = 0 \end{array}$$

$$\text{Normalizing condition: } \sum_j r_{ij}^2 = 0$$

Fig. 7 (continued)

The eigenvectors matrix (atomic orbital coefficients):

	1	2	3	4
1	0.371748	0.601501	0.601501	0.371748
2	0.601501	0.371748	-0.371748	-0.601501
3	0.601501	-0.371748	-0.371748	+0.601501
4	0.371748	-0.601501	0.601501	-0.371748

Substitution of  $\mathbf{H}$  and  $\mathbf{S}$  in (51) and dividing the rows by  $\beta$  results in:

$$\det \left| \begin{array}{c} E_i - \alpha \\ \beta \end{array} * \mathbf{U} - \mathbf{A} \right| = 0 \quad (54)$$

Comparison between eqs. (54) and (43) indicates that the quantities  $(E_i - \alpha)/\beta$  representing the  $\pi$  energies of Huckel orbitals constitute the spectrum of eigenvalues of a Huckel graph (see Fig. 7):

$$E_i = \alpha + x_i \beta; \quad i = 1, 2, \dots, P \quad (55)$$

If  $\beta$  is taken as the energy unit and  $\alpha$  as the zero-energy reference point ( $\beta = 1$ ;  $\alpha = 0$ ), eq. (55) becomes:

$$E_i = x_i; i = 1, 2, \dots, p \quad (56)$$

According to eq. (56), the eigenvalues of  $\mathbf{A}$  are identical with the Huckel orbital (HMO) energy levels. Since the maximal degree in Huckel graphs is  $k_{max} = 3$ , the domain of Huckel eigenvalues (cf. to the Frobenius theorem) is:  $-3 \leq x_i \leq +3$ . In linear polyenes and annulenes.  $k_{max} = 2$ .

The Huckel spectrum  $\{x_1, x_2, \dots, x_p\}$  can be partitioned in three subsets, corresponding to the bonding, nonbonding, and antibonding energy levels,  $P_+$ ,  $P_0$  and  $P_-$ . Their sum equals the number of atoms,  $P$ , in the conjugated system,  $P_+ + P_0 + P_- = P$ .

Since matrices  $\mathbf{H}$  and  $\mathbf{A}$  commute ( $[\mathbf{H}, \mathbf{A}] = 0$ ), they have the same set of eigenvectors. In other words, the eigenvectors of  $\mathbf{A}$  are identical with the Huckel molecular orbitals (sometimes called the *topological orbitals*). An important conclusion one imposes [5]: "the topology of a molecule, rather than its geometry, determines the form of the Huckel molecular orbitals".

From the above considerations, it is obvious that the Huckel theory is equivalent to the graph spectral theory (see also [5]).

Fig. 7 presents an example of Huckel calculation for the butadiene.

**4.2. Conjugation detection.** Baumer et al. [41, 42] used the adjacency matrices and logical multiplication for conjugation perception in unsaturated or aromatic systems. They split the standard adjacency (connectivity) matrix in two logical matrices: **SB** (Single Bond) and **MB** (Multiple Bond) whose elements are respectively TRUE (denoted by \*), if the corresponding element in  $\mathbf{C}$  equals the conventional bond order ( $b_{ij} = 1$  for **SB** and  $b_{ij} > 1$  for **MB**), otherwise FALSE (denoted by .).

The logical multiplication of these matrices will furnish:

- SB** \* **MB** = **P**<sup>1</sup> — all allyl systems in molecule
- MB** \* **P**<sup>1</sup> — butadiene systems (1<sup>st</sup> order conjugation)
- P**<sup>1</sup> \* **P**<sup>1</sup> = **P**<sup>2</sup> — "double allyl" systems (two connected allyls)
- MB** \* **P**<sup>2</sup> — hexatriene systems (2<sup>nd</sup> order conjugation), and so on.

Fig. 8 shows these matrices for hexatriene and benzene, respectively.

Two different situations can determine the end of procedure:

- (i) **P**<sup>*n*</sup> is entirely FALSE, and the corresponding product **MB** \* **P**<sup>*n*</sup> is also FALSE (the case of chain conjugated systems, e.g. the hexatriene, see Fig. 8)
- (ii) **MB** \* **P**<sup>*n-1*</sup>  $\equiv$  **SB** (**MB** \* **P**<sup>*n*</sup>  $\equiv$  **MB**). A ring containing a completely conjugated system was found, i.e. the benzene, Fig. 8. In polycyclic structures, such rings occur when the matrix **MB** \* **P**<sup>*n-1*</sup> contains a submatrix identical to a corresponding one in the **SB** matrix (**MB** \* **P**<sup>*n*</sup> includes a submatrix of **MB**).

(i) hexatriene:

Fig. 8. Conjugation perception in hexatriene and benzene



Fig. 11

C	SB	MB	P
0 2 0 0 0 0	. . . . .	. * . . . .	. . . . .
2 0 1 0 0 0	. . * . . .	* * . . . .	. . . * . . .
0 1 0 2 0 0	. * . . . .	. . . * . . .	* . . . . .
0 0 2 0 1 0	. . . . * . .	. . * . . . .	. . . . . *
0 0 0 1 0 2	. . . * . . .	. . . . * . .	. . * . . . .
0 0 0 0 2 0	. . . . .	. . . . * . .	. . . . .

allyls :

(2-4); (1-3);

(4-6); (3-5)

MB * P	P <sup>2</sup>	MB * P <sup>2</sup>	P <sup>3</sup>
. . . * . . .	. . . . .	. . . . * . .	. . . . .
. . . . * . .	. . . . .	. . . . * . .	. . . . .
* . . . . .	. . . . .	. . . . * . .	. . . . .
. . . . * . .	. . . . .	. . . . * . .	. . . . .
. . . . .	. . . . .	. . . . * . .	. . . . .

butadienes :

(1-4); (3-6)

(1<sup>st</sup> ord. conj.)

double allyls :

(1-5); (2-6)

hexatrienes :

(1-6)

(2<sup>nd</sup> ord. conj.)

Calculation of bond orders :

$$\text{bond a: } (2 + 1 + 0.5)/2 = 1.75$$

$$\text{bond b: } (1 + 2)/2 = 1.50$$

$$\text{bond c: } (2 + 1)/2 = 1.50$$

Fig. 8 (continued)

(ii) benzene :



Fig. 12

C	SB	MB	P
0 2 0 0 0 1	. . . . *	. * . . .	. . . . *
2 0 1 0 0 0	. . * . .	* . . . .	. . . * .
0 1 0 2 0 0	. * . . .	. . * . .	* . . . .
0 0 2 0 1 0	. . . * .	. . * . .	. . . . *
0 0 0 1 0 2	. . . * .	. . . * .	. . * . .
1 0 0 0 2 0	* . . . .	. . . * .	. * . . .

*allyls* : (1-5); (2-4); (1-3); (4-6); (3-5); (2-6)

MB * P	P <sup>2</sup>	MB * P <sup>2</sup>	P <sup>3</sup>
. . . * .	. . * . .	. . . * .	* . . . .
. . . . *	. . . . *	. . * . .	. * . . .
* . . . .	. * . . .	. . . * .	. . . * .
. * . . .	* . . . .	. . . * .	. . . * .
. . * . .	. . . * .	* . . . .	. . . . *

*butadienes* :*double allyls* :*hexatrienes* :

(1-4);(2-5);(3-6) (1-3);(2-6);(3-5) (1-6);(2-3);(4-5)

(1<sup>st</sup> ord. conj.)(2<sup>nd</sup> ord. conj.)MB \* P<sup>2</sup> = SB;(SB)<sup>2</sup> = U;P \* P<sup>3</sup> = P<sup>4</sup> = PMB \* P<sup>3</sup> = MB;(MB)<sup>2</sup> = U;MB \* P<sup>4</sup> = MB \* P*Calculation of bond orders* : (2 + 1)/2 = 1.50

The procedure is included in an algorithm for counting the Pauling's bond orders [43] as arithmetic mean of the conventional bond orders in each resonance forms. Thus, the finding of alternative resonance structures (i.e. Kekule' forms) is done by interchanging of submatrices of SB and the corresponding ones of MB, until all possible combinations are found.

The evaluation of bond orders in cyclic (polycyclic) systems is straitforward (see Fig. 8 for the benzene) In the case of chain conjugated systems, a "long" bond must be considered between the two extreme charged atoms in a resonance structure (see Fig. 8, for the hexatriene). The bond order of such a "long" bond will be taken equal to the conjugation level, multiplied by a damping factor (of 1/2 (n - 1)) with n being the number of double bonds in conjugation). For hexatriene, the calculus of bond orders is given in Fig. 8.

The bond orders thus calculated are used in a procedure of the evaluation of residual charges in molecules [41, 42, 44].

4.3. SP matrices and the ordering of alkanes. Matrices SP, by means of the global sequences M (G), can be used in the ordering of type × (of centro-

complexity) or  $c$  (of centrality) [10, 12, 31, 32], of alkane isomers. Thus, the increasing lexicographic ordering of path sequences furnish an ordering which is identical to that given by the  $x$  - type topological index  $x(\mathbf{LK})$ , [10] or by the superindex  $DM^1$  [45], in the set of heptane isomers (see Table 2).

By applying the centric criteria of Bonchev et al. [16, 17] on the path sequences results in a  $c$  - type ordering which is identical to that induced by the  $c$  - type index  $c(\mathbf{D})$ , [31].

The  $x$  - type and  $c$  - type indices we defined [13] as follows:

$$x(\mathbf{LM})_i = \sum_{j=0}^{ecc_i} [(lm_{ij}) * 10^{-z} \pm li]^{\pm 1} * t_i \quad (57)$$

$$li = fi(lm_{i0}/10 + lm_{i1}/100) \quad (58)$$

$$fi = \sum_u (b_{iu} - l) \quad (59)$$

$$c(\mathbf{LM})_i = [\sum_{j=1}^{ecc_i} (lm_{ij})^{dsp}]^{-1} \quad (60)$$

where:  $z$  - the number of digits of the (integer part of)  $\max lm_{ik}$  value in graph.

$li$  - a local parameter for multiple bonds

$fi$  - a multigraph factor, with  $b_{iu}$  the conventional bond order

$t_i$  - a weighting factor, accounting for heteroatoms (e.g. a Sanderson type of electronegativity [46-48] or fragmental volumes [49, 50]).

$dsp$  - a specified topological distance, usually larger than the diameter of graph (here  $dsp = 10$ , unless otherwise specified)

Table 2 presents the two type of orderings in the set of heptanes.

Table 2

Path sequences in heptanes and the corresponding X - and C - Intermolecular ordering [31]

Path sequence	Xord	X(LK)	DM <sup>1</sup> [45]	C <sub>ord</sub>	C(D) * 100
6 5 4 3 2 1	C <sub>7</sub>	14.39506	13.42462	C <sub>7</sub>	4.56222
6 6 4 3 2 0	2MC <sub>6</sub>	14.61504	14.76562	2MC <sub>6</sub>	6.00622
6 6 5 3 1 0	3MC <sub>6</sub>	14.63682	15.08212	3MC <sub>6</sub>	7.24297
6 6 6 3 0 0	3EC <sub>5</sub>	14.65860	15.36658	24M <sub>2</sub> C <sub>5</sub>	8.34368
6 7 4 4 0 0	24M <sub>2</sub> C <sub>6</sub>	14.83680	16.36313	3EC <sub>5</sub>	9.44105
6 7 6 2 0 0	23M <sub>2</sub> C <sub>5</sub>	14.87640	16.94921	22M <sub>2</sub> C <sub>5</sub>	9.62898
6 8 4 3 0 0	22M <sub>2</sub> C <sub>6</sub>	15.05460	17.94975	23M <sub>2</sub> C <sub>5</sub>	10.29196
6 8 6 1 0 0	33M <sub>2</sub> C <sub>5</sub>	15.09420	18.48528	33M <sub>2</sub> C <sub>5</sub>	12.60393
6 9 6 0 0 0	223M <sub>3</sub> C <sub>4</sub>	15.31200	20.54701	223M <sub>3</sub> C <sub>4</sub>	14.54199

4.4. Structural similarity testing. The term "structural similarity" is an intuitive concept used by the chemists to classify molecules according to

certain structural features. There are more than one measure of similarity which can be relevant in a particular context.

In quantitative terms, the structural similarity can be approached either by means of interstructure distance calculation [51, 52] or in the frame of more sophisticated algorithms, such as SIBIS model [53]. Randić' [51] developed the first procedure by using path sequences as a ground for computing Euclidian distances within various sets of compounds. Basak *et al* [52] performed a PCA (Principal Component Analysis) on a large molecular data base (3692 chemicals) by means of 90 TIs and the Euclidian distance for structure similarity measurements.

One defines the generalized Minkowski distance,  $D_M$ , as [45, 52]:

$$D_M = \left[ \sum_{i=1}^n (x_i - y_i)^2 \right]^{1/2} \quad (61)$$

with  $x_i, y_i$  the coordinates of two structures,  $X(x_1, x_2, \dots, x_n)$  and  $Y(y_1, y_2, \dots, y_n)$  in a  $n$ -dimensional space. For  $z = 2$ ,  $D_M^z$  becomes the Euclidian distance,  $D_E$ . For  $z = 1$ , the Manhattan distance,  $D_{Mh}$ , is obtained:

$$D_{Mh} = \sum_{i=1}^n |x_i - y_i| \quad (62)$$

We used [13] this last distance, with the specification that  $x_i, y_i$  are *LOVIs* of  $c$ - or  $x$ -type (cf. eqs. (57) - (60)), constructed on **LM** matrices. Thus, we applied this procedure on a set of four graphs  $G_8$  to  $G_9$  (Fig. 9), the first three of them being related by Dobrynin [9] as showing degenerate  $\lambda$  and **B** matrices (actually **SD** and **LK** matrices).

Fig. 9. Graphs with degenerated **SD**, **LC**, **LK**, and **LM**<sup>1</sup> matrices.,

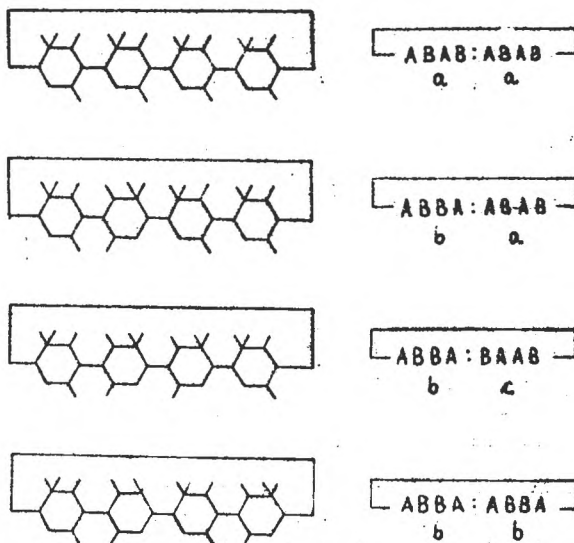


Fig. 13

By inspecting the graphs in Fig. 9, one can see that these structures can be considered as cycles of two types of half hexes, denoted *A* and *B*. Next, one can depart three types of cyclic *AB* — sequences: a) *ABAB*; b) *ABBA* and c) *BAAAB*. It is easily to prove by cyclic permutations, that there are only four distinct combinations of *AB* — sequences: *a — a*; *b — a*; *b — c* and *b — b*. Any other combinations reduce to the above mentioned structures.

Since the **SD** and **LK** (and also **LM**<sup>1</sup> and **LMW**<sup>1</sup>) matrices are degenerated in the set of graphs  $G_6$  to  $G_9$ , it is expected that this graphs are very similar. Indeed, the *x* — type *LOVIs* constructed on **LMD** and **LMW**<sup>*e*</sup> (matrices which do not degenerate in  $G_6$  to  $G_9$ ) gave very low values of  $D_{Mh}$ , which ranged on five orders of magnitude, as *e* varied between 2 and 6.

This result suggested that the rows in the considered **LM** matrices differ only in the remote vertex entries. So, we computed normalized  $D_{Mh}$  values (cf. eq. (63)) by using the *c* — type *LOVIs*:

$$D_{Mh} = \sum_c \sum_i [ |c(\mathbf{LM}^c)_{i1} - c(\mathbf{LM}^c)_{i2}| / (c(\mathbf{LM}^c)_{i1} + c(\mathbf{LM}^c)_{i2}) ] \quad (63)$$

Now, the values of  $D_{Mh}$  are of the order of  $10^{-2}$ , the results being presented in the following distance arrays:

**A**<sub>1</sub>:  $D_{Mh}$  for  $G_6$  to  $G_9$ , computed with  $c(\mathbf{LMD})_i$ , \*  $10^3$  values (*dsp* = 20)

	$G_6$	$G_7$	$G_8$	$G_9$
$G_6$	0	3.3760	5.5463	1.2138
$G_7$		0	2.8633	3.4901
$G_8$			0	5.8184
$G_9$				0

**A**<sub>2</sub>:  $D_{Mh}$  for  $G_6$  to  $G_9$ , computed with  $c(\mathbf{LMW}^e)_i$ , \*  $10^2$  values (*dsp* = 20; *e* = 2 to 6)

	$G_6$	$G_7$	$G_8$	$G_9$
$G_6$	0	11.8007	13.8506	11.0244
$G_7$		0	6.6727	10.0055
$G_8$			0	11.0654
$G_9$				0

From **A**<sub>1</sub> and **A**<sub>2</sub>, one can see that  $G_6$  is more similar with  $G_9$ , in terms of  $c(\mathbf{LM})$ , and  $G_7$  is more close to  $G_8$ . Conversely, the *x*(**LM**) *LOVIs* showed a larger distance (dissimilarity) between  $G_6$  and  $G_9$  than between  $G_8$  and the remaining graphs. However, in both *c* — and *x* — terms,  $G_7$  and  $G_8$  were the most similar structures within the considered set.

**5. Conclusions.** Matrix representation of molecular graphs enables the proper description of their topology and atomic/molecular properties. The symmetric matrices can be processed by classical mathematical operators which can

furnish topological based molecular propertie (i.e. Huckel MO and corresponding energy levels). In opposite, the nonsymmetric matrices can be operated only by special (ad-hoc) designed operators. Both of these types of matrices can serve as a ground for the construction of topological indices (useful in QSPR/QSAR studies). They also can be used in graph ordering and similarity studies.

**Acknowledgements.** Many thanks are addressed to Dr. Ioan Silaghi-Dumitrescu, Department of Chemistry, "Babes-Bolyai" University, Cluj, Romania, for helpful discussions.

## REFERENCES

1. C. Berge, *The Theory of Graphs and Its Applications*, Methuen, London, 1962.
2. M. Randić; W. L. Woodworth; A. Graovac, *Int. J. Quantum Chem.* **24**, 435 (1983).
3. F. Harary, *Graph Theory*, Addison-Wesley, Reading, Mass., 1971.
4. J. J. Sylvester, *Am. J. Math.*, **1**, 64 (1874).
5. N. Trinajstić, *Chemical Graph Theory*, CRC Press, Inc., Boca Raton Florida, 1983.
6. M. V. Diudea; M. Topan; A. Graovac, *J. Chem. Inf. Comput. Sci.* (1993) (in press).
7. S. H. Bertz, *Discr. Appl. Math.* **19**, 65 (1988).
8. V. A. Skorobogatov; A. A. Dobrynin, *MATGH.* **23**, 105 (1988).
9. A. Dobrynin, *J. Math. Chem.*, **14**, 175 (1993).
10. M. V. Diudea; O. M. Minailiuc; A. T. Balaban, *J. Comput. Chem.* **12**, 527 (1991).
11. M. V. Diudea, *Colloquium on Theoretical Chemistry*, October, 14-16, 1992, Cluj, Romania
12. A. T. Balaban; M. V. Diudea, *J. Chem. Inf. Comput. Sci.*, **33**, 421 (1993).
13. M. V. Diudea, *J. Chem. Inf. Comput. Sci.* (1993) (in press).
14. M. V. Diudea; I. E. Kacso'; *MATCH*, **26**, 255 (1991).
15. M. Randić; C. L. Wilkins, *J. Phys. Chem.*, **83**, 1525 (1979).
16. D. Bonchev; O. Mekenyan; A. T. Balaban, *J. Chem. Inf. Comput. Sci.*, **29**, 91 (1989).
17. D. Bonchev; A. T. Balaban; M. Randić, *Int. J. Quantum. Chem.*, **19**, 61 (1981).
18. F. Y. Halberstam; L. V. Quintas, *Distance and path degree sequences for cubic graphs*, Pace University, New York, 1982.
19. M. Randić; L. DeAlba; X. Guo; A. F. Kleiner; H. Krishnapriyan; L. Naylor; T. Oxley, *J. Chem. Inf. Comput. Sci.* (1993) (in press).
20. M. V. Diudea, B. Pary, *MATCH*, **23**, 65 (1988).
21. H. Wiener, *J. Amer. Chem. Soc.*, **69**, 17 (1947).
22. M. Randić, *J. Amer. Chem. Soc.*, **97**, 6609 (1975).
23. A. T. Balaban, *Chem. Phys. Lett.*, **89**, 399 (1982); *Pure Appl. Chem.* **54**, 1075 (1982).
24. B. Mohar, *Prepr. Ser. Dept. Math. Univ. E. K. Ljubljana*, **26**, 385 (1988).
25. M. V. Diudea, "Topologie Moleculara" Synchron Printing House, Cluj, (in press).
26. M. Randić, *J. Math. Chem.*, **7**, 155 (1991).
27. A. T. Balaban, O. Mekenyan, D. Bonchev, *J. Comput. Chim.*, **6**, 538 (1985).
28. D. M. Cvetković, I. Gutman, *Croat. Chem. Acta*, **49**, 115 (1977).
29. M. V. Diudea, I. Bal, *Studia Univ. Babes-Bolyai*, **35**, 17 (1990).
30. L. B. Kier, L. H. Hall, "Molecular Connectivity in Chemistry and Drug Research" Acad. Press, New-York, 1976.
31. M. V. Diudea, D. Horvath, A. Graovac, *J. Chem. Inf. Comput. Sci.* (in press).
32. M. V. Diudea, D. Horvath, I. E. Kacso', O. M. Minailiuc, B. Parv, *J. Math. Chem.*, **11**, 259 (1992).
33. D. H. Rouvray, *Discr. Appl. Math.*, **19**, 317 (1988).
34. A. T. Balaban, I. Motoc, D. Bonchev, O. Mekenyan, *Top. Curr. chem.*, **114**, 21 (1983).
35. E. Huckel, *Z. Phys.*, **60**, 204 (1931); **72**, 310 (1932); **76**, 628 (1932).
36. C. A. Coulson, B. O'Leary, R. B. Mallion, "Huckel Theory for Organic Chemists" Acad. Press, London 1978.

37. H. Sachs, *Publ. Math. (Debrecen)*, **11**, 119 (1964).
38. C. A. Coulson, *Proc. Cambridge Phil. Soc.*, **46**, 202 (1950).
39. F. Bloch, *Z. Phys.*, **52**, 555 (1929).
40. K. Ruedenberg, *J. Chem. Phys.*, **22**, 1878 (1954).
41. L. Baumer, G. Sala, G. Sello, *Tetrahedron Comput. Methodol.*, **2**, 93 (1989).
42. L. Baumer, G. Sala, G. Sello, *Tetrahedron Comput. Methodol.*, **2**, 105 (1989).
43. L. Pauling, "The Nature of the Chemical Bond" 3rd. ed., Cornell Univ. Press, Ithaca, New-York, 1960.
44. L. Baumer, G. Sala, G. Sello, *Tetrahedron Comput. Methodol.*, **2**, 37 (1989).
45. A. T. Balaban, D. Ciubotariu, O. Ivanciuc, *MATCH*, **25**, 41 (1990).
46. R. T. Sanderson, "Polar Covalence" Acad. Press, New-York, 1983.
47. M. V. Diudea, I. E. Kacsó, M. I. Topan, *Rev. Roum. Chim.* (submitting).
48. M. V. Diudea, I. Silaghi-Dumitrescu, *Rev. Roum. Chim.*, **34**, 1175 (1989).
49. I. Motoc, G. R. Marshall, *Chem. Phys. Lett.*, **116**, 415 (1985).
50. M. V. Diudea, *MATCH*, (submitted).
51. M. Randić, *Concepts and Applications of Molecular Similarity*, M. A. Johnson and G. M. Maggiora Eds., John Wiley & Sons, Inc., 1990, pp. 77-145.
52. S. C. Basak, V. R. Magnuson, G. J. Niemi, R. R. Regal, *Discr. Appl. Math.* **19**, 17 (1988).
53. I. Motoc, G. R. Marshall, J. Labanowski, *Z. Naturforsch.*, **40a**, 1121 (1985).

## REACTOR ANALYSIS FOR SOME CONSECUTIVE AND COMPETITIVE-CONSECUTIVE IRREVERSIBLE REACTIONS

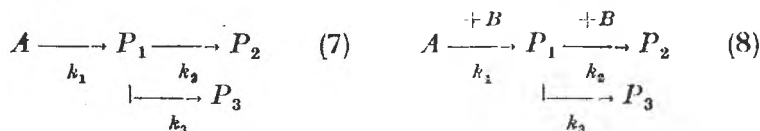
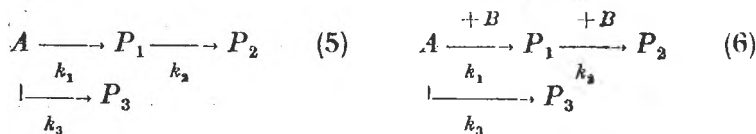
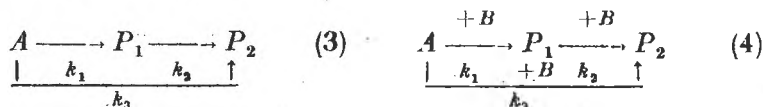
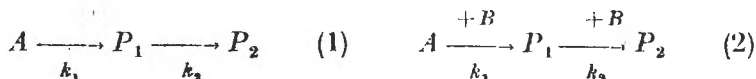
IOAN BĂLDEA and ALEXANDRA RUSTOIU-CAVDARI\*

**ABSTRACT.** Eight complex chemical systems in the class of consecutive and consecutive-competitive processes have been examined concerning the product distribution and selectivity for batch, plug-flow, stirred-tank and series of stirred-tank ideal reactor models, as well as a two-parameter model for a real stirred-tank reactor.

Known relations for relative simple system of a first order succession have been generalized for more complicated kinetic systems. Relations concentration-time (for first-order systems, analytically integrated) and concentration-concentration expression (either for first-order or second-order reactions) have been deduced for the above reactor models.

**1. Introduction.** The design of a chemical reactor is an integral part of the analysis of many industrial chemical processes. For numerous reactions of industrial importance the product distribution, yield of the valuable product and selectivity have a profound effect on the over-all process.

This work examines in detail some classes of homogenous consecutive and competitive-consecutive "elementary" reactions of the type:



These classes of reactions are frequently utilized in the chemical industry. The systems (1), (3), (5) and (7) obey a first-order kinetics, while the systems (2), (4), (6) and (8), a second-order kinetics. The results obtained could be

\* Dept. of Chemistry and Chemical Engineering, Univ. Babeș-Bolyai, Cluj-Napoca.

applied also to some heterogenous processes, following similar rate equations. Table 1 summarizes some of the important industrial reactions categorized by equations (1)–(8).

It is worth mentioning that the system characterized by second-order kinetics could become of first-order kinetics under the conditions of constant concentration of B species. It is the case of many progressive chlorination or oxidation with air of various hydrocarbons used always at concentration well below the explosion limits.

Analytical product distribution expressions namely the ratios  $C_i/C_{A0}$  and selectivity expressions have been obtained for kinetic models of the reactions (1)–(8) taking into consideration the following ideal isothermal reactor models: plug-flow (PFR) and batch reactors (BR), continuous flow stirred-tank reactor (CSTR), tanks-in-series model (CSTR's in series) and a two parameter model (CCM), with a stagnant region and a bypass, describing a non-ideal stirred vessel [1].

It is worth mentioning that a series of  $n$  equal-size stirred tank units could be used as a model for a non-ideal tubular reactor [2], where some axial mixing takes place. Parameters for these ideal combinations, accounting for deviation from ideal flow of the fluid could be determined using residence-time distribution [3]. The CSTR's series model could be used — in principle — for non-isothermal operation, different units being operated at different temperature values.

The problem of developing analytical or approximation techniques for studying complex systems that elucidate important features of the reactions and may be profitably applied to the benefit of the experimental kineticist as well as to the chemical engineers designing reactors or evaluating their performance, has been an active field for a number of years [5, 7–8, 12–14, 16–18]. Although many complex reaction systems have been discussed [3, 18, 19], part of the reactions (1)–(8) have not been treated, and no application to series-of-stirred tank, or two-parameter model has been made.

**2. Reactor Model Equations.** The expressions necessary to determine the product distribution, instantaneous or over-all fractional yield are developed below, assuming "ideal" performance and constant density. To do this, we choose system (3), and present only the final results in tables for the other ones.

*2.1. PFR and BR.* Reactions represented by equation (3) are irreversible and the differential rate expressions describing them are:

$$\frac{dC_A}{d\tau} = -k_1 C_A - k_3 C_A \quad (9)$$

$$\frac{dC_{P1}}{d\tau} = k_1 C_A - k_2 C_{P1} \quad (10)$$

$$\frac{dC_{P2}}{d\tau} = k_2 C_{P1} + k_3 C_A \quad (11)$$

where  $\tau = V/Q_V$  stands for space time or mean residence time for PFR at constant density,  $V$  — the volume of PFR and  $Q_V$  — the volumetric flow

rate respectively. Equations (9)–(11) are valid to BR, changing  $\tau$  with holding time  $t$ . These equations represent the component mass balance relations.

Many reactions taking place in the solutions or some oxidation reactions in gas phase, where a large dilution is used, satisfy these conditions. It is possible to integrate equations (9) and (10) directly [19], and the solutions in the case of initial conditions  $\tau = t = 0$ ,  $C_A = C_{A0}$ ,  $C_{P1} = C_{P2} = 0$  are:

$$\frac{C_A}{C_{A0}} = \exp [-(k_1 + k_3)\tau] = (1 - X_A) \quad (12)$$

where  $X_A$  is the fraction conversion of  $A$  species and

$$\gamma_{P1} = \frac{C_{P1}}{C_{A0}} = \frac{k_1}{k_1 + k_3 - k_2} \{ \exp(-k_2\tau) - \exp [-(k_1 + k_3)\tau] \} \quad (13)$$

the ratio  $C_{P1}/C_{A0}$  is the yield of  $P_1$  species. From the general material balance in terms of concentration

$$C_{A0} - C_A = C_{P1} + C_{P2} \quad (14)$$

the yield of  $P_2$  species could be deduced as:

$$\begin{aligned} \gamma_{P2} = \frac{C_{P2}}{C_{A0}} = 1 + \left[ \frac{k_1}{k_1 + k_3 - k_2} - 1 \right] \exp [-(k_1 + k_3)\tau] - \\ - \frac{k_1}{k_1 + k_3 - k_2} \exp(-k_2\tau) \end{aligned} \quad (15)$$

In order to obtain the concentration–concentration relationship, it is necessary to eliminate space time between equation (9) and (10) or (9) and (11). Let us first consider  $P_1$  as the valuable product. To obtain its yield as a function of  $C_A$ , we express the ratio:

$$\frac{dC_{P1}}{dC_A} = \frac{-k_1}{k_1 + k_3} + \frac{k_2}{k_1 + k_3} \frac{C_{P1}}{C_A} \quad (16)$$

Now we should mention that the same relation is obtained from the second-order sequence (4) or any other rate law, provided that the order with respect to  $A$  is first and all three processes involved present the same order with respect to  $B$  species. Thus, by dividing rate expression (18) by (17).

$$\frac{dC_A}{d\tau} = -k_1 C_A C_B - k_3 C_A C_B \quad (17)$$

$$\frac{dC_{P1}}{d\tau} = k_1 C_A C_B - k_2 C_{P1} C_B \quad (18)$$

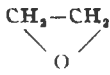
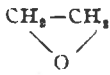
equation (16) is obtained.

To integrate (16), a new variable is needed,  $u$  as the ratio

$$u = C_{P1}/C_A \quad (19)$$

Table 1

Some reactions of industrial importance following the reaction scheme (1)–(8).

A	B	P <sub>1</sub>	P <sub>2</sub>	P <sub>3</sub>	Reference and note
H <sub>2</sub> O		Ethylene glycol $k_1 = 7.37 \times 10^{-7}$ (25°C) (dm <sup>3</sup> · mol <sup>-1</sup> · s <sup>-1</sup> ) E <sub>1</sub> = 19 Kcal/mol	Diethylene glycol $k_2/k_1 = 2.1$ E <sub>2</sub> = 19 Kcal/mol	Triethylene glycol $k_3/k_1 = 2.2$ E <sub>3</sub> = 19 kcal/mol	[10] [9] homogenous
NH <sub>3</sub>		Monoethanolamine $k_1 = 8.2 \times 10^{-3}$ (26°C) (dm <sup>3</sup> · mol <sup>-1</sup> · s <sup>-1</sup> ) E <sub>1</sub> = 14.6 Kcal/mol	Diethanolamine $k_2/k_1 = 4.13$ E <sub>2</sub> = 15.4 Kcal/mol	Triethanolamine $k_3/k_1 = 3.37$ E <sub>3</sub> = 15.4 Kcal	[6], [9], [15] homogenous
C <sub>6</sub> H <sub>6</sub>	Cl <sub>2</sub>	Monochlorobenzene $k_1 = 11.6$ (450°) (dm <sup>3</sup> mol <sup>-1</sup> min <sup>-1</sup> )	Dichlorobenzene $k_2/k_1 = 1.8$	Trichlorobenzene $k_3/k_1 = 1/240$	[4], [11] homogenous or gas-liquid process
CH <sub>4</sub>	Cl <sub>2</sub>	Methyl chloride	Dichloromethane $k_2/k_1 = 2.32$	Trichloromethane $k_3/k_1 = 1.38$	[5] homogenous
C <sub>6</sub> H <sub>5</sub> CH <sub>3</sub>	Cl <sub>2</sub>	Benzylchloride	Phenyl-dichloromethane $k_1/k_2 = 6.0$ (100°C)	Phenyl trichloromethane $k_2/k_3 = 5.7$ (100°C)	[12] gas-liquid process
C <sub>6</sub> H <sub>4</sub>	O <sub>2</sub>	1,4-Benzoquinone	Maleic anhydride	carbon dioxide	heterogenous catalysis
C <sub>10</sub> H <sub>8</sub>	O <sub>2</sub>	phthalic anhydride	carbon dioxide	—	— [20] heterogenous catalysis
C <sub>6</sub> H <sub>12</sub>	O <sub>2</sub>	Cyclohexanol	Cyclohexanone	—	heterogenous catalysis
p-xilen	O <sub>2</sub>	Terephthalic acid	Carbon dioxide	—	heterogenous catalysis
C <sub>6</sub> H <sub>6</sub>	HNO <sub>3</sub>	Nitrobenzene	Dinitrobenzene	Trinitrobenzene	heterogenous liquid-liquid

Differentiation  $du = (C_A dC_{P1} - C_{P1} dC_A)/C_A^2$  and calculation the ratio  $dC_{P1}/dC_A$  gives

$$-\frac{k_1}{k_1 + k_3} + \frac{k_3}{k_1 + k_3} u = u + \frac{du}{d \ln C_A} \quad (20)$$

Separation of variables, integration and introducing  $u$  function, yield the product  $P_1$  distribution as a function of actual relative concentration of  $A$  and value of rate constant ratios:

$$\begin{aligned} \eta_{P1} &= \frac{C_{P1}}{C_{A0}} = \frac{k_1}{k_1 + k_3 - k_2} \left[ \left( \frac{C_A}{C_{A0}} \right)^{\frac{k_3}{k_1 + k_3}} - \left( \frac{C_A}{C_{A0}} \right) \right] = \\ &= \frac{k_1}{k_1 + k_3 - k_2} [(1 - X_A)^{\frac{k_3}{k_1 + k_3}} - (1 - X_A)] \end{aligned} \quad (21a)$$

with  $C_{P10} = 0$  and  $k_2 \neq k_1 + k_3$ . The situation where  $k_2 = k_1 + k_3$ , casually encountered, leads to a different solution:

$$\frac{C_{P1}}{C_{A0}} = \frac{C_A}{C_{A0}} \ln \left( \frac{C_A}{C_{A0}} \right)^{\frac{k_1}{k_1 + k_3}} = (1 - X_A) \ln (1 - X_A)^{\frac{k_1}{k_1 + k_3}} \quad (21b)$$

Introducing equation (21a) into molal balance (14), we obtain the yield of the final product  $P_2$

$$\eta_{P2} = \frac{C_{P2}}{C_{A0}} = 1 + \left( \frac{C_A}{C_{A0}} \right) \frac{k_3 - k_2}{k_1 + k_3 - k_2} - \frac{k_1}{k_1 + k_3 - k_2} \left( \frac{C_A}{C_{A0}} \right)^{\frac{k_3}{k_1 + k_3}} \quad (22)$$

In the case of second-order system (4), the molal balance on the component B

$$C_{B0} - C_B = C_{A0} - C_A + C_{P2} = C_{P1} + C_{P2} \quad (23)$$

leads to the ratio of consumption of B relative to the initial concentration of reference species A:

$$\frac{C_{B0} - C_B}{C_{A0}} = 2 - \frac{k_1 - 2k_2 + 2k_3}{k_1 + k_3 - k_2} \left( \frac{C_A}{C_{A0}} \right) - \frac{k_1}{k_1 + k_3 - k_2} \left( \frac{C_A}{C_{A0}} \right)^{\frac{k_3}{k_1 + k_3}} \quad (24)$$

The over-all fractional yield of  $P_1$  (relative to the reacted  $A$ ) will have the form:

$$\begin{aligned} \sigma_{P1/A} &= \frac{C_{P1}}{C_{A0} - C_A} = \frac{k_1}{k_1 + k_3 - k_2} \{ \exp(-k_2 \tau) - \exp[-(k_1 + k_3) \tau] \} = \\ &= \frac{k_1}{k_1 + k_3 - k_2} \frac{(1 - X_A)^{\frac{k_3}{k_1 + k_3}} - (1 - X_A)}{X_A} \end{aligned} \quad (25)$$

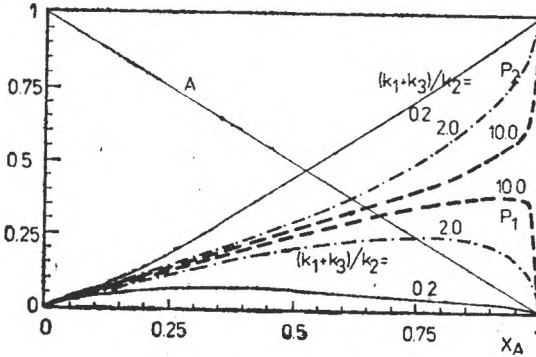


Fig. 1. Dimensionless representation of product distribution for kinetic model (3) in PFR or BR.  $(k_1 + k_3)/k_2 = 0.2; 2.0$  and  $10.0$   $k_1/k_3 = 4.0$

Figure 1 presents product distribution  $C_i/C_{A0}$  as a function of fraction conversion  $X_A$ , taking into account the ratio  $(k_1 + k_3)/k_2$  of 0.2, 2.0 and 10.0 respectively. The ratio  $k_1/k_3$  has been considered always as 4.0.

2.2. CSTR. The analytical product distribution expressions for a stirred-tank reactor are obtained from the component mass balances under the steady-state conditions, these component balances, in term of concentration are :

$$\text{Species A: } Q_1 C_{A0} = Q_V C_A + V(k_1 + k_2)C_A \quad (26)$$

$$\text{Species P}_1: 0 = Q_V C_{P1} + V(-k_1 C_A + k_2 C_{P1}) \quad (27)$$

$$\text{Species P}_2: 0 = Q_V C_{P2} + V(-k_3 C_A - k_2 C_{P1}) \quad (28)$$

They can be solved as a function of space time  $\tau = V/Q_V$  or of the remained A species concentration by elimination of the ratio  $V/Q_V$  between eqs. (27), (28) and (26). The product distribution expressions are :

$$\frac{C_A}{C_{A0}} = 1 - X_A = \frac{1}{1 + (k_1 + k_3)\tau} \quad (29)$$

$$\frac{C_{P1}}{C_{A0}} = \frac{k_1 \tau}{[1 + (k_1 + k_3)\tau](1 + k_2 \tau)} = \frac{k_1}{k_1 + k_3} \frac{X_A}{1 + \frac{k_2}{k_1 + k_3} \cdot \frac{X_A}{1 - X_A}} \quad (30)$$

$$\begin{aligned} \frac{C_{P2}}{C_{A0}} &= \frac{k_2 \tau}{1 + (k_1 + k_3)\tau} + \frac{k_1 k_2 \tau^2}{[1 + (k_1 + k_3)\tau](1 + k_2 \tau)} \\ &= X_A \left[ 1 - \frac{k_1}{k_1 + k_3} \frac{1}{1 + \frac{k_2}{k_1 + k_3} \frac{X_A}{1 - X_A}} \right] = \\ &= \frac{X_A}{k_1 + k_3} \left[ k_3 + \frac{\frac{k_1 k_2}{k_1 + k_3} \frac{X_A}{1 - X_A}}{1 + \frac{k_2}{k_1 + k_3} \frac{X_A}{1 - X_A}} \right] \end{aligned} \quad (31)$$

Instantaneous fractional yield of  $P_1$ , which is equal to over-all fractional yield in CSTR, is calculated as

$$\begin{aligned} \sigma_{P_1/A} &= \frac{C_{P_1}}{C_{A0} - C_A} = \frac{k_1}{k_1 + k_3} \cdot \frac{1}{1 + k_2\tau} = \\ &= \frac{k_1}{k_1 + k_3} \cdot \frac{1}{1 + \frac{k_2}{k_1 + k_3} \frac{X_A}{1 - X_A}} \end{aligned} \quad (32)$$

The ratio  $k_1/(k_1 + k_3)$  represents the fraction of reacted  $A$  on the consecutive processes route. Figure 2 presents the product distribution as a function of fraction conversion  $X_A$ . The same rate constant ratios were considered as for those in figure 1. By comparison with the figure 1, PF behaves better than CSTR, considering  $P_1$  as the valuable product.

When reactions (2) take place in a single stirred-tank reactor, the route to a quantitative relation describing the product distribution involves writing the design equations for species  $A$  and  $P_1$ . When  $C_{P_{10}} = 0$  that is

$$\tau = \frac{C_{A0} - C_A}{k_1 C_A C_B + k_3 C_A C_B} = \frac{-C_{P_1}}{-k_1 C_A C_B + k_1 C_{P_1} C_B} \quad (33)$$

Rearrangement gives

$$\frac{-C_{P_1}}{C_{A0} - C_A} = -\frac{k_1}{k_1 + k_3} + \frac{k_2}{k_1 + k_3} \frac{C_{P_1}}{C_A} \quad (34)$$

which is the difference equation analog of equation (16). It may be solved for  $C_{P_1}$  in terms of  $C_A$  to give

$$\frac{C_{P_1}}{C_{A0}} = \frac{k_1}{k_1 + k_3} \frac{1 - \frac{C_A}{C_{A0}}}{1 + \frac{k_2}{k_1 + k_3} \frac{C_{A0} - C_A}{C_A}} \quad (35)$$

in terms of fraction conversion the result is identical with that given by Equation (30).

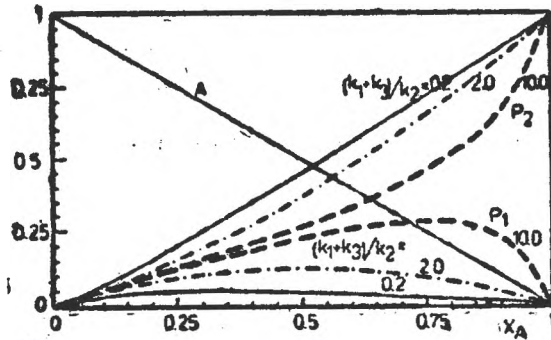


Fig. 2. Dimensionless representation of product distribution for kinetic model (3) in a CSTR taking into consideration the same rate constant ratios as in figure 1.

2.3. *CSTR's in Series.* The use of a series of stirred-tanks is always recommended as compared to a tubular reactor for systems in liquid phase because of better temperature control. The calculation is made applying successively the component balance to each of the reactor in series. Thus, for a series of  $n$  equal-size reactors these are :

$$\begin{aligned} Q_r(C_A)_{i-1} &= Q_r(C_A)_i + (k_1 + k_3)V(C_A)_i & a \\ Q_r(C_{P_1})_{i-1} &= Q_r(C_{P_1})_i - k_1V(C_A)_i + k_2V(C_{P_1})_i & b \\ Q_r(C_{P_2})_{i-1} &= Q_r(C_{P_2})_i - k_2V(C_{P_1})_i - k_3(C_A)_i & c \end{aligned} \quad (36)$$

The subscript "i" designates the order of the tank in the series.

Expressing the remaining concentration of  $A$  or product concentration at the exit of the series as compared to the initial concentration of reference species  $A$  at the entrance of the series we obtained :

$$\left(\frac{C_A}{C_{A0}}\right) = \frac{1}{[1 + (k_1 + k_3)\tau]^n} = 1 - X_A \quad (37)$$

$$\left(\frac{C_{P_1}}{C_{A0}}\right) = \frac{k_1\tau}{[1 + (k_1 + k_3)\tau]^n} \sum_{f,j} [1 + (k_1 + k_3)\tau]^f (1 + k_2\tau)^j \quad (38)$$

with  $f + j = n - 1$ ,  $f = n - 1, n - 2, \dots, 0$  and

$$j = 0, 1, \dots, n - 1.$$

The relative concentration of final product  $P_2$  can be obtained from general balance :

$$\left(\frac{C_{P_2}}{C_{A0}}\right)_n = 1 - \left(\frac{C_A}{C_{A0}}\right)_n - \left(\frac{C_{P_1}}{C_{A0}}\right)_n \quad (39)$$

The value of space time (or mean residence time at constant density) refers to each vessel in the series

$$\tau = \frac{V_{series}}{Q_0 \cdot n} = \frac{\tau_{series}}{n} \quad (40)$$

To express distribution equation as a function of  $C_A/C_{A0}$  ( $1 - X_A$ ) one can deduce from eq (37) that

$$\tau = \frac{1}{k_1 + k_3} \cdot \frac{1 - \left(\frac{C_A}{C_{A0}}\right)^{1/n}}{\left(\frac{C_A}{C_{A0}}\right)^{1/n}} = \frac{1}{k_1 + k_3} \cdot \frac{1 - (1 - X_A)^{1/n}}{(1 - X_A)^{1/n}} \quad (41)$$

and hence,  $k_1\tau$ ,  $(k_1 + k_2)\tau$  and  $k_2\tau$  may be replaced in the above equations. For intermediate product  $P_1$  the result is:

$$\left(\frac{C_{P_1}}{C_{A0}}\right)_n = \frac{k_1}{k_1 + k_2} \cdot \frac{\left(\frac{1}{1 - X_A}\right)^{1/n} - 1}{\frac{1}{1 - X_A} \left\{ 1 + \frac{k_2}{k_1 + k_2} \left[ \left(\frac{1}{1 - X_A}\right)^{1/n} - 1 \right] \right\}^n} \quad (42)$$

$$\times \sum_{f,j} \left(\frac{1}{1 - X_A}\right)^{f/n} \left\{ 1 + \frac{k_2}{k_1 + k_2} \left[ \left(\frac{1}{1 - X_A}\right)^{1/n} - 1 \right] \right\}^j$$

the sum should be performed taking  $f + j = n - 1$ , and  $f$  between  $n - 1$  and zero. The fractional yield at the exit of the series, as a function of the individual space time is:

$$C_{P_1/A} = \left(\frac{C_{P_1}}{C_{A0} - C_A}\right)_n = \quad (43)$$

$$= \frac{k_1\tau}{\{[1 + (k_1 + k_2)\tau]^n - 1\} (k_1 + k_2\tau)^n} \cdot \sum_{f,j} [1 + (k_1 + k_2)\tau]^f (1 + k_2\tau)^j$$

and

$$\sigma_{P_1/A} = \frac{k_1}{k_1 + k_2} \times \frac{\left(\frac{1}{1 - X_A}\right)^{1/n} - 1}{\frac{X_A}{1 - X_A} \left\{ 1 + \frac{k_2}{k_1 + k_2} \left[ \left(\frac{1}{1 - X_A}\right)^{1/n} - 1 \right] \right\}^n} \times \quad (44)$$

$$\times \sum_{f,j} \left(\frac{1}{1 - X_A}\right)^{f/n} \left\{ 1 + \frac{k_2}{k_1 + k_2} \left[ \left(\frac{1}{1 - X_A}\right)^{1/n} - 1 \right] \right\}^j$$

as a fraction conversion of reference component  $A$ .

Figure 3 presents the product distribution obtained in a series of 2, 5 and 10 tanks, taking the same rate constant ratio as for the previous figures. Inspection of figures 2 and 3 reveals that the greatest change occurs by addition of second tank. The performance improvement is not so important when a CSTR's in series of 10 tanks is used, compared to a CSTR's in series with  $n = 5$ . When reactions (2) take place in a series of stirred-tanks, design equation of the type (33) should be solved successively, for each tank in the series to obtain  $C_{P_1}/C_{A0}$ ,  $C_{P_2}/C_{A0}$ .

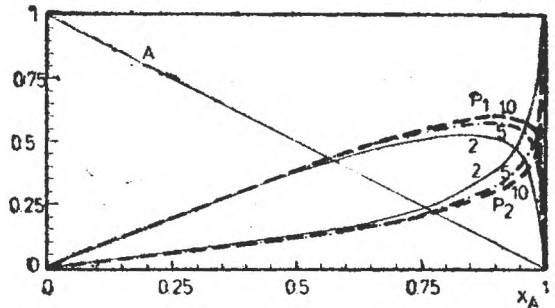


Fig. 3. Product distribution  $C_i/C_{A0}$  as a function of fraction conversion  $X_A$  in a CSTR's in series for  $n = 2, 5$  and  $10$  tanks.  $(k_1 + k_2)/k_2 = 10.0$   $k_1/k_2 = 4.0$

2.4. *Two-parameter model (CCM)* The real stirred-tank has not a perfect mixing. This deviation from ideal flow conditions could be described by a modified ideal model consisting of a volume fraction  $\alpha V$  ideally mixed and a stagnant volume, as well as a fraction of volumetric flow rate  $(1 - \beta)Q_V$  bypassing the reactor. This model was first proposed by Cholette and Cloutier [1]. Under these conditions, the fraction conversion is zero in the bypass and the stagnant region of the fluid in the reactor is inactive for the reaction. Therefore, the maximum fraction conversion  $X_A$  cannot exceed the value of fraction perfectly mixed of entering flow ( $\beta$ ) even if small flow rate (very large mean residence time) is used.

Taking into consideration the material balance of component  $A$  for the fraction of perfectly mixed volume, designated by the subscript " $pm$ ", the following is true:

$$Q_V C_A = (1 - \beta)Q_V C_{A0} + \beta Q_V (C_A)_{pm} \quad (45)$$

The first term in the right side of equation (45) represents the bypass contribution with no reaction, and the second, the contribution of the perfectly mixed region of the total volume of the reactor, where the reaction has taken place.

Division by  $Q_V C_{A0}$  leads to

$$\frac{C_A}{C_{A0}} = (1 - \beta) + \beta \left( \frac{C_A}{C_{A0}} \right)_{pm}; \quad 1 - X_A = (1 - \beta) + \beta(1 - X_A)_{pm} \quad (46)$$

The space time (or mean residence time for constant density) for the perfectly mixed region could be defined as

$$\tau_{pm} = \frac{V_{pm}}{Q_{pm}} = \frac{\alpha V}{\beta Q_V} = \frac{\alpha}{\beta} \tau \quad (47)$$

Following the same procedure as in the case of CSTR, for determining  $(1 - X_A)_{pm}$ , the remained fraction of reference reactant  $A$  at the exit of CCM is:

$$\frac{C_A}{C_{A0}} = 1 - X_A = 1 - \beta + \frac{\beta}{1 + (k_1 + k_2) \frac{\alpha}{\beta} \tau} \quad (48)$$

The ratios  $\left( \frac{C_{P_1}}{C_{A0}} \right)_{pm}$  and  $\left( \frac{C_{P_2}}{C_{A0}} \right)_{pm}$  can be obtained in the same way applied to CSTR. The component balance for  $P_1$  and  $P_2$  required that:

$$\frac{C_{P_1}}{C_{A0}} = \beta \left( \frac{C_{P_1}}{C_{A0}} \right)_{pm}; \quad \frac{C_{P_2}}{C_{A0}} = \beta \left( \frac{C_{P_2}}{C_{A0}} \right)_{pm} \quad (49)$$

The resulting equations for the two successive products are:

$$\begin{aligned} \frac{C_{P_1}}{C_{A0}} &= \frac{k_1 \alpha \tau}{\left[1 + (k_1 + k_3) \frac{\alpha}{\beta} \tau\right] \left(1 + k_2 \frac{\alpha}{\beta} \tau\right)} \\ &= \frac{k_1}{k_1 + k_3} \frac{X_A}{1 + \frac{k_2}{k_1 + k_3} \frac{X_A}{\beta - X_A}} \end{aligned} \quad (50)$$

$$\frac{C_{P_2}}{C_{A0}} = \frac{k_3 \alpha \tau}{1 + (k_1 + k_3) \frac{\alpha}{\beta} \tau} + \frac{k_1 k_3 \frac{\alpha^2}{\beta} \tau^2}{\left[1 + (k_1 + k_3) \frac{\alpha}{\beta} \tau\right] \left(1 + k_2 \frac{\alpha}{\beta} \tau\right)} \quad (51)$$

The first term in eq. (51) accounts for the parallel route of depletion of  $A$ , and the second term the fraction produced by the consecutive route.

An equivalent distribution equation results from the overall material balance (14):

$$\begin{aligned} \frac{C_{P_2}}{C_{A0}} &= \frac{X_A}{k_1 + k_3} \left[ k_3 + \frac{\frac{k_1 k_2}{(k_1 + k_3)} \frac{X_A}{\beta - X_A}}{1 + \frac{k_2}{k_1 + k_3} \frac{X_A}{\beta - X_A}} \right] \\ &= X_A \left[ 1 - \frac{k_1}{k_1 + k_3} \frac{X_A}{1 + \frac{k_2}{k_1 + k_3} \frac{X_A}{\beta - X_A}} \right] \end{aligned} \quad (52)$$

The fractional yield of  $P_1$ , frequently named selectivity, is:

$$\begin{aligned} \sigma_{P_1/A} &= \frac{C_{P_1}}{C_{A0} - C_A} = \frac{k_1}{k_1 + k_3} \frac{1}{1 + k_2 \frac{\alpha}{\beta} \tau} \\ &= \frac{k_1}{k_1 + k_3} \frac{1}{1 + \frac{k_2}{k_1 + k_3} \frac{X_A}{\beta - X_A}} \end{aligned} \quad (53)$$

depending only on  $\beta$  parameter of the model when expressed as a function of  $X_A$ .

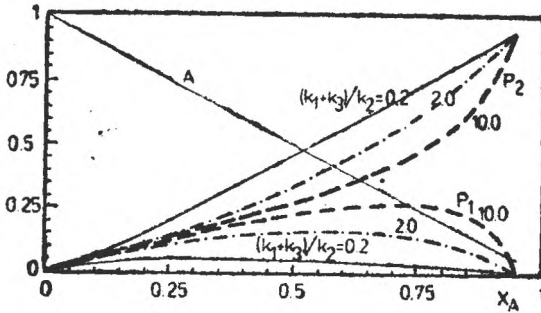


Fig. 4. Dimensionless representation of product distribution for kinetic model (3) in a real stirred vessel (Cholette-Cloutier model) with  $\beta = 0.95$  and  $(k_1 + k_3)/k_2 = 0.2; 2.0$  and  $10.0$   $k_1/k_3 = 4.0$

Figures 4 and 5 present the product distribution at three  $(k_1 + k_3)/k_2$  ratios and the same  $\beta$ , and for one rate constants ratio and 3 values of  $\beta$ , respectively.

Following a similar procedure with the other systems described by the reaction scheme (1)–(8) it is possible to obtain analytically the product distribution as a function of holding time  $t$ , space time  $\tau$  for all the reaction sequence following first-order rate laws, and as a function of concentration (or fraction conversion  $X$ ) for all the systems following either first-order or second-order kinetics. The results are presented in Tables 2, 3 and 4.

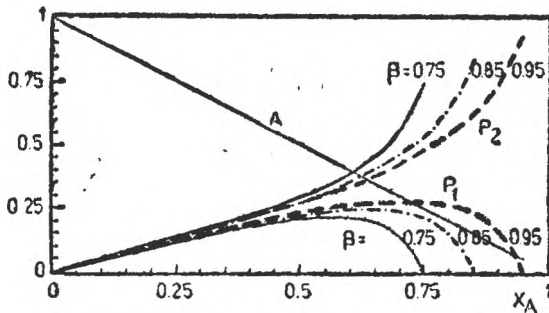


Fig. 5. Dimensionless representation of product distribution for kinetic model (3) in a real stirred vessel (Cholette-Cloutier model) for  $(k_1 + k_3)/k_2 = 10.0$   $k_1/k_3 = 4.0$  and  $\beta = 0.75, 0.85$  and  $0.95$ .

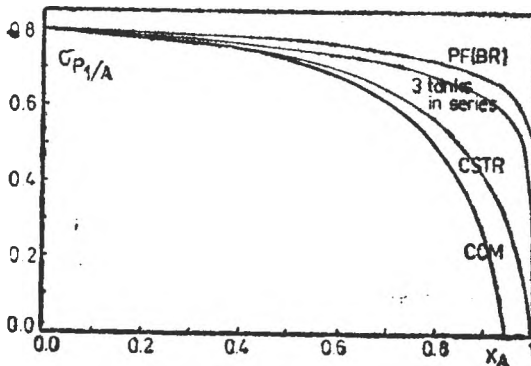


Fig. 6. Fractional yield of intermediate product  $P_1$  as a function of fraction conversion  $X_{11}$  for PFR (BR), CSTR, CSTR's in series and Cholette-Cloutier models.

The selectivity of the intermediate product  $P_1$  depends on the relative values of rate constants. For an easy comparison, figure 6 present selectivity (or fractional yield)  $\sigma_{P_1/A}$  for all the reactor models discussed, as a function of fraction conversion  $X_A$ , and the ratio  $(k_1 + k_3)/k_2 = 10.0$  and  $\beta = 0.95$  (for CCM).

Table 2

**Product distribution and selectivity equations for system (1) in CSTR's in series and two-parameter model (CCM)**

I. CSTR's in series

$$\begin{aligned} \left(\frac{C_A}{C_{A0}}\right)_n &= \frac{1}{(1 + k_1\tau)^n} = 1 - X_A \\ \left(\frac{C_{P_1}}{C_{A0}}\right)_n^* &= \frac{k_1\tau \sum_{f,j} (1 + k_1\tau)^f (1 + k_2\tau)^j}{(1 + k_1\tau)^n (1 + k_2\tau)^n} = \\ &= \frac{\left[\left(\frac{1}{1 - X_A}\right)^{1/n} - 1\right] \sum_{f,j} \left(\frac{1}{1 - X_A}\right)^{f/n} \left\{1 + \frac{k_2}{k_1} \left[\left(\frac{1}{1 - X_A}\right)^{1/n} - 1\right]\right\}^j}{\frac{1}{1 - X_A} \left\{1 + \frac{k_2}{k_1} \left[\left(\frac{1}{1 - X_A}\right)^{1/n} - 1\right]\right\}^n} \\ \left(\frac{C_{P_2}}{C_{A0}}\right)_n^* &= k_1 k_2 \tau^2 \sum_{i=1}^n \frac{\sum_{f,j} (1 + k_1\tau)^f (1 + k_2\tau)^j}{(1 + k_1\tau)^f (1 + k_2\tau)^j} = \\ &= 1 - \frac{1}{(1 + k_1\tau)^n} - \frac{k_1\tau \sum_{f,j} (1 + k_1\tau)^f (1 + k_2\tau)^j}{(1 + k_1\tau)^n (1 + k_2\tau)^n} = \\ &= X_A - \frac{\left[\left(\frac{1}{1 - X_A}\right)^{1/n} - 1\right] \sum_{f,j} \left(\frac{1}{1 - X_A}\right)^{f/n} \left\{1 + \frac{k_2}{k_1} \left[\left(\frac{1}{1 - X_A}\right)^{1/n} - 1\right]\right\}^j}{\frac{1}{1 - X_A} \left\{1 + \frac{k_2}{k_1} \left[\left(\frac{1}{1 - X_A}\right)^{1/n} - 1\right]\right\}^n} \\ \sigma_{P_1/A} &= \frac{k_1\tau \sum_{f,j} (1 + k_1\tau)^f (1 + k_2\tau)^j}{[1 + k_1\tau]^n - 1} (1 + k_2\tau)^n = \\ &= \frac{\left[\left(\frac{1}{1 - X_A}\right)^{1/n} - 1\right] \sum_{f,j} \left(\frac{1}{1 - X_A}\right)^{f/n} \left\{1 + \frac{k_2}{k_1} \left[\left(\frac{1}{1 - X_A}\right)^{1/n} - 1\right]\right\}^j}{\frac{X_A}{1 - X_A} \left\{1 + \frac{k_2}{k_1} \left[\left(\frac{1}{1 - X_A}\right)^{1/n} - 1\right]\right\}^n} \end{aligned}$$

where  $f + j = n - 1$  and  $f \in [n - 1, 0]$

\* To obtain product distribution design equation of the type (36) should be applied step by step when system (2) takes place in a CSTR's in series.

Table 2 (continued)

## II. CCM

$$\frac{C_A}{C_{AO}} = 1 - \beta \left( 1 - \frac{1}{1 + k_1 \tau \frac{\alpha}{\beta}} \right) = 1 - X_A$$

$$\frac{C_{P_1}^{**}}{C_{AO}} = \frac{k_1 \tau \alpha}{\left( 1 + k_1 \tau \frac{\alpha}{\beta} \right) \left( 1 + k_2 \tau \frac{\alpha}{\beta} \right)} = \frac{X_A}{1 + \frac{k_2}{k_1} \frac{X_A}{\beta - X_A}}$$

$$\frac{C_{P_2}^{**}}{C_{AO}} = \frac{k_1 k_2 \tau^2 \alpha^2}{\beta \left( 1 + k_1 \tau \frac{\alpha}{\beta} \right) \left( 1 + k_2 \tau \frac{\alpha}{\beta} \right)} = X_A \left( 1 - \frac{1}{1 + \frac{k_2}{k_1} \frac{X_A}{\beta - X_A}} \right)$$

$$\sigma_{P_1/A}^* = \frac{1}{1 + k_2 \tau \frac{\alpha}{\beta}} = \frac{1}{1 + \frac{k_2}{k_1} \frac{X_A}{\beta - X_A}}$$

\*\* The relation concentration-concentration is valid for the second-order system 2

Table 3

**Product distribution and selectivity for reactions (5) and (6)\* in BR, PF, CSTR, CSTR's in series and CCM.**

I. BR and PF ( $t = \tau$ )

$$\frac{C_A}{C_{AO}} = \exp [-(k_1 + k_2) \cdot t] = 1 - X_A$$

$$\frac{C_{P_1}}{C_{AO}} = \frac{k_1}{k_1 + k_2 - k_3} \cdot \{ \exp [-(k_2 \cdot t)] - \exp [-(k_1 + k_2) \cdot t] \} =$$

$$= \frac{k_1}{k_1 + k_2 - k_3} \cdot \left[ (1 - X_A)^{\frac{k_2}{k_1 + k_2}} - (1 - X_A) \right]$$

$$\frac{C_{P_2}}{C_{AO}} = \frac{k_1}{k_1 + k_2 - k_3} \left\{ (1 - e^{k_2 \tau}) - \frac{k_2}{k_1 + k_2} \left[ 1 - e^{-(k_1 + k_2) \tau} \right] \right\} =$$

$$= \frac{k_1}{k_1 + k_2 - k_3} \left\{ \left[ 1 - (1 - X_A)^{\frac{k_2}{k_1 + k_2}} \right] - \frac{k_2}{k_1 + k_2} X_A \right\}$$

$$\sigma_{P_1/A} = \frac{C_{P_1}/C_{AO}}{1 - e^{-(k_1 + k_2) \tau}} =$$

\* Equations concentration-concentration are valid in the case of second-order system (6), except for CSTR's in series where design equation of the type (36) should be applied step by step to successive tanks in the series.

Table 3 (continued)

$$\begin{aligned}
 &= \frac{k_1}{(k_1 + k_3 - k_2)[1 - e^{-(k_1 + k_3)\tau}]} [e^{-k_2\tau} - e^{-(k_1 + k_3)\tau}] \\
 &= \frac{k_1}{(k_1 + k_3 - k_2)X_A} \left[ (1 - X_A)^{\frac{k_2}{k_1 + k_3}} - (1 - X_A) \right] \\
 \frac{C_{P_2}}{C_{A0}} &= \frac{k_2}{k_1 + k_3} \cdot \{1 - \exp[-(k_1 + k_3) \cdot t]\} = \frac{k_2}{k_1 + k_3} \cdot X_A
 \end{aligned}$$

## II. CSTR

$$\begin{aligned}
 \frac{C_A}{C_{A0}} &= \frac{1}{1 + (k_1 + k_3)\tau} = 1 - X_A \\
 \frac{C_{P_1}}{C_{A0}} &= \frac{k_1\tau}{[1 + (k_1 + k_3)\tau] \cdot (1 + k_2\tau)} = \frac{k_1}{k_1 + k_3} \cdot \frac{X_A}{1 + \frac{k_2}{k_1 + k_3} \cdot \frac{X_A}{1 - X_A}} \\
 \frac{C_{P_2}}{C_{A0}} &= \frac{k_1 k_2 \tau^2}{[1 + (k_1 + k_3)\tau] \cdot (1 + k_2\tau)} = \frac{X_A}{k_1 + k_3} \cdot \frac{\frac{k_1 k_2}{k_1 + k_3} \cdot \frac{X_A}{1 - X_A}}{1 + \frac{k_2}{k_1 + k_3} \cdot \frac{X_A}{1 - X_A}} \\
 \frac{C_{P_3}}{C_A^0} &= \frac{k_3\tau}{1 + (k_1 + k_3)\tau} = \frac{k_3}{k_1 + k_3} \cdot X_A \\
 \sigma_{P_1/A} &= \frac{k_1}{k_1 + k_3} \cdot \frac{1}{1 + \frac{k_2}{k_1 + k_3} \cdot \frac{X_A}{1 - X_A}} \\
 \sigma_{P_2/A} &= \frac{k_2}{k_1 + k_3}
 \end{aligned}$$

## III. CSTR's in series

$$\begin{aligned}
 \left( \frac{C_A}{C_{A0}} \right)_n &= \frac{1}{[1 + (k_1 + k_3)\tau]^n} = 1 - X_A \\
 \left( \frac{C_{P_1}}{C_{A0}} \right)_n &= \frac{k_1\tau \cdot \sum_{f,j} [1 + (k_1 + k_3)\tau]^f \cdot (1 + k_2\tau)^j}{[1 + (k_1 + k_3)\tau]^n \cdot (1 + k_2\tau)^n} \\
 &= \frac{\frac{k_1}{k_1 + k_3} \left[ \left( \frac{1}{1 - X_A} \right)^{1/n} - 1 \right] \sum_{f,j} \left( \frac{1}{1 - X_A} \right)^{f/n} \left\{ 1 + \frac{k_2}{k_1 + k_3} \left[ \left( \frac{1}{1 - X_A} \right)^{1/n} - 1 \right] \right\}^j}{\left( \frac{1}{1 - X_A} \right) \left[ 1 + \frac{k_2}{k_1 + k_3} \left( \frac{1}{1 - X_A} \right)^{1/n} - 1 \right]^n}
 \end{aligned}$$

Table 3 (continued)

$$\begin{aligned} \sigma_{P_i/A} &= \frac{k_1 \tau \sum_{f,j} [1 + (k_1 + k_2)\tau]^f (1 + k_2\tau)^j}{\{[1 + (k_1 + k_2)\tau]^n - 1\} (1 + k_2\tau)^n} = \\ &= \frac{\frac{k_1}{k_1 + k_2} \left[ \left( \frac{1}{1 - X_A} \right)^{1/n} - 1 \right] \sum_{f,j} \left( \frac{1}{1 - X_A} \right)^{f/n} \left\{ 1 + \frac{k_2}{k_1 + k_2} \left[ \left( \frac{1}{1 - X_A} \right)^{1/n} - 1 \right] \right\}^j}{\frac{X_A}{1 - X_A} \left\{ 1 + \frac{k_2}{k_1 + k_2} \left( \frac{1}{1 - X_A} \right)^{1/n} - 1 \right\}^n} \\ \left( \frac{C_{P_i}}{C_{AO}} \right)_n &= k_1 k_2 \tau^2 \cdot \sum_l \frac{\sum_{f,j} [1 + (k_1 + k_2)\tau]^f \cdot (1 + k_2\tau^2)^j}{[1 + (k_1 + k_2)\tau]^l \cdot (1 + k_2\tau)^l} = \\ &= \frac{k_1 k_2}{(k_1 + k_2)^2} \cdot \left[ \left( \frac{1}{1 - X_A} \right)^{1/n} - 1 \right]^2 \cdot \sum_l \frac{\sum_{f,i} \left( \frac{1}{1 - X_A} \right)^{f/n} \cdot \left\{ 1 + \frac{k_2}{k_1 + k_2} \cdot \left[ \left( \frac{1}{1 - X_A} \right)^{1/n} - 1 \right] \right\}^i}{\left( \frac{1}{1 - X_A} \right)^{l/n} \cdot \left\{ 1 + \frac{k_2}{k_1 + k_2} \cdot \left[ \left( \frac{1}{1 - X_A} \right)^{1/n} - 1 \right] \right\}^l} \\ \left( \frac{C_{P_i}}{C_{AO}} \right)_n &= k_2 \tau \cdot \sum_{l=1}^n \frac{1}{[1 + (k_1 + k_2)\tau]^l} = \frac{k_2}{k_1 + k_2} \cdot \left[ \left( \frac{1}{1 - X_A} \right)^{1/n} - 1 \right] \sum_{l=1}^n (1 - X_A)^{l/n} \\ \sigma_{P_i,A} &= \frac{k_2 \tau}{[1 + (k_1 + k_2)\tau]^{1/n} - 1} \sum_{l=1}^n \frac{1}{[1 + (k_1 + k_2)\tau]^{l/n}} \end{aligned}$$

V. Cholette-Cloutier Model (CCM)

$$\begin{aligned} \frac{C_A}{C_{AO}} &= 1 - \beta \cdot \left[ \frac{1}{1 + (k_1 + k_2)\tau \frac{\alpha}{\beta}} \right] = 1 - X_A \\ \frac{C_{P_i}}{C_{AO}} &= \frac{k_1 \tau \alpha}{\left[ 1 + (k_1 + k_2)\tau \frac{\alpha}{\beta} \right] \cdot \left( 1 + k_2 \tau \frac{\alpha}{\beta} \right)} = \frac{k_1}{k_1 + k_2} \cdot \frac{X_A}{1 + \frac{k_2}{k_1 + k_2} \cdot \frac{X_A}{\beta - X_A}} \\ \frac{C_{P_i}}{C_{AO}} &= \frac{k_1 k_2 \tau^2 \alpha^2}{\beta \cdot \left[ 1 + (k_1 + k_2)\tau \frac{\alpha}{\beta} \right] \cdot \left[ 1 + k_2 \tau \frac{\alpha}{\beta} \right]} = \frac{X_A}{k_1 + k_2} \cdot \frac{\frac{k_1 k_2}{k_1 + k_2} \cdot \frac{X_A}{\beta - X_A}}{1 + \frac{k_2}{k_1 + k_2} \cdot \frac{X_A}{\beta - X_A}} \\ \frac{C_{P_i}}{C_{AO}} &= \frac{k_2 \tau \alpha}{1 + (k_1 + k_2)\tau \frac{\alpha}{\beta}} = \frac{k_2}{k_1 + k_2} \cdot X_A \end{aligned}$$

Table 3 (continued)

$$\sigma_{P_i/A} = \frac{k_1}{k_1 + k_2} \frac{1}{1 + k_2 \frac{\alpha}{\beta} \tau} \cdot \frac{k_1}{k_1 + k_3} \frac{1}{1 + \frac{k_3}{k_1 + k_3} \frac{X_A}{\beta - X_A}}$$

$$\sigma_{P_n/A} = \frac{k_n}{k_1 + k_3}$$

Note:  $l \in [1, n]$ ,  $f + j = n - l$ ,  $f \in [n - 1, 0]$

Table 4

Product distribution and selectivity equations for system (7) and (8)\* in BR, PF, CSTR, CSTR's in series and CCM.

I. BR and PF

$$\frac{C_A}{C_{A0}} = \exp [-(k_1 t)] = 1 - X_A$$

$$\frac{C_{P_1}}{C_{A0}} = \frac{k_1}{k_2 + k_3 - k_1} \cdot \{ \exp [-(k_1 \tau)] - \exp [-(k_2 + k_3) \tau] \}$$

$$= \frac{k_1}{k_1 - (k_2 + k_3)} \cdot \left[ (1 - X_A) \frac{k_2 + k_3}{k_1} - (1 - X_A) \right]$$

$$\frac{C_{P_2}}{C_{A0}} = \frac{k_2}{k_2 + k_3} \left[ 1 + \frac{k_2 + k_3}{k_1 - (k_2 + k_3)} e^{-k_1 \tau} - \frac{k_1}{k_1 - (k_2 + k_3)} e^{-(k_2 + k_3) \tau} \right]$$

$$= \frac{k_2}{k_2 + k_3} \left[ 1 + \frac{k_2 + k_3}{k_1 - (k_2 + k_3)} (1 - X_A) \frac{k_2 + k_3}{k_1} - \frac{k_1}{k_1 - (k_2 + k_3)} (1 - X_A) \right]$$

$$\frac{C_{P_2}}{C_{A0}} = \frac{k_2}{k_3} \cdot \frac{C_{P_1}}{C_{A0}}$$

$$\sigma_{P_1/A} = \frac{k_1}{k_1 - (k_2 + k_3)} \cdot \frac{e^{-(k_2 + k_3) \tau} - e^{-k_1 \tau}}{1 - e^{-k_1 \tau}}$$

$$= \frac{k_1}{X_A [k_1 - (k_2 + k_3)]} \left[ (1 - X_A) \frac{k_2 + k_3}{k_1} - (1 - X_A) \right]$$

\* Equations concentration-concentration are valid in the case of second-order system (8), except for CSTR's in series where design equation of type (30) should be applied step by step to successive tanks in the series.

Table 4 (continued)

## II. CSTR

$$\frac{C_A}{C_{A0}} = \frac{1}{1 + k_1\tau} = 1 - X_A$$

$$\frac{C_{P_1}}{C_{A0}} = \frac{k_1\tau}{(1 + k_1\tau) \cdot [1 + (k_2 + k_3)\tau]} = \frac{X_A}{1 + \frac{k_2 + k_3}{k_1} \cdot \frac{X_A}{1 - X_A}}$$

$$\frac{C_{P_2}}{C_{A0}} = \frac{k_1 k_2 \tau^2}{(1 + k_1\tau) \cdot [1 + (k_2 + k_3)\tau]} = X_A \frac{k_2}{k_1} \frac{\frac{X_A}{1 - X_A}}{1 + \frac{k_2 + k_3}{k_1} \cdot \frac{X_A}{1 - X_A}}$$

$$\frac{C_{P_3}}{C_{A0}} = \frac{k_2}{k_1} \cdot \frac{C_{P_2}}{C_{A0}} = \frac{k_1 k_3 \tau^2}{(1 + k_1\tau) [1 + (k_1 + k_3)\tau]} = X_A \frac{k_3}{k_1} \frac{\frac{X_A}{1 - X_A}}{1 + \frac{k_2 + k_3}{k_1} \cdot \frac{X_A}{1 - X_A}}$$

$$\sigma_{P_1/A} = \frac{1}{1 + (k_2 + k_3)\tau} = \frac{1}{1 + \frac{k_2 + k_3}{k_1} \cdot \frac{X_A}{1 - X_A}}$$

## III. CSTR's in series.

$$\left(\frac{C_A}{C_{A0}}\right)_n = \frac{1}{(1 + k_1\tau)^n} = 1 - X_A$$

$$\left(\frac{C_{P_1}}{C_{A0}}\right)_n = \frac{k_1\tau \cdot \sum_{f,j} (1 + k_1\tau)^f \cdot [1 + (k_2 + k_3)\tau]^j}{(1 + k_1\tau)^n \cdot [1 + (k_2 + k_3)\tau]^n} =$$

$$= \left[ \frac{1}{(1 - X_A)^{1/n}} - 1 \right] \cdot \frac{\sum_{f,j} \left[ \frac{1}{(1 - X_A)} \right]^{f/n} \cdot \left\{ 1 + \frac{k_2 + k_3}{k_1} \cdot \left[ \frac{1}{(1 - X_A)^{1/n}} - 1 \right] \right\}^j}{\frac{1}{1 - X_A} \cdot \left\{ 1 + \frac{k_2 + k_3}{k_1} \cdot \left[ \frac{1}{(1 - X_A)^{1/n}} - 1 \right] \right\}^n}$$

$$\sigma_{P_1/A} = \frac{k_1\tau \cdot \sum_{f,j} (1 + k_1\tau)^f [1 + (k_2 + k_3)\tau]^j}{[(1 + k_1\tau)^n - 1] [1 + (k_2 + k_3)\tau]^n} =$$

$$= \frac{\left[ \left( \frac{1}{1 - X_A} \right)^{1/n} - 1 \right] \sum_{f,j} \left( \frac{1}{1 - X_A} \right)^{f/n} \left\{ 1 + \frac{k_2 + k_3}{k_1} \left[ \left( \frac{1}{1 - X_A} \right)^{1/n} - 1 \right] \right\}^j}{\frac{X_A}{1 - X_A} \left\{ 1 + \frac{k_2 + k_3}{k_1} \left[ \left( \frac{1}{1 - X_A} \right)^{1/n} - 1 \right] \right\}^n}$$

Table 4-(continued)

$$\left(\frac{C_{P_i}}{C_{AO}}\right)_n = k_1 k_2 \tau^2 \sum_{j=1}^n \frac{\sum (1 + k_1 \tau)^f [1 + (k_2 + k_3) \tau]^j}{f \cdot j [(1 + k_1 \tau)^f - 1] [1 + (k_2 + k_3) \tau]^j}$$

$$= \frac{\frac{k_2}{k_1} \left[ \left( \frac{1}{1 - X_A} \right)^{1/n} - 1 \right]^2 \sum_{f,j} \left( \frac{1}{1 - X_A} \right)^{f/n} \left\{ 1 + \frac{k_2 + k_3}{k_1} \left[ \left( \frac{1}{1 - X_A} \right)^{1/n} - 1 \right]^j \right\}}{\frac{1}{1 - X_A} \left\{ 1 + \frac{k_2 + k_3}{k_1} \left[ \left( \frac{1}{1 - X_A} \right)^{1/n} - 1 \right]^n \right\}}$$

$$\left(\frac{C_{P_3}}{C_{AO}}\right)_n = \frac{k_3}{k_2} \cdot \left(\frac{C_{P_2}}{C_{AO}}\right)_n$$

IV. CCM

$$\frac{C_A}{C_{AO}} = 1 - \beta \cdot \left[ 1 - \frac{1}{1 + k_1 \tau \frac{\alpha}{\beta}} \right] = 1 - X_A$$

$$\frac{C_{P_1}}{C_{AO}} = \frac{k_1 \tau \alpha}{\left( 1 + k_1 \tau \frac{\alpha}{\beta} \right) \cdot \left[ 1 + (k_2 + k_3) \tau \frac{\alpha}{\beta} \right]} = \frac{X_A}{1 + \frac{k_2 + k_3}{k_1} \cdot \frac{X_A}{\beta - X_A}}$$

$$\frac{C_{P_3}}{C_{AO}} = \frac{k_1 k_2 \tau^2 \alpha^2}{\beta \left( 1 + k_1 \tau \frac{\alpha}{\beta} \right) \left[ 1 + (k_2 + k_3) \tau \frac{\alpha}{\beta} \right]} = \frac{X_A}{k_1} \frac{\frac{k_2}{\beta} \frac{X_A}{\beta - X_A}}{1 + \frac{k_2 + k_3}{k_1} \frac{X_A}{\beta - X_A}}$$

$$\frac{C_{P_2}}{C_{AO}} = \frac{k_1 k_3 \tau^2 \alpha^2}{\beta \left( 1 + k_1 \tau \frac{\alpha}{\beta} \right) \left[ 1 + (k_2 + k_3) \tau \frac{\alpha}{\beta} \right]} = \frac{X_A}{k_1} \frac{\frac{k_3}{\beta} \frac{X_A}{\beta - X_A}}{1 + \frac{k_2 + k_3}{k_1} \frac{X_A}{\beta - X_A}}$$

$$\sigma_{P_1/A} = \frac{1}{1 + (k_2 + k_3) \tau \frac{\alpha}{\beta}} = \frac{1}{1 + \frac{k_2 + k_3}{k_1} \frac{X_A}{\beta - X_A}}$$

**3. Conclusions.** When the product distribution and the total capacity are known, the size of the reactor can be determined and optimized with respect to the total process design or operation. The reactor type is generally selected on the basis of product distribution and/or selectivity for desired product.

Note:  $l \in [1, n]$ ,  $f + j = n - 1$ ,  $f \in [n - 1, 0]$

The equation describing the product distribution and selectivity deduced in this paper for the classes of complex reactions largely encountered in the industry, and for the reactor type and combinations discussed, could be easily used to appreciate these amounts, even if the calculus is made for constant temperature, which holds for CSTR and CSTR's in series. As we have already mentioned in the particular case of CSTR's in series, a temperature programme could be taken into consideration and the result would describe the behaviour of a real tubular reactor operated under nonisothermal conditions.

Diagrams of the type presented in the figures could be easily drawn by means of a simple computer programme at various ratios of rate constants, and conclusion regarding product distribution could be obtained, helping the designer in his choice of the reactor type to be used.

A simple inspection of the figures presented reveals that the PF reactor is always superior to CSTR from the product distribution viewpoint. Less unreacted A should be removed from the final mixture at a given fraction conversion. It follows CSTR's in series, having a reasonable number of tanks. On the other hand, a comparison of experimental product distribution with theoretical values using these models, when kinetics is known, leads to the conclusion regarding nonideality of the flow.

With laboratory reactors, the experimental product distribution compared to that calculated by corresponding equation deduced here will facilitate the determination of rate constant ratios, a very useful tool for a kineticist.

#### REFERENCES

1. A. Cholette, L. Cloutier, *J. Can. Chem. Eng.*, **37**, 105 (1959); A. Cholette, J. Blanchet, L. Cloutier, *J. Can. Chem. Eng.*, **38**, 1 (1960).
2. B. A. Buffham, L. G. Gibilars, *AIChEJ*, **14**, 805 (1968).
3. O. Levenspiel, *Chemical Reaction Engineering* 2nd. Ed. J. Wiley, New York 1972, Cap. 9; R. Mihail, O. Muntean, „*Reactoare chimice*”, EDP, București, 1983, cap. 3.
4. R. B. Macmullin, *Chem. Eng. Progr.*, **44**, 183 (1948).
5. R. J. Maget, *J. Polymer Sci.*, **A2**, 1281 (1964).
6. P. Ferrero, F. Berbe, R. L. Flame, *Bul. Soc. Chim. Belg.*, **56**, 349 (1947).
7. T. W. F. Russel, D. T. Buzzelli, *Ind. Eng. Chem. Proc., Design and Develop.*, **8**, 2 (1969).
8. J. Al. Kabi, P. H. Gore, E. F. Saad, D. N. Waters and G. F. Maxon, *Int. J. Chem. Kinet.*, **15**, 697 (1983).
9. A. M. Eastham, G. A. Latremouille, *Can. J. Chem.*, **31**, 169 (1952).
10. W. A. Parker, J. W. Prados, *Chem. Eng. Progr.*, **60**, 74 (1967).
11. M. H. Friedman, R. R. A. White, *J. Chem. Eng.*, **8**, 74 (1962).
12. H. G. Haring, H. W. Knol, *Chem. Proc. Eng.*, **45**, 560 (1964), **45**, 619 (1964), **45**, 690 (1964), **46**, 38 (1965).
13. W. F. Ames, *Ind. Eng. Chem.*, **52**, 517 (1960).
14. W. F. Ames, *Ind. Eng. Chem.*, **1**, 214 (1962).
15. A. Weidenbacher, S. Șerban, *Rev. Chimie*, **36**, 21 (1985).
16. R. Kerber, O. Gestrich, *Chem. Ing. Techn.*, **38**, 536 (1966).
17. D. Summers, J. N. N. Scott, S. K. Ralph, *Int. J. Chem. Kinet.*, **19**, 553 (1987).
18. J. C. Jungers et al., *Cinétique Chimique Appliquée*, Société des Éditions TECHNIP, Paris, 1958, p. 142-227.
19. C. Capellos, B. H. J. Bielsky, *Kinetic System. Mathematical Description of Chemical Kinetics in Solutions*. Wiley-Intersci., New York, 1972, cap. 9.
20. R. De Maria, J. E. Longfield, G. Butler, *Ind. Eng. Chem.*; **53**, 259 (1961).

## OPTIMAL CHOICE OF SOLVENT SYSTEMS IN BIDIMENSIONAL THIN LAYER CHROMATOGRAPHY

COSTEL SĂRBU\*, IOVANCA HAIDUC\*

**ABSTRACT.** This paper proposes the contingency tables for the optimal choice of sets of solvents in bidimensional thin layer chromatography. The new approach described here is capable of finding the optimal combinations of two TLC solvent systems according to, for instance, Pearson  $\chi^2$ , Cramer's V or gamma criterion. In this order an IBM-PC computer has been used to run the corresponding STATA program.

**Introduction.** A rather common problem in chromatography is to find objective criteria for the evaluation of the most efficient chromatographic system and an optimal choice of combinations to identify the group of compounds.

Regardless of the kind of chromatography used for a sample analysis, e.g. thin layer chromatography (TLC), gas chromatography (GC), paper chromatography (PC), the optimal set of chromatographic systems includes those which differ very much in identification characteristics, e.g.  $hR_f$  values and/or colours in TLC.

The idea of using TLC in qualitative analysis has long been pursued due to the simplicity, the low cost, the rapidity and the sensitivity of the analytical technique. Obviously a single retention factor,  $hR_f$ , is not always sufficient for the identification of any compound and it is evident that more measurements are needed. The  $hR_f$  values in different solvent systems reported either in graphical representations such as the „chromatographic spectrum” [1] and „chromatographic profile” [2], or in tables [3] have been considered to be suitable for identification purposes. In this regard the choice of the minimum number of solvent systems containing different information is of crucial importance for the identification of unknowns and has been the topic of several statistical studies. The individual information provided by each solvent system and the correlation between such systems have been investigated using the „discrimination power” [3—6], information theory [7—10], numerical taxonomy technique [11, 12], while principal components analysis [13—15] and recently fuzzy sets theory [16—17] have been used to evaluate the quality of TLC separations and for the selection of optimum sets of solvent systems.

In this context contingency tables has been proven to have a great potential for the evaluation of the identification power of chromatographic systems considering in this order,  $hR_f$  values and colours of unknowns [18]. As a consequence of these success we here report the results obtained concerning

---

\* Babeș-Bolyai University, Department of Analytical Chemistry R-3400 Cluj-Napoca, Romania.

the optimal choice of solvent systems for a bidimensional TLC separations using contingency tables.

**Theory.** A contingency table provides a way of simplifying the presentation of data and a useful method of comparing two and more variables [19]. We are often interested in the possibility of relationship between two variables. Also of interest are the degree of strength of relation between two variables and the significance of the relationship. Contingency tables are essential with nominal variables but also they may be successfully used with quantitative variables. Each cell of such a table represents the number of observations belonging to a particular category or class of the data. In our case a cell contains the number of compounds of the same  $hR_f$  range e.g. 0–10, 11–20, ..., 91–100 for a combination of two solvent systems. The labels of this class are found in the column and row corresponding to the cell.

Many criteria (indices) were proposed to evaluate the degree of partitional adequacy (association) of two partitions of  $n$  objects. All such indices are derived from the contingency table constructed from two partitions as is shown in Table 1. The two partitions of  $n$  objects are denoted  $U$  and  $V$ . The partitions are identified with the clustering algorithm and a priori information when a specific index is defined.

Contingency Table of Two Partitions

Table 1

	$v_1$	$v_2$	...	$v_q$	
$u_1$	$n_{11}$	$n_{12}$	...	$n_{1q}$	$n_{1.}$
$u_2$	$n_{21}$	$n_{22}$	...	$n_{2q}$	$n_{2.}$
$u_p$	$n_{p1}$	$n_{p2}$	...	$n_{pq}$	$n_{p.}$
	$n_{.1}$	$n_{.2}$	...	$n_{.q}$	$n_{..} = n$

$$U = \{u_1, u_2, \dots, u_p\} \text{ and } V = \{v_1, v_2, \dots, v_q\}$$

Entry  $n_{ij}$  ( $i = 1, 2, \dots, p; j = 1, 2, \dots, q$ ) in Table 1 is the number of objects that are both in group  $u_i$  and in group  $v_j$ . The term  $n_{i.}$  (1) is the row sum for the  $i$ th row, or the number of objects in group  $u_i$  and  $n_{.j}$  (2) is the number of objects in group  $v_j$ . If the data are not weighted,  $n_{ij}$  is just a count. If the data are weighted,  $n_{ij}$  is the sum of weights of all data corresponding to the  $(i, j)$  cell.

$$n_{i.} = \sum_{j=1}^q n_{ij} \quad (1), \quad n_{.j} = \sum_{i=1}^p n_{ij} \quad (2)$$

with

$$n = \sum_{i=1}^p \sum_{j=1}^q n_{ij}$$

Also define the concordance (3) and discordance (4)

$$A_{ij} = \sum_{k>1} \sum_{l>j} n_{kl} + \sum_{k<1} \sum_{l<j} n_{kl} \quad (3) \quad D_{ij} = \sum_{k>1} \sum_{l<j} n_{kl} + \sum_{k<1} \sum_{l>j} n_{kl} \quad (4)$$

along with twice the number of concordances  $P$  and number of discordances  $Q$

$$P = \sum_{i=1}^p \sum_{j=1}^q n_{ij} A_{ij}, \quad Q = \sum_{i=1}^p \sum_{j=1}^q n_{ij} D_{ij}$$

Now we are able to define some statistics used within the contingency tables [20-21].

The Pearson  $\chi^2$  statistic with  $(p-1)(q-1)$  degrees of freedom is defined as

$$\chi^2 = \sum_{i=1}^p \sum_{j=1}^q \frac{(n_{ij} - m_{ij})^2}{m_{ij}}$$

where

$$m_{ij} = n_i n_j / n$$

The likelihood - ratio  $\chi^2$  statistic with  $(p-1)(q-1)$  degrees of freedom is defined in a similar way as the mutual information [18] having the following expression

$$G = 2 \sum_{i=1}^p \sum_{j=1}^q n_{ij} \ln(n_{ij}/m_{ij})$$

Cramer's  $V$  is a measure of association designed so that the attainable upper bound is 1. For  $2 \times 2$  tables,  $-1 \leq V \leq 1$ , and otherwise  $0 \leq V \leq 1$ .

$$V = (n_{11}n_{22} - n_{12}n_{21}) / (n_1 n_2 n_{.1} n_{.2})^{1/2} \quad \text{for } 2 \times 2$$

and

$$V = [(\chi^2/n) / \min(p-1)(q-1)]^{1/2} \quad \text{otherwise.}$$

Goodmann and Kruskal's gamma  $\gamma$  ignores tied pairs and is based only on the number of concordant and discordant pairs of observations

$$\gamma = (P - Q) / (P + Q)$$

with asymptotic variance

$$16 \sum_{i=1}^p \sum_{j=1}^q n_{ij} (Q A_{ij} - P D_{ij})^2 / (P + Q)^4$$

Kendall's  $\tau$  is similar gamma except that it considers a correction for ties

$$\tau_b = (P - Q) / (w_r w_c)^{1/2}$$

with asymptotic variance

$$\frac{\sum_{i=1}^p \sum_{j=1}^q n_{ij}(2w_r w_c d_{ij} + \tau_b v_{ij})^2 - n^2 \tau_b^2 (w_r + w_c)^2}{(w_r w_c)^2}$$

where

$$w_r = n^2 - \sum_i n_i$$

$$w_c = n^2 - \sum_j n_j$$

$$d_{ij} = A_{ij} - D_{ij}$$

$$v_{ij} = n_i w_c + n_j w_r$$

Kendall's  $\tau_b$  ( $-1 \leq \tau_b \leq 1$ ) and Goodmann and Kruskal's gamma ( $-1 \leq \gamma \leq 1$ ) are relevant only when both dimensions of the table can be ordered say from low-to-high or worst to best. The other statistics, however, are applicable in all cases.

**Results and discussion.** For the choice of the most appropriate solvent system recommended in the literature for the TLC of carotenoids, the information content (I) has been calculated using the Shannon entropy [7]. In the same respect the informational energy ( $E = \sum_i p_i^2$ ) has been also used [9].

The  $hR_f$  values for 11 components and 7 solvent systems presented in Table 2 are divided into 10 groups of  $hR_f$  values in the range 0–10, 11–20, ..., 91–100. Comparing I and E values (see Table 2) it appears that system IV is the best one because the highest I and the lowest E have been attained.

Table 2

$hR_f$  values of 11 carotenoids, information content, I, and information energy, E.

Substance	Solvent*						
	I	II	III	IV	V	VI	VII
Cryptoxanthine	62	70	76	74	39	21	4
Rubixanthine	45	60	64	45	15	4	0
Lycioxanthine	29	37	40	32	8	0	0
Isozeaxanthine	34	56	92	91	36	36	10
Escholtzanthine	12	22	25	22	8	1	0
Lycophyll	8	20	22	20	7	0	0
Euglenanone	62	68	81	80	54	34	9
Canthaxanthine	58	65	79	80	55	37	20
Rhodoxanthine	28	42	43	40	14	7	1
8'-apo- $\beta$ -carotenic acid	28	38	30	15	5	0	0
Torularhodin	6	10	9	2	1	0	0
I	2.66	2.91	3.08	3.26	2.11	1.79	1.49
E	0.17	0.14	0.12	0.11	0.19	0.36	0.57

\* 50:50 methanol-methyl-ethyl-ketone mixture with light petroleum of water in various proportions.

As none of the 7 solvent systems achieves a complete separation of the carotenoids the bidimensional TLC has to be used. In this order Pearson  $\chi^2$ , Cramer's  $V$  and gamma were calculated. In Table 3 the results obtained for different solvent system combinations are presented together with the conditional information energy  $E_{ij}$  calculated in the same respect [9].

Considering only the group of the best solvent systems (I, II, III, IV and V), from Table 2, it can be seen that there is a little practical difference between the sequence of values obtained for Pearson  $\chi^2$ , Cramer's  $V$  and gamma.

Table 3

Values obtained for Pearson  $\chi^2$ , Cramer's  $V$ , gamma  $\gamma$  and conditional information energy,  $E_{ij}$ .

Pairs of solvent	$\chi^2$	V	$\gamma$	$E_{ij}$
I-IV	50.40	0.87	0.78	0.0032
II-IV	49.50	0.86	0.83	0.0020
III-IV	47.67	0.85	1.00	0.0016
I-II	44.00	0.82	1.00	0.0050
I-III	36.00	0.74	0.91	0.0020
I-V	22.36	0.82	0.87	0.0032
III-V	22.00	0.81	0.95	0.0036
IV-V	21.81	0.81	0.90	0.0048
II-V	20.17	0.78	1.00	0.0042
III-VI	14.67	0.81	1.00	0.0036
I-VI	14.67	0.81	0.80	0.0204
V-VI	14.66	0.81	1.00	0.0253
IV-VI	12.22	0.74	1.00	0.0352
I-VII	11.00	1.00	0.60	0.0153
II-VI	9.6	0.66	0.93	0.0706
III-VII	4.95	0.67	0.55	0.0204
V-VII	4.95	0.67	1.00	0.0443
IV-VII	2.93	0.52	0.75	0.0793
II-VII	2.93	0.52	1.00	0.0443
VI-VII	2.93	0.52	1.00	0.166

From the point of view of Pearson  $\chi^2$  which appears to be the most objective and sensitive criterion it is easy to observe that the best combination is within solvent system I and IV because the highest value was obtained (50.4), the second being II-IV (49.5) and the third III-IV (47.7). The same sequence is obtained using Cramer's  $V$  and gamma. Comparing with the conditional information energy one may see that the latter can only occasionally reveal the same situation. The plot of  $hR_{fi}$  vs.  $hR_{fj}$  values, as may be seen in Fig. 1 illustrates the fact that Pearson  $\chi^2$  objectively reveals the (non)similarity between two solvent systems in TLC.

**Conclusions.** Taking into account the results obtained in this paper one may conclude that contingency tables can be very useful to appreciate the efficiency of combinations of solvent systems in TLC considering Pearson  $\chi^2$ , Cramer's  $V$  or gamma and/or more sophisticated indices as the likelihood-ratio  $\chi^2$  and Fischer's test [21-23].

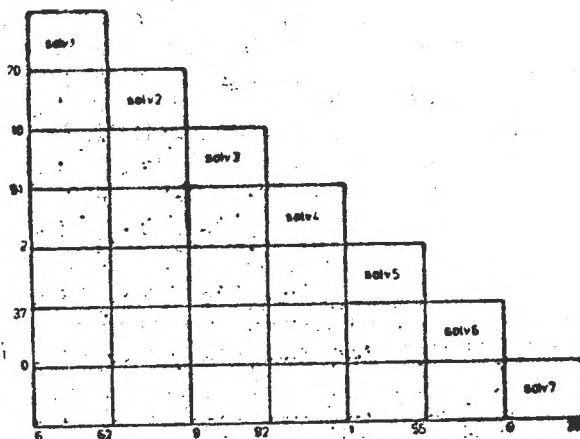


Fig. 1. Plot (matrix) of  $hR_f$  pairs for solvent System I-VII.

The mathematics used to obtain these results are quite complex and of minor importance for our purpose. Of greater importance, however, are the rules for qualitative analysis which can be derived from them. The rules are as follows.

- (1) Optimal combined methods for qualitative analysis make use of individually good system.
- (2) Individually good systems are characterized by high spread of analytical signals (for instance, many different  $hR_f$  values or colours) and low errors (substances with small difference in  $hR_f$  values can be discriminated).
- (3) Optimal combinations also require that the individual systems should yield uncorrelated information, meaning that very dissimilar should be combined. This explains the power of combinations of methods with very different principles such as GC/MS (combination of a chromatographic method with a spectrometrical one).

#### REFERENCES

1. J. Franc and Z. Stransky, *Collect. Czech. Chem. Commun.*, **24**, 3611 (1959).
2. V. Milan, G. Romano and G. Scarlata, *Minerva Medicoleg.*, **99**, 15 (1979).
3. A. H. Stead, R. Gill, T. Wright, J. P. Gibbs and A. C. Moffat, *Analyst* (London) **107**, 1106 (1982).
4. A. C. Moffat and K. W. Smalldon, *J. Chromatogr.*, **90**, 9 (1974).
5. P. Owen, A. Pendlebury and A. C. Moffat, *J. Chromatogr.*, **161**, 187 (1978).
6. P. Owen, A. Pendlebury and A. C. Moffat, *J. Chromatogr.*, **161**, 195 (1978).
7. D. L. Massart, *J. Chromatogr.*, **79**, 157 (1973).
8. C. Sărbu and H. Nașcu, *Rev. Chim. (Bucharest)*, **41**, 276 (1990).
9. C. Sărbu and H. Nașcu, *Rev. Roum. Chim.*, **37**, 945 (1992).
10. C. Sărbu, *Anal. Chim. Acta*, **271**, 269 (1993).
11. D. L. Massart and H. De Clercq, *Anal. Chem.*, **46**, 1988 (1974).
12. H. De Clercq and D. L. Massart, *J. Chromatogr.*, **115**, 1 (1975).
13. G. Musumarra, G. Scarlata, G. Romano and S. Clementi, *J. Anal. Toxicol.* **7**, 286 (1983).

14. G. Musumarra, G. Scarlata, G. Romano, S. Clementi and S. Wold, *J. Chromatogr. Sci.*, **22**, 538 (1984).
15. G. Musumarra, G. Scarlata, G. Cirma, G. Romano, S. Palazzo, S. Clementi and G. Giulietti, *J. Chromatogr.*, **295**, 31 (1984).
16. C. Sârbu, D. Dumitrescu and H. Pop, *Rev. Chim. (Bucharest)*, **44** (5), 450 (1993).
17. D. Dumitrescu, C. Sârbu and H. Pop, *Anal. Lett.*, **26** (5), 123 (1994).
18. C. Sârbu, *Conferința națională de chimie și chimie industrială*, București, 1993, vol. 1, pag. 311.
19. A. K. Jain and R. C. Dubes, *Algorithms for Clustering Data*, Prentice-Hall, New Jersey 1988.
20. W. J. Conover, *Practical Nonparametric Statistics*, 2nd, Ed., John Wiley & Sons, New York, 1980.
21. A. Agresti, *Analysis of Ordinal Categorical Data*, John Wiley & Sons, New York, 1984.
22. K. J. Rothman, *Modern Epidemiology*, Little, Brown and Company, Boston, 1986.
23. *The Statistics Problem Solver*, Research and Education Association, Piscataway, New Jersey, 1991.



MONTE-CARLO SIMULATION IN THE REACTION OF *p, p'*-DINITRO-DIBENZYL ELECTROREDUCTION TO *p, p'*-DIAMINODIBENZYL.

## I. THE MATHEMATICAL MODEL

MARIA OLEA\*, LIVIU ONICIU\*, ZOLTÁN KUBASZEK\*

**ABSTRACT.** The purpose of the paper is the determination of the Faradaic yield as well as the chemical one, in the case of the electroreduction of *p, p'*-Diaminodibenzyl using a stochastic model of Monte-Carlo type.

**Introduction.** An electrochemical synthesis variant is suggested for obtaining *p, p'*-diaminodibenzyl, an intermediate in the leather substitutes synthesis. The numerous advantages of organic electro-synthesis as compared to the traditional method of aromatic nitroderivates reduction have been considered.

The type of synthesis suggested here is based on the mediated electroreduction of *p, p'*-dinitrodibenzyl in a divided batch reactor of filter-press type [1].

A previous study [2] was concerned with the optimum reactions conditions.

Since the experimental determination of the quantity of hydrogen formed parallel with the main reaction is extremely difficult, a stochastic Monte-Carlo type model is employed for describing the process. By solving this model, both the Faradaic and the chemical yield are determined.

**The Monte-Carlo model.** The basic equation of the model is the theoretical formation rate of *p, p'*-diaminodibenzyl:

$$\frac{[(dm)_t]}{dt} = \frac{iAM}{zF}, \quad (1)$$

where

$i$  = current density,  $A \cdot m^{-2}$

$A$  = electrode area,  $m^2$

$M$  = molecular mass of *p, p'*-Diaminodibenzyl (DADB), g. mole

$z$  = the number of transferred electrons

$F$  = Faraday's constant.

$m$  = mass of DADB, g

$t$  = time, s

This equation is easy to integrate, with a view to determining the imposed quantities of DADB under (the conditions) of constant current density and of 100% Faradaic yield.

A considerable shortening of the reaction time is achieved operating the reactor according to a certain profile of current density,  $i = i(t)$  [3].

\* University Babeş-Bolyai, Faculty of Chemistry, 3100 Cluj-Napoca, Romania.

This profile is obtained by the numerical solving of the analytical mathematical model that is applied to the electrochemical reactor [4]. The ensuing problem is the one of determining the Faradaic, respectively, chemical yield.

Let us have  $r$  = the chemical yield of the reaction (time dependent),  $r = r(t)$ . If  $(dm)_t$  is the theoretical DADB quantity that is accumulated during  $dt$ , while  $dm$  is the practical quantity accumulated within the same time  $dt$ , then the following can be written for the chemical yield at the moment  $t$ :

$$r(t) = \frac{dm}{(dm)_t}; \quad (2)$$

hence :

$$\frac{dm}{dt} = \frac{(dm)_t}{dt} r(t) \quad (3)$$

and, considering the equation (1) we infer :

$$\frac{dm}{dt} = \frac{AM}{zF} i(t) r(t). \quad (4)$$

Obviously, the numerical integration of the equation (4) could be possible only if we know  $r(t)$  at different moments. As we do not have enough experimental measurements at our disposal, a stochastic model, of Monte-Carlo type, is suggested for the variation  $r = r(t)$ .

$$\text{We note } \alpha(t) = \frac{AM}{zF} i(t) r(t), \quad (5)$$

subsequently, by re-writing the equation (4) by means of finite differences, we obtaine

$$\frac{m_j - m_{j-1}}{t_j - t_{j-1}} = \alpha_j, \quad (6)$$

where  $m_j$  = DADB mass at the  $t_j$  moment  
 $m_{j-1}$  = DADB mass at the  $t_{j-1}$  moment,

or

$$m_j = m_{j-1} + \alpha_j t_j - \alpha_j t_{j-1} \quad (7)$$

By further applying the equation (7) for other moments, we get :

$$\left\{ \begin{array}{l} m_j = m_{j-1} + \alpha_j t_j - \alpha_j t_{j-1} \\ m_{j-1} = m_{j-2} + \alpha_{j-1} t_{j-1} - \alpha_{j-1} t_{j-2} \\ \vdots \\ m_2 = m_1 + \alpha_2 t_2 - \alpha_2 t_1 \\ m_1 = m_0 + \alpha_1 t_1 - \alpha_1 t_0, \end{array} \right. \quad (8)$$

with the conditions  $m_0 = 0$ , and  $T_0 = 0$ .

By a member by member addition of the above equation, we get

$$m_j = \alpha_j t_j + \alpha_{j-1} t_{j-1} + \alpha_{j-2} t_{j-2} + \dots + \alpha_2 t_2 + \alpha_1 t_1 - (\alpha_j t_{j-1} + \alpha_{j-1} t_{j-2} + \dots + \alpha_2 t_1); \quad (9)$$

or, by re-grouping the terms, we obtain:

$$m_j = \alpha_j t_j + (\alpha_{j-1} - \alpha_j) t_{j-1} + (\alpha_{j-2} - \alpha_{j-1}) t_{j-2} + \dots + (\alpha_1 - \alpha_2) t_1, \quad (10)$$

which represents the DADB quantity accumulated at the moment  $t_j$ :

A method of Monte Carlo simulation is employed in order to infer the coefficients from the equation (10). That is:  $t_j$  aleatory numbers are generated within the time interval  $0 - t_m$  (where  $t_m$  is the maximum reaction time

The corresponding value  $m_j$  is generated according to a law:  $m_j = f(t_j)$ . The law is chosen in such a way that the suggested empirical model  $m_j = f(t_j)$  should prove the value  $m_j$  as accurately as possible. After several attempts, the law has the form:

$$m_j = a [1 - \exp(-bt_j)]. \quad (11)$$

*An Iterative Method of Determination for Coefficients a and b*

After a  $N$  experimental measurements  $(t_j, m_j)$  the parameters are determined from the condition:

$$m = a [1 - \exp(-bt_m)], \quad (12)$$

where  $m$  = the final DADB quantity.

Step 1:

For a first approximation we take  $a^{(1)} = m$ ; a value for the parameter  $b$  is determined in the case of each pair  $(t_j, m_j)$ :

$$m_j = m [1 - \exp(-bt_j)]; \quad (13)$$

hence

$$b_j^{(1)} = \frac{1}{t_j} \ln \frac{m}{m - m_j}, \quad j = \overline{1, N}. \quad (14)$$

At this step the value assigned to the  $b$  parameter is:

$$b^{(1)} = \frac{\sum_{j=1}^N b_j^{(1)}}{N} \quad (15)$$

Step 2:

From the equation:

$$a^{(2)} = \frac{m}{1 - \exp(-b^{(1)} t_m)} \quad (16)$$

$a^{(2)}$  is recalculated with the value we inferred during step 1.

The values of the parameters  $b_j^{(2)}$  are recalculated with the value  $a^{(2)}$  and the pairs  $(t_j, m_j)$ :

$$b_j^{(2)} = \frac{1}{t_j} \ln \frac{a^{(2)}}{a^{(2)} - m_j}; \quad j = 1, N \quad (17)$$

Then, the new value assigned to the parameter  $b^{(2)}$  at this step is:

$$b^{(2)} = \frac{\sum_{j=1}^N b_j^{(2)}}{N}. \quad (18)$$

Step  $k$ :

$$a^{(k)} = \frac{m}{1 - \exp(-b^{(k-1)} t_m)}, \quad (19)$$

$$b_j^{(k)} = \frac{1}{t_j} \ln \frac{a^{(k)}}{a^{(k)} - m_j}, \quad j = 1, N \quad (20)$$

$$\text{and } b^{(k)} = \frac{\sum_{j=1}^N b_j^{(k)}}{N}. \quad (21)$$

The algorithm stops the moment:

$$|a^{(k)} - a^{(k-1)}| < \varepsilon, \quad (22)$$

where  $\varepsilon$  is an imposed accuracy and  $a = a^{(k)}$  and  $b = b^{(k)}$ , being now capable of generating  $m_j$  (according to the equation (12)).

As compared to the values  $m_j^*$  calculated by means of equation (9), the values  $m_j$  calculated by means of equation (12) have to satisfy the condition:

$$\sum_{j=1}^n (m_j - m_j^*)^2 \stackrel{!}{=} \min, \quad (23)$$

where  $n$  = the number of randomly generated points  $t_j$ .

#### Determination of $\alpha_j$ coefficients [6]

We note

$$Q = \sum_{j=1}^n (m_j - m_j^*)^2 \stackrel{!}{=} \min. \quad (24)$$

This sum can also be written:

$$\begin{aligned} & (m_1 - \alpha_1 t_1)^2 + (m_2 - \alpha_1 t_1 - \alpha_2 (t_2 - t_1))^2 + \dots + (m_n - \alpha_1 t_1 - \\ & - \alpha_2 (t_2 - t_1) - \dots - \alpha_n (t_n - t_{n-1}))^2 \stackrel{!}{=} \min. \end{aligned} \quad (25)$$



**Conclusions :** The model suggested here allows the determination of the chemical yield and subsequently of Faradaic yield, during the electroreduction of p, p' - Dinitrodibenzyl to p, p'-Diaminodibenzyl.

As practice has shown, hydrogen evolution reaction depends on many factors, having therefore a random evolution, the stochastic model of Monte-Carlo type can be asserted as the best to describe the behaviour of the system.

#### REFERENCES

1. Oniciu, L., Olea Maria, Schinteie Monica, *Revista de chimie*, **41** (4), 1990 (345-347).
2. Oniciu, L., Olea Maria, Danciu, Virginia, *Revista de chimie*, **41** (10), 1990 (799-801).
3. Olea Maria, Oniciu, L., unpublished data.
4. Pickett, D., *Electrochemical Reactor Design*, Elsevier Scientific Publishing Company, Amsterdam, 1977 (171).
5. Unwin, P. R., Bard, J. A., *J. Phys. Chem.*, **95** (20), 191 (7814-7824).
6. Rosenblatt, M., *Stationary Sequences and Random Fields*, Birkhäuser, 1985 (111).

## THE SENSITIVITY OF ETHYL-ACETATE SYNTHESIS REACTOR (I)

MARIA OLEA\*, LIVIU ONICIU\*, ȘTEFAN OIȚĂ\*

**ABSTRACT.** The paper proposes a method of operation based on the direct sensitivity analysis of the ethyl-acetate synthesis reactor (I) and in that of the p, p'-diaminodibenzyl electrosynthesis reactor (II).

A mathematical model, verified in practice has been used in the former case.

## Nomenclature:

- $x$  — the vector of state variables  
 $u$  — the vector of control variables  
 $p$  — the vector of parameters  
 $\tau$  — the independent variable (time or space)  
 $S_{x_0}^x(\tau)$  — the matrix of state sensitivity reported to initial state  
 $S_p^x(\tau)$  — the matrix of state sensitivity reported to parameters  
 $f(x, u, p, \tau)$  — the vector of functions  
 $f_x$  — the Jacobian of the vector of functions reported to  $x$   
 $f_p$  — the Jacobian of the vector of functions reported to parameters ( $p$ )  
 $c$  — the concentration of acetaldehyde, mol. l<sup>-1</sup>  
 $a$  — the catalyst concentration, mol. l<sup>-1</sup>  
 $\xi_A$  — the acetaldehyde conversion  
 $T$  — the reacting mass temperature, K  
 $T_S$  — the cooling agent temperature, K  
 $K_T$  — the global constant of the heat transfer, Kcal · m<sup>2</sup> · s<sup>-1</sup> · K  
 $Q_{vo}$  — the volumetric input flow, m<sup>3</sup> · s<sup>-1</sup>  
 $Q_{so}$  — the volumetric flow of brine, m<sup>3</sup> · s<sup>-1</sup>  
 $Q_{mo}$  — the massic input flow [kg · s<sup>-1</sup>]  
 $Q_{ms}$  — the brine massic flow [kg · s<sup>-1</sup>]  
 $c_0$  — the initial acetaldehyde concentration [mol · m<sup>-3</sup>]  
 $d$  — the diameter of the reactor [m]  
 $d_e$  — the equivalent diameter of the cooling coil [m]  
 $c_p$  — the specific heat of the reaction mass [kcal · mol<sup>-1</sup> · K<sup>-1</sup>]  
 $C_{pS}$  — the specific heat of brine [kcal · mol<sup>-1</sup> · K<sup>-1</sup>]  
 $b$  — the volumetric contraction  
 $z$  — the space [m]

**Introduction.** Let us start with a short presentation of the method of the direct sensitivity analysis (DSA) [1].

A system can be described by the concentrated equation:

$$\dot{x} = f(x(\tau), u, p, \tau) \quad (1)$$

where  $\dot{x}$  is the vectorial state equation.

\* University Babeș-Bolyai, Faculty of Chemistry, 3400 Cluj-Napoca, Romania.

The deviation of the system's state evolution is to be obtained by adding the effects on the variations of all parameters as below :

$$\Delta x(\tau) = \Delta_{x_0} x(\tau) + \Delta_u x(\tau) + \Delta_p x(\tau) \quad (2)$$

In the case of small variations for  $\Delta x_0$ ,  $\Delta u$ ,  $\Delta p$ , we have :

$$\Delta_{x_0} x(\tau) \approx S_{x_0}^x(\tau) \cdot \Delta x_0 \quad (3.1.)$$

$$\Delta_u x(\tau) \approx S_u^x(\tau) \cdot \Delta u \quad (3.2)$$

$$\Delta_p x(\tau) \approx S_p^x(\tau) \cdot \Delta p \quad (3.3)$$

where  $\Delta x_{0(u, p)} x(\tau)$  is the trajectory deviation state reported to  $x_0$  (or  $u$ , or  $p$ ).

These sensitivity matrices may be obtained by solving the sensitivity equations.

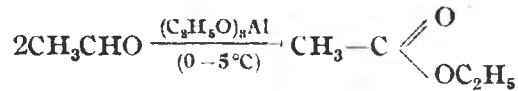
The state's sensitivity reported to the parameters can be written as below :

$$S_p^x(\tau) = f_i S_p^x(\tau) + f_p \quad (4)$$

With the initial condition :

$$S_p^x(0) = 0 \quad (5)$$

### 1. The Tischenko reaction for obtaining the ethyl-acetate [2]



The kinetic equation is :

$$r = kCa, \quad (6)$$

$$\text{where : } k = k_0 \exp(-E_a/RT), \quad (7)$$

$$\text{with } k_0 = 1,9 \cdot 10^8 \text{ l/mol} \cdot \text{s},$$

$$E_a = 12,5 \text{ kcal} \cdot \text{mol}^{-1}$$

$$\Delta_r H = -10560 \text{ kcal} \cdot \text{mol}^{-1}$$

$$\text{and } a = 0.0539 \text{ mol} \cdot \text{l}^{-1}$$

2. *The physical model of the reactor and the identification of the variables and parameters.* It is a long tube reactor with coat cooling in parallel flow. The length is dependent on the imposed conversion [2].

We have chosen  $x$ ,  $T$ ,  $T_s$  as state variables,  $K_T$ ,  $a_0$ ,  $c_0$  as parameters and  $Q_c$ ,  $Q_{s0}$  as control variables.

3. The mathematical model equations [2]

$$\frac{d\xi_A}{dz} = \frac{k_0 \exp(-E_a/RT)\pi d^2 a_0 (1 - \xi_A)}{4Q_{T_0} (1 - b\xi_A)^2} \tag{8.1}$$

$$\frac{dT}{dz} = \frac{-\Delta_r H \cdot k_0 \exp(-E_a/RT)c_0 a_0 (1 - \xi_A)\pi d^2}{4Q_{m_0} C_P (1 - b\xi_A)^2} - \frac{K_T \pi d (T - T_S)}{Q_{m_0} C_P} \tag{8.2}$$

$$\frac{dT_S}{dz} = \frac{K_T \pi d_e (T - T_S)}{Q_{m_S} C_{PS}} \tag{8.3}$$

with the initial conditions:

$$\xi_A = \xi_{A_0} \tag{9.1}$$

$$T = T_0 \tag{9.2}$$

$$T_S = T_{S_0} \tag{9.3}$$

This system was solved by means of Euler's method. The solving of the mathematical model has led to the variations presented in figure 1.

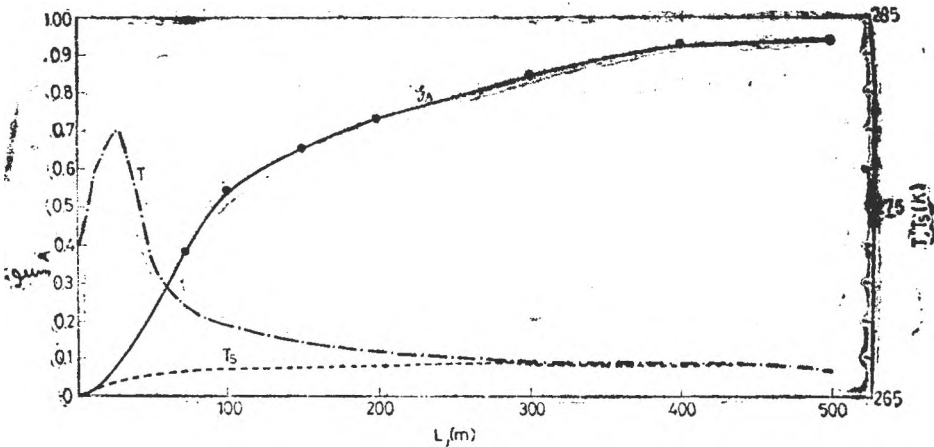


Fig. 1.  $\xi_A$ , T and  $T_S$  variation with reactor length.

4. The parametric sensitivity. We have approached only the impact of the above parameters on the state of the system.

The solving of the system (4)–(5) led to the following curves of parametric sensitivity (fig. 2, 3, 4, 5, 6, 7, 8, 9, 10).

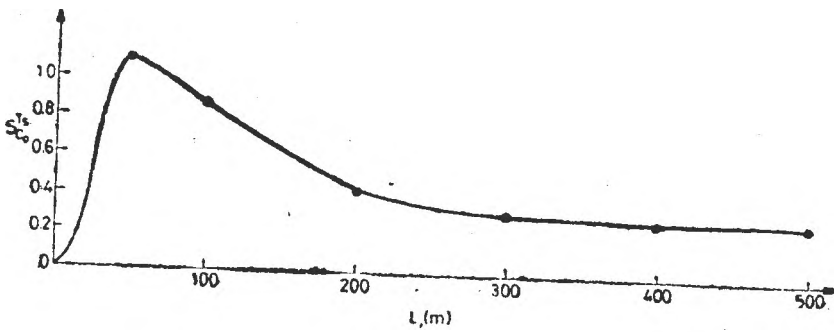
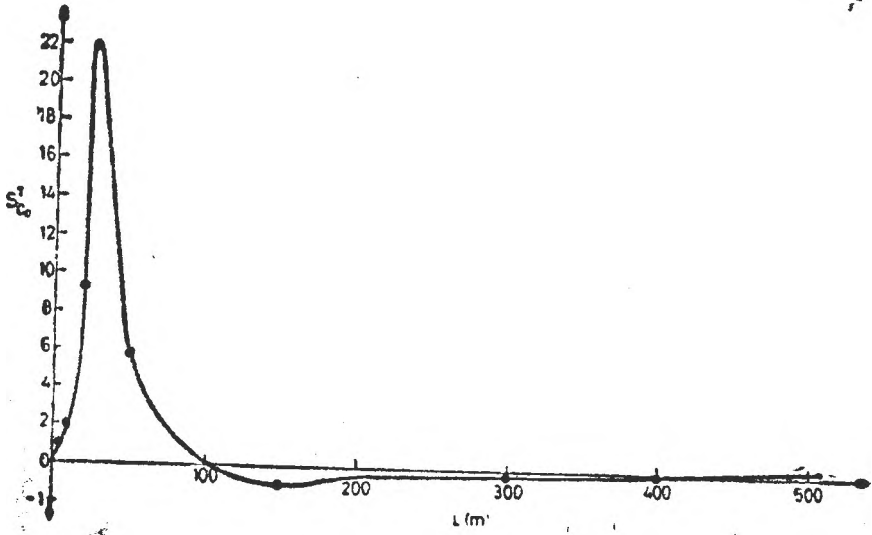
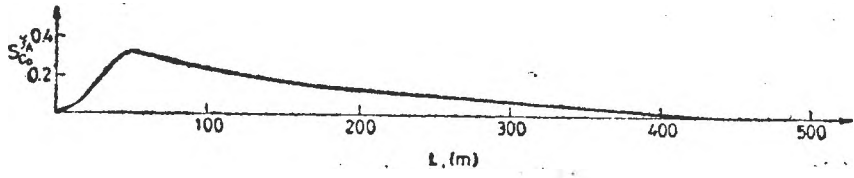


Fig. 2, 3, 4. Variation of the state sensitivity  $S_{C_a}^{(T_A, T_s)}$  as a function of the reactor length.

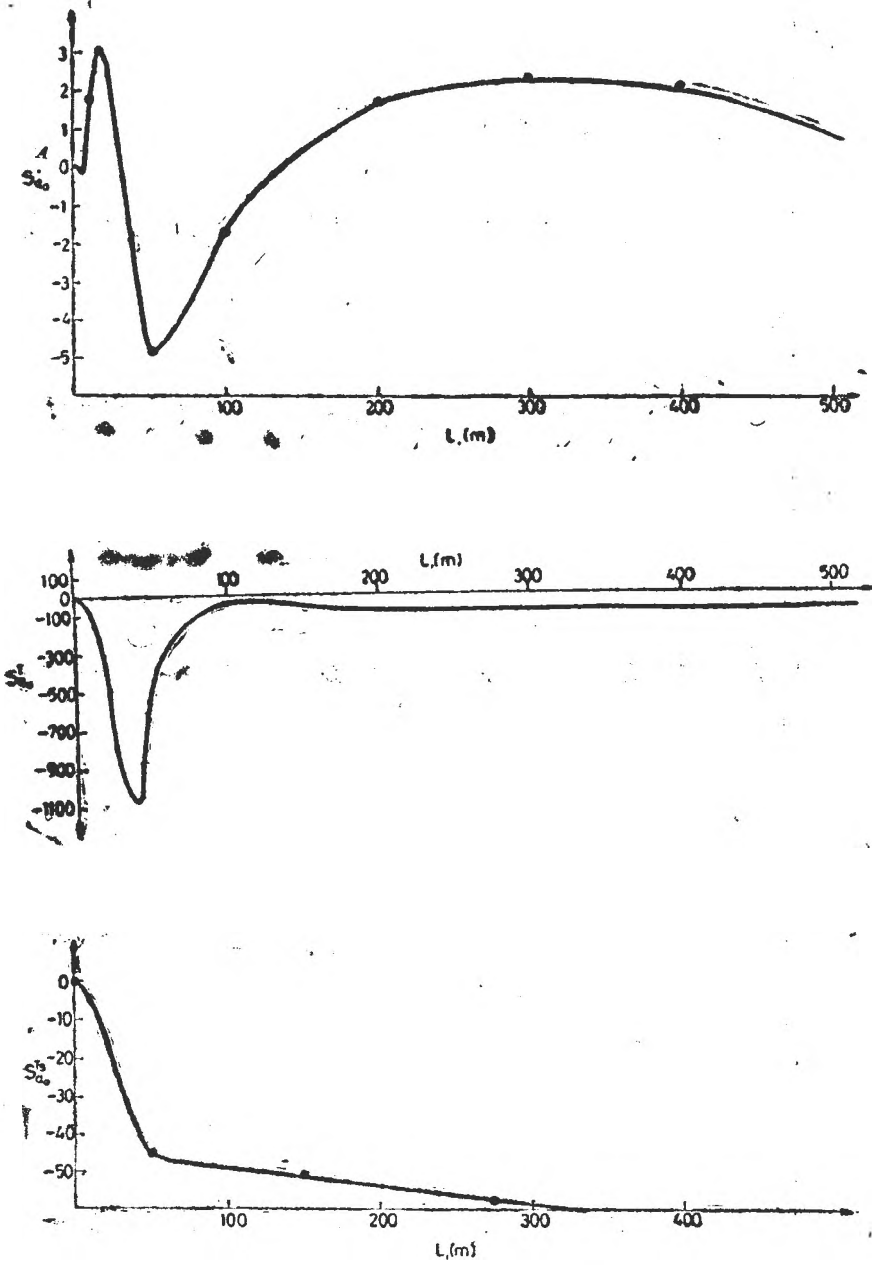


Fig. 5, 6, 7. Variation of the state sensitivity  $S_{a_i}^{(T_A, T, T_S)}$  as a function of the reactor length.

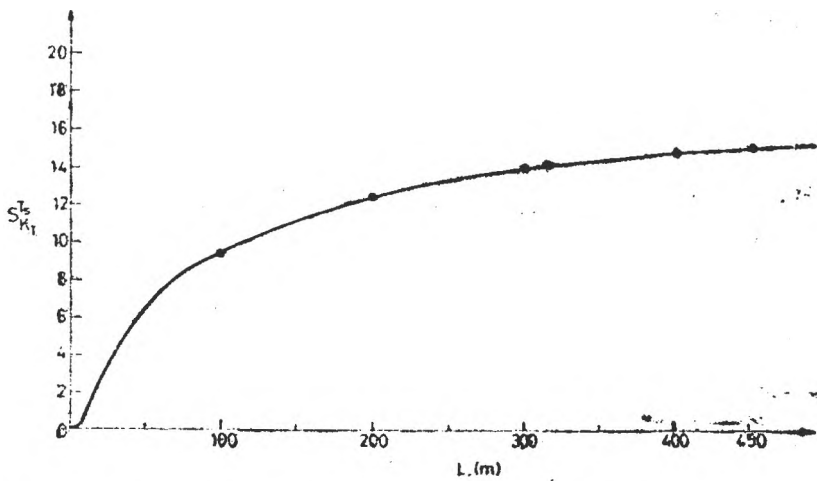
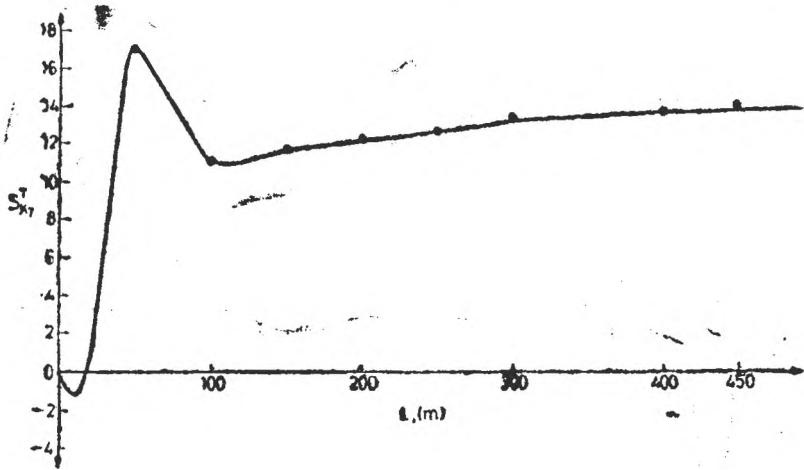
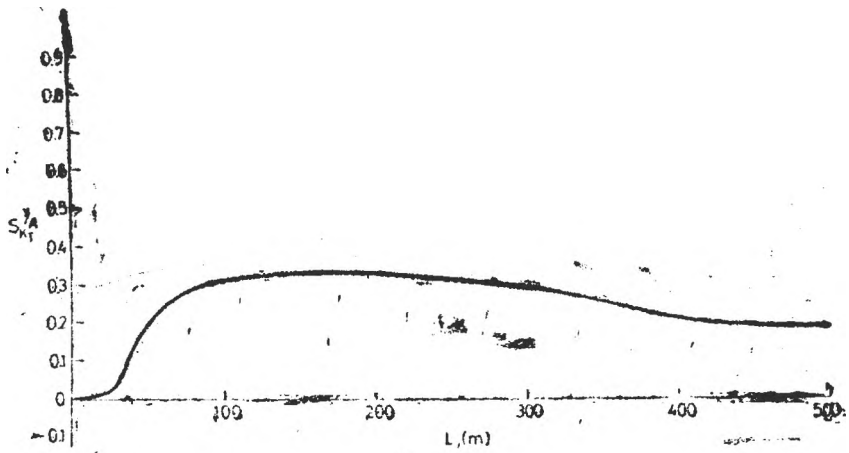


Fig. 8, 9, 10. Variation of the state sensitivity  $S_{K_T}^{(T_A, T_T, T_S)}$  as a function of the reactor length.

5. *Conclusions.* a) The sensitivity increases in the warm spot for all the parameters in question:  $a_0$ ,  $c_0$ ,  $K_T$ .

b) As we obtained the matrix of state sensitivity reported to the parameters, it is now possible to calculate (using (3.3)), the state's variation reported to those parameters.

For example, at  $z = 200$  m

$$S_p^x(200) = \begin{bmatrix} S_{K_T}^x(200) & S_{a_0}^x(200) & S_{c_0}^x(200) \\ S_{K_T}^T(200) & S_{a_0}^T(200) & S_{c_0}^T(200) \\ S_{K_T}^T(200) & S_{a_0}^T(200) & S_{c_0}^T(200) \end{bmatrix} = \begin{bmatrix} 0.831 & 1.687 & 0.137 \\ 12.351 & -85.90 & -0.514 \\ 12.5183 & -53.617 & 0.593 \end{bmatrix}$$

For a small variation of the parameters:

$$\Delta_p = \begin{bmatrix} \Delta K_T \\ \Delta a_0 \\ \Delta c_0 \end{bmatrix} = \begin{bmatrix} -0.05 \\ 0.001 \\ 0 \end{bmatrix}$$

The state variation is:

$$\Delta_p x(200) = \begin{bmatrix} \Delta x(200) \\ \Delta T(200) \\ \Delta T_5(200) \end{bmatrix} = S_p^x \cdot \Delta_p = \begin{bmatrix} -0.0148 \\ -0.7035 \\ -0.6795 \end{bmatrix}$$

#### REFERENCES

1. Ungureanu, S., *Sensibilitatea sistemelor dinamice*, Ed. Tehnică, București, 1988, Sect. III, (75-143).
2. Munteanu, O., and all. *Reactoare chimice. Studii de caz*, Institutul Politehnic București, 1989 (109-115).
3. Bucur, C. M., Popocea, C. A., Simion, G. H. G. H., *Calcul numeric*, Ed. Tehnică, București, 1983, Cap. V (138).
4. Watanabe N., Nishimura Y., and Matsubara M., *Chem. Eng. Sci.*, **28**, 7, 905 (1973).
5. Welsnaere Van R. J., and Froment F., *Chem. Eng. Sci.*, **25**, 10, 1503 (1970).
6. Bailey I. E., *Chem. Eng. Sci.*, **28**, 7, 1417 (1973).



## A POTENTIOMETRIC METHOD FOR LEAD DETERMINATION IN ALKALINE ZINC-PLATING ELECTROLYTE

ELENA HOPIRTEAN\* and MONICA HORN\*

**ABSTRACT.** A method for the determination of low concentrations of lead ions, in zinc plating electrolyte has been accomplished. The method is based on the separation of the lead ions by selective extraction from the strongly alkaline aqueous cyanide solution, as lead dithizonate, into a chloroformic phase, the de-complexation of this in acidic medium, followed by potentiometric, complexometric determination of  $Pb^{2+}$ , by back-titration of the EDTA excess, with standardized lead acetate solution, using a home-made Pb ion selective membrane electrode (Pb-ISM).

The experimental data have been statistically worked out, and compared to those obtained by atomic absorption spectrometry.

The method is estimated to prove high precision and accuracy.

**Introduction.** The quantitative determination of lead in various electroplating electrolytes is the main topic of a great number of papers in this field [1-9].

Among the most frequently used methods are: polarography [1-4], spectrochemical methods [5], chromatography [6], anodic stripping voltametry [7-9].

A potentiometric method [10] is useful for the determination of low concentration of lead in samples of residual water, resulted from electroplating baths. The determination was carried out by direct potentiometry using a  $Pb^{2+}$  selective membrane electrode. The major drawback of the method is the interference of  $Ag^+$ ,  $Hg^{2+}$  and  $Fe^{3+}$  ions.

It is known that strongly alkaline zinc-plating electrolyte is mainly characterised by the following chemical composition: NaCN (90-100 g/L); NaOH (70-80 g/L);  $Zn^{2+}$  (36-38g/L). As the time of use increases, the electrolyte becomes contaminated with cadmium, lead and iron ions, which interferes with the zinc-plate process, especially when their concentration reaches the critical values of 0.2 g  $Cd^{2+}$ /L; 0.5 g  $Pb^{2+}$ /L and 3-4 g  $Fe^{3+}$ /L. Zinc, cadmium and iron are present as cyanocomplexes.

Lead ions are present as natriumplumbit, that is why they cannot be determined by direct potentiometry. On the other hand, zinc, cadmium and iron ions resulting in the reaction of these cyanocomplexes with formaldehyde, interfere the Pb-ISM response towards lead ions.

Taking into account these interferences, our potentiometric method for lead determination (Pb-ISM [11]), in this case is preceded by its extraction in chloroform as lead dithizonate [12, 13].

**Experimental. Devices and working conditions:** The potential measurements were performed at room temperature, under stirring conditions, by using a digital pH-meter, accurate to 1 mV.

\* Institute of Chemistry, Str. Fărtâncle 30, 3400 - Cluj-Napoca, Roumania.

A home-made Pb ion-selective membrane electrode of type Pb-ISME [11], based on a mixture of PbS and Ag<sub>2</sub>S as well as a double junction saturated calomel electrode (SCE) as a reference electrode have been used. The second salt bridge of the reference electrode consists of 1 M KNO<sub>3</sub> solution. The following solutions are necessary: Dithizone  $3 \times 10^{-3}$  M and  $3 \times 10^{-4}$  M in chloroform, 0.2 M HNO<sub>3</sub>;  $10^{-1}$  M NaCN; 2 M NaOH; buffer solution of pH = 4.7 (acetic acid — sodium acetate);  $10^{-2}$  M EDTA;  $5 \times 10^{-3}$  M lead acetate.

**Principle of the method:** the method involves the following steps:

- selective and quantitative extraction of Pb<sup>2+</sup> in chloroform (pH = 10 — 10.2) as lead dithizonate [12, 13],
  - decomposition of the extracted lead dithizonate with 2 M nitric acid when lead ions are transferred into the aqueous solution;
  - addition of standard EDTA solution in excess;
  - potentiometric titration of the EDTA excess with a standardized lead acetate solution.
- For the determination of the equivalence point, an electrode pair formed by a Pb-ISME and a double junction saturated calomel electrode is used.

**Procedure:** Samples of 5 ml of the zinc plate bath electrolyte were diluted to 10 ml with distilled water and the pH was adjusted to 10 — 10.2 with 2.5 M nitric acid.

In order to separate lead as lead dithizonate in chloroform, following way has been chosen:

The prepared sample was quantitatively transferred into a separation funnel and was vigorously stirred with 10 ml of  $3 \times 10^{-3}$  M dithizone in chloroform. Chloroformic phase containing lead dithizonate was transferred in another separation funnel. Three successive such extractions have been performed, chloroformic phases being collected in the same separation funnel and afterwards washed with  $10^{-1}$  M NaCN. Then solution of lead dithizonate in chloroform was vigorously stirred in separation funnel with 10 ml solution of 0.2 M HNO<sub>3</sub>, in order to transfer lead ions in the aqueous phase. This operation was repeated three times and respective aqueous phases were collected in the same beaker.

The pH of the aqueous lead extract was adjusted to pH = 4 by adding dropwise 2 M NaOH, then 5 ml of buffer solution of pH = 4.7 and 5 ml of  $10^{-2}$  M standard EDTA solution ( $V_{EDTA}$ ) were subsequently added; The excess of EDTA was potentiometrically titrated with standardized  $5 \times 10^{-2}$  M lead acetate solution ( $V_e$ ). A microburette was used for titrant addition. Titration curves obtained were very well shaped and showed a sharp potential jump of at least 120 mV at the equivalence point. The equivalence volumes are determined by Hahn-Weiller method [14]. Lead content expressed in g/L, was calculated according to the formula:

$$\text{Pb (g/L)} = (V_{EDTA} \times f_{EDTA} - 5 \times V_e \times f_{PbAc_2}) \frac{M_{Pb}}{100 \times V_S}$$

where  $f$  represents the correction factor for the EDTA and lead acetate solution respectively, and  $V_S$  — the titrated solution volume. Nine determinations have been performed. Data obtained were statistically processed, according to the literature recommendations [15].

**Results.** Experimental results are given in Table 1.

Table 1

Experimental data obtained for lead determination in zinc — plating electrolyte

Nr. crt.	V ml	g Pb/L sample
0	1	2
1	0.73	$5.687 \times 10^{-1}$
2	0.73	$5.687 \times 10^{-1}$
3	0.725	$5.797 \times 10^{-1}$
4	0.725	$5.797 \times 10^{-1}$
5	0.73	$5.687 \times 10^{-1}$
6	0.73	$5.687 \times 10^{-1}$
7	0.73	$5.687 \times 10^{-1}$
8	0.73	$5.687 \times 10^{-1}$
9	0.72	$5.908 \times 10^{-1}$

Statistically, the following results have been obtained:  $\bar{X} = 5.74 \times 10^{-1}$  g Pb/L;  $n = 9$ ;  $s^2 = 6.39 \times 10^{-5}$ ;  $s = 8 \times 10^{-3}$  and  $s_{\bar{X}} = 2.66 \times 10^{-3}$ . Taking into account the low value of dispersion  $s^2$ , the method is estimated to prove a high precision.

The data were compared to those obtained by atomic absorption spectrometry (value A), by applying the test  $t$ . The following results have been obtained:  $\bar{X} = 5.74 \times 10^{-1}$ ;  $A = 5.68 \times 10^{-1}$  and  $t_{calcd} = 2.25$ . Since  $t_{calcd} = 2.25 < t_{tab} = 2.31$  ( $P = 95\%$ ;  $k = 8$ ), the two data do not differ from the statistical point of view, a fact that leads us to the conclusion that the proposed method is accurate.

The described method has been used also for the determination of traces of Pb in waste water samples from electroplating baths as well as in the determination of small amounts of Pb ( $< 1\%$ ) in brass samples.

**Conclusions.** The method is characterized by simplicity and rapidity.

The experimental results prove that it has a high precision and accuracy.

The method can be easily and efficiently applied to an industrial laboratory.

#### REFERENCES

1. A. Kuntze, *Galvanotehnik*, **60**, 802 (1969).
2. P. W. Wild, *Galvanotehnik*, **60**, 757 (1969).
3. J. Royon and M. T. Descarson, *Trait. Surface*, **12**, 27 (1971); cf. Chem. Abstr., **75**, 126042 (1971).
4. P. N. Kovalenko, *Uchenye Zapiski Rostov-no-Donu Univ.*, **41**, (1958).
5. A. Frank Lupino, *Plating*, **52**, 44 (1965); cf. Chem. Abstr., **62**, 12426 (1965).
6. M. V. Mahmud, J. Rains and D. Cote, *Anal. Sci.*, **2**, 311 (1986).
7. A. M. Bond, R. W. Knight and O. M. G. Newman, *Anal. Chem.*, **60**, 2445 (1988).
8. T. G. Mashchenko, *Technol. Organ. Proizvod.*, **1**, 49 (1980).
9. P. L. Buldini, P. Saxena, V. Saxena and A. Poponi, *Analyst* (London) **115**, 1073 (1990); cf. *Anal. Abstr.*, **53**, 4E 12 (1991).
10. A. N. Lavrona and V. A. Belyaev, *Tr. Mosvodokanalnii proiect*, **1**, 197 (1977); cf. *Chem. Abstr.*, **91**, 44134 (1980).
11. E. Hopirtean and M. Horn, *Revista de Chimie*, **41**, 252 (1990).
12. I. M. Kolthoff and Ph. J. Elving, *Treatise on Analytical Chemistry, Analytical Chemistry of the Elements*, Part II, Vol. 6, Interscience Publishers, J. Wiley and Sons, New York, p. 101 (1966).
13. E. B. Sandell, *Colorimetric Determinations of Traces of Metals*, Interscience Publishes, Inc., New York, p. 555 (1959).
14. F. L. Hahn and G. Weiller, *Z. Analyt. Chem.*, **69**, 417 (1926).
15. C. Liteanu and E. Hopirteanu, *Chimie analitică cantitativă. Volumetrie*. Ed. Didactică și Pedagogică, București, p. 17–23 (1972).



## OXYGEN ELECTROREDUCTION BY CYCLIC VOLTAMMETRY AND CHRONOPOTENTIOMETRY

ELENA M. PICĂ\*, ILEANA TEUCA\*\*

**ABSTRACT.** The electroreduction of oxygen by cyclic voltammetry method has been studied in comparison with chronopotentiometric one on stationary silver gold and carbon paste electrodes.

One wave has been obtained on silver and two waves on gold and carbon paste respectively, in 1 M KCl and 1 M KCl + 0,01 M KOH solutions, saturated with air.

**Introduction.** The electrochemical reduction of oxygen has been studied by cyclic voltammetry [1-4] both on stationary and rotating electrodes and by chronopotentiometry on stationary platinum [5-7], paladium [6-8] and gold [9] electrodes, respectively.

Although the mechanism of this electroreduction has not been yet completely elucidated, it is admitted that regarding this mechanism the electrodic materials used may be divided in two distinct groups, namely [10, 11]: a.) platinum, platinum group metals (Pd, Rh, Ir), silver and nickel. The reduction of oxygen at their surface takes place in two paralel reaction: in „direct”, one step reduction to water and the “succesive”, two step reduction with the intermediate formation of hydrogen peroxide, and b.) gold, mercury and carbon based electrodes: the reduction of oxygen at their surface occurs only as a result of two step “succesive” reaction with the formation of hydrogen peroxide.

The paper presents a comparative study of reduction of oxygen by cyclic voltammetry and chronopotentiometry on stationary electrodes used at the manufacturing of sensors for the determination of dissolved oxygen.

**Results and discussions.** The cyclic voltammetric and chronopotentiometric reduction curves of oxygen on silver, exhibit only one wave, corresponding to the direct reduction of oxygen to water, in both electrolyte media (Figures 1 and 2; curves 1 and 2).

The half-peak potentials determined from voltammetric curves are displaced towards more negative values in the 1 M KCl solution as compared to the 1 M KCl + 0,01 M KOH solution (Table 1), showing that the process is more reversible in the case of 1 M KCl + 0,01 M KOH. The same behaviours has been encountered from the potentials at  $\tau/4$ , determined from chronopotentiometric curves, (Table 1). As a consequence, a decrease of reduction overvoltage of oxygen takes place with the increase of the pH value, in accordance with the literature [11] data.

\* Technical University, Department of Chemistry, B-dul Muncii 105, 3400 - Cluj-Napoca, Roumania.

\*\* Institute of Chemistry, Str. Fântânelor 30, 3400 - Cluj-Napoca, Roumania.

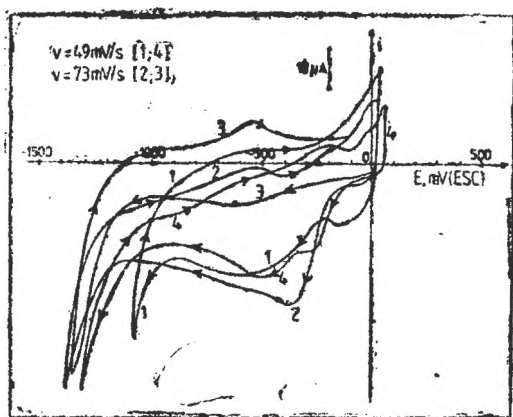


Fig. 1. Cyclic voltammograms of the reduction of oxygen on Ag in air saturated solution: 1 M KCl (1), 1 M KCl + 0,01 M KOH (fresh surface (2) and aged surface (4)), and the cyclic voltammogram of Ag in 1 M KCl + 0,01 M KOH, deaerated with purified Ar (3), respectively.

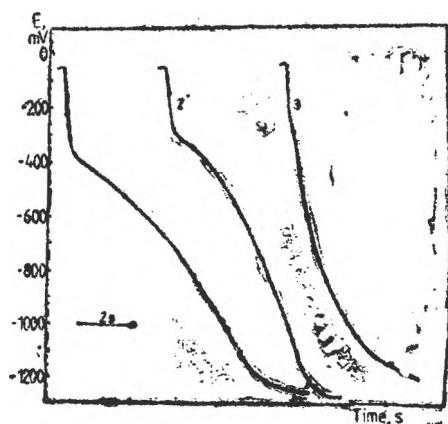


Fig. 2. Chronopotentiograms of the reduction of oxygen on Ag in air saturated solutions: KCl 1 M (1), KCl 1 M + KOH 0,01 M (2) and the chronopotentiogram of Ag in KCl 1 M solution deaerated with purified Ar (3), respectively.

With the aging of the surface two peaks (Figure 1, curve 4) can be observed on the cyclic voltammograms, with the half-peak potentials between  $(-193,0) - (-225,0)$  mV for the first, and  $(-351) - (420)$  mV for the second wave, respectively. In the region of the anodic scanning for negative potentials, only one peak is observed at  $(-184,0)$  mV, that doesn't correspond to a reversible oxidation  $H_2O_2/O_2$ . These data confirm the mechanisms presented in literature.

The curves of reduction of oxygen on gold, registered both by cyclic voltammetry and chronopotentiometry, exhibit two waves, corresponding to the two steps reduction of oxygen in the two electrolyte media (Figures 3 and 4, curves 1 and 2).

From the voltammetric curves, for the first reduction wave, the determined half-peak potentials are more negative in 0,1 M KCl solution than in the 1 M KCl + 0,01 M KOH solution (Table 1), resulting that the process is more rapid and more reversible in basic medium. For the second reduction wave the half-peak potentials are more positive in the 1 M KCl solution than in the 1 M KCl + 0,01 M KOH solution (Table 1), indicating that the process is slower and more irreversible in alkaline medium. For both waves the results are in good agreement with the chronopotentiometric ones, (Table 1). As a result, the overvoltage of the oxygen reduction to hydrogen peroxide decreases with the increase of pH, while the overvoltage of the reduction of hydrogen peroxide to water increases with the increase of pH.

The curves of the reduction of oxygen on carbon paste, registered by cyclic voltammetry or chronopotentiometry present two reduction waves in both electrolyte media. (Figures 5 and 6, curves 1 and 2).

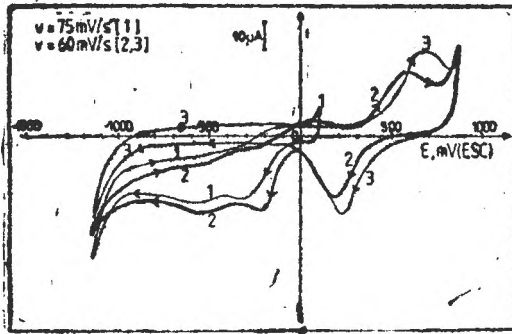


Fig. 3. Cyclic voltammograms of the reduction of oxygen on Au in air saturated solutions: KCl 1 M (1), KCl 1 M + KOH 0,01 M (2) and the cyclic voltammogram of Au in KCl 1 M + KOH 0,01 M deaerated with purified Ar (3), respectively.

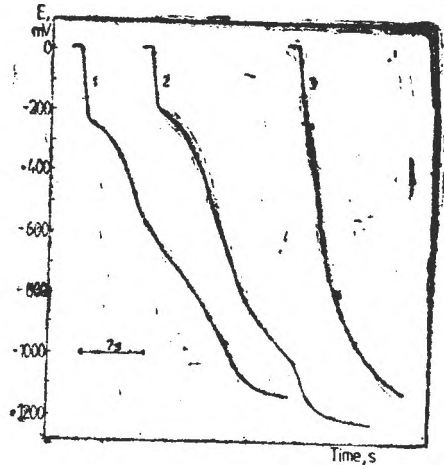


Fig. 4. Chronopotentiograms of the reduction of oxygen on Au in air saturated solutions: KCl 1 M (1), KCl 1 M + KOH 0,01 M (2) and the chronopotentiogram of Au in KCl 1 M solution deaerated with purified Ar (3), respectively.

The half-peak potentials determined from the voltammograms for the two waves are more negative in 1 M KCl + 0,01 M KOH solution than in 0,1 M KCl solution (Table 1). The values of the potentials are not in agreement with those obtained in the case of chronopotentiometry (Table 1). Thus, the

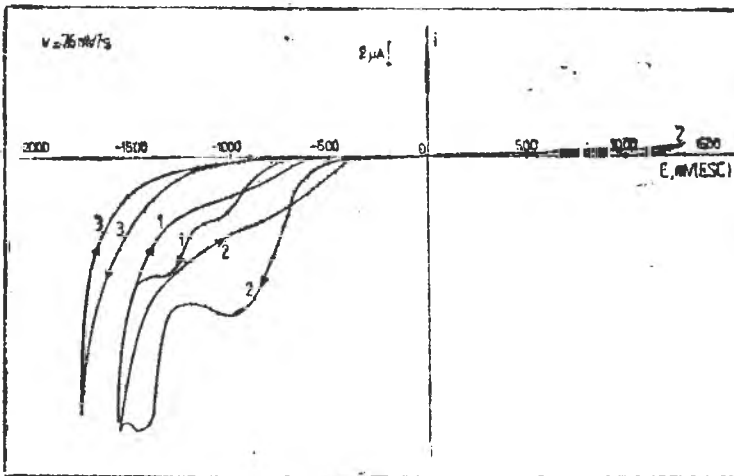


Fig. 5. Cyclic voltammograms of reduction of oxygen on carbon paste in air saturated solution: KCl 1 M (1), KCl 1 M + KOH 0,01 M (2) and the cyclic voltammogram of the carbon paste in KCl 1 M solution deaerated with purified Ar (3), respectively.

Experimental values of the half-peak and  $\tau/4$  voltages for different electrode materials and electrolyte solutions, saturated with air; T = 293 K.

Electrode material	Half-peak potential ( $E_{p/2}$ ) in mV*, determined from voltammograms				$\tau/4$ voltages, in mV* determined from chronopotentiograms			
	1 M KCl		1 M KCl + 0,01 M KOH		1 M KCl		1 M KCl + 0,01 M KOH	
	$O_2/H_2O_2$	$H_2O_2/H_2O$	$O_2/H_2O_2$	$H_2O_2/H_2O$	$O_2/H_2O_2$	$H_2O_2/H_2O$	$O_2/H_2O_2$	$H_2O_2/H_2O$
Silver	298-371	( $O_2/H_2O$ )	252-259	( $O_2/H_2O$ )	327-380	( $O_2/H_2O$ )	300-336	( $O_2/H_2O$ )
Gold	200-210	464-482	144-235	473-587	215-245	533-593	202-231	835-925
Carbon paste	800-1055	1283-1357	1050-1185	1434-1534	1190-1350	1380-1520	1050-1260	1270-1440

\* All values in the Table are negative.

values of the half-peak potentials determined from the voltammogram show that the overvoltage of the reduction of hydrogen peroxide increases with increase of the pH, while the values of the potentials determined from the chronopotentiograms illustrate that the overvoltage of reduction of hydrogen peroxide decreases with the increase of the pH.

In solution free of oxygen, the cyclic voltammograms of silver and gold exhibit two peaks, one anodic and other cathodic, corresponding to the formation and reduction of the oxides on the surface, respectively (Figures 1 and 3, curve 3). The chronopotentiograms of silver and gold present (at the voltage of  $\sim 400$  mV) a wave (curves 3, figures 2 and 4) attributed to the reduction of oxides formed on the two surfaces. In the case of carbon paste electrode, neither the voltammograms, nor the chronopotentiograms, do not exhibit peaks, indicating the formation of oxides (Figures 5 and 6, curves 3).

**Experimental.** A common used experimental setup for cyclic voltammetry [12] and for amperostatic chronopotentiometry [13] was used.

The working electrodes were a silver wire electrode of  $r_0 = 4 \cdot 10^{-3}$  m radius and  $A = 0,2059 \cdot 10^{-4}$  m<sup>2</sup> area and carbon paste disc electrode (CPE) of  $r_0 = 1,5 \cdot 10^{-3}$  m radius, and  $A = 7,065 \cdot 10^{-6}$  m<sup>2</sup>. As auxiliary electrode served a platinum helix with  $A = 12,59 \cdot 10^{-4}$  m<sup>2</sup> area and as reference electrode the saturated calomel electrode (SCE) through Luggin capillary.

The studies have been focussed on the reduction of oxygen on untreated electrodes, in 1 M KCl and 1 M KCl + 0,01 M KOH solutions, saturated with air. The cyclic voltammograms have been registered at constant scanning rates, ranging between 42–84 mV/s. The chronopotentiograms have been registered at five constant values of the current, between  $1,6 - 5,0 \cdot 10^{-6}$  A, with 5–6 measurements at each value of the applied current.

The cyclic voltammograms on silver, gold and carbon paste electrodes have been obtained in same solution deaerated with purified argon.

The half-peak potentials ( $E_{p/2}$ ) [12], corresponding to the half-wave potential in polarography, has been calculated from the voltammograms. The transition time  $\tau$  have been calculated from the chronopotentiograms using the Kuwana method described by Russel and Petterson [14]. The  $\tau/4$  voltages, corresponding to the half-wave potential in polarography was calculated with the equation of Karagianof [15, 16].

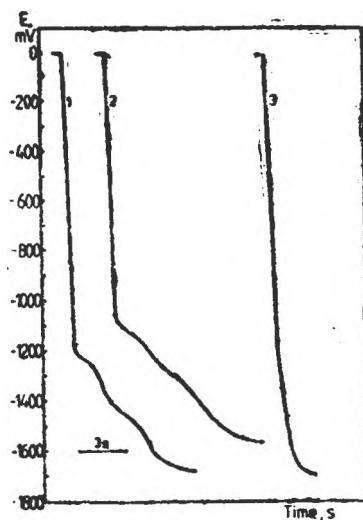


Fig. 6. Chronopotentiograms of the reduction of oxygen on carbon paste in air saturated solution: KCl 1 M (1), KCl 1 M + KOH 0,1 M (2) and the chronopotentiogram of the carbon paste in KCl 1 M solution deaerated with purified Ar (3), respectively.

#### REFERENCES

1. Brezina M., Koryta J. and Musilova M., *Coll. Czech. Chem. Commun.* 1968, **33**, 3397–4013.
2. Koryta J., Brezina M. and Kriz N., *Rev. Roum. Chim.*, 1972, **17**, 171–196.
3. Elzing H., Van Der Putten A., Visscher W. and Barendrecht E., *J. Electroanal. Chem.*, 1987, **233**, 99–108.

4. Paliteiro C., *J. Electroanal. Chem.*, 1987, **233**, 147–151.
5. Lingane J. J., *J. Electroanal. Chem.*, 1961, **2**, 296–309.
6. Sawyer D. T., and Interante I. V., *J. Electroanal. Chem.*, 1961, **2**, 310–327.
7. Peters D. G., and Mitchell R. A., *J. Electroanal. Chem.*, 1965, **10**, 306–318.
8. Blackburn T. R. and Lingane J. J., *J. Electroanal. Chem.*, 1963, **5**, 210–235.
9. Evans D. H. and Lingane J. J., *J. Electroanal. Chem.*, 1963, **6**, 283–299.
10. Fischer P. and Hetbaum J., *J. Electroanal. Chem.*, 1980, **112**, 231–242.
11. Tarasevich M. R., Sadkowskii A. and Yeager E., *The Electrochemistry of Oxygen in Comprehensive Treatise of Electrochemistry* Conway B. E., Bockris J. O'M., Yeager E., Khan S. U. M. and White R. E. (editors), vol. 7. New York -- London, 1983, 301.
12. Teuca I., *Cercetări privind perfecționarea senzorului de oxigen și lărgirea domeniilor de utilizare în economia noastră* — teză de doctorat Univ. „Babeș-Bolyai” Cluj-Napoca, 1990.
13. Pică E. M., *Elaborarea și studiul unui senzor electrochimic pentru determinarea continuă a oxigenului* — teză de doctorat, Univ. „Babeș-Bolyai” Cluj-Napoca, 1990.
14. Russel C. D. and Petterson J. M., *J. Electroanal. Chem.* 1963, **5**, 467–476.
15. Adams R. N., *Electrochemistry at Solid Electrodes*, M. Dekker Inc., New York, 1969, 165–186.
16. Pică E. M. and Kékedy L., *Rev. Chim.*, 1989, **40**, 910–915.

## INTERACTION OF SOME DRUGS WITH MONOMOLECULAR MEMBRANES AT THE FLUID INTERFACES

MARIA TOMOAIÀ-COTIȘEL\*, E. CHIFU\*\*, J. ZSAKÓ\*\*, P. T.  
FRANGOPOL\*\*\*, P. J. QUINN\*\*\*\*, AURORA MOCANU\*\*

**ABSTRACT.** — By compressing stearic acid monolayers spread onto aqueous solutions of different pH values and containing procaine and Gerovital H<sub>3</sub>, respectively, the penetration of these drugs into the stearic acid monolayer was studied, by using Gibbs' equation. This penetration is more important in the case of Gerovital H<sub>3</sub> as component to pure procaine.

**Introduction.** Adsorption of soluble surfactants at the air/water interface may be increased by the presence of a monolayer of insoluble surfactant. This phenomenon is frequently called monolayer penetration [1].

Compression isotherms, i.e. surface pressure ( $\pi$ ) vs. mean molecular area ( $A$ ) curves of stearic acid (SA) monolayers spread at the air/aqueous solution interface show that drugs as procaine ( $P$ ) or gerovital H<sub>3</sub> ( $G$ ) dissolved in the subphase have an important influence upon the behaviour of the SA monolayer.  $P$  and especially  $G$  have an expanding and fluidizing effect upon the SA monolayer and in addition they stabilize the monolayer, i.e. increase its collapse pressure [2]. These phenomena are presumed to be due to the penetration of drug molecules into the SA monolayer.

**Experimental.** Surface tension of aqueous solutions of procaine chlorhydrate of different concentrations is measured by using du Nouy's ring method.

Compression isotherms of SA monolayers are recorded by using the Wilhelmy method. In these experiments both buffered and unbuffered subphases were used, i.e. measurements were performed at pH = 2, ensured by 10<sup>-3</sup> M HCl, at pH values comprised between 4 and 5.6 as generated by the dissolved procaine chlorhydrate, and at pH = 8 ensured by phosphate buffered solution.

The concentration of  $P$  in the subphase was varied between 0 and 10<sup>-2</sup> M.

In the case of gerovital H<sub>3</sub> having  $P$  as active component in the subphase the  $P$  concentration was of 10<sup>-3</sup> M. All measurements were performed at 22°C.

**Results and discussion.** Surface tension ( $\sigma$ ) of  $P$  solutions of different concentrations ( $c_2$ ) was plotted vs.  $\ln c_2$ , allowing us to derive the procaine adsorption ( $\Gamma_2^c$ ) by means of Gibbs' equation:

$$\Gamma_2^c = - \frac{1}{kT} \left( \frac{\partial \sigma}{\partial \ln c_2} \right)_T \quad (1)$$

\* National Institutes of Health, Physical Biology Laboratory, Bethesda, Maryland 20892, USA.

\*\* Department of Physical Chemistry, University of Cluj-Napoca, 3400 Cluj-Napoca, Romania.

\*\*\* Institute of Physics and Nuclear Engineering, PO Box MG-6, R-76900, Măgurele-Bucharest, Romania.

\*\*\*\* Department of Biochemistry, King's College London, Campden Hill, London W8 7AH, U.K.

where  $k$  and  $T$  stand for Boltzmann's constant and absolute temperature, respectively.  $P$  adsorptions calculated for a subphase  $P$  concentration  $c_2 = 10^{-3}$  M are presented in Table 1.

Table 1

$P$  adsorption at  $c_2 = 10^{-3}$  M, and mean molecular area at saturation, as function of pH values.

pH	2	4.3	8
$\Gamma_2^s \cdot 10^{18}$ , molec./cm <sup>2</sup>	0.267	0.694	1.463
$A_2$ , nm <sup>2</sup> /molec.	2.07	1.96	0.91

As seen in Table 1,  $\Gamma_2^s$  increases very much with increasing pH values. This is due to the protolytic equilibria in which participate the  $P$  molecules. At pH = 2 in the subphase there are almost equal amounts of protonated  $PH^+$  and double protonated  $PH_2^{2+}$  molecules. At pH = 4.3, practically  $PH^+$  is the only species. At pH = 8 besides  $PH^+$  there is a considerable amount of neutral  $P$  molecules. Therefore, results presented in Table 1 are very reasonable since the increase of the surface activity may be expected in the order  $PH_2^{2+} < PH^+ < P$ .

From the maximum adsorption, derived by means of the least square method from the linear portion of the  $\pi$  vs.  $\ln c_2$  curve obtained at high  $c_2$  values, the mean molecular area  $A_2$  of  $P$  can be calculated. These values are also indicated in Table 1. In view of their interpretation molecular models were constructed and area necessities were calculated for the  $P$  molecule in a vertical position, perpendicular to the air/water interface, and for its horizontal-lying down position. By comparing the calculated molecular area values of  $P$  in different conformations and for different modes of packing in the surface lattice with those presented in Table 1 one may conclude that  $P$  is adsorbed at the air/water interface in a horizontal position.

The influence of the subphase drugs upon the behaviour of SA monolayers was studied by recording the compression isotherms of the monolayers. As an example, in Fig. 1 such compression isotherms are shown in the case of subphase having pH = 4.3. Both in the absence of subphase drugs (curve 1) and in their presence (curves 2 and 3), the isotherms exhibit two linear portions corresponding to the solid state (S) of the SA monolayer (at high  $\pi$  values) and to the liquid condensed state (LC) of the monolayer (at intermediate  $\pi$  values), and at compression the LC  $\rightarrow$  S phase transition occurs at about the same surface pressure of 26 mN/m, as observed also at pH = 2 [2].

The presence of  $P$  in the subphase ( $c_2 = 10^{-3}$  M, curve 2) entails a shift of the isotherm towards higher  $A$  values, i.e.  $P$  has an expanding effect. The slope of the linear portions is less than with curve 1, indicating the fluidizing effect of  $P$  upon the SA monolayer (its compressibility is increased).

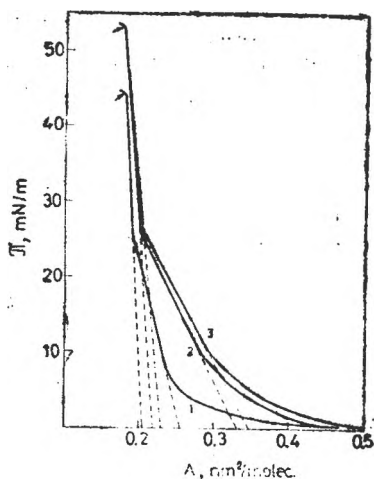


Fig. 1. Compression isotherms of SA monolayers; pH = 4.3  
 Subphase: 1—without drugs;  
 2— $10^{-3}$  M, P;  
 3—G( $10^{-3}$  M in P).

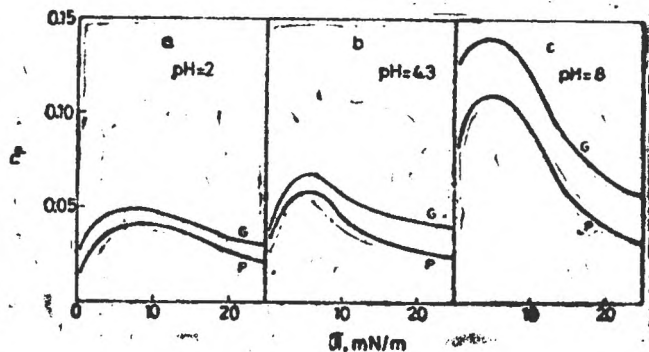


Fig. 2. The  $n_p$  values for P and G as function of  $\pi$ .

Further, one observes that the collapse area  $A_c$  is not affected but the collapse pressure  $\pi_c$  (see arrows in Figure 1) is considerably increased. These phenomena may be explained in the following way:  $P$  penetrates into the SA monolayer, leading to the increase of  $A$ . At compression, at large  $\pi$  values, the  $P$  molecules may be squeezed out from the monolayer, since  $A_c$  has practically the same value in all cases. Presumably, the expelled  $P$  molecules form a subjacent monolayer, which interacts with the SA monolayer, leading to the increase of  $\pi_c$ .

In the case of gerovital  $H_3$  (curve 3), the effects are similar to those observed with  $P$ , but they are a little higher, showing that  $P$  penetration into the SA monolayer is increased by the ingredients of  $G$ .

In order to obtain information concerning the amount of  $P$  penetrated into the monolayer, the Gibbs' equation adapted to the presence of a monolayer of insoluble surfactant [1, 3] was used. At constant mean molecular area ( $A$ ) of the insoluble surfactant ( $A = A_3$ ), the adsorption of the soluble surfactant  $\Gamma_2$  per unit area of the interface not covered by insoluble surfactant molecules is the following:

$$\Gamma_2 = \frac{1}{kT} \left( \frac{\partial \pi}{\partial \ln c_2} \right) A_3, T \quad (2)$$

The adsorption per unit area of the interface can be obtained as:

$$\Gamma_2 = \Gamma_2' (1 - \bar{A}_3/A_3) \quad (3)$$

where  $\bar{A}_3$  stands for the partial molecular area of the insoluble surfactant.

We presumed that  $\bar{A}_3$  can well be approximated by the collapse area of SA.

From compression isotherms of SA monolayer recorded on subphases with varying  $P$  concentrations  $\Gamma_2$  values can be derived by using Eqs. (2) and (3). Results are summarized in Table 2.

Table 2

$P$  adsorption ( $\Gamma_2 \cdot 10^{-12}$ , molee/cm<sup>2</sup>) at  $c_2 = 10^{-3}$  M as function of  $A_2$  and pH.

pH	$A_2$ , nm <sup>2</sup>				
	50	40	30	25	20
2	0.41	0.59	1.54	0.90	0.42
4.3	0.58	1.09	1.79	1.34	0.25
8	2.12	2.06	1.39	0.87	0.27

By comparing  $\Gamma_2$  values with  $\Gamma_2^0$  values presented in Table 1, one can see that the  $P$  adsorption is generally enhanced in the presence of the SA monolayer. Further, one observes that the maximum  $\Gamma_2$  value increases with increasing pH, similarly as  $\Gamma_2^0$  values (see Table 1).

These results enable us to calculate the ratio between the number of  $P$  and of SA molecules per unit area, which will be referred to as penetration number ( $n_p$ ). For subphases with  $c_2 = 10^{-3}$  M the maximum  $n_p$  values at pH = 2; 4.3 and 8 are equal to  $n_p = 0.045$ ; 0.058 and 0.11, respectively.

For other systems, penetration number values were derived also from the mean molecular area increments  $\Delta A$  observed at constant  $\pi$  values [4] as  $n_p = \Delta A/A_2$ , where  $\Delta A$  represents the difference between the mean molecular area of the insoluble surfactant in the presence and in the absence of the drug, measured at the same  $\pi$ , and  $A_2$  stands for the molecular area of the drug. We derived a more correct expression (by presuming that in the monolayer the molar fraction of water is a unique function of  $\pi$ ), viz.:

$$n_p = \Delta A / (A - A_3 + A_2) \quad (4)$$

where  $A_2$  and  $A_3$  stand for the actual area necessity of the soluble and of the insoluble surfactant molecules, respectively.

The penetration number values were derived by means of Eq. (4) from the compression isotherms recorded in the absence of surfactant drugs in the aqueous subphase, on subphases containing  $10^{-3}$  M procaine, and on G-containing subphases, the  $P$  concentration being also  $10^{-3}$  M. In these calculations  $0.18 \text{ nm}^2$  was taken for  $A_3$ . In the case of  $A_2$  for  $\pi = 0$  the  $A_2 = 1.5 \text{ nm}^2$  value was taken and  $A_2$  was presumed to be a linear function of  $\pi$ , at the phase transition of SA becoming equal to  $0.4 \text{ nm}^2$ .

The  $n_p$  values calculated by means of the above procedure are visualized in Figure 2. As a general feature one observes that  $n_p$  has a maximum at about 5 mN/m. This maximum value obtained for  $P$  is in very good agreement with the  $n_p$  value derived above for  $10^{-3}$  M  $P$  solutions by means of the Gibbs' Equation.

Further, one observes that the penetration is more important in the case of  $G$  as compared to  $P$ . The increase of pH entails increasing of  $n_p$ , indicating that neutral  $P$  molecules penetrate more easily into the SA monolayers, than the cationic species do.

#### REFERENCES

1. Pethica, B. A., *Trans. Faraday Soc.*, **51**, 1402 (1955).
2. Tomoaia - Cotisel, M., Chifu, E., Mocanu, A., Zsakó, J., Sălăjan, M., Frangopol, P. T., *Rev. roumaine Biochim.*, **25** (3), 227 (1988).
3. Nakagaki, M., Okamura, E., *Bull. Chem. Soc. Japan*, **55**, 1332 (1982).
4. Seelig, A., *Biochem. Biophys. Acta*, **539**, 196 (1987).



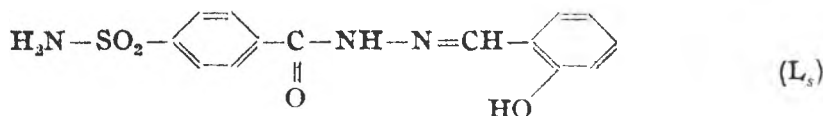
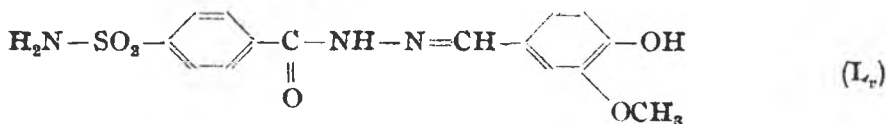
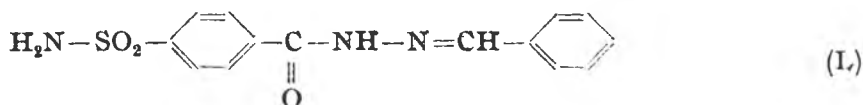
METAL COMPLEXES WITH HIDRAZONE TYPE  
LIGANDS. III. SYNTHESIS AND ESR SPECTRA  
OF CU(II) COMPOUNDS WITH  
SULFONAMIDOBENZHYDRAZONES

LUMINIȚA SILAGHI-DUMITRESCU\*, RADU SEMENIUC\* and RODICA  
MICU - SEMENIUC\*

**ABSTRACT.** Cu(II) complexes of the type  $\text{CuX}_2(\text{Lig})_2$ ,  $\text{CuX}(\text{Lig})$  and  $\text{Cu}(\text{Lig})_2$ , where X =  $\text{NO}_3$ , Cl, Br and Lig = benzhydrazone type ligands have been synthesized and characterized by elemental analysis, infrared and ESR spectra. Isotropic spectra were found for  $\text{Cu}(\text{NO}_3)_2(\text{L}_v)_2$ ,  $\text{Cu}(\text{L}_s)_2$  and  $\text{CuBr}(\text{L}_s)$  and axial symmetry for the other compounds.

**Introduction.** The coordination behavior towards metals of the ligands with known or potential biologic activity has been in our attention for several years [1-5]. After the solution studies of Co(II) and Ni(II) complexes [4] and the synthesis and characterization of  $\text{UO}_2(\text{II})$  complexes [4, 5] with sulfonamidobenzhydrazone ligands we report now the synthesis and ESR spectra of some Cu(II) complexes of the same ligands.

The title compounds have been synthesised by reacting  $\text{CuX}_2$  (X =  $\text{NO}_3$ , Cl, Br) with the following sulfonamidobenzhydrazone ligands:



**Results and discussion.** The reaction of sulfonamidobenzhydrazone ligands mentioned above with Cu(II) salts lead to three types of compounds (according to the elemental analysis):  $\text{CuX}_2(\text{Lig})_2$  where Lig = L and  $\text{L}_v$  and X =  $\text{NO}_3$  and Cl,  $\text{CuX}(\text{Lig})$ , for Lig =  $\text{L}_s$  and X = Cl and Br and  $\text{Cu}(\text{L}_s)_2$ . The last

\* University of Cluj-Napoca, Chemistry Department, 3400 Cluj-Napoca, Roumania.

two types of compounds were obtained with the anionic form of the  $L_v$  ligand in basic solutions. The data regarding the synthesis, elemental analysis and some physical properties of the complexes are listed in Table 1. Infrared and ESR spectra are discussed for the synthesised compounds.

Table 1

Elemental Analysis and Physical Properties of the Title Compounds

Compound	CuX <sub>2</sub> (g)	Ligand (g)	M.p. (d) (°)	Colour	% (found/calculated)		
					Cu	N	halogen
1. Cu(NO <sub>3</sub> )(L <sub>v</sub> ) <sub>2</sub>	0.06	0.15	(220d)	green-brown	8.43/8.00	13.86/14.11	—
2. Cu(NO <sub>3</sub> ) <sub>2</sub> (L <sub>v</sub> ) <sub>2</sub>	0.12	0.34	128–130	green-brown	6.94/7.16	11.83/12.61	—
3. CuCl <sub>2</sub> (L <sub>v</sub> ) <sub>2</sub>	0.07	0.15	(100d)	dark-green	9.00/8.58	11.02/11.34	9.00/9.59
4. CuCl <sub>2</sub> (L <sub>v</sub> ) <sub>2</sub>	0.07	0.18	*	green-brown	7.90/7.61	9.83/10.06	8.25/8.50
5. CuBr <sub>2</sub> (L <sub>v</sub> ) <sub>2</sub>	0.16	0.15	(270d)	brown	7.08/7.66	—	19.00/19.28
6. CuBr <sub>2</sub> (L <sub>v</sub> ) <sub>2</sub>	0.16	0.18	(180d)	dark-green	7.40/6.88	8.71/9.09	17.80/17.02
7. Cu(L <sub>s</sub> ) <sub>2</sub>	0.12	0.32	*	green	9.59/9.07	11.60/12.00	—
8. CuCl(L <sub>s</sub> )	0.07	0.16	*	green	15.20/15.23	9.92/10.07	17.60/17.02
9. CuBr(L <sub>s</sub> )	0.16	0.15	*	green	14.40/13.77	8.58/9.10	17.40/17.33

\* stable until 340°

**Infrared Spectra.** As expected, the IR spectra of the title compounds are very complex, due the organic groups present in the ligand molecules, the assignment of the bands being difficult. The comparison of the IR spectra of the starting materials (Cu(II) salts and sulfonamidobenzhydrazone) with the spectra of the Cu(II) complexes show changes in the range of  $\nu(\text{NH}_2)$  and  $\nu(\text{C}=\text{O})$  frequencies. The shift of the  $\nu(\text{NH}_2)$  in the spectra of compounds (1) and (6) was related to a coordination through a sulfonamidic groups [6]. For the complexes with the ligand  $L_v$  changes in the position of  $\nu(\text{C}=\text{O})$  frequency were observed. The  $L_s$  ligand has a different behavior: the  $\nu(\text{O}-\text{H})$  stretching, present in the IR spectrum of the ligand is missing in the spectrum of the Cu(II) complexes (compounds 7, 8, 9), in accordance with the formation of Cu—O bonds. No other obvious changes were observed in the IR spectra of the compounds.

**ESR Spectra.** Isotropic spectra were obtained for compounds (2), (7) and (9) (Fig. 1) and spectra with axial symmetry for compounds (1), (3), (4) and (8) (Fig. 2). The parameters calculated from the ESR spectra are listed in Table 2.

Table 2

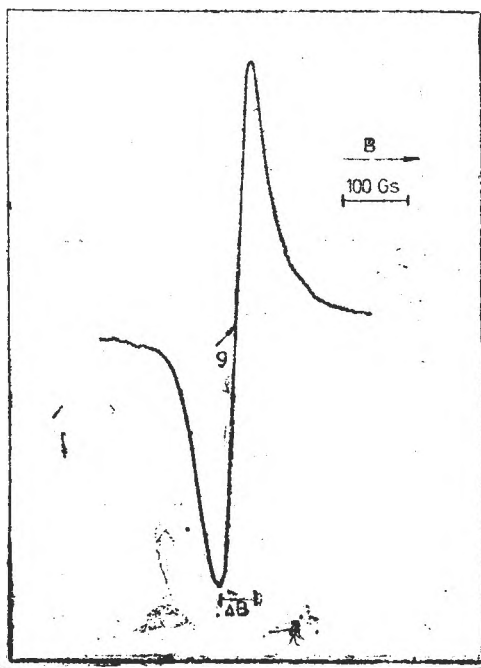
ESR spectra parameters

Compound	g	$\Delta B$ (GSS)	$I_{\parallel} / I_{\perp}$ (cm)
1. $\text{Cu}(\text{NO}_3)_2(\text{L}_s)_2$	2,036 2,25	58,70	6/13
2. $\text{Cu}(\text{NO}_3)_2(\text{L}_V)_2$	2,018	58,7	7/6,8
3. $\text{CuCl}_2(\text{L}_s)_2$	2,043 2,196	70,5	7/2/11,2
4. $\text{CuCl}_2(\text{L}_V)_2$	2,047 2,140	47	7/12,5
7. $\text{Cu}(\text{L}_s)_2$	2,054	35,2	8,8/11,2
8. $\text{CuCl}(\text{L}_S)$	2,050 2,170	53	6,5/10,5
6 $\text{CuBr}(\text{L}_S)$	2,073	205,6	8/9,2

The assignment of the local symmetry of the central ion was made in accordance with the literature data [7, 8]. (Fig. 3).

An octahedral symmetry ( $O_h$ ) with Jahn-Teller distortions usual for Cu(II) could be the source of the isotropic spectra. For nitrate containing compounds (1) the hexacoordination is most probably realised by a bidentate coordination of the nitrate groups (four sites) and the coordination of the ligand through the sulfonamidic groups (in accordance with the infra-red data) (Structure I). For  $\text{CuX}_2(\text{L}_V)_2$  ( $X = \text{Cl}, \text{Br}$ ) the organic ligand is coordinated via  $\text{C}=\text{O}$  and  $-\text{N}=\text{}$  groups (Structure I) with the two halogens in the axial position.

Either a tetra- or hexacoordination of the central ion can determine the presence of the ESR spectra with axial symmetry. A tetracoordination of Cu(II) was assigned for compound (7) (Structure III). The bridging of the chlorine in compound (3) can fulfill the coordination number six (Structure IV) accompanied by significant distortion. The smallest value of giromagnetic factor  $g$ , lower than 2.03 [7, 8] can be related to a tetragonal distortion compressed along the  $z$  axis. (compound 2).

Fig. 1. ESR spectrum of  $\text{Cu}(\text{NO}_3)_2(\text{L}_V)_2$ .

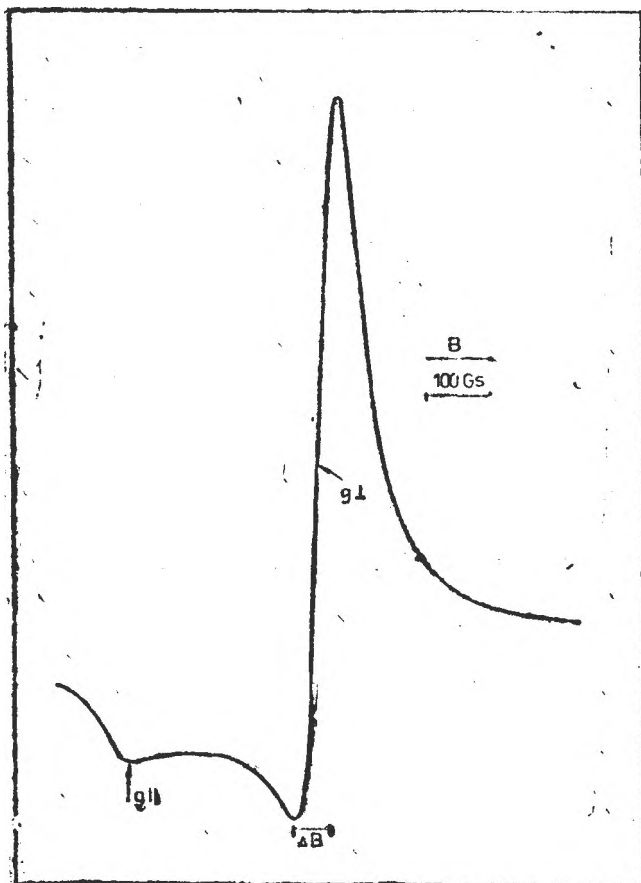


Fig. 2. ESR spectrum of  $\text{Cu}(\text{NO}_3)_2(\text{L})_2$ .

The structure of the compounds (8) and (9) can be represented by a square-planar geometry with bidentate organic ligand and bridging halogens (Structure V).

As a result of the distortions present in these molecules there are remarkable high differences between the values of  $I_{\parallel}$  and  $I_{\perp}$ . (Table 2.)

The values of  $\Delta B$  calculated from the ESR spectra, listed in Table 2. are in the range 35.2 Gss (compound 7) and 205.6 Gss (compound 9). The high values of  $\Delta B$  for the compound 9 suggest the presence of the magnetic interaction between the paramagnetic centers, via the halogen monoatomic bridges (Structure V). The  $\Delta B$  values for nitrate complexes are lower than for the halogen containing complexes (Table 2.), which can be related to the lower degree of covalence in the first case.

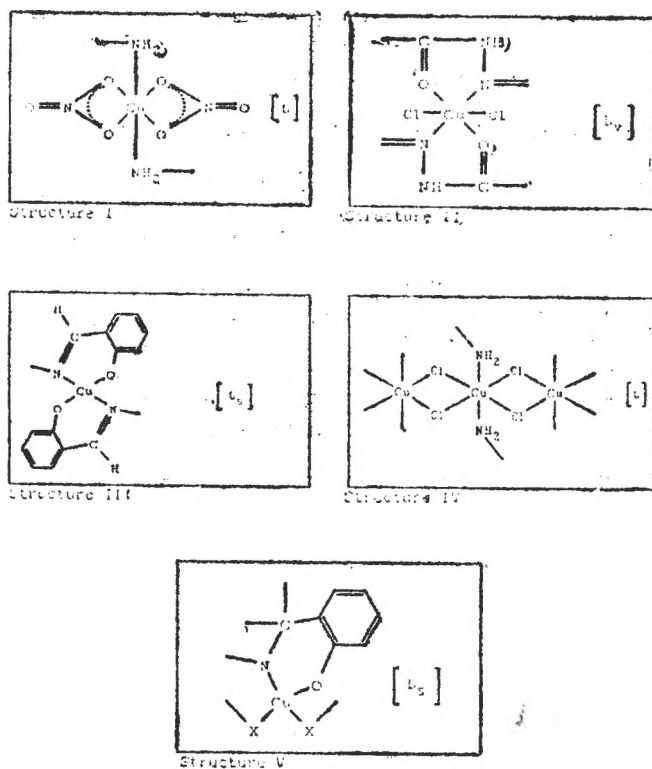


Fig. 3. Proposed structure of studied compounds.

**Experimental Part.** Copper (II) salts were commercial products of analytical grade purity. The sulfonamidobenzhydrazone ligands were synthesised according the literature data [9].

The synthesis of the complexes have been performed in ethanolic solutions, using stoichiometric amounts of the appropriate Cu(II) salt and ligand. The data concerning the synthesis, elemental analysis and some physical properties are summarised in Table I. For the synthesis of the complexes with the  $L_5$  ligand the ionisation of the  $-O-H$  group improved the yield, a found previously for  $UO_2(II)$  complexes [5]. Using the same ligand ( $L_5$  in anionic form, with no nitrate ion present) a complex with molar ratio 1 M: 2L ( $L_5$  in anionic form, with no nitrate ion present) was obtained at pH = 8 - 9 when  $Cu(NO_3)_2$  was the starting material, while  $CuX(L_5)$  type complexes were obtained for X = Cl, Br. This is in agreement with the coordination ability of the halogens compared to the nitrate anion.

The elemental analysis (Table I) were performed using Spacu method [10] for copper (II), reaction with  $AgNO_3$  for chlorides and bromides and combustion (micro-Dumas) method for the nitrogen.

Infrared spectra were recorded in KBr pellets with a Specord IR-75 Carl Zeiss Jena spectrophotometer and ESR spectra with a JES-3B apparatus, on polycrystalline powders, at room temperature.

## REFERENCES

1. R. Micu -- Semeniuc, L. Silaghi -- Dumitrescu and I. Haiduc, *Inorg. Chim. Acta*, **17**, 5 (1976).
2. R. Micu -- Semeniuc, L. Silaghi -- Dumitrescu and I. Haiduc, *Inorg. Chim. Acta*, **33**, 281 (1979).
3. R. Micu -- Semeniuc, S. Barbu and M. S. Mihaiu, *Rev. Roumaine Chim.*, **28**, 365 (1993).
4. R. Micu -- Semeniuc and L. Silaghi -- Dumitrescu, *Rev. Roumaine Chim.*, in press.
5. R. Micu -- Semeniuc and L. Silaghi -- Dumitrescu, *Revista de Chimie*, in press.
6. N. B. Colthup, L. H. Daly and S. E. Wiberly, *Introduction to Infrared and Raman Spectroscopy*, Academic Press, New York, 1964.
7. B. J. Hathaway and A. A. Thompson, *Coord. Chem. Rev.*, **5**, 1 (1970).
8. B. J. Hathaway and D. R. Billing, *Coord. Chem. Rev.*, **5**, 143 (1970).
9. \* \* \* *ORGANICUM. Chimie organică practică*, Scientific and Encyclopedic Publ., Bucharest, 1982, p. 424.
10. G. Spacu, *Bull. Soc. Sc. Cluj.*, **1**, 284, 314 (1921).

STUDY OF THE FORMATION OF  
HETEROPOLYMOLYBDOTUNGSTATES  
OF DAWSON-TYPE WITH La(III),  
Ce(III) AND Ce(IV) AS CENTRAL IONS

CRISTINA RAȚIU\*, MARIANA RUSU\*\*, ALEXANDRU BOTAR\*

**ABSTRACT.** The lanthanide ions Ce(III), La(III) and Ce(IV) react quite easily with unsaturated Dawson structure heteropolymolybdotungstates giving rise to heteropolycompounds of types  $ZL$  and  $ZL_2$ , where  $Z = Ce(III), La(III)$  and  $Ce(IV)$ , and  $L = P_3MoW_{10}O_{61}^{10-}$ . The conductometric, spectrophotometric and photocolometric investigations, performed by using the method of molar ratios, have pointed out that in all the three cases, heteropolycomplexes with two ratios of metal: ligand combination, of 1:1 and 1:2 respectively, are formed.

**Introduction.** As a result of the degradation with  $KHCO_3$  of the heteropolycompounds of the type  $K_6P_2W_{18}O_{62}$  with complete Dawson structure, the series of lacunary heteropolycompounds of the type  $K_{10}P_2W_{17}O_{61}$  with modified Dawson structure [1, 2] have been obtained. The absence of a  $WO_4^{2-}$  group from the structure of the lacunary heteropolyanions confers them an "unsaturated" character which manifests itself in a special affinity towards the di- and trivalent metal cations, with which  $ZX_2W_{17}O_{61}^{(10-z)-}$  are formed, where  $Z^{2+} =$  the di- or trivalent metal cation as a secondary heteroatom and  $X = P(V), As(V)$  as a primary heteroatom.

In these complexes, the ratio metal cation: heteropolyanion is 1:1.

Weakley and co-workers [3] previously reported that lanthanides and actinides, together with the "unsaturated" heteropolyanions of Dawson type, give rise to complexes with the ratio metal cation: heteropolyanion 1:2. In these complexes, the unsaturated heteropolyanion functions as a tetradentate ligand versus the secondary heteroatom  $Z$  with octahedral coordination capacity with eight oxygen atoms in a square antiprism.

More recently, R. Contant and co-workers [4] have extended the series of unsaturated heteropolyanions with Dawson structure to molybdotungstic heteropolyanions of  $K_{10}P_2MoW_{16}O_{61}$  type, which can be obtained from the saturated series  $\alpha-K_6P_2W_{18}O_{62}$  by reaction with  $Na_2MoO_4 \cdot 2H_2O$  at an acidic pH.

The present paper has aimed at investigating the action of the heteropolycompound  $K_{10}P_2MoW_{16}O_{61}$  on some lanthanide cations (La(III), Ce(III) and Ce(IV)), thus establishing both the stoichiometry of the compound formation reactions and the chemical individuality of the series of the complexes formed.

\* Institute of Chemistry Cluj-Napoca, Romania.

\*\* Faculty of Chemistry and Chemical Engineering, University "Babeș-Bolyai" Cluj-Napoca, Romania.

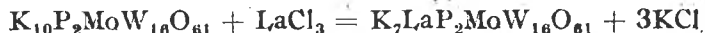
**Experimental.** The extinction of the mixtures formed from the colourless solution of  $\text{LaCl}_3 \cdot 7\text{H}_2\text{O}$  with the concentration  $10^{-3}$  mol.  $\text{L}^{-1}$  and  $\text{K}_{10}\text{P}_2\text{MoW}_{16}\text{O}_{61} \cdot 19\text{H}_2\text{O}$  with the concentration  $10^{-3}$  mol.  $\text{L}^{-1}$ , have been determined spectrophotometrically, in different mole ratios. The measurements have been made on a Specord UV-VIS spectrophotometer by recording the extinction variations of the absorption band situated at  $48\,000\text{ cm}^{-1}$ .

The extinctions of the violaceous-brownish solutions containing the mixtures of  $\text{CeCl}_3 \cdot 7\text{H}_2\text{O}$  and  $\text{K}_{10}\text{P}_2\text{MoW}_{16}\text{O}_{61} \cdot 19\text{H}_2\text{O}$  with the concentrations  $5 \cdot 10^{-3}$  mol.  $\text{L}^{-1}$  and  $10^{-3}$  mol.  $\text{L}^{-1}$  respectively, in different mole ratios, have been determined photocolometrically by using a green filter, whereas the extinctions of the yellow solutions containing mixtures of the solutions  $\text{Ce}(\text{SO}_4)_3 \cdot 4\text{H}_2\text{O}$  and  $\text{K}_{10}\text{P}_2\text{MoW}_{16}\text{O}_{61} \cdot 19\text{H}_2\text{O}$  with the concentrations  $5 \cdot 10^{-3}$  mol.  $\text{L}^{-1}$  and  $10^{-3}$  mol.  $\text{L}^{-1}$  respectively, in different mole ratios, have been determined photocolometrically, this time by using a blue filter. A PEK-K-M photocolimeter has been used.

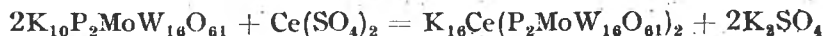
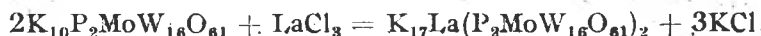
An A.T.C. 1100 conductometer (The Enterprises of Industrial Electronics and Automation, Cluj-Napoca, Romania) has been used for measuring the conductivities of the mixtures formed as a result of the reaction taking place between the solutions of  $\text{CeCl}_3 \cdot 7\text{H}_2\text{O}$ ,  $\text{LaCl}_3 \cdot 7\text{H}_2\text{O}$  and  $\text{Ce}(\text{SO}_4)_2 \cdot 4\text{H}_2\text{O}$  with the concentrations  $10^{-2}$  mol.  $\text{L}^{-1}$ , on one hand, with the ligand solution  $\text{K}_{10}\text{P}_2\text{MoW}_{16}\text{O}_{61} \cdot 19\text{H}_2\text{O}$  with the concentration  $10^{-3}$  mol.  $\text{L}^{-1}$ , in different molar ratios, on the other hand.

The UV spectra, characteristic to the studied ligand and complexes have been effected on solutions with concentrations  $10^{-5}$  mol.  $\text{L}^{-1}$ , and the recordings have been performed on a UV-VIS spectrophotometer.

**Results and Discussion.** Provided the solutions containing La(III), Ce(III) and Ce(IV) ions are added to solutions containing the molybdotungstic heteropolycompound, in different molar ratios, the following chemical reactions will take place quite rapidly:



respectively:



In order to study the formation in solution of the heteropolymolybdotungstates of the types  $\text{ZL}$  and  $\text{ZL}_2$ , where  $\text{Z} = \text{La(III), Ce(III) and Ce(IV)}$  and  $\text{L} = \text{P}_2\text{MoW}_{16}\text{O}_{61}^{10-}$ , conductometric, spectrophotometric and photocolometric studies have been completed through the agency of the method of molar ratios. The spectrophotometric study on the formation of  $\text{La(III)-L}$  and  $\text{La(III)-L}_2$  complexes, has revealed changes in intensity of the adsorption band at  $48\,000\text{ cm}^{-1}$ , shown in their absorption spectrum. The variation of the extinctions peculiar to  $\text{Ce(III)-L}$  and  $\text{Ce(III)-L}_2$  mixtures and also to  $\text{Ce(IV)-L}$  and  $\text{Ce(IV)-L}_2$  mixtures has been pursued photocolometrically, by using a green filter for the  $\text{Ce(III)}$  violaceous-brownish heteropolycomplex and a blue filter for the  $\text{Ce(IV)}$  yellow heteropolycomplex.

The extinction variation of the solutions containing mixtures of lanthanide-heteropoly ligand ions in different molar ratios, is shown in Fig. 1.

The curves drawn-up for the Ce(III) and Ce(IV) complexes consist of three segments crossing one another at a point corresponding to the two values obtained for the molar ratios metal cation : ligand 1 : 1 and 1 : 2. By examining the first and the second portion of the curves, it becomes apparent that the extinction increases proportionally with the increase of the concentration of the reaction products  $ZL$  and  $ZL_2$ . On the third portion of the curves, the increase of the extinction is slightly less as a result of the entrance of the lanthanide cation outside the coordination cavity of the heteropolycomplexes.

As a result of the slight curvature of the first inflexion point corresponding to the molar ratio metal cation : ligand of 1 :

1, a conductometric study has been effected in order to establish and confirm the stoichiometry of the formation reactions of the studied heteropolycomplexes also by using the molar ratio method.

The solutions of the reagents in different molar ratios have been mixed up and then their conductivities have been measured.

The conductivity variation depending on different molar ratios has been presented then in Fig. 2.

The conductometric curves, like the extinction ones, depending on the reagent molar ratio also consist of three seg-

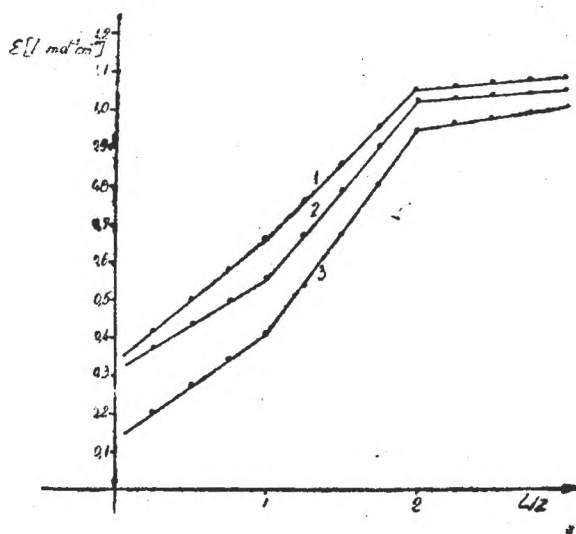


Fig. 1. The curves of the extinction variation of the mixtures formed from  $K_{10}P_2MoW_{16}O_{61}$  and La(III) (curve 1), Ce(III) (curve 2) and Ce(IV) (curve 3) in different molar ratios.

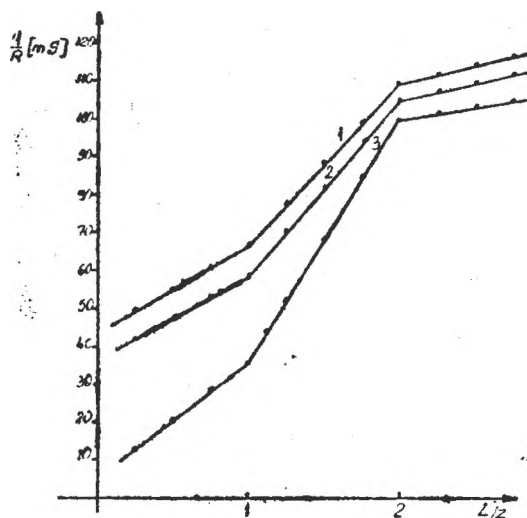


Fig. 2. The curves of the variation of the electric conductivity of the mixtures formed from  $K_{10}P_2MoW_{16}O_{61}$  and La(III) (curve 1), Ce(III) (curve 2) and Ce(IV) (curve 3) in different molar ratios.

ments that intersect in two points corresponding to the molar ratios metal cation : ligand of 1 : 1 and 1 : 2.

The first segment of the curves exhibit a rapid increase of the conductivity of the  $\text{Cl}^-$  and  $\text{SO}_4^{2-}$  ions, present within the system. A similar remark applies to the second segment of the curves, which also shows an increase of conductivity, corresponding to the formation of the second complex which is completed with a release of  $\text{Cl}^-$  and  $\text{SO}_4^{2-}$  ions. The third portion of the curve shows a less abrupt slope and hence, a diminished increase of the conductivity within the systems, which is due to the formation of hard-soluble salts, obtained as a result of the lanthanide cation entrance outside the coordination cavities of the heteropolyanions.

The spectrophotometric, photocolometric curves, as well as the conductometric titration curves prove that the equivalence point corresponding to the ratio of metal cation : ligand combination 1 : 1 is less outlined in contrast with that one corresponding to the ratio of metal cation : ligand combination 1 : 2. This is currently explained, in structural terms, by Weakley and co-workers [3] on the basis of the octahedral coordination of the lanthanide ions by two ligands  $\text{P}_2\text{MoW}_{16}\text{O}_{61}^{10-}$ , each of them contributing with four oxygen atoms shared with four different octahedral groups  $\text{WO}_6$ , with no participation of the inner oxygen shared by the tetrahedral group  $\text{PO}_4$  at the coordination.

In the complexes with the molar ratio metal cation : ligand 1 : 1, the lanthanide ion which is a rather big cation, being compelled to occupy the lacunary hole of a single ligand, thus encountering a steric hindrance which leads to the instability of the  $\text{ZL}$  compound and consequently facilitates the formation of the  $\text{ZL}_2$  compound.

The chemical individuality of the newly-formed species has been put into evidence by recording the UV spectra on solution, containing both the ligand and the mixtures formed by lanthanide cation : ligand in a ratio of 1 : 2. These spectra are characterized by a prominent absorption band titrated at  $48000\text{ cm}^{-1}$  for the ligand, due to the charge transfer from the terminal  $\text{M}=\text{O}$  groups, where  $\text{M} = \text{Mo}$  or  $\text{W}$  addendum atom. In the tail of these bands, we can notice a wider absorption band within the range  $34000\text{--}40000\text{ cm}^{-1}$  superimposed on the background and as such, concealing the two bands, specific to the compounds with unsaturated Dawson structure, at about  $34000\text{ cm}^{-1}$  and  $40000\text{ cm}^{-1}$  respectively. In the case of the anion  $\text{P}_2\text{MoW}_{16}\text{O}_{61}^{10-}$ , this band splits into two parts, occurring as two shoulders in the spectra of the studied ligand and heteropolycomplexes, see Table 1.

The attenuation of the absorption band and the absence of an absorption maximum within this range are due to the decrease of the symmetry of the ligand  $\text{L} = \text{P}_2\text{MoW}_{16}\text{O}_{61}^{10-}$ , as well as to the occurrence of some distortions in the polytungstic edifice, as a result of the mixed addenda  $\text{M}$  which have a strong effect on the charge transfer in  $\text{M}-\text{O}-\text{M}$  bonds (where  $\text{M} = \text{Mo}$  or  $\text{W}$ ).

The compensation of the defect structure in the lacunary heteropolyanions because of the complexation with lanthanide cations exerts a narrow influence on the UV absorption spectra and consequently, the same shape for the

Table 1

The electronic transition in the electronic spectra of  $L$  and  $ZL_n$ , where  
 $L = P_2MoW_{16}O_{61}^{10-}$  and  $Z = La(III), Ce(III)$  and  $Ce(IV)$

Complex	Absorption Band cm <sup>-1</sup>	Assignment
$L$	4800	charge-transfer M=O terminal
	42000 sh	charge-transfer M—O—M
	32200 sh	
$Ce(III)L_n$	48400	charge-transfer M=O terminal
	43800 sh	charge-transfer M—O—M
	33800 sh	
$Ce(IV)L_n$	48500	charge-transfer M=O terminal
	43900 sh	charge-transfer M—O—M
	33850 sh	
$La(III)L_n$	48800	charge-transfer M=O terminal
	44000 sh	charge-transfer M—O—M
	34000 sh	

complex and the ligand, that is, with a weaker maximum and a shift of the lacunary heteropolyanions within the complexes towards higher energies, is formed out, owing to the involvement of the oxygen atoms, out of the polyanions, in the lanthanide cation coordination, followed by a strengthening of the terminal bonds M=O engaged in the charge transfer. Henceforth, the complexation reaction brings about an increase in the symmetry of the heteropolyanions and a strengthening of the double bond M=O, thus displacing the absorption band from about 48000 cm<sup>-1</sup> of the studied heteropolycomplexes towards greater energies of the free heteropolyligand.

**Conclusions.** The stoichiometry of the reaction of formation in solution of the heteropolycompounds of types  $ZL$  and  $ZL_2$  where  $Z = La(III), Ce(III)$  and  $Ce(IV)$  and  $L = P_2MoW_{16}O_{61}^{10-}$  has been determined.

The results of the conductometric, spectrophotometric and colorimetric studies performed on the mixtures of the solutions of lanthanide cations and heteropolymolybdotungstate  $P_2MoW_{16}O_{61}^{10-}$  with Dawson structure of the 1:1:16 series, point out the formation of heteropolycomplexes with the molar ratios lanthanide cation: heteropolyanion 1:1 and 1:2, the latter being more stable.

By means of the UV spectrophotometric studies developed on mixtures of the solutions of lanthanide cations and the heteropolymolybdotungstic anion in a ratio of 1:2, evidence for the formation of some new species, probably implying the octahedral coordination of the lanthanide ion to two ligands in a square antiprism structure is reported.

## REFERENCES

1. P. Souchay, *Ions Minéraux Condensés*, Masson, Paris, 1969.
2. M. T. Pope, *Heteropoly and Isopoly Oxometalates* Springer, Berlin, Heidelberg, New York, Tokyo, 1983.
3. R. D. Peacock and T. J. R. Weakley, *J. Chem. Soc. (A)*, 1836 (1971).
4. R. Contant, J. M. Fruchard, G. Hervé, A. Tézé, *C. R. Acad. Sci., Ser. C*, **273**, 199 (1974).
5. R. Contant, J. P. Ciabrini, *J. Chem. Res. (S)* **222**, (1977).

ON THE DIOXIMINE COMPLEXES OF TRANSITION METALS.  
Part XCII. Spectrophotometric study on the formation of copper(II)  
chelates with some  $\alpha$ -substituted alicyclic oximes

FERENC MAKKAY\*, CSABA VÁRHELYI\*\*, JÁNOS ZSAKÓ\*\* and ZSUZSANNA  
SZÁSZ\*

ABSTRACT. The composition and in some cases the stability constants of the Cu(II)-chelates with several 1,2,3-cyclohexane trione derivatives: 1,2,3-cyclohexane trione dioxime (1,3), ... trioxime, 1,2,3-cyclohexane trione dioxime (1,3) semicarbazone (2), ... thiosemicarbazone (2) were determined using the continuous variation (isomolar series) and the molar ration methods. The electronic spectra of these Cu(II) compounds were recorded and discussed. Some derivatives were proposed for the spectrophotometric determination of this metal.

**Introduction.** Chugaev [1, 2] observed, that the copper (II)-salts form brown coloured solutions with dimethylglyoxime and some other aliphatic  $\alpha$ -dioximes. Unlike the sparingly soluble Ni, Pd and Pt chelates of the type  $M(\text{Diox.H})_2$ , some analogous copper derivatives were isolated in a pure form from aqueous alcoholic solutions only with serious difficulties.

The x-ray measurements show a dimeric structure for the  $[\text{Cu}(\text{Diox.H})_2]_2$  derivatives with pentacoordinated Cu central atoms [3, 4]. In solutions the dimeric structure decomposes. Monomeric hexacoordinated species:  $[\text{Cu}(\text{Diox.H})_2(\text{H}_2\text{O})_2]$ ,  $[\text{Cu}(\text{Diox.H})_2(\text{H}_2\text{O})(\text{OH})]^-$ ,  $\text{Cu}(\text{Diox.H})_2(\text{OH})_2^{2-}$  or  $[\text{Cu}(\text{OH})_4]^{2-}$  are formed as function of the pH of the system.

The interaction of the copper halides ( $\text{CuCl}_2$ ,  $\text{CuBr}_2$ ) with some aliphatic dioximes in acetone leads to the formation of green coloured  $\text{CuX}_2$ . Dioxime type derivatives with only a single coordinated ligand molecule [5, 6]. Analogous compounds with alicyclic dioximes and with  $X = \text{F}, \text{I}, \text{NCS}, \text{N}_3$  were not described in the literature. In the presence of water the mentioned green coloured compounds decompose and  $\text{Cu} : \text{Diox.H}_2 = 1 : 2$  chelates are formed.

In the present paper in a wide pH range the reaction of some  $\text{C}_6$  alicyclic oxime derivatives with  $\text{Cu}(\text{NO}_3)_2$  solutions was studied spectrophotometrically.

**Results and Discussion.** We observed that the 1,2,3-cyclohexane trione dioxime (1,3) obtained by isonitrozation of the cyclohexanone [7] can be easily condensed with hydroxylamine, semicarbazide and thiosemicarbazide. All these products give various colour reactions with Cu(II) - salts as function of the pH value of the solutions.

\* Faculty of Chemistry Babeș-Bolyai University, Cluj, Romania.

\*\* Dept. of Nat. Sciences and Mathematics, Transilvanian Museum Association, Cluj, Romania.

The electronic spectra of these coloured derivatives were recorded in ethanol (or in ethanol-dimethylsulphoxide: 3:1, in the case of very sparingly soluble chelating agents). Molar ratio  $\text{Cu}^{2+}$  — chelating agent: 1:4, 1:5.

The spectral data, as compared to those of the dimethyl-glyoximine and 1,2-cyclohexane dione dioximine derivatives are presented in Table 1.

Table 1

Chelating agent	Origin of the absorption band				
	$\pi \rightarrow \pi^*$		d-d	d-d	d-d
dimethylglyoxime	42 000	35 400	30 710	27 510	21 000
	43 000	37 000	—	25 000	17 000
		33 000			
1,2-cyclohexane dione dioxime	47 500	40 500	30 400	25 000	18 000
1,2,3-cyclohexane trione trioxime	40 800	38 900	33 000	23 000	—
	39 700	37 900			
1,2,3-cyclohexane trione dioxime (1,3)	37 000	30 000	—	—	—
1,2,3-cyclohexane trione dioxime (1,3)-semicarbazone (2)	47 800	38 500	—	—	—

The spectra of some derivatives of this type are shown in Fig. 1. and 2.

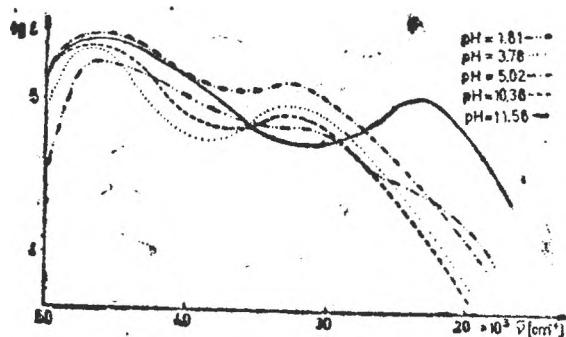


Fig. 1. Electronic spectra of the  $\text{Cu(II)}$ -1,2,3-cyclohexane trione dioxime (1,3)-complex at various pH-values.

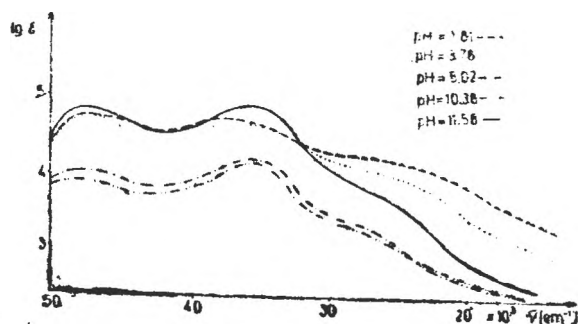


Fig. 2. Electronic spectra of the  $\text{Cu(II)}$ -1,2,3-cyclohexane trione trioxime systems at various pH values.

The electronic spectrum of  $\text{Cu}(\text{DH})_2$  studied in various solvents [8, 9] presents five bands with some superpositions, splitted in the individual bands using the corresponding mathematical methods.

At 42 and 35.4 kK appear two intraligand bands, corresponding to  $\pi \rightarrow \pi^*$  transitions in the co-ordinated dimethylglyoxime molecule. Three weak bands can be observed at 30.7, 27.5 and 21.0 kK, which were assigned to d-d crystal field transitions (i.e.  $d(yz) \rightarrow d(xy)$ ,  $d(x^2 - y^2) \rightarrow d(xy)$ , and the latter  $dz^2 \rightarrow d(xy)$ ).

These bands can be observed also in the spectra of other  $\alpha$ -dioximine complexes of  $\text{Cu}(\text{II})$ ; e.g.  $\text{Cu}(\text{Niox. H})_2$  etc.

In the case of the  $\text{Cu}^{2+} - \text{Triox. H}_3$  system ( $\text{Triox. H}_3 - 1,2,3\text{-Cyclohexane trione trioxime}$ ) the UV bands are splitted. Presumably these bands correspond also to  $\pi \rightarrow \pi^*$  transitions and the splitting might be due to a more delocalized  $\pi$  - system as compared to the case of the  $\alpha$ -dioximine derivatives (e.g.  $\text{Cu}(\text{Niox. H})_2$ ).

In the case of the  $\text{Cu}^{2+} - 1,2,3\text{-cyclohexane trione dioxime (1, 3)}$  derivative appears only a single band at 37 kK in acidic medium and at 30 kK in basic solutions, respectively, indicating a protolytic equilibrium (this problem will be the subject of a forthcoming paper).

Under analogous experimental conditions in the  $\text{Cu}^{2+} - \text{trione} - \text{dioxime (1, 3)}$  semicarbazone (2) and ... thiosemicarbazone (2) systems ligand field transitions cannot be observed.

In the  $\text{Cu}^{2+} - 1,2\text{-dioxime (1,2,3-trioxime)}$  -systems brown coloured complexes are formed. Using the above mentioned  $\alpha$ -ketoxime, the semi- and thiosemicarbazone derivatives as chelating agents for the reaction, green and blue colorations appear. Generally, the colour intensity increases with increasing pH - value up to a limit. At higher pH values (pH > 6-7) in some cases amorphous, brown precipitates are separated.

At various acidic pH-values, for the  $\text{Cu}^{2+} - \text{trione dioxime (1, 3)}$  and  $\text{Cu}^{2+} - \text{trioxime}$  systems the Job's curves and the molar ratio ones are presented in Fig. 3-6.

The analogous representations for some  $\text{Cu}^{2+} - \text{...-semicarbazone (2)}$  and  $\text{Cu}^{2+} - \text{...-thiosemicarbazone (2)}$  systems are shown in Fig. 7. and 8.

The optical density measurements prove that in all the studied cases, with exception of the  $\text{Cu}^{2+} - \text{trioxime}$  system,  $\text{Cu}^{2+} : \text{L} = 1 : 2$  complexes are formed.

The continuous variation - and the molar ratio absorption curves enabled us, in some cases, to determine the stability constants of the formed copper chelates. The  $\text{Cu}^{2+} - \text{trioxime}$  systems were not suitable for this purpose because the very high stability of the complex.

The stability constant of  $\text{CuL}_2$  can be given as

$$K = \frac{[\text{CuL}_2]}{[\text{Cu}][\text{L}]^2}$$

This constant was determined in the following way. Job's curve was recorded by using an isomolar series of solutions with a total concentration  $[\text{Cu}]^0 + [\text{L}]^0 = c$  and by plotting the extinction  $E$  vs. the formal molar frac-

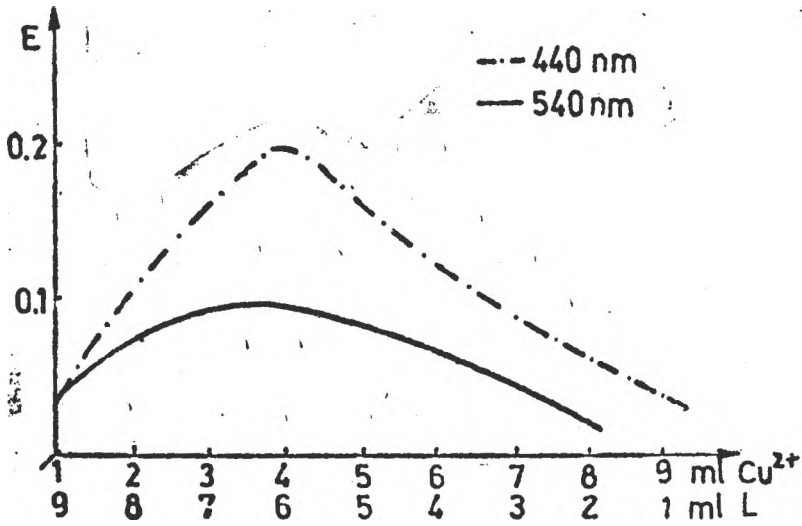


Fig. 3. Job's curve for the  $\text{Cu}(\text{NO}_3)_2$ -1,2,3-cyclohexane trione dioxime (1,3) system,  $\text{pH} = 3.78$ .

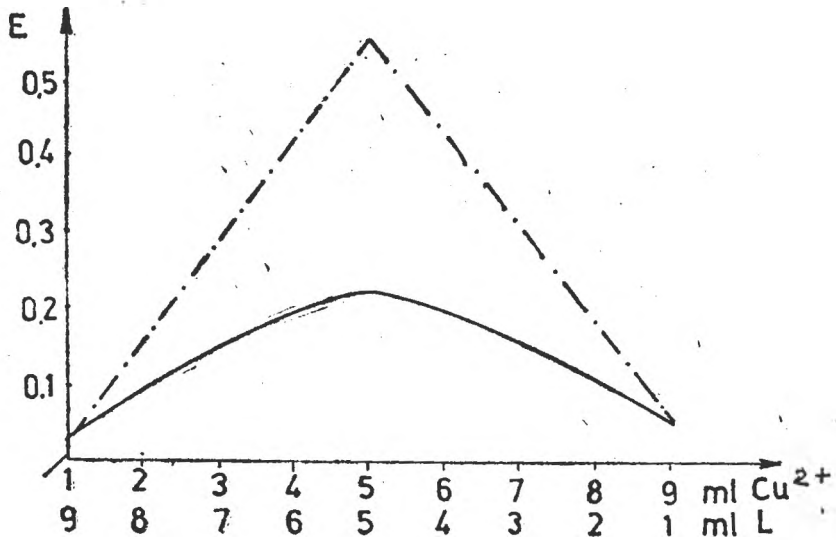


Fig. 4. Job's curve for the  $\text{Cu}(\text{NO}_3)_2$ -1,2,3-cyclohexane trione trioxime system,  $\text{pH} = 1.81$  (—);  $\text{pH} = 2.56$  (- - -).

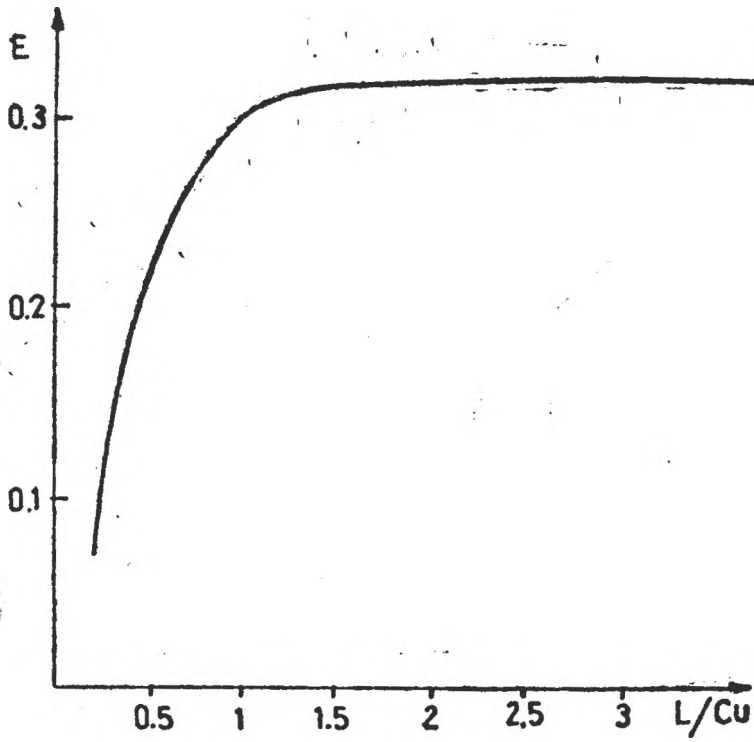


Fig. 5. Molar ratio absorptions curve for the  $\text{Cu}(\text{NO}_3)_2$ -1,2,3-cyclohexane trione dioxime (1,3) system, pH = 3.78.

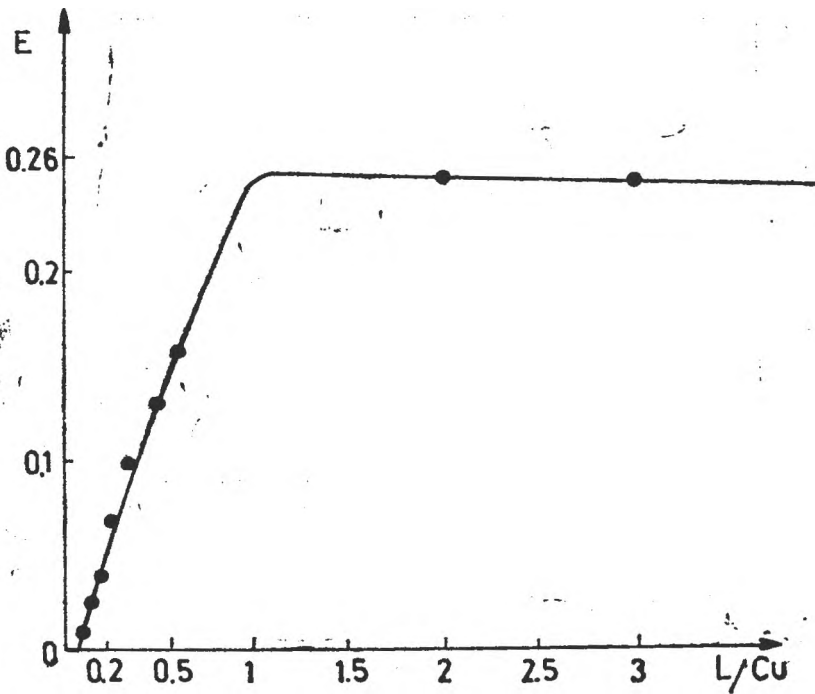


Fig. 6. Molar ratio absorptions curve for the  $\text{Cu}(\text{NO}_3)_2$ -1,2,3-cyclohexane trione trioxime system, pH = 1.81.

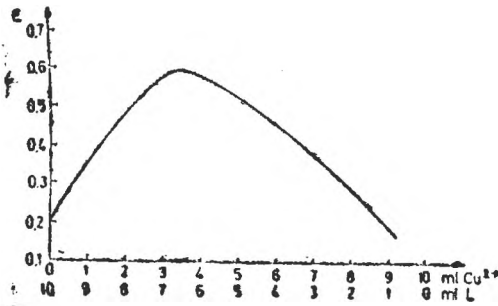


Fig. 7. Job's curve for the  $\text{Cu}(\text{NO}_3)_2$ -1,2,3-cyclohexane trione dioxime (1,3)-semicarbazone (2) system,  $\text{pH} = 2.56$ .

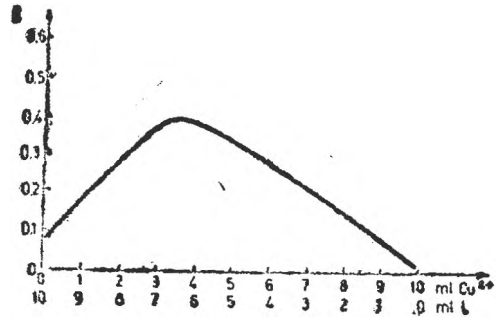


Fig. 8. Job's curve for the  $\text{Cu}(\text{NO}_3)_2$ -1,2,3-cyclohexane trione dioxime (1,3)-thiosemicarbazone (2) system,  $\text{pH} = 2.56$ .

tion of Cu:  $X_{\text{Cu}} = \frac{[\text{Cu}]^0}{c}$ . By constructing the tangency of the curve corresponding to the beginning and to the end of the curve, respectively, the two straight lines intersected each other at  $X_{\text{Cu}} = 0.33$ , as shown in Fig. 9, indicating for the complex obtained the molar ratio  $\text{Cu} : \text{L} = 1 : 2$ .

One may presume the ordinate value of the intersection to correspond to the extinction of a solution in which  $[\text{CuL}_2] = 0.33c$ , since this extinction would be observed if Cu were completely transformed into  $\text{CuL}_2$ . On the basis of

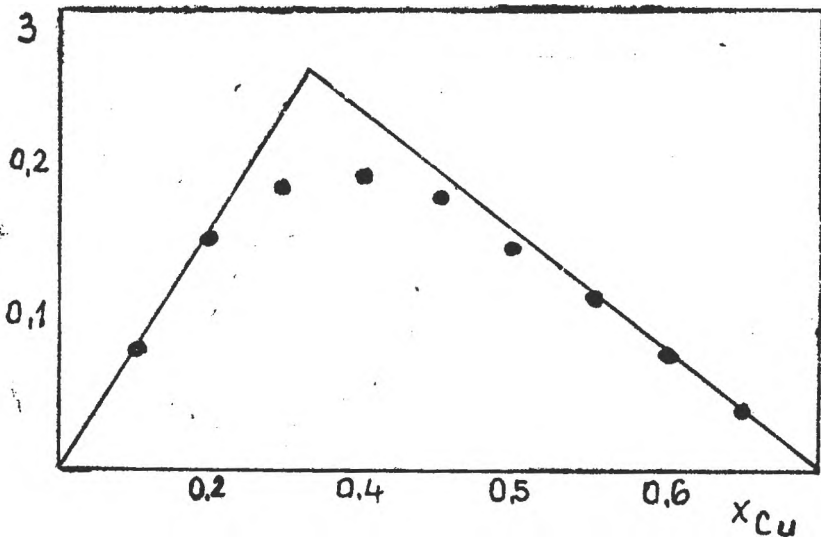


Fig. 9. Determination of the stability constant of the  $\text{Cu}^{2+}$ -1,2,3-cyclohexane trione dioxime (1,3)thiosemicarbazone (2) complexes from the Job's curve.

this hypothesis the actual concentration  $[\text{CuL}_2]$  may be calculated from the experimental  $E$  value. The concentration of the free reagents are obtained as

$$[\text{Cu}] = [\text{Cu}]^{\circ} - [\text{CuL}_2]$$

$$[\text{L}] = [\text{L}]^{\circ} - 2[\text{CuL}_2]$$

Thus, a stability constant value can be derived from each experimental  $E$  value. These calculations could be performed with the 1,2,3-...trione dioxime (2) and the ... thiosemicarbazone (2) derivatives. In the region  $0.2 \leq X \leq 0.5$  the  $K$  values calculated showed a systematic increase with increasing  $X$ , but it did not exceed  $\pm 50\%$  of the mean value.

The following mean stability constant values were obtained:

$$L = 1,2,3, - \text{cyclohexane trione dioxime (1,3)}$$

$$K = 6.6 \times 10^6$$

$$L = 1,2,3\text{-cyclohexane trione dioxime(1,3) thiosemicarbazone (2)}$$

$$K = 2.8 \times 10^7$$

(Concentrations were given in mole/l units.)

**On the structure of the Cu -oxime complexes.** As known, the  $\text{Cu}(\text{Diox.H})_2$  - groupings in weak acidic or neutral aqueous solutions have a square planar structure stabilized by two strong intramolecular hydrogen bondings ( $\text{O}-\text{H}\cdots\text{O}$ ), similar to the analogous Ni and Pb derivatives ( $\text{Diox.H}_2$  - aliphatic, aromatic or alicyclic dioximes) (I. Fig. 10).

In the case of the 1,2,3-cyclohexane trione - oxime derivatives the situation is more complicated. The third functional group, especially the free oxime can be co-ordinated to a second copper atom, forming a dimeric or trimeric derivative. The turbidity or in some cases amorphous precipitate, observed especially in basic media, proves the formation of a polymeric product.

One can presume that the ..trione dioxime (1,3) forms pentaatomic heterocycles (II). The ..semicarbazone (2) and ... thiosemicarbazone (2) derivatives can co-ordinate to the  $\text{Cu}(\text{II})$  as tridentate ligands (III. Fig. 10).

**Analytical applications.** The brown coloured solutions of the  $\text{Cu}^{2+}$  - trioxime systems obey the Lambert - Beer's law in weak acidic media ( $\text{pH} = 1.81 - 4.0$ ) in a concentration range of  $0.5 - 10 \times 10^{-4}$  mole/l. Some deviations from the linearity appear in the case of the other .. trione dioxime (1,3) derivatives. (Fig. 11.)

The stability of the colour in time is the best in the case of the  $\text{Cu}^{2+}$  - trioxime system (12-24 hours). This phenomenon presents an advantage for

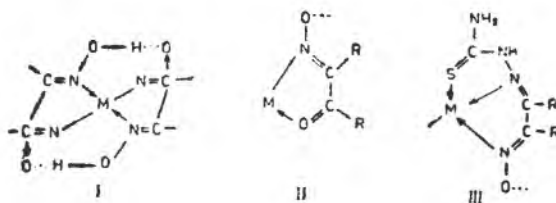


Fig. 10. Chelate rings in the  $\text{Cu}(\text{II})$ -nyoxime (I),  $\text{Cu}(\text{II})$ -... trione dioxime (1,3)(II) and  $\text{Cu}(\text{II})$ -trione dioxime (1,3) thiosemicarbazone (2)(III) complexes.

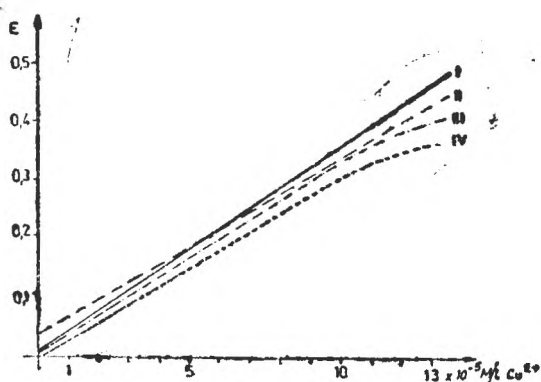


Fig. 11. Validity of the Lambert-Beer's law: I.  $\text{Cu}^{2+}$ -trioxime system; II.  $\text{Cu}^{2+}$ -nyoxime system; III.  $\text{Cu}^{2+}$ -trione dioxime (1,3)-system; IV.  $\text{Cu}^{2+}$ -trione dioxime (1,3)-thiosemicarbazone (2) system.

This  $\alpha$ -ketoxime is formed by isonitrosation of cyclohexanone with gaseous ethyl-nitrite in alcoholic solution in the presence of hydrochloric acid. [9, 10].

**Electronic spectra** were recorded in aqueous buffered solutions or in a mixture of water-dimethylsulphoxide-ethanol, respectively, in the case of in water sparingly soluble reagents, using a Specord recording spectrophotometer (Jena, Germany).

The colorimetric measurements were made with a FEK -Colorimeter (USSR).

The isomolar solutions and the samples for the molar ratio measurements were prepared from  $10^{-2}$  mole/l  $\text{Cu}(\text{NO}_3)_2$  and  $10^{-2}$  mole/l oxime and 5–5 ml Britton-Robinson buffer solutions in 50 ml volume.

#### REFERENCES

1. A. Chugaev, *J. prakt. Chem.*, **76**, 88 (1907).
2. A. Chugaev, *Z. anorg. allg. Chem.*, **46**, 144 (1905).
3. E. Frasson, R. Bardi, S. Berzi, *Acta Crystallogr.*, **12**, 201 (1959).
4. A. Vacilago, L. Zambonelli, *J. Chem. Soc., A*, **1970**, 218.
5. M. Bélombé, M. Novotny, *Inorg. Chem.*, **19**, 2470 (1980).
6. D. H. Svedung, *Acta Chem. Scand.*, **23**, 2865 (1969).
7. A. Treibs, H. Kuhn, *Chem. Ber.* **90**, 1691 (1957).
8. D. Dyrssen, D. Petkovich, *Acta Chem. Scand.*, **19**, 653 (1965).
9. B. Roos, *Acta Chem. Scand.*, **21**, 1855 (1967).
10. J. Zsákó, A. Benkő, J. Horák, Cs. Várhelyi, *Acta Chim. Acad. Sci. Hung.*, **103**, 51 (1980).

ON THE DIOXIMINE COMPLEXES OF TRANSITION METALS. XCIII.  
Alicyclic  $\alpha$ -substituted oximes as chelating agents for the determination of cobalt

FERENC MAKKAY\*, CSABA VÁRHELYI\*\*, ENIKŐ SZAKÁCS\* and  
ERNEST GRÜNWARD\*\*

**ABSTRACT.** The formation of cobalt(II)-chelates with 1,2,3-cyclohexane trione dioxime (1,3) and with its condensation products (partner: hydroxylamine semicarbazide, thiosemicarbazide) was studied spectrophotometrically using the continuous variation method and the molar-ratio method, respectively. The electronic spectra of these complexes were recorded and discussed. Some derivatives of this type were proposed for the analytical determination of the cobalt.

**Introduction.** The colour reaction of the cobalt(II)-salts in the presence of some aliphatic  $\alpha$ -dioximes was observed even at the beginning of the century by Chugaev and al. [1, 2].

The complexes can be stabilized in aqueous solutions in the absence of oxygen, ensuring favourable conditions for this purpose by deaeration with nitrogen, methane, argon or by addition of reducing agents. The cobalt(II) derivatives in aqueous media oxidize with the time, generally quickly, in function of the nature of the oxidizing agent ( $O_2$ ,  $H_2O_2$ , free halogens etc.) and the anionic or neutral ligands present in the solution. Some nucleophilic monodentate anions (e.g.  $NCS^-$ ,  $NCS_2^-$ ,  $N_3^-$ ,  $I^-$ ) stabilize the Co(II) form in some extent [3, 4].

The Co(III) mixed chelates formed by oxidation are very stable and can be used for various ligand exchange kinetic and preparative studies [5-8].

The formation of the Co(II)-chelates with some aliphatic and heterocyclic  $\alpha$ -dioximes [9-12] and alicyclic mixed oxime-thiosemicarbazones obtained from alkyl-cyclopentane dione and dimedone [5, 5-dimethyl-cyclohexane dione (1,3)] were examined [13-16].

In continuation of our physico-chemical investigations [17-21] on the formation of transition metal complexes with  $\alpha$ -substituted oximes in this paper the formation conditions of the cobalt(II)-complexes with 1,2,3-cyclohexane trione dioxime (1,3) and its condensation products with hydroxylamine, semicarbazide and thiosemicarbazide was studied spectrophotometrically.

**Results and Discussion.** Our preliminary tests show that the aliphatic  $\alpha$ -ketoximes, e.g. diacetymonoxime and methyl-isopropyl-2,3-dione monoxime (2) form yellow, soluble complexes with cobalt(II)-salts at higher pH-values

\* Faculty of Chemistry, Babeș-Bolyai University, Cluj-Napoca, Romania.

\*\* Dept. of Nat. Sciences and Mathematics, Transylvanian Museum Association, Cluj-Napoca, Romania

(pH > 8). In acidic media this phenomenon cannot be observed. Using 1, 2, 3-cyclohexane trione dioxime (1, 3) and its condensation products with above mentioned partners, the colour reaction is more significant and appears also in slightly acidic media (pH ~ 3.5–4.0). The alicyclic monoximes with C<sub>5</sub>, ... C<sub>8</sub> are not suitable for this purpose.

The electronic spectra of the coloured complexes were recorded in diluted ethanol (in the case of the Co(II)-1, 2, 3-cyclohexane trione dioxime (1, 3) semicarbazone (2) in ethanol-dimethylsulphoxide mixture (1:3)) in the presence of Na<sub>2</sub>SO<sub>3</sub> or hydroxylamine as reducing agents. The spectral data, as compared with those of the Co(II)-1, 2-cyclohexane dione dioxime (1, 2-cycloheptane dione dioxime) systems are presented in Table 1.

Table 1

Electronic spectral data of some cobalt(II)- $\alpha$ -substituted oxime derivative (in cm<sup>-1</sup>)

Chelating agent	Origin of the absorption band			
	d-d	$\pi \rightarrow \pi^*$	d-d	$\pi \rightarrow \pi^*$
	acid medium		basic medium	
1,2-cyclohexane dione dioxime	28 000	47 000	28 000	48 000
		41 000	32 000	40 000
1,2-cycloheptane dione dioxime	28 000	47 000	28 000	48 000
		41 000	32 000	40 000
1,2,3-cyclohexane trione trioxime	26 000	38 000	33 000	38 800
		47 200		47 900
1,2,3-cyclohexane trione-dioxime (1,3)-thiosemicarbazone (2)	?	38 700	24 000	33 500
		48 000	26 500	37 200
1,2,3-cyclohexane trione dioxime (1,3)-semicarbazone (2)	?	37 000	26 000	34 000
		48 000		38 000
				48 000

The electronic spectra of some Co(II)-oxime chelates are shown in Figs. 1–3.

As seen from the spectral data, the position and in some cases also the number of the absorption bands show differences in acidic and in basic media, respectively. This phenomenon is in agreement with the existence of protolytic equilibria in the studied systems. For the clarification of this problem further spectrophotometric and potentiometric measurements are required.

It is worth to mention that the electronic spectra of the [Co(Diox. H)<sub>2</sub>XY] type complexes (Diox.H – deprotonated  $\alpha$ -dioxime) show generally 3–4 bands at 300–375 nm (A) and 340–400 nm (B) and a weak band in the visible region. The B band can be attributed to a charge transfer X, Y  $\rightarrow$  Co (X, Y anionic or neutral monodentate ligands). The A band corresponds to a charge transfer Co  $\rightarrow$  dioxime. The ligand field parameters of these Co(III)-chelates were calculated using the Co(Diox.H)<sub>3</sub> nonelectrolyte as „parent compound” for this purpose [22, 23].

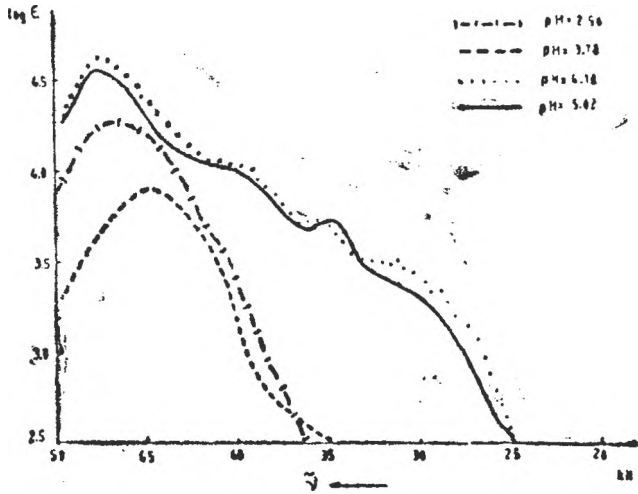


Fig. 1. Electronic spectra of the Co(II)-1,2-Cycloheptane dione dioxime complex in Britton-Robinson buffer solutions.

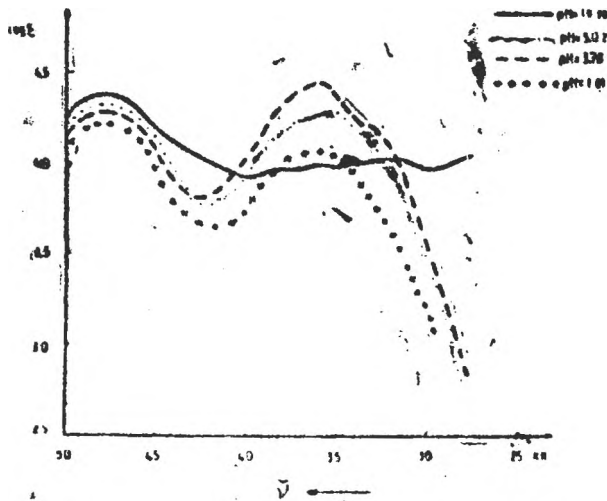


Fig. 2. Electronic spectra of the Co(II)-1,2,3-Cyclohexane trione dioxime (1,3)-thiosemicarbazone (2) complex in Britton-Robinson buffer solutions.

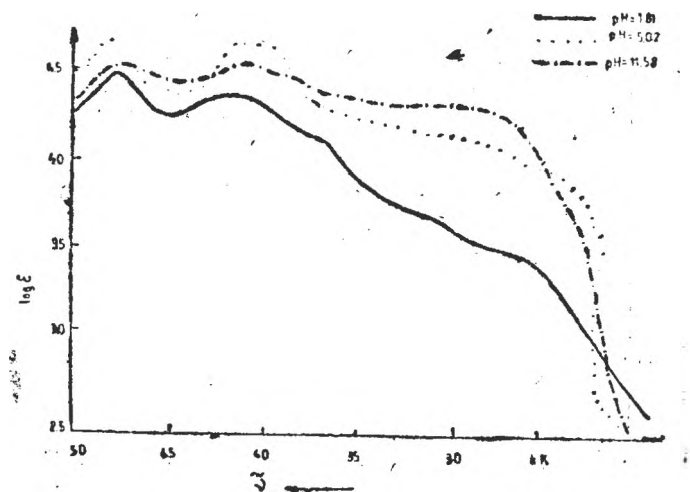


Fig. 3. Electronic spectra of the Co(II)-1,2,3-Cyclohexane trione trioxime complex in Britton-Robinson buffer solutions.

The composition of the Co(II)-1,2,3-cyclohexane trione derivative complexes was determined by means of the continuous variation and the molar-ratio methods. The Job's curves are presented in Figs. 4-5.

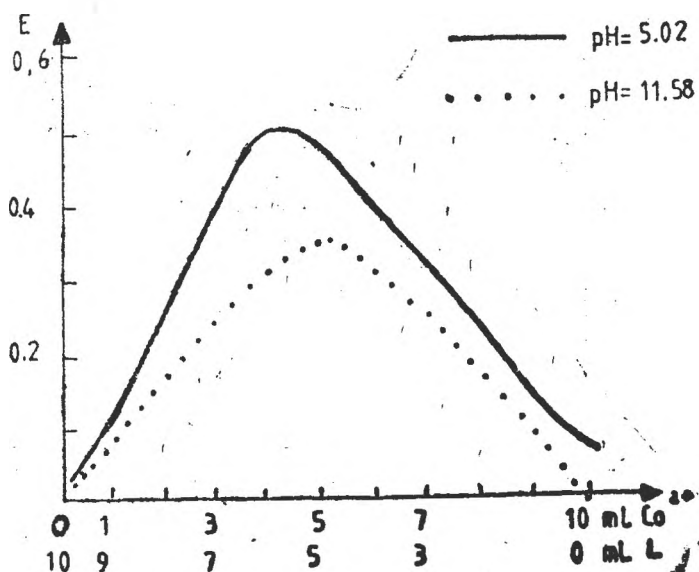


Fig. 4. Job's curves of the Co(II)-1,2,3-Cyclohexane trione dioxime (1,3) semicarbazone (2) systems at various pH-values.

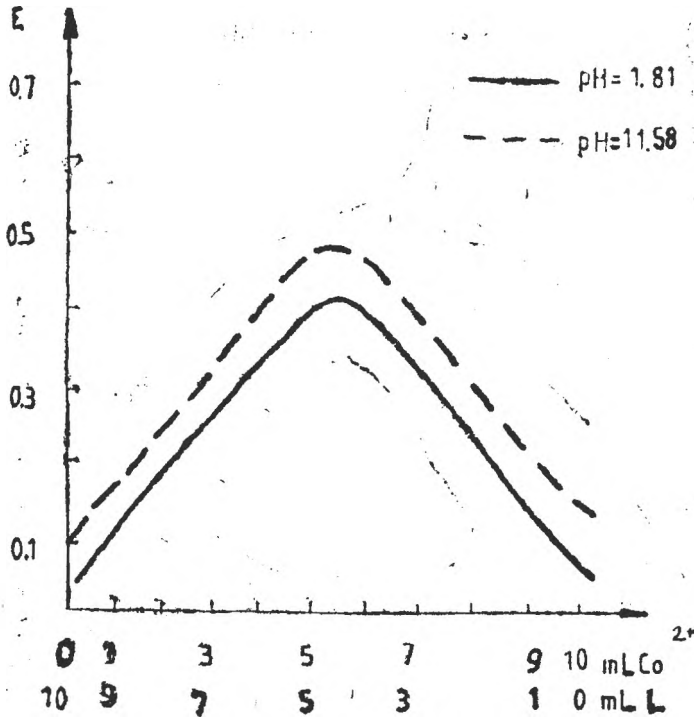


Fig. 5. Job's curves of the Co(II)-1,2,3-Cyclohexane trione trioxime systems at various pH-values

As seen, at lower pH-values Co : L = 1 : 2 complexes are formed with 1,2,3-cyclohexane trione dioxime (1,3) semicarbazone (2) and 1,2,3-cyclohexane trione dioxime (1,3) thiosemicarbazone (2) ligands. The basic media favourize the formation of Co : L = 1 : 1 complexes (Fig. 4). The molar ratio curves for these systems are in agreement with this observation (Fig. 6.).

An analogous representation for the Co(II)-trione dioxime (1,3) system pleads also for Co : L = 1 : 2 composition in acidic media and for Co : L = 1 : 1 in basic ones respectively.

For the Co(II)-trioxime system in a wide pH range only a Co : L = 1 : 1 ratio was observed (Fig. 5).

The shape of the continuous variation and molar ratio curves do not enable us to determine the stability constants of the Co(II)-chelates.

**On the structure of the Co(II)-oxime complexes.** The  $\alpha$ -dioximes form  $[\text{Co}(\text{Diox.H})_2\text{X}_2]$  type complexes with Co : Diox.H = 1 : 2 ratio, where the  $\text{Co}(\text{Diox.H})_2$  grouping have a square planar structure stabilized by two strong intramolecular hydrogen bridges (O—H...O), similarly with the  $\text{M}(\text{Diox.H})_2$  derivatives (M = Ni, Pd, Pt). The axial X ligands influence the stability of

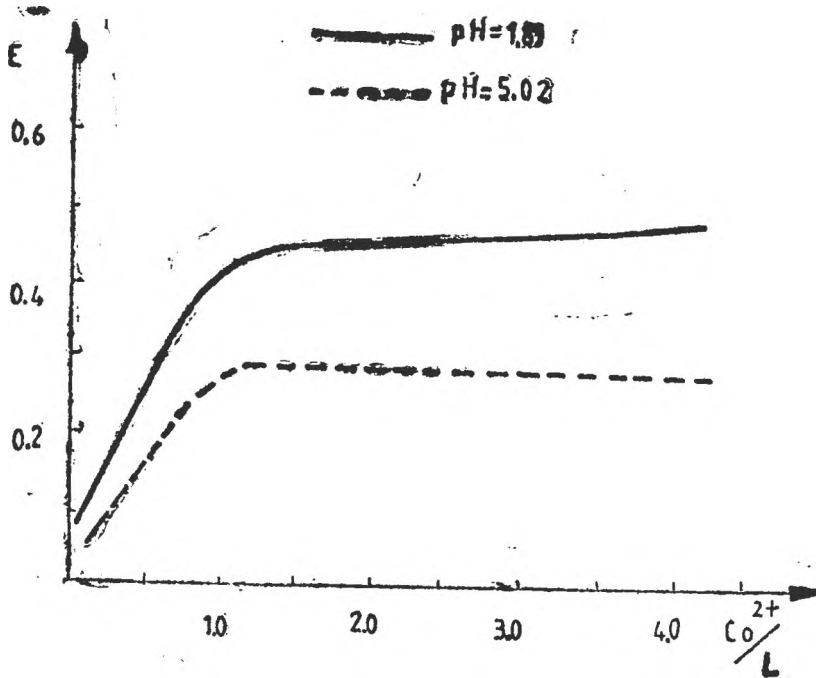


Fig. 6. Molar-ratio curves of the Co(II)-1,2,3-Cyclohexane trione dioxime (1,3)-semicarbazone (2) systems at various pH-values.

these compounds ( $X$  = solvent molecule, amine, phosphine). In the case of the 1,2,3-cyclohexane trione dioxime (1,3) and its condensation products the structure of the cobalt complexes is more complicated. The third functional group, especially the free oxime, promotes the formation of di- or polymeric structures in function of the pH value of the medium. One can presume, that the 1,2,3-cyclohexane trione dioxime (1,3) forms pentaatomic heterocycles. The 1,2,3-cyclohexane trione dioxime (1,3) semicarbazone (2) and ... thiosemicarbazone (2) act as tridentate ligands in the above mentioned complexation reaction [24].

**Analytical applications.** The 1,2,3-cyclohexane trione derivatives studied are middle sensitive reagents for the analytical detection of cobalt(II).

Reagent :	Detection limits :	
	acidic medium	basic medium
	pH = 3-4	pH = 8-9
1,2,3-cyclohexane trione-dioxime (1,3)	10 ppm	8 ppm
" trioxime	8 ppm	6 ppm
" dioxime (1,3) semicarbazone(2)	5 ppm	6 ppm
" dioxime(1,3) thiosemicarb.(2)	3 ppm	2 ppm

The yellow-brown solutions of the Co(II)-oxime systems obey the Beer's law in weak acidic and weak basic media in a concentration range of  $0.5-10 \times 10^{-4}$  mole/L. Some deviations from the linearity appear in the case of the Co(II)-1,2,3-cyclohexane trione dioxime (1,3) semicarbazone (2) derivative.

The spectrophotometric measurements were made in the presence of  $\text{Na}_2\text{SO}_3$  or  $\text{NH}_2\text{OH}$  for the elimination of the interference of the oxygen. The stability of the colour in time is the best in the case of trione dioxime (1,3) and trione trioxime.

The Cu(II) and Fe(II) interfere the spectrophotometric determination of cobalt(II). The other 3 d transition metals, the alkali and alkaline earth metals do not influence this analytical procedure.

**Experimental.** The synthesis of the chelating agents was described in an earlier paper [24].

Electronic spectra were recorded in aqueous buffered solutions or in a mixture of water-dimethylsulphoxide-ethanol (1:3:1), respectively, in the case of in water sparingly soluble reagents, in the presence of an excess of  $\text{Na}_2\text{SO}_3$ , using a SPECORD recording spectrophotometer (Carl Zeiss Jena, Germany).

The analytical measurements were made with a colorimeter-nefelometer photoelectric FFK-56M-U4.2 (URSS).

The samples for the spectrophotometric measurements were prepared from  $10^{-2}$  mole/L  $\text{Co}(\text{NO}_3)_2$  and  $10^{-3}$  mole/L oxime and 5-5 ml Britton-Robinson buffer solution in the presence of 1 ml 2%  $\text{Na}_2\text{SO}_3$  or  $\text{NH}_2\text{OH}\cdot\text{HCl}$  (Volume: 50 ml).

#### REFERENCES

1. L. A. Chugaev, *Ber. dtsh. Chem. Ges.*, **38**, 2520 (1905); **39**, 3382 (1906); **40**, 3498 (1907); **41**, 2219 (1908).
2. L. A. Chugaev, *J. Chem. Soc.*, **105**, 2187 (1914).
3. K. Burger, *Anal. Univ. Scient. Budapest, Sect. Chim.*, **10**, 61 (1968).
4. K. Burger, B. Pintér, *J. Inorg. Nucl. Chem.*, **29**, 1717 (1967).
5. N. Maki, *Bull. Chem. Soc., Japan*, **38**, 2013 (1965).
6. A. V. Ablov, G. P. Syrzova, *Zhur. neorg. Khim.*, **10**, 1980 (1965).
7. A. V. Ablov, D. G. Batir, M. P. Starih, *Zhur. neorg. Khim.*, **16**, 690 (1971).
8. Cs. Várhelyi, Z. Finta, J. Zsakó, *Z. anorg. allg. Chem.*, **374**, 326 (1970).
9. Nobusuke Masuda, Meisetsu Kojiiwara, *Japan Analyst*, **19**, 1613 (1970).
10. J. L. Jones, J. Gasterfield, *Anal. Chim. Acta*, **51**, 130 (1970).
11. W. J. Holland, J. Bozic, *Talanta*, **15**, 843 (1968).
12. J. Losada del Barrio, E. Lorenzo Abad, S. Vicente Perez, *Ann. Quim. Ser. B.* **82**, 66 (1986).
13. R. Belcher, S. A. Ghonaim, A. Townshend, *Talanta*, **21**, 191 (1974).
14. J. Rojas, J. M. Lopez Fernandez, M. Valcarcel, *Mikrochem. J.*, **27**, 445 (1982).
15. A. Quamieh, A. H. Laila, R. Salim, *Spectrosc. Lett.*, **21**, 411 (1988).
16. M. Roman Ceba, J. A. Munoz Leyva, J. C. Jimenez Sanchez, *Afinidad*, **38**, 431 (1981).
17. Cs. Várhelyi, F. Makkay, A. Benkó, E. Kazinczy, *Chem. analit. (Warsaw)*, **37**, 219 (1992).

18. Cs. Várhelyi, B. Burus, F. Makkay Stud. Univ. Babeş-Bolyai, *Chem.*, **34**, (2), 61 (1989)
- 19 Cs. Várhelyi, F. Makkay, T. Czier, G. Perint, Stud. Univ. Babeş-Bolyai, *Chem.*, **34**, (1), 64 (1989).
20. Cs. Várhelyi, F. Makkay, H. Székely, G. Liptay, *Periodica Polytechnica Ser. Chem.* (Budapest), **35**, (4), 187 (1991).
21. F. Mánok, E. Kőszegi, Cs. Várhelyi, G. Liptay, *Periodica Polytechnica Ser. Chem.* (Budapest), **33**, (1), 11 (1989).
22. J. Zsakó, J. Sata, Cs. Várhelyi, *Revue Roum. Chim.*, **18**, 1759 (1973).
23. J. Zsakó, J. Sata, Cs. Várhelyi, Stud. Univ. Babeş-Bolyai, *Chem.*, **18**, (1), 37 (1973).
24. F. Makkay, Cs. Várhelyi, J. Zsakó, Zs. Szász, Stud. Univ. Babeş-Bolyai, *Chem.* **38**, **99** (1993).

## PREPARATION AND CHARACTERIZATION OF SOME NEW NITROFURANHYDRAZOMETHINES

FLORIAN JÜGREȘTAN\*, VASILE MICLÄUȘ\*\*, MONICA TOȘA\*\*, GABRIELA CÎMPAN\*\*, DANIELA HOMORODEAN\*\*\*

**ABSTRACT:** Some new nitrofuranydrazomethines have been prepared from hydrazides generated through the reaction of saccharin's derivatives with hydrazine hydrate. The structures of the compounds were confirmed by NMR IR, UV-VIS spectroscopy. Biological tests have pointed out an antibacterial activity.

**Introduction.** The biological activity of 5-nitro-2-furaldehyde as azomethines is well known and now these compounds are on large scale commercially available. The sulfonamides are biologically active too, representing a group of successfully employed chemotherapeutics [1].

The structures of 5-nitro-2-furyl-hydrazomethines series prepared by us contain in their molecule the biologically active sulfonamide group and also the nitrofuranyl moiety, which are expected to give interesting biological properties. In this scope we condensed 5-nitro-2-furaldehyde with a series of hydrazides derived from saccharine.

**Results and Discussion.** In the literature [2, 3] saccharine gives with hydrazine hydrate a salt in the first stage and then it suffers a reaction of splitting of the heterocyclic ring into compounds II<sub>a</sub>.

This behaviour was confirmed in our work.

The action of Hydrazine hydrate on N-alkoxy-carbonyl-methylen-saccharines I<sub>c-e</sub> wasn't studied yet. In the molecule of this

substance there are two carbonyl groups accessible to the nucleophilic attack. This difference of reactivity between the two sites (exocyclic and endocyclic) can be used in laboratory syntheses.

In our first attempt the molar ratio was I<sub>c-e</sub> : N<sub>2</sub>H<sub>4</sub> · H<sub>2</sub>O = 1 : 1. The major products were the monohydrazides II<sub>c-e</sub>, with small amounts of dihydrazide II<sub>f</sub>. The elemental and chromatographic analyses pointed out the same results, even if we have used an excess of esters I<sub>c-e</sub>.

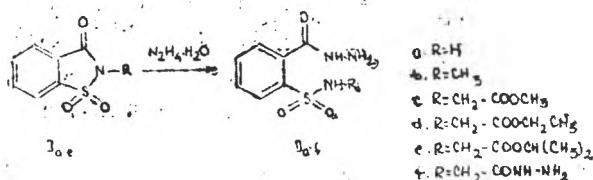


Fig. 1. Scheme 1.

\* Medical Enterprise "Terapia", 3400 Cluj-Napoca, Romania.

\*\* Babeș-Bolyai University, Department of Technological Chemistry, 3400, Cluj-Napoca, Romania.

\*\*\* "Leon Danielli" Fiziological Clinic 3400 Clu-Napoca, Romania.

In order to find out in what measure the difference of reactivity is due to the fact that one of the carbonyl group is engaged in a cyclic system, we opened the ring of compounds  $I_{c-e}$  with alcoxides into the structures  $VII_{c-e}$ .

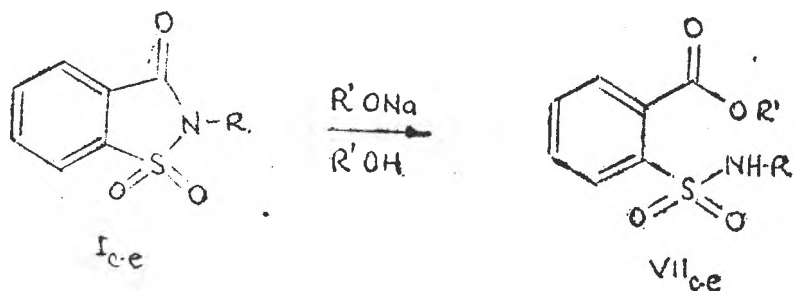


Fig. 2. Scheme 2.

Patek M. and Hampe F. [4], Schapira C. & Co. [5] showed that with molar ratio  $I_{c-e} : R'ONa = 1 : 1$  have been obtained the structures  $VII_{c-e}$ , while in the condition of a molar ratio  $1 : 2$  the reaction lead to the corresponding structure  $III_{c-e}$ .

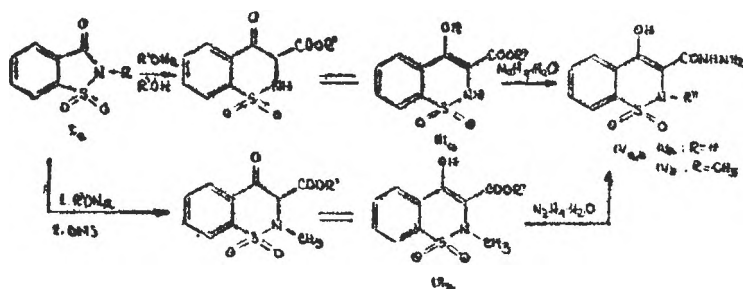


Fig. 3. Scheme 3.

During the reproduction of Czech researchers experiments we realized that in anhydrous conditions and  $70^\circ C$ , the catalytic amount of alcoxide determines the quantitative changes of compounds  $I_{c-e}$  into derivatives  $VII_{c-e}$ .

The estheric Structures  $VII_{c-e}$  were treated with hydrazine hydrate and the same monohydrazide derivatives  $II_{c-e}$  were obtained with dihydrazide,  $II_f$  as impurity.

The difference of behaviour to hydrazinolyze of compounds  $I_{c-e}$  towards  $VII_{c-e}$  would be the subject of a quantitative study in the near future.

Hydrazides  $IV_{a,b}$  were prepared through the reaction of ester compounds  $III_{a,b}$  which were obtained in the Dieckman reaction from  $I_c$  in the condition exhibited by Svoboda J. and Palacek J. [6].

During the reaction of Hydrazides  $II_{a-f}$  with 5-nitro-2 furanidehyde resulted the structures  $V_{a-f}$  and  $VI_{a,b}$ .

The structures of the newly synthesized compounds were confirmed by elemental and spectral analyses (Table I). The characteristic spectral data are given in Table 2.

Without the aim of a detailed analysis of recorded spectra, we emphasize some observations.

In all cases the characteristics of absorption bands have shown that they are generated by electronic transitions of a conjugated system which involve compulsorily the furan ring. At the structures VI<sub>a,b</sub> we found an unexpected difference of about 55 nm between the position of the highest wavelength band, probably due to the absence of the tautomeric sulphonamidic interactions which disappeared after methylation.

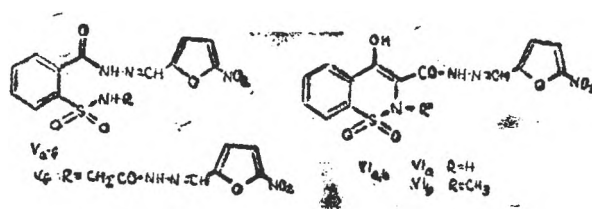


Fig. 4. Scheme 4.

Table I

Hydrazides and Nitrofuranhydrazomethines

Compound	Molecular formula	Molecular weight	Melting point	Yield %	Analysis Calcd.	N% Found
II <sub>a</sub>	C <sub>7</sub> H <sub>9</sub> N <sub>5</sub> O <sub>5</sub> S	201.21	187-89	76	28.08	27.98
II <sub>b</sub>	C <sub>9</sub> H <sub>11</sub> N <sub>5</sub> O <sub>5</sub> S	215.21	147-48	78	18.23	18.70
II <sub>c</sub> <sup>+</sup>	C <sub>10</sub> H <sub>10</sub> N <sub>5</sub> O <sub>5</sub> S	287.19	—	90	14.63	14.72
II <sub>d</sub> <sup>+</sup>	C <sub>11</sub> H <sub>11</sub> N <sub>5</sub> O <sub>5</sub> S	301.32	66-68	81	13.94	14.09
II <sub>e</sub> <sup>+</sup>	C <sub>11</sub> H <sub>17</sub> N <sub>5</sub> O <sub>5</sub> S	315.35	62-64	83	13.32	13.13
II <sub>f</sub> <sup>+</sup>	C <sub>9</sub> H <sub>11</sub> N <sub>5</sub> O <sub>5</sub> S	289.29	158-59	87	24.37	24.46
IV <sub>a</sub> <sup>+</sup>	C <sub>9</sub> H <sub>9</sub> N <sub>5</sub> O <sub>5</sub> S	255.52	187-89	80	16.46	16.61
IV <sub>b</sub> <sup>+</sup>	C <sub>10</sub> H <sub>11</sub> N <sub>5</sub> O <sub>5</sub> S	269.28	189-90	75	15.60	15.12
V <sub>a</sub> <sup>+</sup>	C <sub>15</sub> H <sub>16</sub> N <sub>5</sub> O <sub>5</sub> S	338.32	197-98	94	16.35	16.43
V <sub>b</sub> <sup>+</sup>	C <sub>15</sub> H <sub>19</sub> N <sub>5</sub> O <sub>5</sub> S	352.32	216-17	96	15.90	15.73
V <sub>c</sub> <sup>+</sup>	C <sub>16</sub> H <sub>14</sub> N <sub>5</sub> O <sub>5</sub> S	410.36	152-54	95	13.65	13.79
V <sub>d</sub> <sup>+</sup>	C <sub>16</sub> H <sub>16</sub> N <sub>5</sub> O <sub>5</sub> S	424.39	191-93	95	13.20	13.61
V <sub>e</sub>	C <sub>17</sub> H <sub>16</sub> N <sub>5</sub> O <sub>5</sub> S	438.41	112-14	95	12.78	12.96
V <sub>f</sub>	C <sub>9</sub> H <sub>13</sub> N <sub>5</sub> O <sub>5</sub> S	287.29	218-20 <sub>d</sub>	90	24.37	24.46
VI <sub>a</sub>	C <sub>9</sub> H <sub>9</sub> N <sub>5</sub> O <sub>4</sub> S	255.25	243-45 <sub>d</sub>	94	15.02	14.81
VI <sub>b</sub>	C <sub>15</sub> H <sub>12</sub> N <sub>5</sub> O <sub>7</sub> S	292.11	267-68 <sub>d</sub>	92	14.28	14.50

<sup>+</sup> new compound

\* for II<sub>a-c</sub>, relating to I<sub>a-c</sub>; for II<sub>f</sub>, relating to I<sub>c</sub>; for IV<sub>a,b</sub>, relating to I<sub>c</sub>; for V<sub>a-f</sub>, relating to II<sub>a-f</sub>; for VI<sub>a,b</sub>, relating to IV<sub>a,b</sub>.

Table 2

## SPECTRAL DATA OF NITROFURANHYDRAZOMETHINES

Coni pound	UV-VIS spectra max (nm)		IR-spectral bands (cm <sup>-1</sup> )	<sup>1</sup> H-NMR, values (ppm)
V <sub>a</sub>	368	19311	3260, 3120, 1660, 1550, 1480, 1400, 1360, 1250, 1170, 1020, 970	7.8(4H,m); 6.9(2H,d); 9.75(2H); 9.5(aH); 9.1(1H)
V <sub>b</sub>	368	18978	3450, 3220, 1650, 1550, 1360, 1290, 1250, 1160, 960	3.9(3H,s); 7(2H,d); 7.7(4H,m); 9.7(1H); 9.4(1H); 9.0(1H)
V <sub>c</sub>	370	20076	3236, 3016, 1764, 1532, 1482, 1342, 1228, 1164, 1016, 966	3.6(3H,s); 4(2H,s); 7.1(2H,d); 7.8(4H,m); 9.1(1H); 9.75(1H); 10.5(1H)
V <sub>d</sub>	370	19387	3280, 3020, 1730, 1674, 1530, 1480, 1250, 1160, 1025, 970	2.2(3H,t); 2.7(2H,q); 4(2H,s); 7.2(2H,d); 7(4H,m); 9(1H); 9.5(1H); 9.9(1H)
V <sub>e</sub>	370	14396	3242, 3016, 1736, 1674, 1528, 1480, 1420, 1246, 1164, 1104, 1016, 964	0.98(6H,d); 3.8(2H,s); 4.9(1H,m); 7.1(2H,d); 7.6(4H,m); 9.1(1H); 9.5(1H); 9.9(1H)
V <sub>f</sub>	385	14776	3100, 1730, 1674, 1530, 1480, 1440, 1360, 1250, 1170, 1020, 970	4(2H,s); 7(4H,d); 7.7(4H,m); 9(1H); 9.5(1H); 10.1(1H)
VI <sub>a</sub>	385	16421	3324, 3116, 1658, 1476, 1374, 1202, 1098, 1060, 924	8(4H,m); 7.3(2H,d); 9(1H); 9.4(1H); 9.9(1H)
VI <sub>b</sub>	440	9955	3260, 3120, 1660, 1550, 1480, 1375, 1270, 1220, 1190, 1180, 1160, 980	3(3H,s); 7.2(2H,d); 8(4H,m); 9.2(1H); 9.7(1H)

In the course of the antibacterial biologic screening the synthesised compounds exhibited interesting properties that will be the subject of a separate communication.

**Experimental.** Infrared spectra were recorded on a "Perkin Elmer" spectrophotometer instrument using the KBr techniques. UV-VIS spectra were measured on a Sp. cord M40 (Carl Zeiss, Jena). <sup>1</sup>H-NMR spectra were taken on a Tesla BS 487 C (80 MHz) using tetramethylsilan as internal standard and CF<sub>3</sub>-COOH as solvent. The melting points are determined in capillaries and are uncorrected. Thin layer chromatography was performed on precoated Silica gel 60F<sub>254</sub> plates (5 × 10 cm, 0.25 mm layer of silica gel) from Merck (Darmstadt, Germany).

1. Esthers I<sub>c-e</sub> were prepared according to [7, 8].

2. Structures VII<sub>c-e</sub>: A solution of 0.1 g of sodium in 100 ml methanol was successively treated with 0.1 mole of compound I<sub>c-e</sub>. The mixture was heated to 80 °C for 20 minutes. It was cooled and poured in 50 ml water. The separated product was filtered, washed with water and dried.

3. Esthers III<sub>a,b</sub> were prepared according to [4].

4. *Monohydrazides II<sub>a,b</sub>*: To 0.1 mol saccharin (or 2-methylsaccharin) solved in 50 ml benzene 0.15 mols of hydrazine hydrate (97%) were added. The water was removed under reflux as azeotropic mixture. After the mixture was cooled, 20 ml of water was added. The solid was filtered, washed with water and recrystallized from methanol.

5. *Structures II<sub>c-e</sub>*: A suspension of I<sub>c-e</sub> in 50 ml benzene at 0°C was treated with 0.1 mol hydrazine hydrate (97%). The reaction was perfected 30 minutes at 10°C and then 30 minutes at 25°C. The solid formed was filtered and suspended in NaHCO<sub>3</sub> (soln. 20%). The unsolved products were filtered off. The filtrate was treated with acetic acid. All the hydrazides II<sub>c-e</sub> were purified with II. The recrystallization in usual solvents doesn't lead any results. The reaction mixture was chromatographed on silicagel with benzene: methyl-ethylacetone = 3:1 afforded pure II<sub>c-e</sub>.

6. *Dihydrazides II*: 0.1 mol II<sub>c-e</sub> in 50 ml benzene and 0.25 mols hydrazine hydrate (97%) were heated under reflux removing the alcohol and water. The solid formed was filtered off and crystallized from methanol.

7. *Hydrazides III<sub>a,b</sub>*: 0.25 mols III<sub>a,b</sub>, 100 ml benzene and 0.75 mols hydrazine hydrate was kept under reflux for 2 h with azeotropic remove of water and alcohol. After cooling, the precipitate was filtered. The solid obtained was solved in water, purified with charcoal and precipitated with acetic acid.

8. *Structures V<sub>a-c</sub> and VI<sub>a,b</sub>*: 0.11 mols of 5-nitro-2-furaldehyde in 15 ml methanol and 0.1 mol II<sub>a-c</sub> or IV<sub>a,b</sub> (0.05 mols of II<sub>f</sub>) in 50 ml methanol gave after 50 minutes at 50°C expected nitro-furanhydrazomethines. The yellow solid was recrystallized from dimethylformamide.

**Acknowledgement:** The authors are grateful to Mr. Prof. Dr. Valer Parcasan for his permanent assistance in the achievement of this work. Our thanks to Mr. Nicolae Lungu and Mrs. Adriana Matei for their recorded spectra.

#### REFERENCES

1. K. Spirková, P. Bobal, *Collect. Czech. Chem. Comm.*, 1992, **57**, 2157.
2. Maunesier - Mamelli, *Gazz. Chim. Ital.*, 1941, **71**, 18.
3. C. W. Whitehead, J. T. Travesa, *J. Org. Chem.*, 1960, **25**, 413.
4. M. Patek, H. Hampe, *Collect. Czech. Chem. Comm.*, 1989, **54**, 3267.
5. C. Schapira, I. Prillo, *J. Heterocycl. Chem.*, 1980, **17**, 1281.
6. J. Svoboda, J. Paleček, *Collect. Czech. Chem. Comm.*, 1986, **51**, 1133.
7. F. Pahlborg, A. List, *Chem. Ber.*, 1887, **20**, 1596.
8. H. L. Rice, G. R. Petit, *J. Amer. Chem. Soc.*, 1954, **76**, 302.



NEW BIS-( $\gamma$ -L-GLUTAMYL)-DIAMIDE DERIVATIVES. PART II.

IOAN CRISTEA\* and CARMEN BĂTIU\*

ABSTRACT: New bis-( $\gamma$ -L-glutamyl)-diamides 1a-d were obtained by regioselective acylation of some aromatic diamines 3a-d, using N-phthalyl-L-glutamic anhydride followed by hydrazinolysis of protecting group with hydrazine hydrate.

$\gamma$ -L-Glutamyl-amides are important compounds with various applications in clinical diagnosis for detection of enzymes [1, 5], or compounds with biological activity [6]. Some  $\gamma$ -L-glutamyl amides as glutamine transport inhibitors are used for the treatment and diagnosis of cancer [7].

In our last paper [8], we have prepared some new  $\gamma$ -L-glutamyl-amides which can be used in clinical diagnosis of  $\gamma$  GT. Diagnosis of some diseases of the pancreas is based on the determination of enzymatic activity of the  $\gamma$ -glutamyl-transpeptidase ( $\gamma$ GT).

**Results and Discussion.** In this view, we have extended our studies in synthesis of some bis-( $\gamma$ -L-glutamyl)-diamides 1a-d.

This class of diamides has not yet been reported in literature.

The compounds 1a-d were prepared, starting from phthalyl-L-glutamic anhydride 2 by a regioselective acylation of some aromatic diamines 3a-d, followed by hydrolysis of phthalyl group with hydrazine hydrate.

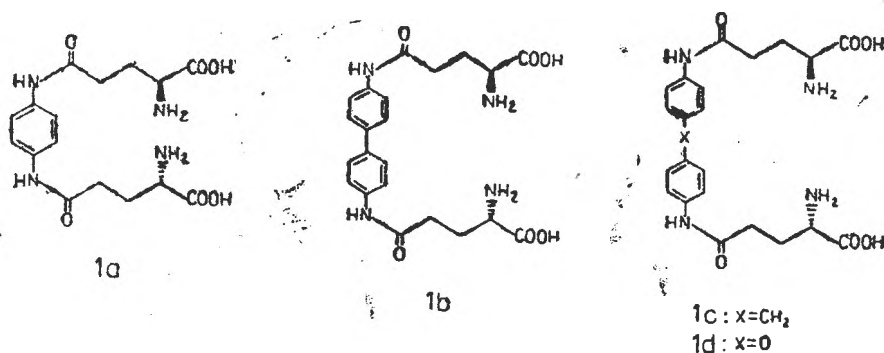


Fig. 1.

An interesting comparison can be made between phthalyl-L-glutamic anhydride and carbobenzoxy-L-glutamic anhydride; the first one reacts with amines to give only  $\gamma$ -L-glutamyl-amides by a high regio-selective reaction, while the

\* Department of Chemistry, "B-B" Univ. Str. Arany Janos 11, 3100 Cluj-Napoca, Romania.

second gives a mixture of  $\alpha$ - and  $\gamma$ -glutamyl-amides regioisomers. Phthalyl-L-glutamic anhydride **2** obtained by King and Kidd's method [9], can be used extensively for preparation of  $\gamma$ -L-glutamyl-amides in very high optical purity, due a preferential fission of the  $\gamma$ -carbonyl-to-oxygen bond. More details for this regioselective synthesis are given in another our paper [8].

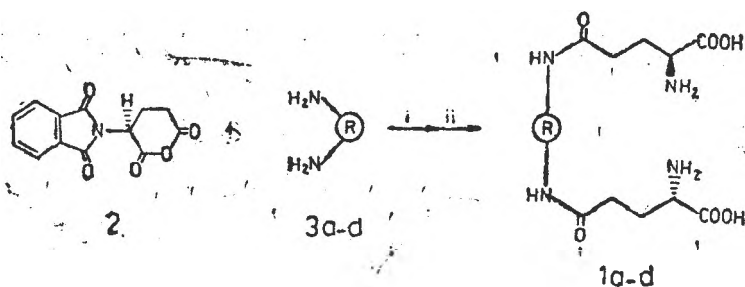


Fig. 2. Scheme 1. i: solvent  $\text{CHCl}_3$ ,  $60^\circ\text{C}$ ; ii:  $(\text{H}_2\text{N})_2\text{H}_2\text{O}$ , solvent MeOH,  $65^\circ\text{C}$ ; R = phenyl, diphenyl, diphenylmethane, diphenylether, substituted in 4, 4' position.

The reaction of acylation was studied in different solvents and basic catalysis, with p-phenylenediamine **3a** as substrat. Thus 2 equiv. of **2** and 1 equiv. of **3a** were reacted in chloroform or THF, under mild conditions ( $60^\circ\text{C}$ ) with  $\text{Et}_3\text{N}$  or pyrrolidine as bases, to give the N-protected bis-( $\gamma$ -L-glutamyl)-diamide **1a**. The best yields were obtained in all cases, using chloroform as solvent and  $\text{Et}_3\text{N}$  as catalyst.

Table 1

Acylation of some aromatic diamines **3a-d** with phthalyl-L-glutamic anhydride **2**.

Starting materials Ratio (2 : 3a-d)	Solvent	Catalyst	Yield %*	Product m.p. $^\circ\text{C}$
2equiv. : 1equiv.(3a)	$\text{CHCl}_3$	—	70	220
2equiv. : 1equiv.(3a)	$\text{CHCl}_3$	$\text{Et}_3\text{N}$	80	
2equiv. : 1equiv.(3a)	$\text{CHCl}_3$	Pyrrolidine	75	
2equiv. : 1equiv.(3a)	THF	$\text{Et}_3\text{N}$	72	
2equiv. : 1equiv.(3b)	$\text{CHCl}_3$	$\text{Et}_3\text{N}$	80	182
2equiv. : 1equiv.(3c)	$\text{CHCl}_3$	$\text{Et}_3\text{N}$	93	170
2equiv. : 1equiv.(3d)	$\text{CHCl}_3$	$\text{Et}_3\text{N}$	90	162

\* isolation of the product

Our investigations on the crude maerial by TLC (eluent ; 2-propanol : AcOH :  $\text{H}_2\text{O}$ ; 10 : 4 : 1) have shown that only one compound was obtained by acylation, with a little unreacted strating material.

No  $\gamma$ -monoamide was detected. These intermediates isolated without purification, were further converted to 1a-d by hydrazinolysis of the protected group. This reaction was performed in boiling methanol, for 1–2 h, using hydrazine hydrate 100%.

These diamides 1a-d are insoluble in many organic solvents.

For purification the compounds were dissolved in basic medium ( $\text{Na}_2\text{CO}_3$  1M,  $\text{NaHCO}_3$  1M) and then precipitated with 0.5N HCl at pH = 6,5.

This proceeding was repeated two times and then the purity was checked by TLC. The free diamides 1a-d obtained by this method were characterized by elemental analysis and IR spectra. The  $^1\text{H-NMR}$  spectra were not recorded due a very low solubility of these compounds in usual solvents.

The IR spectra shown the strong stretching bands at  $3380\text{ cm}^{-1}$  ( $\text{NH}_2$ ),  $3050\text{ cm}^{-1}$  ( $\text{NH}_3^+$ ),  $1680\text{ cm}^{-1}$  ( $\text{COOH}$ ),  $1420\text{ cm}^{-1}$  ( $\text{COO}^-$ ) and  $1610\text{ cm}^{-1}$  (amide). The IR absorption bands at  $3050\text{ cm}^{-1}$  and  $1410\text{ cm}^{-1}$  are very characteristic for the amphionic structure of the amino acids.

**Experimental.** The m.p. were determined in capillaries and are uncorrected. IR spectra were recorded in KBr pellets using a Karl Zeiss Jena UR-20 spectrophotometer. TLC was performed with Merck Kieselgel 60 F 254.

**General procedure for the preparation of bis-(N-phthalyl- $\gamma$ -L-glutamyl)-diamides.** To a mixture of N-phthalyl-L-glutamic anhydride 2 (20 mmol) and aromatic diamines 3a-d (10 mmol) in 30 ml chloroform,  $\text{Et}_3\text{N}$  or pyrrolidine (1 ml) was added. After being stirred at  $60^\circ\text{C}$  for 1–2 h, the reaction mixture was filtered, washed with chloroform and diethylether and dried. The precipitate was suspended in 15 ml HCl 0.5 N, stirred 5 min, filtered, washed with water and dried to give a pure product (TLC, eluent; 2-propanol: AcOH:  $\text{H}_2\text{O}$ ; 8:3:2).

**General procedure for the preparation of bis-( $\gamma$ -L-glutamyl)-diamides 1a–d.** 1a–d. A suspension of bis-(N-phthalyl-L-glutamyl)-diamide (6 mmol) in 35 ml MeOH was treated with 2.8 ml hydrazine hydrate 100%, the mixture was refluxed under stirring for 2 h and set aside at room temperature overnight. The precipitate was filtered and well washed with acetone and ether. The dried material was suspended in 30 ml HCl 1 N, filtered after 10 min from phthalhydrazide, and aqueous layer was adjusted to pH = 6–6,5 with  $\text{Na}_2\text{CO}_3$  1 M and the solid filtered. For purification the precipitate was dissolved in 20 ml  $\text{Na}_2\text{CO}_3$  1 M, 1 g charcoal was added under stirring, the suspension filtered after 5 min and the pure product 1a–d was precipitated from aqueous solution with HCl 2 N at pH = 6.

The purity was checked by TLC using as eluent 2-propanol: AcOH:  $\text{H}_2\text{O}$  10:4:1.

*Bis- $\gamma$ -L-glutamyl)-p-phenylenediamide 1a.* m. p.  $226^\circ\text{C}$ ; yield 62%;  $\nu\text{ cm}^{-1}$ : 3340s, 3030s, 1675s, 1620s, 1420s. Anal for  $\text{C}_{16}\text{H}_{22}\text{O}_6\text{N}_4$ : C, H, N calcd. 52.45, 6.01, 15.3; found 51.6, 5.9, 15.

*Bis- $\gamma$ -L-glutamyl)-4,4-diphenyldiamide 1b.* m.p.  $232^\circ\text{C}$ ; yield 52%;  $\text{cm}^{-1}$ : 3380s, 3040s, 1680s, 1620s, 1415s. Anal for  $\text{C}_{22}\text{H}_{20}\text{O}_6\text{N}_4$ : C, H, N calcd. 59.72, 5.88, 12.66; found 60.0, 6.1, 12.1.

*Bis- $\gamma$ -L-glutamyl)-4,4-diphenylmethane-diamide 1c.* m.p.  $218^\circ\text{C}$ ; yield 59%;  $\nu\text{ cm}^{-1}$ : 3320s, 3080s, 1670s, 1605s, 1410s. Anal for  $\text{C}_{23}\text{H}_{28}\text{O}_6\text{N}_4$ : C, H, N calcd. 60.52, 6.14, 12.28; found 61.0, 6.5, 11.9.

*Bis- $\gamma$ -L-glutamyl)-4,4-diphenylether-diamide 1d.* m.p.  $225^\circ\text{C}$ ; yield 71%;  $\text{cm}^{-1}$ : 3350s, 3050s, 1700s, 1600s, 1410s. Anal for  $\text{C}_{22}\text{H}_{20}\text{O}_6\text{N}_4$ : C, H, N calcd. 57.64, 5.67, 12.22; found 57.2, 6.0, 11.8.

## REFERENCES

1. M. Orłowski, *Arch. Immun. Therapie*, **13**, 538 (1965).
2. W. L. W. Jacobs, *Clin. Chim. Acta*, **31**, 175 (1971).
3. G. A. Moss, *Clin. Chem.*, **20**, 315 (1974).
4. I. Makoto, S. Masao, *Rinsho Kenso (Jap.)*, **18**, 10 (1974), C. A. 84, 134595z (1975).
5. H. Munakat, T. Tsutsui, S. Soto, *Jap. Kokai (pat.)*, 8836428 (1980), C. A. 94,66064w (1981).
6. A. Szent — Györgyi, *J. Org. Chem.*, **41**, 1603 (1974).
7. T. Nogotsu, S. Sakakibara, *Jpn. Kokai (pat.)*, 77568869 (1977), C. A., 89, 110416k (1978).
8. I. Cristea, S. Mager, C. Bătiu, G. Plé, *Rev. Roum. Chim.*, (1993), in press.
9. F. E. King, D. A. A. Kidd, *J. Chem. Soc.*, 3315 (1949).

## SOME NEW HYDRAZONES AND HYDRAZIDO-HYDRAZONES OF TERPENOIDS AND RELATED COMPOUNDS.

IOAN BĂȚIU\*, IOAN CRISTEA\* and VALER FĂRCĂȘAN\*

**ABSTRACT.** It were prepared some new condensation products between various type of terpenoids (IV, V, VI, VII, VIII, IX) and hydrazines (I, II) or hydrazide of isonicotinic acid (III). The new hydrazones and hydrazido-hydrazones were characterized by UV-VIS and IR spectra.

**Introduction.** As part of our larger program to contribute in the chemistry of terpenoids, we report as a preliminary note the preparation of some new hydrazones and hydrazido-hydrazones of this class of compounds.

As starting material we used the hydrazines: I (2-hydrazino-4-hidroxy-6-methyl pyrimidine), II (5-buthyl-2-hydrazino-4-hydroxy-6-methyl pyrimidine) [1], the hydrazide of isonicotinic acid(III) and various type of terpenoids, namely citral(IV), (+)-carvone(V), ( $\pm$ )- $\alpha$ -ionone (VI),  $\beta$ -ionone(VII), (-)-verbenone (VIII) (+)-fenchone(IX).

Such compounds may present interest as potential biological active. Species as show e. g. the hydrazones of menthone with hidrazide of isonicotinic acid [2], present biological activity.

The reaction were performed in the conditions described in the experimental section.

Tables 1, 2 and 3 listed the compounds prepared (XI ... XV a, b and c). From the spectral data only IR and UV-VIS were given, last one useful for an easliy handled quantitative analysis. As can be seen, the condensation of I, II and III ( $\lambda_{max}$  299,6, 305,260.3 nm) with the carbonyl compounds determine, a bathochromic shift of the band from longest the wave lenght in the electronic spectrum.

The compounds XI-c, XIII-c and XIV-c were prepared earlier [3, 4] in another experimental conditions, XIII-c was isolated only as hydrochloride [4]

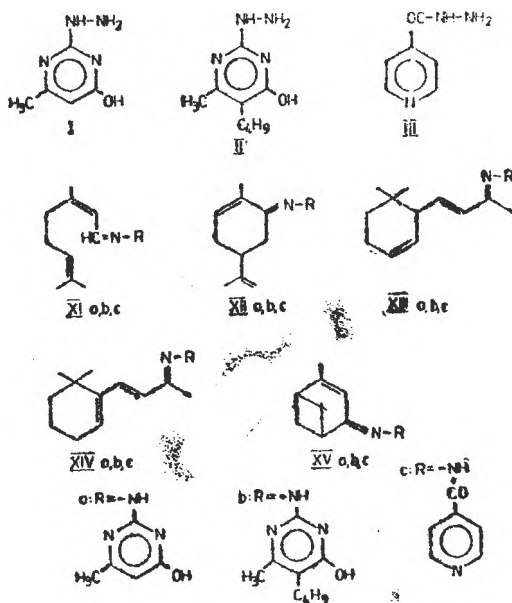


Fig. 1. Formulae.

\* University of Cluj-Napoca, Faculty of chemistry and industrial chemistry, 3400 Cluj-Napoca, Romania.

Table 1

## Condensation products of I (XI-a ... XV-a)

No.	Substance	Starting carbonyl compound	Melting point [°C]	Formula (Mol. wt.)	Analysis, N [%]		IR spectra* 1/λ, cm <sup>-1</sup>	Electronic** spectrum λ <sub>max</sub> , nm ε <sub>max</sub> × 10 <sup>-3</sup>
					Calcd.	Found		
1.	XI-a	Citraf (IV)	144-5	C <sub>15</sub> H <sub>20</sub> N <sub>4</sub> O (274.36)	20.42	19.8	1585, 1635, 2890, 1480, 1315, 1105, 820, 960, 700	316.0 (22.6)
2.	XII-a	(+)-Carvone (V)	173-4	C <sub>15</sub> H <sub>20</sub> N <sub>4</sub> O (272.34)	20.57	20.5	1590, 1670, 2910, 815, 1300, 1100, 1190, 1040, 690	316.0 (22.0)
3.	XIII-a	(±)-α-Ionone (VI)	218-20	C <sub>15</sub> H <sub>20</sub> N <sub>4</sub> O (314.42)	17.82	18.0	1595, 1610, 2910, 1120, 1260, 965, 1450, 1355, 855	304.5 (23.1)
4.	XIV-a	β-Ionone (VII)	169-70	C <sub>14</sub> H <sub>18</sub> N <sub>4</sub> O (314.42)	17.82	18.2	1570, 1665, 2920, 1110, 1450, 1340, 970, 1170, 820	316.8 (17.5)
5.	XV-a	(-)-Verbenone (VIII)	186-8	C <sub>15</sub> H <sub>20</sub> N <sub>4</sub> O (272.34)	20.57	20.6	1580, 1665, 2940, 1430, 1090, 1275, 810, 970, 1245	319.4 (22.7)

\* Only some of the more intense bands were given

\*\* The band of the longest wave length in the electronic spectrum

Table 2

## Condensation products of II (XI-b ... XV-b)

No.	Substance	Starting carbonyl compound	Melting point [°C]	Formula (Mol. wt.)	Analysis, N [%]		IR spectra* 1/λ, cm <sup>-1</sup>	Electronic** spectrum λ max, nm ε <sub>max</sub> × 10 <sup>-3</sup>
					Calcd.	Found		
1.	XI-b	Citral (IV)	141-3	C <sub>19</sub> H <sub>30</sub> N <sub>4</sub> O (330.47)	16.95	16.6	1650, 1695, 2920, 1435, 1500, 1335, 1375, 1100, 975	325.1 (22.1)
2.	XII-b	(+)-Carvone (V)	174-6	C <sub>19</sub> H <sub>22</sub> N <sub>4</sub> O (328.45)	17.06	16.9	1615, 1640, 2920, 1125, 1430, 1050, 1310, 775, 1240	322.5 (25.5)
3.	XIII-b	(±)-α-Ionone (VI)	182-3	C <sub>22</sub> H <sub>34</sub> N <sub>4</sub> O (370.53)	15.12	15.2	1650, 1580, 2960, 1445, 1375, 1335, 1110, 970, 535	320.1 (23.8)
4.	XIV-b	β-Ionone (VII)	178-9	C <sub>23</sub> H <sub>34</sub> N <sub>4</sub> O (370.53)	15.12	14.9	1655, 1690, 2930, 1455, 1545, 970, 1340, 1375, 1100	325.1 (23.2)
5.	XV-b	(-)-Verbenone (VIII)	159-60	C <sub>19</sub> H <sub>28</sub> N <sub>4</sub> O (328.45)	17.06	17.0	1675, 1610, 2930, 1540, 1465, 1280, 1045, 1080, 1235	311.0 (13.0)

\* Only some of the more intense bands were given

\*\* The band of the longest wave length in the electronic spectrum

Table 3

## Condensation products of III (XI-e ... XV-e)

No.	Substance	Starting carbonyl compound	Melting point [°C]	Formula) (Mol. wt.)	Analysis, Calcd.	N [%] Found	IR spectra* 1/λ, cm <sup>-1</sup>	Electronic** spectrum λ max, nm ε <sub>max</sub> × 10 <sup>-3</sup>
1.	XI-c	Citral (IV)	127-8	C <sub>16</sub> H <sub>21</sub> N <sub>3</sub> O (271.36)	15.48	15.5	1635, 1650, 3050, 1550, 1300, 690, 1390, 1410, 870	300.2 (20.2)
2.	XII-c	(+)-Carvone (V)	140-2	C <sub>16</sub> H <sub>19</sub> N <sub>3</sub> O (269.34)	15.60	15.8	1650, 1540, 3180, 1290, 1040, 1430, 1120, 995, 680	282.8 (12.3)
3.	XIII-c	(±)-α-Ionone (VI)	163-5	C <sub>19</sub> H <sub>25</sub> N <sub>3</sub> O (311.42)	13.49	13.8	1660, 1525, 3320, 1555, 1275, 970, 1380, 840, 680	284.1 (16.3)
4.	XIV-c	β-Ionone (VII)	172-3	C <sub>18</sub> H <sub>23</sub> N <sub>3</sub> O (311.42)	13.49	13.7	1645, 1530, 2920, 1400, 755, 1145, 670, 835, 960	312.2 (19.0)
5.	XV-c	(-)-Verbenone (VIII)	206-7	C <sub>16</sub> H <sub>19</sub> N <sub>3</sub> O (269.34)	15.60	15.9	1645, 1530, 2940, 1615, 1285, 1540, 1590, 685, 1135	302.0 (13.7)

\* Only some of the more intense bands were given

\*\* The band of the longest wave length in the electronic spectrum

If (+)-fenchone (IX) was reacted with I, II or III in the condition used for us by IV . . . VIII, no condensation was observed. This behaviour may be attributed to a steric hindrance.

In the case of IV,V, VII and VIII  $\alpha$ ,  $\beta$ -unsaturated carbonyl compounds, beside the 1,2 addition, which precede the formation of the corresponding hydrazone, an 1,4 addition may be expected. Our preliminary observations by the condensation of III with IV support this fact.

Exposed to the sunlight, XII-a, give a new compound, as indicate TLC.

The detailed studies of the two last mentioned behaviours and that of related compounds will be the topic of our subsequent work.

The investigations of the TLC and the biological activity of the new compounds are in progress.

**Experimental.** The melting points determined in glass capillaries are not corrected. The electronic spectra UV-VIS were recorded in ethanol on a "Specord M 40" Carl Zeiss Jena spectrometer. For recording IR spectra (in KBr pellets) a "Specord M 80" Carl Zeiss Jena was used.

**General method.** A mixture of 0.0075 M hydrazine (I, II) or hydrazide (III) and 0.0085 M carbonyl compound\* in 30 ml ethanol (in the case of I, 150–200 ml) was refluxed for 6–10 hours. After 24 hours in the refrigerator, the precipitate was filtered and dried. If after 24 hours no precipitation occurred, the ethanol was distilled off and the residue (viscous or solid product) was macerated with ligroin and the solvent decanted. This procedure was repeated until a powder was obtained. After the last maceration, the solid was filtered and washed with ligroin and acetone. In the case of the reaction products of III, also a washing with warm water was useful. The crude dried products were recrystallized from acetone.

The yields are between 25% to 75%. We were interested only in the obtained of the new pure substances (compounds) not in yields.

#### REFERENCES

1. I. E. Brady, K. M. Herbst, *J. Chem. Soc.*, **24**, 922 (1959).
2. C. H. Budeanu, E. Budeanu, A. Toma, *Analele științifice univ. Al. I. Cuza, Iași*, Sect. I, **2**, 281–90 (1956).
3. G. Carrara, V. D'Amato, G. Rolland, E. Fusarpoli, *Gazz. chim. ital.*, **83**, 459 (1953).
4. Peter P. T. Sah, S. A. Peoples, *J. Amer. Pharm. Assoc.*, **43**, 513 (1954).

\* For the condensation pure or technical acyclic compounds were used. Namely: citral (96.22%), (+)-carvone (90.5%), ( $\pm$ )- $\alpha$  and  $\beta$ -ionone (99.90%), (-)-verbenone (82.80%).



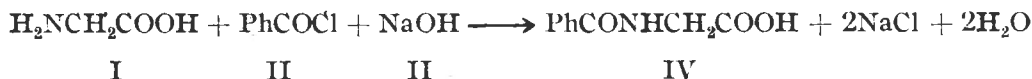
## OPTIMIZATION OF HIPPURIC ACID SYNTHESIS

IONEL HOPĂRTEAN\*, ALEXANDRU LUPU\*\*, IRINA TARSICHE\*\*\* and  
IOANA HOPĂRTEAN\*\*\*

ABSTRACT. This paper presents a new experimental method to obtain the optimum technology for the synthesis of hippuric acid and purity determination by potentiometric titration.

Hippuric acid is an important compound in some essential aminoacids synthesis (tryptophan, phenylalanine, histidine).

Hippuric acid is obtained by the reaction between glycine (Gly, I) and benzoyl chloride (II) in alkaline medium (NaOH, III). This seems to be the most favorable method to obtain it [1-3].



This paper deals with a method for the optimization of the hippuric acid synthesis. The influence of the molar ratios of the reagents upon the yield hippuric acid was studied by an experiment which consists in the adequate change of the molar ratios of the reagents.

This experiment begins with the identification of the independent variables (amounts of the reagents) then continues with the choice of the quantities, according to the stoichiometric molar ratios of the reagents (the base level). Then the molar ratio Gly : PhCOCl : NaOH is changed as follows : PhCOCl : Gly = 0.9 : 1(-1) and 1.1 : 1(+1) and the molar ratio NaOH : Gly = 1.5 : 1(-1) and 2.5 : 1(+1). Each combination of these ratios is tested. The Gly concentration is maintained at the constant level of 0.031 M (2.325 g/l) and then the concentrations of the other reagents (II, III) are changed according to the figure 1.

The change takes place systematically following the change of the experimental matrix and the resulted amount of hippuric acid is observed.

As can be seen in figure 1 the molar ratio PhCOCl : Gly is modified with the increment  $\Delta_1 = \pm 0.1$  and the molar ratio NaOH : Gly with  $\Delta_2 = \pm 0.5$ . The point in the center of the figure corresponds to the base level.

\* Department of Organic Chemistry "Babeș-Bolyai University" Cluj-Napoca.

\*\* Military Institute "Nicolae Bălcescu" Sibiu, Romania.

\*\*\* Chemical Institute Cluj-Napoca, Romania.

The coefficients in the regression equation are determined by solving the equation:

$$A = (X_T X)^{-1} (X_T Y) \text{ where: } \begin{array}{l} X \text{ independent variables matrix} \\ Y \text{ dependent variables matrix} \end{array}$$

The regression equation obtained is:  $y = 0.657 + 0.586x_1 + 0.28x_2$  where:

$y$  is the quantity of hippuric acid obtained (g)

$x_1$  is the volume of PhCOCl used ( $\text{cm}^3$ )

$x_2$  is the quantity of NaOH used (g)

This equation describes a surface of the experimental data, each experimental  $y$  having the coordinates  $x_1$  and  $x_2$  [4].

The experimental data (table 1, 2) show that the best yield of the hippuric acid is obtained for the molar ratio Gly : PhCOCl : NaOH = 1 : 1.1 : 2.5.

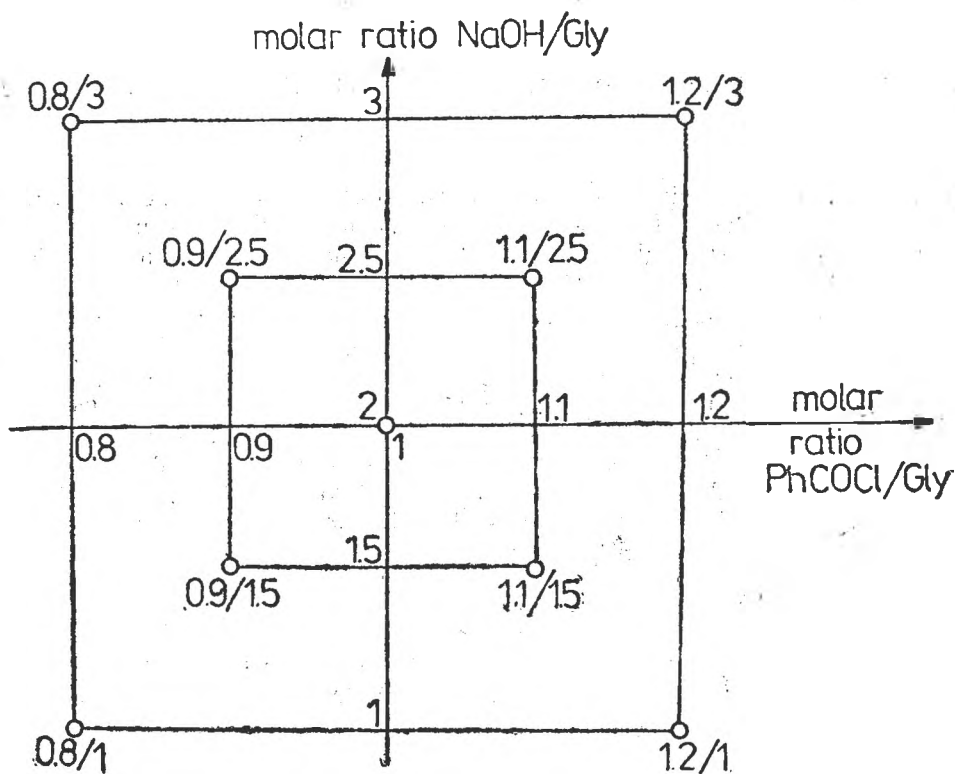


Fig. 1. Molar ratios of the reagents during the experiment

Table 1

Experimental data obtained in the proposed experimental

Nr.	Molar ratio I/II/III	PhCOCl cm <sup>3</sup>	NaOH g	Hippuric acid		m.p. °C	Yield %
				Taw	pure		
0	1	2	3	4	5	6	7
1	1/1/2	2.89	2.0	3.1	2.5	188	56.00
2	1/0.9/1.5	2.60	1.5	2.7	2.2	189	54.76
3	1/0.9/2.5	2.60	2.5	3.0	2.1	189	54.74
4	1/1.1/1.5	3.18	1.5	3.3	2.0	187	44.85
5	1/1.1/2.5	3.18	2.5	3.4	3.1	190	69.50
6	1/1.2/3	3.47	3.0	3.3	2.9	190	65.10
7	1/0.8/3	2.31	3.0	2.2	1.9	189	53.17
8	1/0.8/1	2.31	1.0	2.1	1.9	190	53.20
9	1/1.2/1	3.47	1.0	2.2	1.8	188	40.33

Table 2

Experimental data obtained when CCl<sub>4</sub> was used to wash hippuric acid crystals

0	1	2	3	4	5	6	7
10	1/1/2	2.89	2.0	3.0	2.1	190	47.04
11	1/1.1/2.5	3.18	2.5	3.7	3.0	190	67.21

**Experimental.** In a 250 ml round bottom flask, 0.031 M Gly, 0.032 M PhCOCl and 0.031 M NaOH are mixed under continuous stirring. PhCOCl is slowly added. The reaction is exothermic. After 45 minutes, HCl is added under stirring for the precipitation of hippuric acid. The obtained hippuric acid is filtered in vacuum. The crystals are washed with ethyl ether or CCl<sub>4</sub> to remove secondary products, and dried. Hippuric acid is purified by recrystallisation from water; 2.5g hippuric acid were obtained, m.p. 188°C, yield 56%.

Table 2 presents the results obtained when the filtered crystals of hippuric acid were washed with CCl<sub>4</sub>.

**The determination of hippuric acid purity.** The purity of hippuric acid is determined by titration with an aqueous solution of NaOH 0.1 M. Hippuric acid was solved in EtOH (0.4479 g in 25 ml EtOH). Samples of 5 ml were tested. Titration was carried out under continuous stirring, successively adding NaOH solution (of known concentration). The pairs: NaOH volume (ml) — potential

(mV), were recorded. A titration curve was built up. The equivalence point was calculated using the Hahn-Weiller method [5].

$V_{\text{NaOH}}$ (ml)	E (mV)	$\Delta E^I$	$\Delta E^{II}$
4.5	40	40	235
5.0	0		
5.5	-275	275	269
6.0	-281	6	504

$$V = 5.0 + 0.5 \frac{235}{504} = 5.23 \text{ ml}$$

The experimental results obtained at the determination of hippuric acid by potentiometric titration on samples no. 5 and 11 from tables 1 and 2 are shown in fig. 2.

The amount of pure hippuric acid in the samples is calculated as follows:

$$m = \frac{M V_e N f}{V}$$

where:

M — molar weight of hippuric acid (179.17 g)

$V_e$  — average equivalence volume (ml NaOH)

N — normality of the NaOH solution

f — factor of the NaOH solution

V — volume of sample (ml)

m — concentration of hippuric acid in the sample (g/l)

The amount of hippuric acid found was:

$$m = \frac{179.17 \times 5.14 \times 0.1 \times 0.972}{5.0} = 17.903 \text{ g/l}$$

The purity of the hippuric acid was calculated as follows:

$$\text{purity} = \frac{m}{17.917} \times 100\%$$

The purity of the prepared hippuric acid is:

$$\text{purity} = \frac{17.903}{17.917} \times 100\% = 99.92\%$$

**Conclusions.** As the experimental results show, the best molar ratio of the reagents for the synthesis of hippuric acid is: Gly : PhCOCl : NaOH = 1 : 1.1 : 2.5. The excess of II and III leads to the increase of the rate of the reaction. A

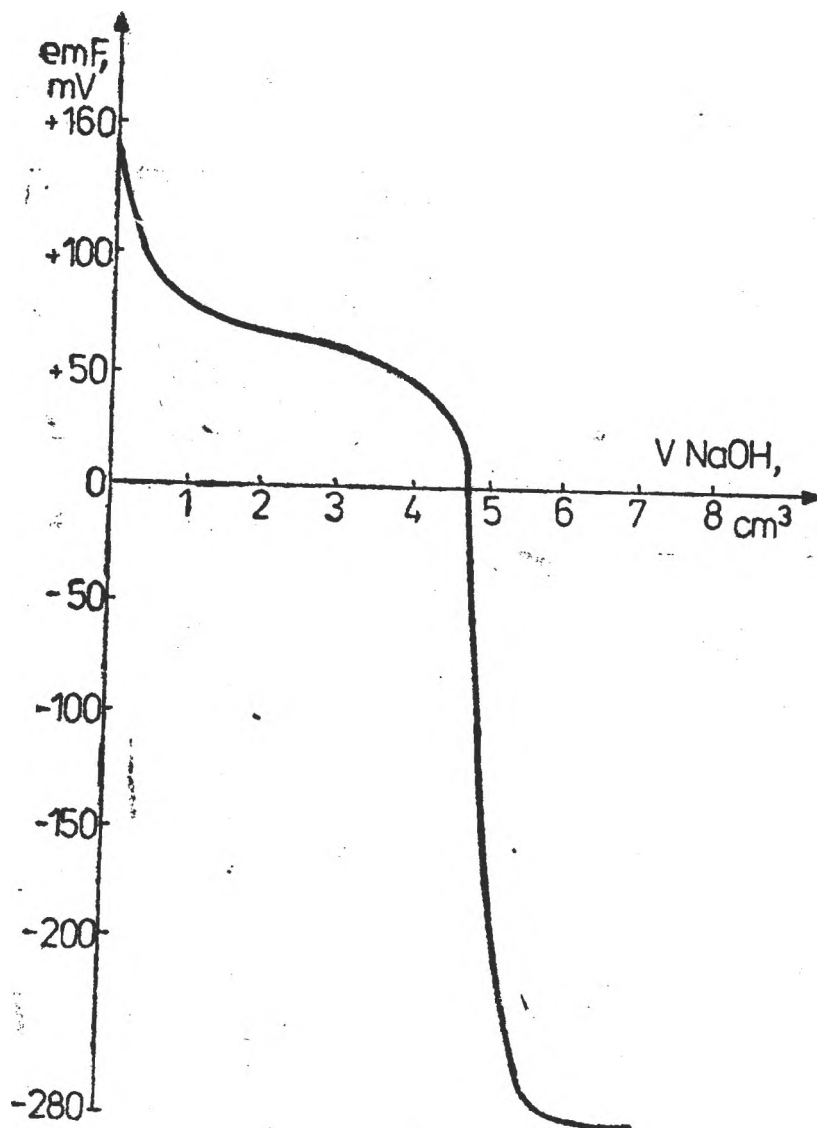


Fig. 2. Potentiometric titration curve.

further increase in  $\text{PhCOCl}$  and  $\text{NaOH}$  excess doesn't lead to the improvement of yield (70%).

The secondary products were washed off with  $\text{CCl}_4$  which is not inflammable. The determination of hippuric acid purity leads to the conclusion that a high purity product was obtained (99.92%).

## REFERENCES

1. E. Fischer, *Ber. dtsh. Chem. Ges.*, **38**, 612 (1905).
2. H. Tauchy, C. F. Van Sumere, *Arch. Int. Physiol. Biochim.*, **79** (3), 589 (1971).
3. R. K. Huckle, D. H. Hutson and P. Millburn, *Drug. Metab. Dispos.*, **9** (4), 352 (1981).
4. Dumitru Ceaușescu, „*Utilizarea statisticii matematice în chimia analitică*”, Ed. Tehnică București, 1982.
5. E. Cordos, I. Kekedy, *Lucrări practice de analiză instrumentală*, Babeș-Bolyai University Cluj-Napoca, 1985.

## THE MASS SPECTRUM OF 3-PHENYL-2,1-BENZISOXAZOLE.

IONEL HOPÂRTEAN\*, MIRCEA VLASSA\* and IOANA HOPÂRTEAN\*\*

**ABSTRACT.** — The mass spectrum of 3-phenyl-2,1-benzisoxazole has been recorded and the similarity between mass spectra of the title compound, acridone and acridine-N-oxide is discussed.

Although the behaviour of some aromatic heterocyclic ring systems like oxazole, benzoxazole and 2,1-benzisoxazole under electron impact have been discussed [1-3], a study of the mass spectrum of 3-phenyl-2,1-benzisoxazole has not been reported.

Details of the mass spectrum of this compound, recorded by us, are presented in Tabel 1 and Scheme 1. As we can notice the spectrum is typical for heterocyclic compounds, dominated by a peak at  $m/e$  195 (the molecular ion is the base peak). The molecular ion undergoes two fragmentation pathways, analogous with 2,1-benzisoxazole [3]. A first one consists in the loss

Tabel 1

Mass spectral data  $m/e$  (I%) of compounds I-III\*\*\*

I	39(8), 51(20), 63(6), 71(4), 77(45), 84 (5), 90(8), 92(12), 105(7), 113(6), 151(7), 120(6), 138(8), 139(18), 140(10), 166(23), 167(55), 168(8), 195(100, M)
II	39(9), 61(18), 63(7), 69.5(12), 71(5), 77(40), 84(10), 90(10), 102(5), 113(14), 115(8), 138(7), 139(18), 140(20), 151(7), 166(24), 167(52), 179(17), 194(87), 195(100, M), 196(18), 197(10).
III	39(10), 51(17), 63(8), 68(6), 70(8), 71(6), 77(29), 83(8), 84(10), 89(5), 90(6), 91(11), 102(6), 113(9), 115(12), 138(8), 139(20), 140(18), 151(6), 166(25), 167(54), 168(71), 195(100, M), 196(19), 197(11).

of a CO molecule by a skeletal rearrangement leading to the ion **a**  $m/e$  167, which fragments further by loss of HCN and of a hydrogen radical yielding ions **b**  $m/e$  140 and **c**  $m/e$  139, respectively [4, 5]. The ion **c** in its turn eliminates acetylene giving the ion **d**  $m/e$  113 (see Scheme 1, the asterisk denotes the presence of an appropriate metastable ion). The second degradation sequence of molecular ion involves the cleavage of the 2,1-benzisoxazole ring generating the ion **e**  $m/e$  105 and **f**  $m/e$  90, respectively. The ion **e**  $m/e$  105 losses CO

\* Department of Organic Chemistry, "Babeș-Bolyai University", str. Arany Janos 11, 3100 Cluj-Napoca, Romania.

\*\* Chemical Institute Cluj-Napoca, Romania.

\*\*\* The peaks corresponding to less than 2% relative intensities were not tabulated.

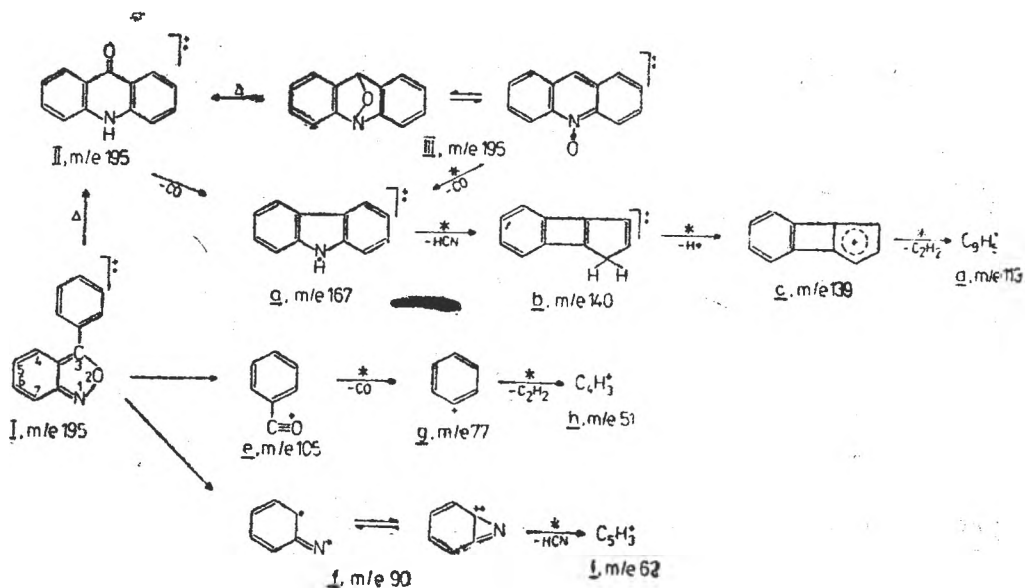


Fig. 1. Scheme 1.

molecule and then acetylene giving the abundant ion **g** m/e 77 and **h** m/e 51; the ion **f** eliminates HCN leading to the ion **i** m/e 63.

The first fragmentation mode presented above involves an intramolecular skeletal rearrangement process which have also been noticed in the case of the acridine [6, 7], azoxybenzene and phenazine-N-oxide [8] derivatives.

If we compare the spectrum of 3-phenyl-2,1-benzisoxazole (I) with those of acridone (II) and acridine-N-oxide (III) the similar behaviour of these compounds in the mass spectrometer conditions is obvious (see Table I and Scheme 1). Thus the ions m/e 167, 140, 139 and 113 are common for all these compounds. It can be accounted for by the fact that the molecular ion undergoes a skeletal rearrangement to II, which is common for I, II and III; then it fragments further to ions m/e 167, 140, 139 and 113. This statement is supported by the fact that at 150°C 3-phenyl-2,1-benzisoxazole [9, 10] and acridine-N-oxide [11, 12] suffer a thermal rearrangement to acridone.

**Experimental.** The substances were prepared by literature methods [13–15]. The purity was checked by TLC on silica gel. The mass spectra were recorded using a Perkin-Elmer GL mass spectrometer operating at 70 eV and 100  $\mu$ A.

Metastables peaks were measured by scanning the electrostatic field (DADI) and the accelerating voltage (defocusing technique). Metastables peaks: 143.2, calculated, 143.02 (for ion **a**); 117.40, calculated 117.36 (for ion **b**); 91.80, calculated 91.86 (for ion **d**); 56.40, calculated 56.46 (for ion **g**); 33.70, calculated 33.77 (for ion **h**), 44.04, calculated 44.10 (for ion **i**).

## REFERENCES

1. J. H. Bowie, P. F. Donagaue, H. J. Rodda, R. G. Cooks and D. H. Williams, *Org. Mass Spectrom.*, **1**, 13 (1968).
2. H. Ogura S. Sugimoto and T. Itoh, *Org. Mass Spectrom.* **3** (10), 1341 (1970).
3. A. Maguestian and J. van Haverbeke, *Org. Mass Spectrom.*, **9** (1), 199 (1974).
4. M. Ishikawa, Ch. Kanebo and S. Yamado, *Tetrahedron Letters*, **43**, 4519 (1968).
5. *Catalogue of Mass Spectral Data*, American Petroleum Institute Research Project 44, Carnegie Institute of Technology, Pittsburg, spectrum 638.
6. J. H. Bowie, R. G. Cooks, R. H. Prager and H. M. Thredgold, *Austral. J. Chem.*, **20** (6), 1179 (1967).
7. H. H. Mantsch, *Rev. Roumaine Chim.*, **14**, 549 (1969).
8. J. H. Bowie, R. G. Crooks and G. E. Lewis, *Austral. J. Chem.*, **20**, 1601 (1967).
9. P. L. Coe, A. E. Jukes and J. C. Tatlow, *J. Chem. Soc. C*, 1966, 2020.
10. R. Kwok and P. Franc, *J. Org. Chem.*, **33**, 2880 (1968).
11. I. Tănăsescu, L. Almași and A. Hantz, *Sudii și Cercetări Chim.*, fil. Cluj, **11**, 105 (1960).
12. I. Tănăsescu and E. Ramonțian, *Bull. Soc. Chim. France* 1934, 547.
13. I. Hopârtean, S. Mager and M. Ionescu, *Stud. Univ. Babeș-Bolyai, Chem.*, **22**, 6 (1976).
14. M. Ionescu and M. Hopârtean, *Stud. Univ. Babeș-Bolyai, Chem.*, **21**, 6 (1976).
15. M. Ionescu, H. Mantsch and I. Goia, *Chem., Ber.*, **16**, 1726 (1963).



## THIAZOL XIII. NITRIERUNGSREAKTION IN DER PHENYLTHIAZOLREIHE.

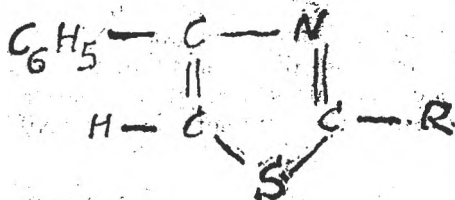
ANDRÁS BENKŐ und ILDIKÓ SZATMÁRI \*\*

**ABSTRACT.** The nitration reaction in the phenylthiazole series. The orientation effect exerted by the substituents located on the thiazole ring upon the nitration reaction within the phenylthiazole series was investigated. The nitration of 2-phenyl-4-R-thiazoles was carried out. The nature of the substituent on the thiazole ring was the decisive factor in orienting the nitration of the phenyl moiety in the para or meta position. The meta-substituted products represented less 5% of the obtained nitrated derivativeis.

**Einleitung.** Im Fall der Phenylthiazolderivaten, wenn man den Thiazolring als ein Substituent von ersten Rang betrachte, welcher in dem Benzolring sich befindet, kann man die Orientierungseffekte studieren. Für diesem Zweck wurden die Mononitroderivaten gewählt und es wurde mit eine Nitrierungsmischung gearbeitet, berechnet in der streng stöchiometrischen Quantität.

Die Nitrierungsreaktion von Phenylthiazolderivaten die mit ein Substituent von ersten Rang substituiert sind, findet unabhängig von der Stellung des Substituentes in der para Stellung des Phenylrings statt.

In der Mitteilung XII wurde dargestellt, dasz Phenylthiazolderivate von den Typen: oder Substituenten von zweiten Rang.



R: -COOH  
-COOCH<sub>3</sub>

Fig. 1.

Im Fall der Nitrierungsreaktion die NO<sub>2</sub>-Gruppe würde anabhängig von dem Charakter des Substituentes nur in der para Stellung eintreten.

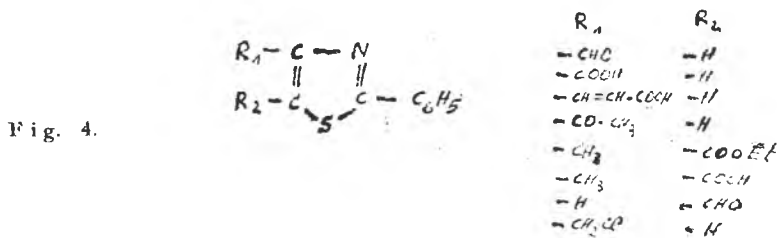
**Diskussion:** Unsere nachtragliche Untersuchungen beweisen, dasz, wenn R ein Substituent von zweiten Rang ist, wurde auch das m-Nitrophenylderivat gebildet sein, aber einem kleinem Anteil. Nach der Oxidation der Nitrierungsprodukten erhält man eine Mischung von meta und para Nitrobenzoesäure mit einem Schmelzpunkt von 190°C und das beweist, dasz auch die meta Nitrobenzoesäure, dessen Schmelzpunkt 141°C beträgt, gebildet ist. Nach wiederholter Re-

\* Universität Babeş-Bolyai Cluj-Napoca Rumänien.

\*\* Mitteilung XII: A. Silberg, A. Benko, und I. A. Panczel, Studia Univ. Babeş-Bolyai.

kristallisation erhebt sich der Schmelzpunkt bis 241°C (der Schmelzpunkt der reinen p-Nitrobenzoesäure beträgt 241°C). In diesem Fall gibt es das meta Nitroderivate in einer sehr kleinen Quantität (weniger als 5%) und es wurde aus der Mutterlauge erhalten.

In unseren Untersuchungen haben wir Derivaten von folgenden Typen betrachtet :



Die Derivaten von 2-Phenyl-4-R<sub>1</sub>-5-R<sub>2</sub> thiazolen sind mit einer Nitrierungsmischung nitrirt worden, die in eine strengstöchiometrische Quantität berechnet ist. Die erhaltenen Nitroderivaten sind danach mit KMnO<sub>4</sub> oxydiert worden und es wurde die Nitrobenzoesäure erhalten.

Es wurde die Solubilität im Wasser der Nitrobenzoesäure festgestellt :

	Schmelzpunkt C	Solubilität (20°C)
1. orto Nitrobenzoesäure	146—148	—
2. meta Nitrobenzoesäure	140—141	1,245 g/100 ml
3. para Nitrobenzoesäure	241	0,15 g/100 ml

Die Tabelle zeigt eindeutig, dass (nach der Oxydation von 2-Phenylthiazolen, die in der 4 und 5 Position substituiert sind) von allen Nitrobenzoesäuren die meta Derivate in der Lösung bleiben weil diese ungefähr eine 8,5 mal größere Solubilität hat, para Derivat sich heraus schlagen. Man stellte fest, dass das Hauptprodukt der Oxydationsreaktion immer die para Nitrobenzoesäure ist.

Wenn R<sub>1</sub> oder R<sub>2</sub> ein Substituent von ersten-Rang ist, wurde aus der Reaktionsmischung, nach der Isolierung der p-Nitrobenzoesäure aus der Mutterlauge, in allen Fällen auch die m-Nitrobenzoesäure erhalten (Schmelzpunkt 140—141 C), aber nur in einem kleinen Anteil (weniger als 5%). Es ist zu bemerken dass die orto-Nitrobenzoesäure in keinem Fall erhalten wurde wahrscheinlich wegen des primären sterischen Effektes.

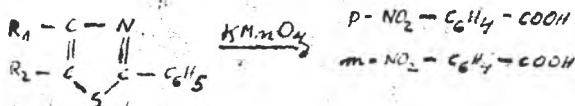


Fig. 2.



Es wurden nach der Nitrierungsreaktion ein Gemisch von p- und m-Nitrophenylderivaten erhalten. Sch. p. 236°C.

*2-Phenyl-4-thiazolil-acrilsäure*: Man erwärmt am Rückfluszkühler auf dem Wasserbade 6 Stunden in Gemisch von 15 g (0,08 Mol) 2-Phenyl-4-formylthiazol, 9,3 g (0,08 Mol) Malonsäure, 69 ccm Pyridin und 6 ccm Triäthylamin. Die Erwärmung des Gemisches wurde noch 6 Stunden noch 120–125°C auf dem Oelbad fortgesetzt. Man kühlt die Lösung und neutralisiert mit verdünnter HCl-Lösung. Man filtriert den gebildeten Niederschlag, dann wird mit Wasser gewaschen und aus Benzol umkristallisiert. Man erhielt 2-Phenyl-4-thiazolylacrilsäure mit Sch.p. 190°C. Ausb. 87%. In Nitrierungsreaktion wurde ein Substanz mit Sch. p. 217–218°C erhalten.

*Methylester von 2-Phenyl-4-thiazolylacrilsäure*: Man löst 2,3 g 2-Phenyl-4-thiazolylacrilsäure in 10 ccm Methanol, beträgt 3 Tropfen  $H_2SO_4$  und das Reaktionsgemisch wurde am Rückfluszkühler 1 Stunde auf dem Wasserbad erwärmt. Man filtriert den gebildeten Niederschlag und dann wird er aus dem wässriger Methanol (3:1) mehrmalig umkristallisiert. Man erhielt eine weisse kristallinische Substanz. Sch. p. 124–125°C. Ausb. 80%.

In der Nitrierungsreaktion wurde ein p-Nitrophenylderivat erhalten. Sch. p. 178°C.

*Ester der  $\alpha$ -Chloracetyllessigsäure*: In einem rundlichen unterlagenen Kolben versehen mit Tropftrichter, mechanischer Turbinierungsgesetz und Gasableitung leitet man 39 g (0,3 Mol) Ester der acetyllessigsäure ein und unter Turbinieren des Gemisches tropft man 42,5 g  $SO_2Cl_2$  (ein Überschuss von 5%). Nachdem Tropfen der  $SO_2Cl_2$  (ein lebhaftige Gasentwicklung von HCl und  $SO_2$  stattfindet) destilliert man das Reaktionsgemisch in Vakuum. S.p. 105–110°C/30 Hg mm oder 193°C.

*2-Phenyl-4-methyl-5-carboxythiazolsäure*: Man erwärmt am Rückfluszkühler ein Gemisch von 16,5 (0,1 Mol) Ester der  $\alpha$ -Chloracetyllessigsäure und 13,7 g (0,1 Mol) Thiobenzamid [3], der vorherige in 25 ccm Methanol gelöst wurde. Die erhaltene Lösung, in der Ester der 2-Phenyl-4-methyl-5-carboxy thiazolsäure bildet wurde, hydrolisiert man mit 10 g NaOH in einer minimalischen Quantität Wasser gelöst, man erwärmt noch ein halb Stunde und giesst man in 80 ccm Wasser und einsäuert mit konz. HCl Lösung. Der ausgefallene Niederschlag der 2-Phenyl-4-methyl-5-carboxythiazolsäure wird filtriert und aus Essigsäure umkristallisiert. Sch. p. 204–205°C. Ausb. 90%.

In Nitrierungsreaktion wurde eine schwachgelbliche Substanz erhalten. Sch. p. 201°C die ein Gemisch von der p- und meta Nitrophenylderivat ist.

*2-Phenyl-4-methyl-5-acetylthiazol*: Man kocht am Rückfluszkühler 1 Stunde ein Gemisch aus 2,6 g (0,019 Mol) Thiobenzamid, in 26 ccm Benzol gelöst und 2,6 g (0,019 Mol) 3-Chlor-2,4-pentandion (erhält man in einem Chlorierungsreaktion der Acetylaceton mit Hilfe  $SO_2Cl_2$ ). Nach dem Erkalten der Reaktionsmischung wurde 2-Phenyl-4-methyl-5-acetyl thiazol ausgefällt, filtriert und umkristallisiert. Sch. p. 85°C. Ausb. 89%.

In Nitrierungsreaktion wurde ein Substanz erhalten, das ein Gemisch von der p- und meta-Nitrophenylderivat ist. Sch. p. 96°C.

*2-Phenyl-5-formylthiazol*: Man erwärmt 10 Min. am Rückfluszkühler ein Gemisch aus 1 g (10 mMol) Chlormalondialdehyd [4] und 1,37 g (10 mMol) Thio-

benzamid in 10 ccm Aceton. Nach der Entfernung des Lösungsmittels wird die bleibende Substanz aus Wasser umkristallisiert (ergab Aktivkohle), man erhält 2-Phenyl-5-formylthiazol. Sch. p. 94,6. Ausb. nahe Quantitativ.

In der Nitrierungsreaktion wurde ein Gemisch p- und m-Nitrophenylderivat gebildet

*2-Phenyl-5-carboxylthiazolsäure*: Man erwärmt 1 Stunde am Rückfluszkühler auf dem Wasserbad bei 65–70°C ein Gemisch aus 0,95 g (5 mMol) 2-Phenyl-5-formylthiazol und 2,1 g (15 mMol) Ag<sub>2</sub>O (frisch ausgefällt) suspendiert in 15 ccm Wasser und 15 ccm Dioxan. Nach der Oxydation der Aldehydgruppe versetzt man ungefähr 20 ccm NaOH 2N. Der ausgefallene Niederschlag wird filtriert und aus Wasser umkristallisiert. Sch. p. 188°C. Ausb.: nahezu Quantitativ.

In der Nitrierungsreaktion wurde ein Gemisch p- und m-Nitrophenylderivat gebildet Sch. p. 205°C

*2-Carboxy-4-phenylthiazolsäure*: Man kocht 1 Stunde am Rückfluszkühler ein Gemisch von 16,8 g (0,125 Mol) thioxamethan (Ethylerster der Oxalsäuretioamid) [5] und 25 g (0,125 Mol) -Bromacetophenon gelöst in 100 ccm Methanol. Nach dem Erkalten filtriert man den gebildeten Niederschlag, es wurde der Ethyleszter der 2-Carboxy-4-phenylthiazolsäure erhalten. Die Hydrolisation des Esters kann nur bei Kalte stattfindet, weil die Säure eine Decarboxylations-tendenz hat. Die Decarboxylation der Thiazolsäuren wurde hauptsächlich begünstigt, wenn die Carboxygruppe sich in 2-tem Position des Thiazolrings bindet. Man gibt dem Reaktionsgemisch (womöglichst vor dem Filtrations) 20 g KOH das löst in 15 ccm Wasser und man lässt 1 Stunde bei Zimmertemperatur. Das gebildeten K-Salz wurde abfiltriert dann löst man den Niederschlag in kaltem Wasser und säuert mit HCl (konz) unter auszern Kühlung. Es wurde 2-Carboxy-4-Phenylthiazolsäure gefällt. Sch. p. 85–86°C Ausb. 87%.

In der Nitrierungsreaktion wurde ein Substanz mit Sch. p. 175–176°C erhalten: die ist ein Gemisch von p- und m-Nitrophenylderivat.

*2-Acetyl-4-Phenylthiazol*: Man löst bei Wärme 18,8 g 4-Phenyl-2-thiazolyl- $\alpha$ -ethanol in 50 ccm Essigsäure, dann wurde eine Lösung von 7,5 g Na<sub>2</sub>Cr<sub>2</sub>O<sub>7</sub> · 2H<sub>2</sub>O in 15 ccm Essigsäure zu der warmen Lösung in 15 Min. portionsweise unter Kühlung und Mischung gegeben. Während man die Bichromatlösung dazugeht erwärmt man nicht das Reaktionsgemisch. Nach dem ungefähr die Hälfte der Bichromatlösung zugegeben wurde, scheidet sich aus dem Reaktionsgemisch 2-Acetyl-4-Phenylthiazol. Wenn es nötig ist, gibt man 10–15 ccm Eisessig. Nach dem die ganze Menge des Oxydationsmittels zugegeben wurde, erwärmt man noch auf dem Wasserbade 2 Stunden, dann wird das Reaktionsgemisch filtriert und wäscht (bis zur Entfernung der grüne Färbung der Cr<sup>III</sup>). Auskristallisation aus Essigsäure erhält man ein Substanz mit 77–78°C Sch. p. Aus dem Mutterlauge man ein bedeutliche Menge von 2-Acetyl-4 phenylthiazol. Ausb. nahezu Quantitativ.

In der Nitrierungsreaktion wurde ein Substanz. Sch. p. 185°C. Das Nitrierungsprodukt ist ein Gemisch von p- und m-Nitrophenylderivaten.

**Allgemeine Methoden für die Nitration der Phenylthiazolderivaten.** Im jeden Fall hat die Nitrationsreaktion mit streng stöchiometrischen berechneten Mengen Nitrierungsgemisch stattgefunden. Die Substanz wurde bei 0°C in konz H<sub>2</sub>SO<sub>4</sub> (minimalischen Menge) gelöst; die so erhaltene Lösung kühlt man unter 0°C und unter stetige Mischung, tropfenweise, gibt die strenge stöchiometrische Menge rauchende HNO<sub>3</sub> (D: 1,5 g/ccm). Man lässt 15 Min bei Zimmertemperature dann gieszt man auf Eis, der ausgefallene Niederschlag wird filtriert und auskristalisiert aus Methanol.

**Allgemeine Methoden für Oxydation der Nitrophenylthiazol derivaten mit KMnO<sub>4</sub>.** Im jeden Fall, für die Oxydation der Nitrophenylthiazol derivaten wurde 1 g abwiegt, man gibt 80 ccm Wasser und 5 g KMnO<sub>4</sub> in Dreiportion und das Reaktionsgemisch erwärmt man am Rückfluszkühler 1 Stunde, dann wurde noch warm de MnO<sub>2</sub> abfiltriert und säuert man mit HCl konz. Wenn die Nitrobenzoesäure nicht abfällt wurde die Lösung bis zur Hälfte verdunst. Nach der Erscheinung des Niederschlags wurde abfiltriert, trocknet und bestimmt die Sch.p.. In jedem Fall wurde auch das Filtrat verdunst, weil die m-Nitrobenzoesäure löslicher als die p-Derivaten ist, sie es gibt in der Lösung und auch in diesem Fall wurde die Sch.p. bestimmt.

**Konklusion:** Es wurde das Orientierungseffekt der am Thiazolring befindlichen Substituenten bei der Nitrierungsreaktion der Phenylthiazols untersucht. Die Nitrierung der 2-Phenyl-4-R-thiazol derivaten wurde ausgeführt. Man stellte fest, dasz abhängig von der Natur des Substituenten R die Nitrogruppe sowohl in die para Stellung als auch in die meta Stellung des Phenyring eintreten. Die meta-Derivaten sind nur in einem kleinen Anteil (weniger als 5%) gebildet worden.

#### L I T E R A T U R

1. S. Archer und M. G. Pratt, *J. Am. Chem. Soc.*, 66 1656 (1944).
2. P. F. Kruse und Mitarbeiter, *J. Am. Chem. Soc.*, 76 5796 (1954).
3. V. V. Spanova, *Preparatnyha Organiczwa Selte*, 758 Warsava 1954.
4. *Denicho Patent* 261689 C 394 II (1913).
5. A. Reissert, *Ber. dtch. chemGes.* 37 37 21 (1904).

## ETHYLBENZENE DEHYDROGENATION ON Fe-Cr-K CATALYST. I. THE INFLUENCE OF THE ADDITION OF SEVERAL MATERIALS WITH VANADIUM ON THE CATALYTIC PERFORMANCES AND MECHANICAL STRENGTH OF THE CATALYST

N. DULĂMIȚĂ\*, M. STANCA and F. BUCIUMAN\*\*

**ABSTRACT.** — The addition of some materials with vanadium in the Fe-Cr-K catalyst, followed by a thermal treatment with a steam-ethylbenzene mixture, increases mechanical strength and the catalytic performances in the ethylbenzene dehydrogenation at temperatures over 640°C are sensibly improved.

**Introduction.** The styrene is obtained mainly through the catalytic ethylbenzene dehydrogenation in the presence of steam. Many catalysts have used in this process and many attempts have been made in order to improve their catalytic performances and mechanical strength [1,9]. The most utilised catalysts contain  $\text{Fe}_2\text{O}_3$ — $\text{Cr}_2\text{O}_3$ — $\text{K}_2\text{CO}_3$  with addition of some metal oxides as promoters, e.g. vanadium [1-4], magnesium [3,5], zinc and copper [1, 6, 7], molybdenum, cerium and calcium [5], nickel and copper [8], calcium and aluminium [9].

In this paper was studied the influence of some materials containing vanadium precisely the fresh catalysts from the manufacturing of the sulphuric acid, on the yield, conversion, selectivity and mechanical strength of some Fe—Cr—K catalyst in the ethylbenzene dehydrogenation to styrene.

Table 1

Composition and mechanical strength of the catalysts

Cat. no.	Composition (wt. %)				Compressive strength (kg/pellet)	Abrasion resistance (%)
	$\text{Fe}_2\text{O}_3$	$\text{Cr}_2\text{O}_3$	$\text{K}_2\text{CO}_3$	$\text{V}_2\text{O}_5/\text{SiO}_2$		
1 <sup>+</sup>	85	5	10	—	6.5	85
2 <sup>+</sup>	87	3	10	—	7.0	87
3	62	3	10	25*	13.4	95
4	63	3	10	24*	13.8	94
5	60	3	10	27*	15.2	98

\* Department of Technological Chemistry, Faculty of Chemistry "Babeș-Bolyai" University, 3400 Cluj-Napoca, Romania  
+ Industrial catalyst (1), catalyst prepared in laboratory (2).

\*\* Fresh catalysts added, provided from the sulphuric acid industry of Craiova, Romania (3), Wolfen (4) and Grillo (5), Germany, in a quantity corresponding to 2.5%  $\text{V}_2\text{O}_5$ .

**Experimental:** - *Catalyst preparation and mechanical strength.* The catalyst composition is shown in Table 1. The  $\text{Fe}_2\text{O}_3$ ,  $\text{Cr}_2\text{O}_3$ ,  $\text{V}_2\text{O}_5/\text{SiO}_2$  powders with the granulation within the range of 2–10 microns were mixed in a stirrer for 30 min., then the  $\text{K}_2\text{CO}_3$  solution was added and the mixing continued for another 30 min. The wet paste was extruded in 4 mm diameter and 5–6 mm length cylinders. The pellets were dried for 4–5 hours at room temperature, 5–6 hours at 110–120°C, then calcinated at 700°C for 1–2 hours. The heating rate was 100°C/hour to avoid the crushing. For a good mechanical strength, the humidity of the paste must be within the range of 15–25% in rapport to the solid mass. The compressive strength and abrasion resistance of the pellets are shown in table 1.

**Ethylbenzene dehydrogenation.** In a tubular isothermal reactor, a bed of 40  $\text{cm}^3$  catalyst with the granulation of 0.8–1 mm was charged, between two layers of silicon carbide. Over the catalyst a steam-ethylbenzene mixture is passed in a mass ratio of  $\text{H}_2\text{O}:\text{EB}=3:1$ . The space velocity, calculated as  $\text{cm}^3$  liquid EB feed per hour per  $\text{cm}^3$  catalyst, were 0.5. The composition of the EB feed was, in weight % :EB–99.08; benzene plus toluene – 0.40, styrene – 0.40; diethylbenzene – 0.10.

The catalytic properties of the ferric oxide and the capacity of adsorption for  $\text{Cr}^{3+}$  ions were improved by the thermal treatment at 640°C in steam-EB flood, for 4 hours. The coked catalyst was regenerated with air and steam until the absence of  $\text{CO}_2$  in the effluent gas; during this operation the temperature in the catalytic bed must not exceed 700°C. After regeneration, the catalytic activity was tested at work temperature in the ethylbenzene dehydrogenation. The effluent vapors were cooled and condensed, the organic product was separated, measured and the liquid yield calculated.

The composition of the product was determined using the gas-chromatography method [10]. The catalytic performances at temperature were then calculated.

**Results and discussion.** The addition of vanadium materials and the lower humidity of the paste bring about the increase of the compressive strength and the abrasion resistance, as one can see in Table 1.

The dependence of the styrene percent, and light hydrocarbons (i.e. benzene + toluene = B + T) per cent, in the organic product, with the work temperature, in the ethylbenzene dehydrogenation, is shown in Fig. 1, and Fig. 2,

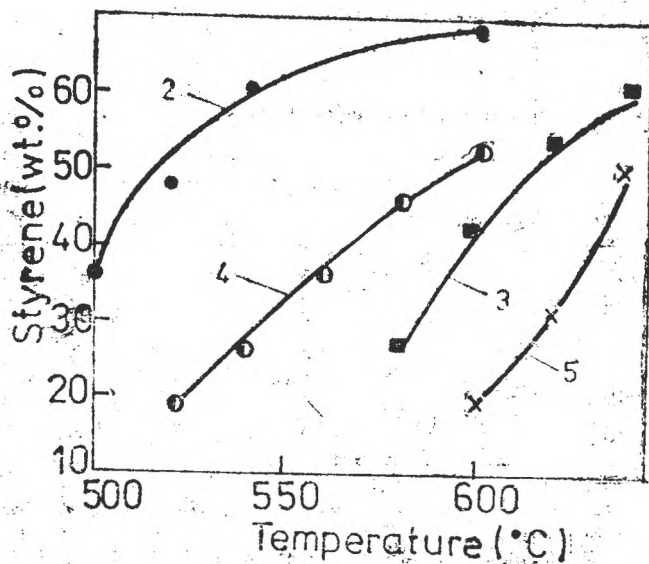


Fig. 1. The variation of the styrene content in the organic product, function of temperature.

respectively. The selectivity (benzene plus toluene) as a function of the styrene percent is presented in Fig. 3.

A content of 50% styrene in the product (see Fig. 1.) was obtained at 520°C on catalyst no.2, at 595°C on catalyst no. 4, at 615°C on catalyst no. 3 and at 640°C on catalyst no. 5. It means that, by introducing the vanadium materials in catalyst no. 2, the thermal level was enhanced with 75–120°C. At the same time, the light hydrocarbons content at 50% styrene in product (see Fig. 3) increased from 4.4% (catalyst no. 2) to 5–6% (catalyst no. 4 and 3, respectively). The vanadium material added to catalyst no. 3 and 4, lead practically to the same performances and mechanical strength. Catalyst no. 5 is less active and nonselective below 640°C.

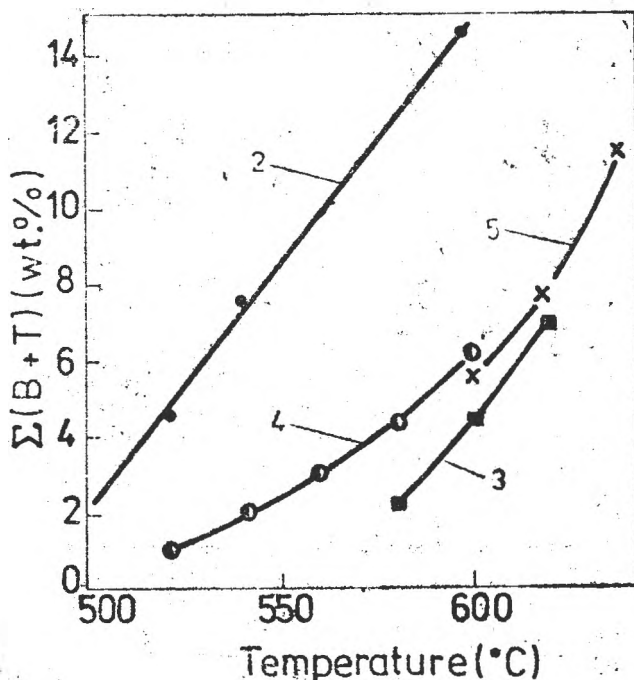


Fig. 2. The variation of light hydrocarbons (sum B+T) content in the organic product, function of temperature.

From the analysis of the experimental data one can find that, even if catalyst no. 2 has a poor mechanical strength, it possesses higher catalytic performances than catalysts no. 3 and 4, at temperatures below 600°C.

Table 2 shows the composition of the products, the performances of catalysts no. 1 and 3 at the same styrene content in the organic product and the performances of catalysts no. 2 and 3 at 600°C. One can also see that the vanadium material added to the Fe-Cr-K catalyst rises the thermal level with 80°C and diminishes the selectivity with 2.1% at the same conversion, at temperatures below 620°C.

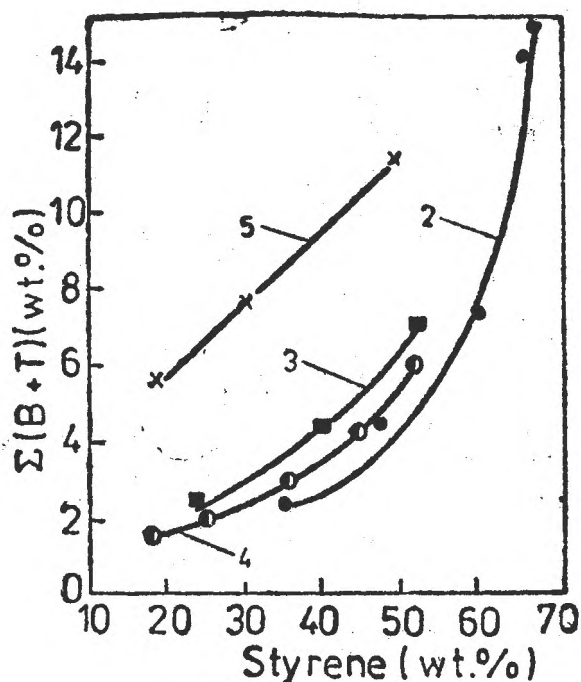


Fig. 3. The variation of selectivity (sum B+T) with the styrene content in the organic product at different temperatures.

At great quantities of styrene in product, of about 61%, the performances and mechanical strength of catalyst no.3 are better than those of catalyst no.1, although the thermal level still remains greater. In the same time, at 600°C, catalyst no.3 is more selective (with 7%) than catalyst no.2. After 5 days, the conversion over catalyst no. 2 decreases to 50% than remains constant for more than a month. Catalyst no.3 keeps its performances unmodified for the same time.

As a result of the thermal treatment of the catalyst,  $\text{Fe}_3\text{O}_4$  forms which allows the  $\text{Cr}^{3+}$  and  $\text{K}^+$  superficial ions to penetrate inside the crystal lattice. The promoter role of the chromium consists in  $\text{FeCr}_2\text{O}_4$  formation, which is isomorphous with  $\text{Fe}_2\text{O}_3$  (the lattice constant is  $a = 8.37 \text{ \AA}$  for  $\text{Fe}_2\text{O}_3$  and  $a = 8.34 \text{ \AA}$  for  $\text{FeCr}_2\text{O}_4$ );  $\text{K}_2\text{Cr}_2\text{O}_4$  also forms.

Table 2

#### Experimental results and catalytic performances

Cat. no.	Temp. (°C)	Composition of the products (wt. %)			Performances (wt. %)		
		B+T	EB	St	R	C	S
1	520	3.66	54.90	41.44	40.66	47.70	85.25
3	600	4.36	53.89	41.75	40.09	48.24	83.10
1	540	4.59	47.71	47.70	46.24	55.29	83.63
3	620	6.80	46.20	47.00	44.01	54.00	81.50
1	560	9.05	29.79	61.16	36.06	72.80	77.00
3	640	7.55	31.05	61.40	62.52	78.00	80.15
2	600	14.70	17.45	67.87	63.49	83.70	75.85

B - benzene; T - toluene; St - styrene; EB - ethylbenzene; R - yield; C - conversion; S - selectivity

At 640°C, the SiO<sub>2</sub> from the vanadium material allow the supplementary penetration of Cr<sup>3+</sup> and K<sup>+</sup> ions, which explains the enhancement of catalytic performances at high temperatures.

**Conclusion.** Over the Fe-Cr-K catalyst below 560°C, yields of 41–56% styrene in organic product and 85–77% selectivities are obtained, so the catalyst is active at low temperatures but its mechanical strength is weak.

The catalyst which contains materials with vanadium, proportional to 2.5% (wt.) V<sub>2</sub>O<sub>5</sub>, has a double compressive strength and proves 62% yield with 80% selectivity in styrene, at 640°C, so it is active at high temperatures in ethylbenzene dehydrogenation.

The improvement of ethylbenzene dehydrogenation could be achieved by using both catalysts, laid in two layers in the adiabatic reactor.

## REFERENCES

1. W. R. Guttman: *U. S. Pat.* 3, 361, 683 (1968).
2. G. Csomontanyi, S. Barabas, A. Bădărău, G. Muscă, G. Pogonaru: *Rom. Pat.* 90, 697 (1985).
3. D. E. Andreescu, D. Ploșu: *Rom. Pat.* 88, 850 (1986).
4. N. Dulămiță, G. Csomontanyi, I. Hopârtean, H. Podorean, Fl. Irimie: *Al IV-lea simpozion național de ingineria proceselor chimice*, Piatra Neamț, p. 313, 1988.
5. Un-Ei Hidemi/Sekybai, 33(1), 9 (1991), Ref. J., 24B4305 (1991).
6. E. H. Lee: *U. S. Pat.* 3, 387, 052 (1968).
7. E. H. Lee: *Catal. Rev.*, 8(2), 285 (1973).
8. C. C. Brewer, R. C. Richard: *U. S. Pat.* 3, 424, 808 (1969).
9. G. Mocearov: *Rev. Roumaine Chim.*, 19 (7), 1271 (1974).
10. N. Dulămiță, I. Hopârtean, M. Podorean: *Studia Univ. Babeș-Bolyai, Ser. Chem.*, 28 (1), 40 (1983).



THE STUDY OF HYDROGEN ADSORPTION ON THE SURFACE OF Pd/Al<sub>2</sub>O<sub>3</sub> CATALYST USING THE GAS-CHROMATOGRAPHY METHOD

MARIA STANCA, NICU DULĂMIȚĂ and FLORINA BUCIUMAN\*

**ABSTRACT.** — Using the gas-chromatography, the processes of adsorption-desorption of hydrogen on the surface of Pd/Al<sub>2</sub>O<sub>3</sub> catalyst have been studied. The adsorption isotherms, the isosteric heats of adsorption and the kinetics of hydrogen desorption have been settled, and three forms of hydrogen adsorbed on the catalyst surface have been found, their influence being determined in cyclohexane dehydrogenation and benzene hydrogenation, respectively.

**1. Introduction.** By studying the adsorption of gases on the surfaces of solid catalysts, many important experimental data can be obtained, which allow the settlement of the mechanism of some heterogeneous catalytic processes.

The gas chromatography method was used for the research of physisorption, chemisorption and chemical reactions catalysed by solid catalysts, because it allows the execution of fast and precise dynamic runs.

By means of gas chromatography a study was performed on the hydrogen adsorption — desorption processes on Pd/Al<sub>2</sub>O<sub>3</sub> catalyst, used in the hydrogenation — dehydrogenation processes of hydrocarbons.

The research of the kinetics of cyclohexane dehydrogenation [2] and benzene hydrogenation [3], using as catalyst the paladium supported on various materials (asbestos, alumina, silica gel) showed that, in the absence of hydrogen, the catalyst was quickly deactivated. In the range of temperatures of 200–320°C the rate pressure of the hydrogen. The experimental data verified satisfactorily the (Eq. (1)):

$$w = k \cdot p_{C_6H_{12}}^m \cdot p_{H_2}^n \quad (1)$$

where:  $w$  = reaction rate;  $k$  = rate constant;  $p_{C_6H_{12}}$  and  $p_{H_2}$  = partial pressures of cyclohexane and hydrogen, respectively;  $m$  and  $n$  indicate the order of reaction in respect cyclohexane and hydrogen.

The values of the partial reaction orders depend on temperature as follows:

$$m = 0.5 \quad n = 0.2 \quad \text{at } 250^\circ\text{C}$$

and

$$m = 0.6 \quad n = 0.5 \quad \text{at } 322^\circ\text{C}$$

As the partial reaction order of hydrogen doesn't exceed 0.5 one can understand that in the cyclohexane dehydrogenation participate those hydrogen atoms which are adsorbed on catalyst surface.

\* University "Babeș-Bolyai", Department of Chemistry and Chemical Engineering, 3400 Cluj-Napoca, Romania.

This paper presents a study carried out by using the gas chromatography method, on the  $\text{Pd}/\text{Al}_2\text{O}_3$  system, in order to evaluate the nature of the adsorption processes, the shape of the adsorption isotherms, the isosteric heats of adsorption and the kinetics of hydrogen desorption.

**2. Experimental.** A catalyst was used which contained 0.4–0.5% (mass) of Pd supported on alumina. The thermal analysis of the catalyst were carried out using a Paulik–Paulik derivatograph in the range of 20–1.000°C. Fig. 1 shows that the physically adsorbed water was eliminated up

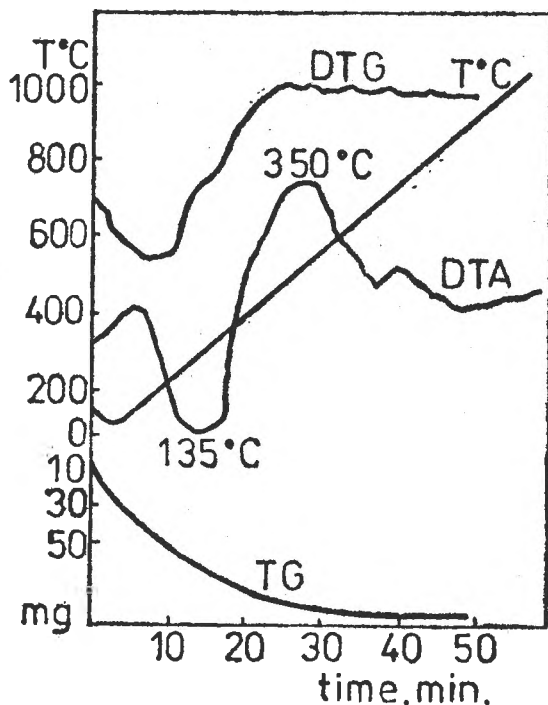


Fig. 1. Thermal analysis of a typical  $\text{Pd}/\text{Al}_2\text{O}_3$  catalyst sample.

to 230°C, the greatest desorption rate being at 135°C. The exothermal peak at 400°C corresponds to the structural modification of alumina.

According to these results catalyst samples were selected in the 0.125 – 0.160 mm range of granulation, which were thermally pretreated at 500°C firstly in air flow, then in hydrogen flow at the same temperature, during 8 hours.

The study of the adsorption-desorption processes was performed using an experimental device similar to that presented in the paper [5]. The argon was employed as a carrier gas with a flow rate of 20  $\text{cm}^3/\text{min}$ . The hydrogen was injected in the argon flow in proportion of 5% (vol) to the argon. The dead space of the device was determined with nitrogen. The mass of the catalyst sample was in the 4–7 g field. Because the catalyst activates the hydrogenation-dehydrogenation processes only in the 150–330°C range of temperature, the tests of adsorption-desorption of hydrogen were carried out within the same range.

For the kinetic study of the hydrogen desorption within the range 150–300°C, the elution technique was employed, in the zone where the adsorption-desorption process is reversible. The runs were carried out at 150, 200 and 250°C using the device presented in [5] and preparing the catalyst samples as in the frontal measurements.

### 3. Results and discussions. 3.1. Adsorption isotherms of hydrogen.

In order to study the hydrogen adsorption on the surface of the  $\text{Pd}/\text{Al}_2\text{O}_3$  catalyst the frontal technique was used, because it can be extended also in the nonlinear area of the isotherm. The desorption curve was used in calculations assuming that, at a given coverage of the catalyst surface, the partial pressure of the hydrogen is proportional to the height of the chromatogram peak while the area of the surface enclosed under this height is proportional to the volume of hydrogen adsorbed on the catalyst surface. Knowing the flow rate and the hydrogen concentration in the hydrogen – argon mixture, the hydrogen volume corresponding to each of the adsorption area can be calculated.

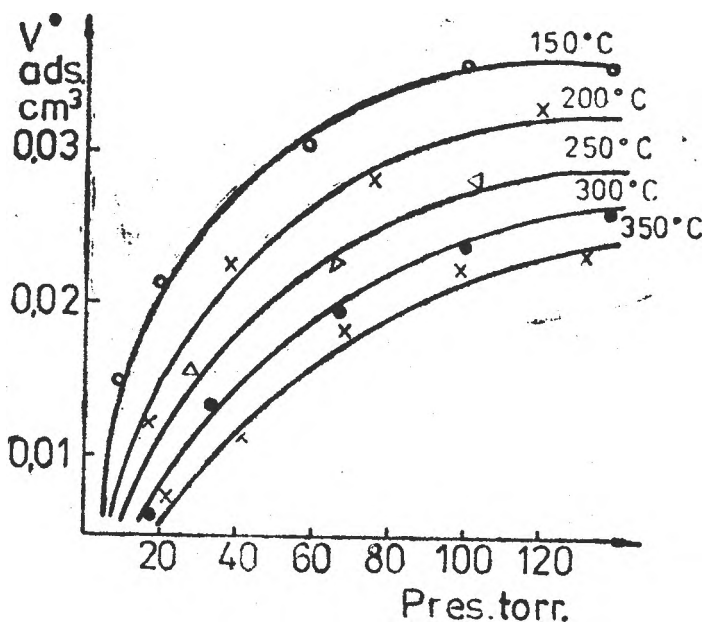


Fig. 2. Langmuir-type adsorption isotherms per Hydrogen an Pd/Al<sub>2</sub>O<sub>3</sub> catalyst.

Adsorption isotherms showed in Fig. 2 are Langmuir — type and can be used for the determination of adsorption heat.

3.2. *Isosteric adsorption heats of hydrogen on Pd / Al<sub>2</sub>O<sub>3</sub>.* They were calculated from the isosteres provided by the adsorption isotherms (see Fig. 2) using the Clausius — Clapeyron eq.:

$$\log p = - \frac{Q}{2 \cdot 303 \cdot R \cdot T} + \log \theta \quad (2)$$

where:  $p$  = hydrogen pressure;  $Q$  = isosteric heat of adsorption;  $\theta$  = degree of surface coverage.

Plotting  $\log p$  as a function of  $1/T$  a straight line was obtained; its slope allowed the calculation of isosteric heats of adsorption (see Tab. 1).

Table 1

**Isosteric Heats of Adsorption**

Surface coverage $\theta$ cm <sup>3</sup> H <sub>2</sub> /g	Heat of adsorption $Q$	
catalyst	kcal/mol	kJ/mol
0.010	-2.90	-12.13
0.015	-2.87	-12.00
0.020	-2.64	-11.04
0.025	-2.60	-10.87

The small values of the isosteric heats of adsorption are in agreement with those existing in literature [4], proving that the hydrogen is weakly linked on the solid surface and can be removed by elution in isothermal conditions.

**3.3. Irreversible adsorption of hydrogen.** Comparing the volume of the hydrogen adsorbed by 1 g of catalyst  $V_a^0$ , with the volume of the hydrogen desorbed in isothermal conditions,  $V_d^0$ , one can notice that  $V_d^0$  is smaller than  $V_a^0$  at the same working temperature (see Tab. 2). The volume of hydrogen adsorbed irreversibly, noted  $V_i^0$ , was defined as the gas volume which was not eluated after 30 minutes of desorption at the working temperature.

Table 2

The  $V_a^0$ ,  $V_d^0$ ,  $V_i^0$  and  $V_{dt}^0$  Values at Different Work Temperatures

Temperature, °C	$V_a^0$ cm <sup>3</sup> /g	$V_d^0$ cm <sup>3</sup> /g	$V_i^{0*}$ cm <sup>3</sup> /g	$V_{dt}^0$ cm <sup>3</sup> /g
150	0.09123	0.02022	0.07101	0.02783
200	0.09123	0.03210	0.05913	0.02543
250	0.09123	0.04079	0.05044	0.01493
300	0.09123	0.04382	0.04741	0.01241

$$* V_i^0 = V_d^0 - V_a^0$$

To confirm the fact that the irreversible adsorption is due strictly to the slow removing of the hydrogen at low coverages and not to the reaction of hydrogen with the oxygen atoms of the support, tests of thermal desorption were carried out. The volume of hydrogen thermally desorbed is  $V_{dt}^0$ . The thermal desorption was realised by heating the sample from the working temperature to 400°C.

As one can see, the hydrogen cannot be completely removed even at this temperature (see Tab. 2).

The irreversible adsorption of hydrogen could be explained by the existence of some forms of activated adsorbed hydrogen on the catalyst surface. The hydrogen fixed on the surface by weak bondings is removed from the surface in isothermal conditions, while the strongly bonded hydrogen can be removed only at high temperatures. In some cases the slow desorption could be caused by a mass — transfer phenomenon. It was observed experimentally that the passing rate of the gas over the catalyst sample didn't influence the desorption rate, which excluded this possibility.

To establish which form of activated adsorbed hydrogen is involved in the hydrogenation — dehydrogenation reactions on the Pd/A<sub>2</sub>O<sub>3</sub> catalysts saturated with hydrogen, samples of 10 μl cyclohexane and benzene, respectively were introduced. In both cases a chemical reaction resulted, taking into account that the branch of the isotherm corresponding to the desorption laked from the chro-

matogram. On the same sample the thermal desorption was performed, by heating the sample at 400°C. We found the presence of hydrogen thermally desorbed. This means that, in the hydrogenation — dehydrogenation reactions is involved the weakly bounded hydrogen, i.e. the hydrogen which was desorbed in isothermal conditions.

The decreasing of the catalyst activity [2] when temperature rises from 150 to 400°C could be explained by the existence, at high temperatures, of irreversible adsorbed hydrogen which doesn't participate in the benzene hydrogenation and cyclohexane dehydrogenation.

**3.4. Kinetics of hydrogen desorption.** The desorption process was treated as a first order reaction and the conversion was calculated as the ratio of the amount of hydrogen desorbed in the time  $\tau$  and the total amount of hydrogen desorbed in isothermal conditions at the working temperature. Because at 300°C the differences between the areas of the chromatographic peaks, recorded at high desorption times, are insignificant, the recordings at this temperature couldn't be taken into account. It was also noticed that, at room temperature, the catalyst retained a five times greater ( $5 \times 1.08 \text{ cm}^3$ ) volume of hydrogen to reach the surface saturation. We considered that, at this temperature, the hydrogen was physically adsorbed on catalyst surface and the adsorption processes was inactivated.

The results obtained allowed the plotting of the kinetic curves showed in Fig. 3. From the slopes of these lines the rate constants were calculated and the values are indicated in Tab. 3. It can be observed a diminishing of the reaction rate depending on time in isothermal conditions.

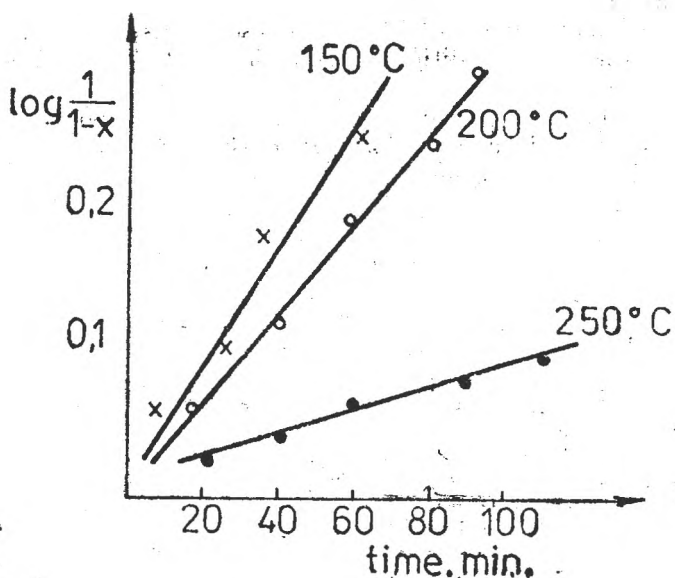


Fig. 3. Kinetics plots per isothermal desorption of hydrogen from Pd/Al<sub>2</sub>O<sub>3</sub> catalyst.

The Rate Constants Values and the Activation Energy

Temperature, °C	Rate constant min <sup>-1</sup>	Activation energy	
		kcal/mol	kJ/mol
150	17.700 · 10 <sup>-3</sup>		
200	4.430 · 10 <sup>-3</sup>	12.5	52.28
250	0.875 · 10 <sup>-3</sup>		

Using the Arrhenius equation, the activation energy for the isotherma desorption of hydrogen ( $E_a$ ) was calculated from the values of rate constant  $k$ . The value of activation energy of 12.5 kcal/mol confirms the fact that the hydrogen desorbed in isothermal conditions is weakly bonded on the surface of catalyst. The low value of the activation energy could also show that the desorption rate could be controlled by diffusional or intermediary (kinetic-diffusional) processes.

**4. Conclusions.** The energetics of the adsorption-desorption processes in the  $H_2$  — Pd/Al<sub>2</sub>O<sub>3</sub> system have been studied in dynamic conditions using the gas-chromatography. The hydrogen physically adsorbed, weakly bonded and irreversible adsorbed, could be identified on the catalyst surface.

The weakly bonded hydrogen participates in the cyclohexane dehydrogenation and the benzene hydrogenation, while the irreversible adsorbed hydrogen is responsible for the diminishing of the catalytic activity when the temperature rises in these processes. The volumes of irreversible adsorbed hydrogen at each working temperature were measured.

The activation energy of 12.5 kcal/mol ascertains the fact that the hydrogen desorbed in isothermal conditions is linked on the catalyst surface by weak bondings.

The gas chromatography can be employed, with good results, in the fast control of activity, poisoning and aging of the catalyst, at working temperature, in the catalytic processes.

## REFERENCES

1. Cremer E., *J. Anal. Chem.*, **170**, 219, (1959).
2. Erianov V. M., Pavlov I. F., River P. Rosen A., Huacs A., *Kinet. Katal.*, **12** (5), 1197, (1971).
3. Nakama K., Kusunoki K., *Kagaku Kogaku Ronbunshu*, **8** (2), 162 (1982) in *Planum Metals Revew.* **27** (1) 45, (1983).
4. Tsuckiya S., Amenomyiya Y., Cvetanovic R. J., *J. Catal.*, **19**, 245, (1970).
5. Pop A., Stanca M., *Revista de Chimie*, **30** (3), 227, (1979).
6. Hansen A., Gruber H. L., *J. Catal.*, **20** (1), 97, (1971).
7. Gruber H., *Anal. Chem.*, **34**, 1828, (1962).
8. Parravanon G., *J. Catal.*, **16** (1), 1, (1970).

## INTERCALATION COMPOUNDS. II. PHYSICAL, INVESTIGATION METHODS OF THE INTERCALATION COMPOUNDS

GEORGETA ȚARĂLUNGĂ\*, L. ONICIU\*\*, C. BOLLA\*\* and L. D. BOBOȘ\*\*

**ABSTRACT.** — Physical methods used for the research of the intercalation compounds and some correlations between the electrochemical performances of lithium batteries and the structure of the host material are shown in this review paper.

During the power delivery of the nonconventional galvanic batteries with lithium anode, intercalation compounds by the insertion of the lithium ion in the crystal lattice of the cathodic depolarisant are formed [1].

There is a strong marked correlation between the electrochemical performances and the crystal structure of the host material where has placed the intercalation. The cyclability, the life as well as other characteristics of the batteries are dependent on the lithium insertion degree.

Among the methods used for the research of the intercalation compounds there are:

- microscopy
- X-ray diffraction, electron diffraction and neutron diffraction
- nuclear magnetic resonance spectroscopy and electron spin resonance spectroscopy.

**1. Microscopy.** The microscopical methods have offered informations about the constituent micrography, kind number and their form about the sizes and their distribution and about the lattice planes, as well as about the different types of the structural defects. In accordance with the used radiations (light, electron or ionic beams) must be used the metallographic, electronic or ionic microscope.

The metallographic microscope does not have a very high resolution and cannot give the conclusive information about the inner structure of the intercalation compounds, but it can offer data on the granulometry

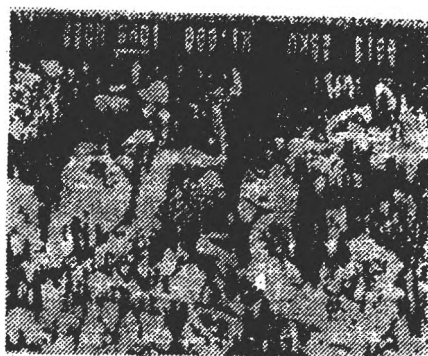


Fig. 1. Distribution of the  $MnO_2$ , acetylen black and teflon particles into the  $MnO_2$  depolarisant

\* Laboratory of Electrochemistry of University Babeș-Bolyai Cluj-Napoca.

\*\* Physical Chemistry Dept. of University "Babeș-Bolyai" Cluj-Napoca.

and granulometrical distribution of the constituent particles of the cathodic depolarisant [2]. Thus, the Fig. 1 gives the distribution of constitutive parts of the depolarisant made up of the magnesse dioxide, acetylen black and teflon.

Electronic microscope, relying on the propagated and focusing properties of electron beam, is the only instrument wich permits the direct observation of the isolated atoms, as well as the structural details [3—6]. Thus, it can observe the different types of the structural defects, phase transformations, plastic deformations, defect interactions, interactions of the defects with impurities, and the reactions on the surface, too.

The continous improvements, bringing of the electron optics, led towards the considerable increments until  $10^7$  times, the electron microscope becoming the more efficient instrument for investigation the crystalline structure.

The electrochemical activity of the cathodic depolarisants from the lithium batteries is strongly bound by the particle sizes of the constituents as well as by the crystal structure. The intercalation phenomenon which corresponds to the electromotive active reaction, is favoured by the presence or the absence of the defects inner the host microstructure.

By means of scanning electron microscopy (SEM) could put onself forward both the size of the cathodic cristallites, which must be by the order of the microns and structural details, bound by the lattice periodicity and the existence of some defects of a vacancy type, which facilitated the intercalation of the lithium ions.

One of the cathodic depolarisants from the lithium cells is the copper oxide, which may present only two crystallographic modifications: the monoclinic and the tetragonal [7]. The structure of the monoclinic copper oxide approaches that of  $\text{TiO}_2$  (a rutile-type structure), which permits  $\text{Li}^+$  intercalation and formation of the intercalation compound  $\text{LiCuO}$  [8].

The non-stoichiometric  $\text{CuO}$  has a relatively regular crystallographic lattice and the lattice dfects are favourable for the diffusion of the lithium ions. The thermal treated stoichiometric samples about  $400^\circ\text{C}$  maintain some crystalline defects of the mosaic texture type with strains between crystallites, which allow a good interstitial diffusion of the lithium ions, too [9].

In the figure 2 are shown two microphotographs of some  $\text{CuO}$  samples obtained by means of the scanning electron microscope. The two samples were prepared from the same copper powder: one by slow oxidation at about  $400^\circ\text{C}$ , when a mosaic texture is formed (fig. 2a, active sample), and another by rapid oxidation at about  $800^\circ\text{C}$  when the structure is more compact (fig. 2b, inactive sample).

Although the size of the crystallites is the same ( $\sim 1 \mu\text{m}$ ) their compactness, more pronounced than in the mosaic structure, determines a lower discharge capacity, approximately half that characteristic of the sample with the mosaic texture. The thing is illustrated in figure 3, where the discharge curves are shown for the two types of the  $\text{CuO}$  samples. Discharge was made with a current  $I = C_t/24$  at  $25^\circ\text{C}$  ( $C_t$  — theoretical discharge capacity). It follows that the good electrochemical properties of the  $\text{CuO}$  electrode are influenced by both the sizes of the particles and the presence of the defects into the crystalline structure.



Fig. 2. SEM microphotographs of CuO: (a) — sample with mosaic texture and (b) — sample prepared at a high temperature (800 °C).

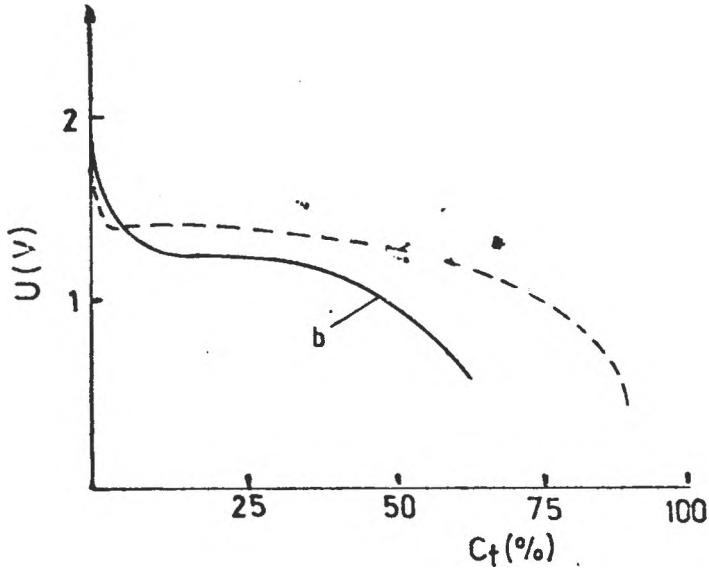


Fig. 3. Discharge curves for CuO cathodes: (a) with mosaic texture, (b) — with high compactness.

The transition metal dichalcogenides have layered structures and the most studied system is titanium disulfide. The compound is nonstoichiometric, the excess element found in the „van der Waals” layer and it steadies the compound, but the following intercalation will be more difficult [10, 11].

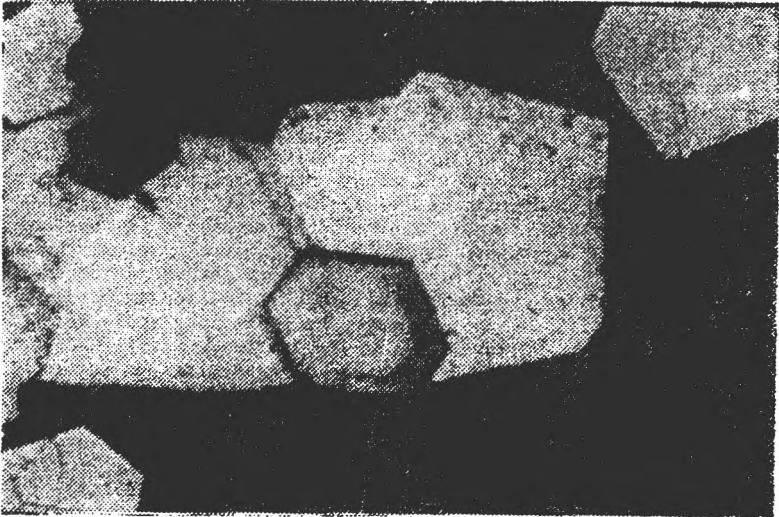


Fig. 4. Microphotograph of a single crystal of  $\text{TiS}_2$  which contains intercalated lithium.

The product of the intercalation,  $\text{Li}_x\text{TiS}_2$ , appears during the discharge on the secondary galvanic cell  $\text{Li}/\text{TiS}_2$ . The diffusion of the lithium ions takes place only in the "van der Waals" layer which binds the  $\text{TiS}_2$  sandwiches [1].

Chianelli [12] has succeeded in obtaining of a single crystal of  $\text{TiS}_2$  with intercalation lithium ion by the electron microscopy the micrography (fig. 4).

**2. Diffractometry.** In spite of the performances obtained because of a high resolution (under 1 Å), the microscopical methods generally remain a qualitative investigation method of the structure of the intercalation compounds. Among the quantitative methods count the diffractometrical methods as: X-ray, electron and neutron diffractometry.

These methods offer up the quantitative data about the internal structure, as well as the characteristic sizes of these structures [13]. It is a matter of the symmetry of the crystalline lattice (crystal unit cell) and characteristic parameters of the lattice, as well as about the position of the atoms in the unit cell.

X-ray diffractometry uses the radiations having the wavelength of about 1 Å, by the order of the size with the dimensions of the atoms. The electrons from the placed atoms in the lattice modes can scatter partly or totally X-ray radiation with the same frequency with the incident.

Therefore, the lattice planes of the crystal have a reflection properties for X radiation, while the crystal as a whole, has a diffraction property of the incident beam, plying the part of the diffraction grating.

Through the interference of the reflected rays by the atomic planes, the emerged rays will be intensified if the optical path difference,  $\delta$ , in accordance with the Bragg relationship will be a integer multiple of the wavelength,  $\lambda$ :

$$\delta = 2d \sin \theta = n\lambda, \quad (n = 0, 1, 2, \dots) \quad (1)$$

where  $d$  is the distance between the lattice planes, and  $\theta$  the scattering angle of the radiations. The Bragg relationship is available only for  $\lambda \leq 2d$ .

Because of the wave nature of the electron, the propagation of a electron beam is equivalent to the propagation of associate waves, which can diffract into the crystals. The wavelength of the de Broglie wave associated to the electron, is given by:

$$\lambda = \frac{h}{\sqrt{2m_0eU}}, \quad (2)$$

where  $h$  is the Planck constant,  $m_0$  — electron mass,  $e$  — unit charge and  $U$  the driving potential. At a driving potential of 100 kV, usually used in the electronography and the electron microscopy, it has obtained  $\lambda = 0,037$  Å, therefore a value of the range of the little interatomic distances, much smaller than that of X-ray.

The obtained results by the X-ray diffraction have remained available with the some specific features for the electron diffraction [6, 13–16]. Thus unlike the X-ray, the electron beam is scattered both by the atomic electrons

and by the nuclei of the sample. The advantage of the electron diffractometry consists in the fact that method, unlike X-ray diffractometry, a very short time is required for the obtaining of the diagrams.

For the investigation of the very thin samples has used the thermal neutron diffraction, with energy  $E \leq 1 \text{ eV}$  and with de Broglie wavelength of about  $1,5 \text{ \AA}$ , therefore comparable with the sizes of the atoms [16, 17].

The neutron diffraction distinguishes the isotopes of the same element and established the distribution of the atoms, into the unit cell, electron density, texture of the materials, crystalline defects and magnetic structure of the materials, too.

Between the electrochemical performances of the lithium cells and the crystalline structure of the cathodic depolarisants is a strong relation. The cyclability and the life time of these galvanic cells are also dependent on the structure of the intercalated compounds formed during the discharge.

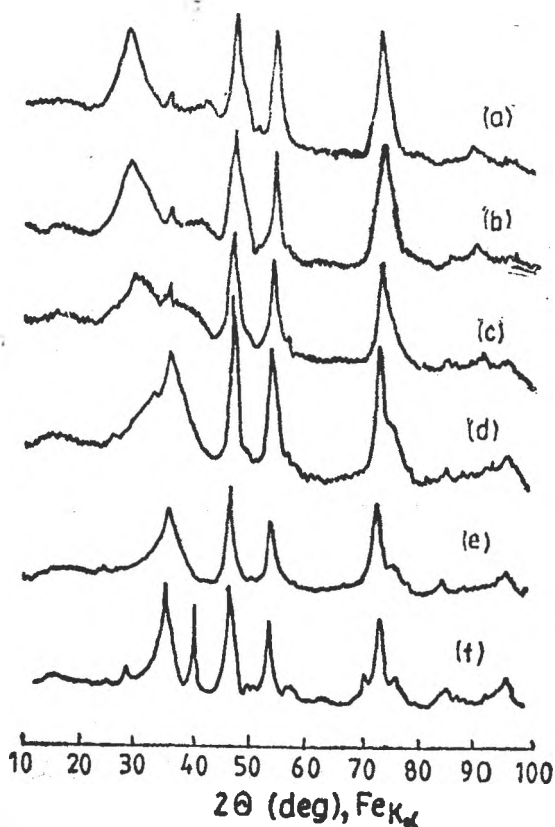


Fig. 5. X-ray diffractograms of heat-treated electrolytic  $\text{MnO}_2$  at: a —  $200^\circ\text{C}$ ; b —  $250^\circ\text{C}$ ; c —  $300^\circ\text{C}$ ; d —  $350^\circ\text{C}$ ; e —  $400^\circ\text{C}$  and f —  $450^\circ\text{C}$ .

Ikeda et al. [18–20] established the necessary thermal treatment to obtain crystalline  $\text{MnO}_2$  favourable to lithium ion intercalation for the primary galvanic cell  $\text{Li}/\text{MnO}_2$ . The behaviour of heat treated  $\text{MnO}_2$  has been examined by using electrochemical and analytical techniques and has been explained by ignoring the crystal structure of cathodic depolarisants [21–23]. Ohzuku et al. [24–25] through X-ray diffraction measurements have brought some explanations about the reduction mechanism of  $\text{MnO}_2$  in correlation with the structure of the crystalline lattice.

It is known the crystal structure of the intercalation compounds  $\text{Li MnO}_2$  is the same of manganese dioxide, which is formed by the hexagonally close-packed oxygen layers, existing two types of symmetric centers: octahedral and tetrahedral sites. Half of the octahedral sites are occupied by the manganese ions, but lithium ions are intercalated in the tetrahedral sites [26, 27]

The octahedra of  $\text{MnO}_6$  can form the simple rectilinear layers

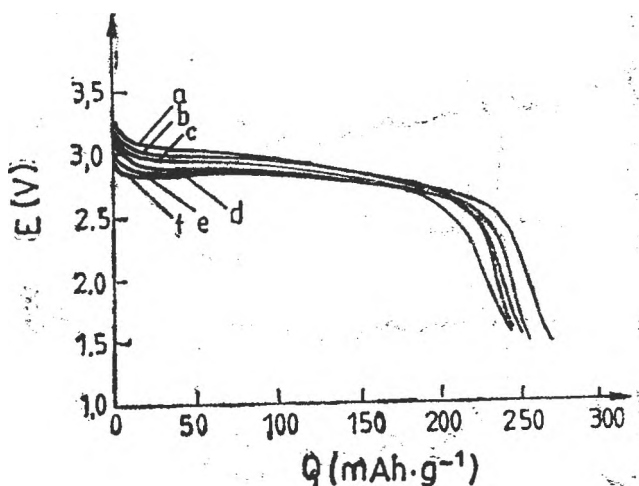


Fig. 6. Discharge curves of EMD: a — 200°C; b — 250°C; c — 300°C; d — 350°C; e — 400°C and f — 450°C.

with  $1 \times 1$  rutile-type structure, double layers with  $1 \times 2$  ramsdellite-type structure or even triple layers with  $1 \times 3$  - type structure, the last resulting by the superposition of the first two structures. The intercalation compounds  $\text{Li MnO}_2$  with a rutile-type structure have the tetragonal unit cells, with the lattice parameters  $a = 4.9 - 5.0 \text{ \AA}$ ;  $b = 4.95 \text{ \AA}$  and  $c = 2.85 - 2.86 \text{ \AA}$ . In the case of ramsdellite-type structure, the unit cell is orthorhombic, in fact it is formed from two tetragonal sublattice with the parameters  $a = 2 \times 2.95 \text{ \AA}$ ,  $b = 4.95 \text{ \AA}$  and  $c = 2.85 \text{ \AA}$ .

Figure 5 shows the X-ray diffractograms (XRD) of the some electrolytic manganese dioxide (EMD) which was treated thermally at several temperatures, for 7 days. It has been found that all the samples have six diffraction lines with diffraction angles of  $2\theta$ . With the increase of temperature, only the lines corresponding at  $28^\circ \leq 2\theta \leq 44^\circ$  will be modified, the other three main diffraction lines at ca.  $47.5^\circ$ ;  $54.7^\circ$  and  $73.6^\circ$  in  $2\theta$  remain unchanged.

These modifications of the first diffraction lines, which appear when  $\text{MnO}_2$  was heated at elevated temperature, are also reflected in the electrochemical parameters of the cells. Thus, to all appearances from figure 6, where the discharge curves are illustrated, the prepared samples at higher temperatures correspond to a lower working voltages and to a larger voltage plateau; the curves were drawn at  $0,1 \text{ mA/cm}^2$ . Exception was made the treated electrolytic manganese dioxide (EMD) sample at  $450^\circ\text{C}$  (curve f), which had both the lower working voltage and lower discharge capacity. Likely, this matter can be explained by the fact  $\text{MnO}_2$  was contaminated by  $\text{Mn}_2\text{O}_3$ .

The roentgenograms of the intercalated  $\text{Li MnO}_2$  products, which resulted in the cathodic reduction are presented in figure 7. The discharge was made until  $Q = 250 \text{ mAh/g}$  discharge capacity. It has been found that the intercalation compounds of  $\text{MnO}_2$ , thermal treated at several temperatures, have 6-8 main diffraction lines. From these, five lines have been found in the same place at  $46^\circ - 47^\circ$ ,  $51^\circ - 52^\circ$ ,  $66^\circ - 67^\circ$ ,  $82^\circ - 83^\circ$ ,  $85^\circ - 86^\circ$  in  $2\theta$  angels

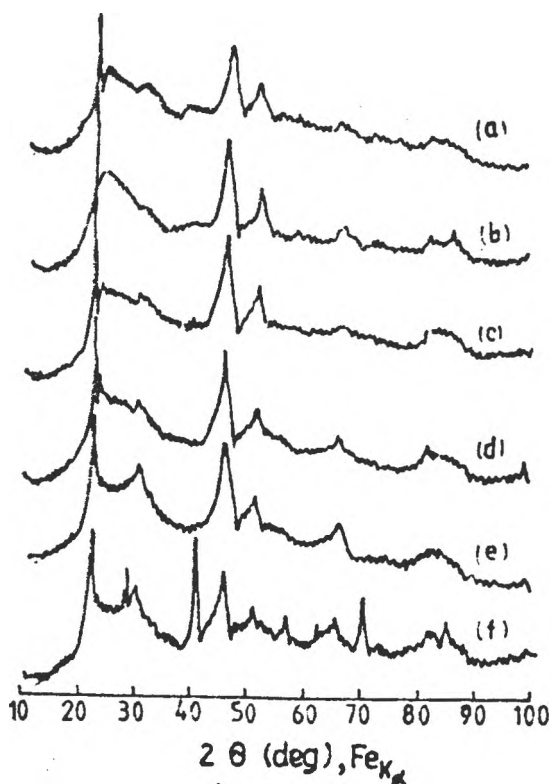


Fig. 7. X-ray diffractograms of intercalation compounds  $\text{LiMnO}_2$ : a - EMD (200°C); b - EMD (250°C); c - EMD (300°C); d - EMD (350°C); e - EMD (400°C) and f - EMD (450°C).

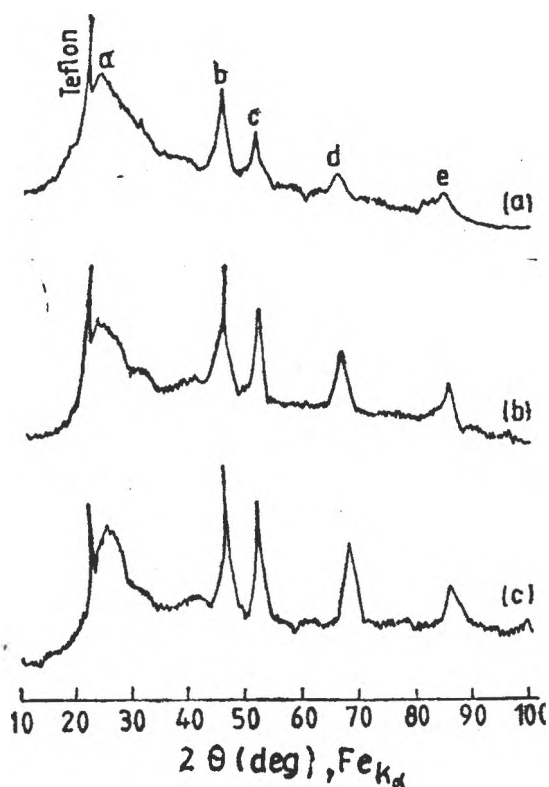


Fig. 8. X-ray diagram charges of  $\text{LiMnO}_2$  by oxidation.

and were had approximately the same relative intensity. On the basis of X-ray measurements, were calculated the parameters of the unit cell, and were found approximately the same values for the all discharge products; this fact suggests that the intercalation compounds have about the same crystalline structure, unlike the  $\text{MnO}_2$  samples used.

The intercalation reaction of lithium in  $\text{MnO}_2$  lattice takes place in a homogenous phase, which suggests the cell rechargeability through an oxidation reaction. Figure 8 shows comparatively the roentgenograms of the intercalated compound, obtained from the reduced EDM (250°) at 245 mAh/g depth of discharge (curve a) as well as the diagrams of two intercalated products which were oxidated during the recharged process of the cell. The pattern (b) was  $\text{LiMnO}_2$  sample at 148 mAh/g state of discharge which was formed by 232 mAh/g of reduction, followed by 84 mAh/g of oxidation. The pattern (c) was  $\text{LiMnO}_2$  sample at 74 mAh/g formed by 233 mAh/g of reduction, followed by 159 mAh/g of oxidation.

As can be seen in figure 8, the intercalation compounds have six main diffraction lines, which were shifted toward higher diffraction angles,  $2\theta$ , with oxidation degree. The shape and intensity of the spectral lines suggest that  $a/1 \times 2/-$ -type structure predominates in the  $\text{Li}_x\text{MnO}_2$  matrix, with a orthorhombic unit cell. The reaction mechanism of  $\text{Li}_x\text{MnO}_2$  in the rechargeable region was shown to be a homogeneous-phase reaction in  $\text{Li}_x\text{MnO}_2$  matrix, with the lattice parameters  $a = 9.7-10.3 \text{ \AA}$ ,  $b = 4.7-5.0 \text{ \AA}$  and  $c = 2.82-2.85 \text{ \AA}$ , which anisotropically shrinks and expands during the oxidation and reduction, respectively, within 10% unit cell volume.

The difference between these three  $1/1 \times 1/-$ ,  $1/1 \times 2/-$ ,  $1/1 \times 3/-$ -type structures, which have the same hexagonal close-packed oxygen matrix, is due to the distribution of manganese ions in the octahedral sites. The regular distribution of one fourth of  $\text{Mn}^{4+}$  at octahedral sites in a ramsdellite-type structure converts this structure into a  $1/1 \times 3/-$ -structure, and the regular displacement of one fourth of manganese ions in a  $1/1 \times 3/-$ -structures converts this structure into a rutile-type structure. The precise location of manganese ions in these structures only by the neutron diffraction can be obtained.

A diagram of rutile-type structure, which was obtained by neutron diffraction, in figure 9 is shown. The diffractogram contains five main diffraction lines, whence the line at  $47.8^\circ$  in the  $2\theta$  diffraction angle, has relatively a reduced intensity [28].

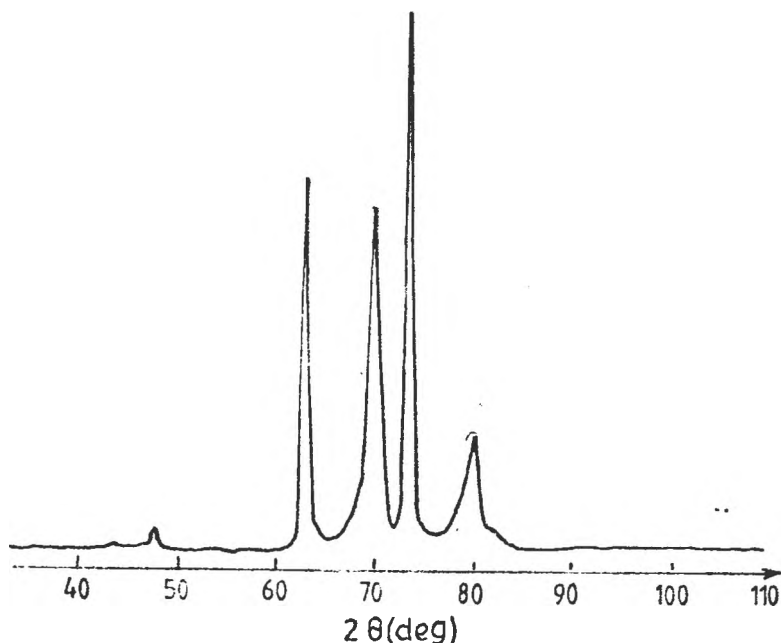


Fig. 9. Neutron diffractogram of  $\beta\text{-MnO}_2$ .

Also, from the neutron diffraction measurements can be determined at what temperature appear  $Mn^{3+}$  ions in  $MnO_2$ . This deed is very important to establish the right thermal treatment of electrolytic manganese dioxide.

**3. Spectroscopy.** The radiospectroscopical methods rely on the intrinsic properties of the electron, nucleus and other particles which are characterized by mass, charge, impulse moment and magnetic moment. These particles interact with the external fields (electric and magnetic) and thus take place to the phenomeny of energetical absorption, whence can be established the kind of interactions, the type and the characteristics of the interatomic bonds, the chemical structure etc. [5, 13, 16].

Among the radiospectroscopical methods the most frequent utilized in the research of crystalline structure are nuclear magnetic resonance (NMR) and electron spin resonance (ESR).

From the NMR point of view, the movement limitation at the microscopical level into the solids have two main consequences. In the first place, because the magnetic field, produced by the magnetic dipoles, is steady, the NMR spectras of solids are more broad than these of liquids. In the second place, the spin-lattice relaxation time  $T_1$ , habitually is more smaller for the solids, because the fluctuations of dipole magnetic field, through which the spin-lattice relaxation was realized, have a more smaller amplitude. Consequently, the solids are characterized by the spin-lattice relaxation times more greates than the spin-spin relaxation times  $T_2$ , which are inversely proportional to the width of signals.

During the discharge of lithium cells having transition metal dichalcogenides as depolarisants were formed the  $Li_xMS_2$  intercalation compounds. The intercalation of lithium ion takes place by diffusion only in the van der Waals layers, there being no significant mobility through the sulfide layers. The lithium ion can be occupy the octahedral/tetrahedral sites or trigonal prismatic symmetry sites, remaining unoccupied by the transition metal [29, 30].

When the diffusion takes place through octahedral and tetrahedral sites, the released energy which accompains the occupancy of one tetrahedral site is considerable lower than the realised at occupancy of one octahedral site. Generally, the released middle energy at the occupancy of the one octahedral/tetrahedral site is more smaller than that released at occupancy of one trigonal prismatic site (fig. 10) than in the case of prismatic trigonal sites.

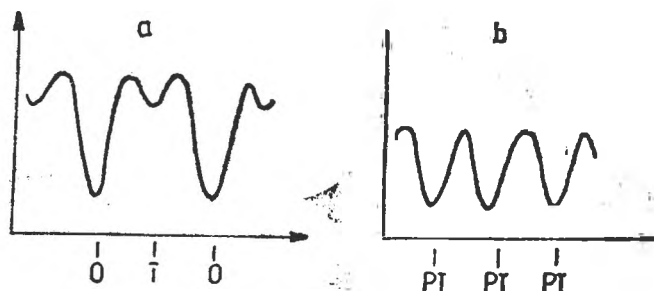
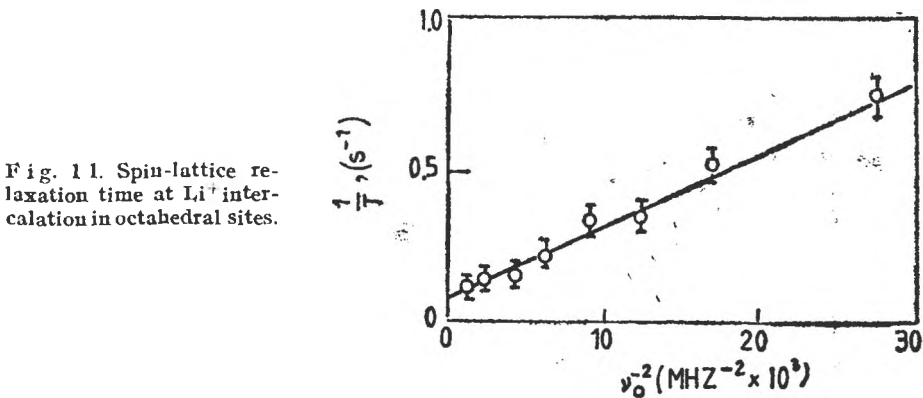


Fig. 10. Energy profiles of  $Li^+$  ions in the two coordination types.

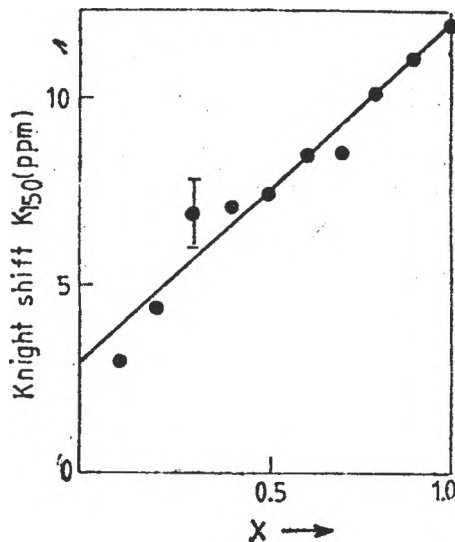
The difference of the activation energy should diminish as the sulfide layers are separated and all the sites increase in size. The situation is more complicated when in the host crystal inter simultaneously different structures of trigonal prismatic or tetrahedral/octahedral type there are. In this case, during intercalation, the diffused species must cross the boundaries which separate these domains [31–33].

Experimental studies of lithium diffusion in  $\text{TiS}_2$  are limited enough. By the NMR measurement have been determined the variation of the spin-lattice relaxation time as a function of the applied frequency (fig. 11) for the



intercalated lithium ions in the octahedral sites. From these measurements were calculated the diffusion coefficient as being by order of  $\sim 10^{-9}$   $\text{cm}^2/\text{sec}$ , as well as the activation energy of  $\sim 30$   $\text{kJ/mol}$  for  $x = 1$ .

In the figure 12 the variation of the  $^7\text{Li}$  Knight shift as a function of the lithium intercalation coefficient,  $x$ , in the  $\text{Li}_x\text{TiS}_2$  compound is shown.



The very small values of the Knight shift, 3–12 ppm compared with 240 ppm in lithium metal, show that the lithium are essentially ionized, but that the degree of ionization decreases slightly with increasing lithium content.

The variation of the quadruple coupling constant as a function of the lithium content (fig. 13) gives also information about the ionization degree of lithium, an important role playing the more pronounced deformation of the occupied sites by lithium; the deformation increases from octahedral to trigonal prismatic symmetry.

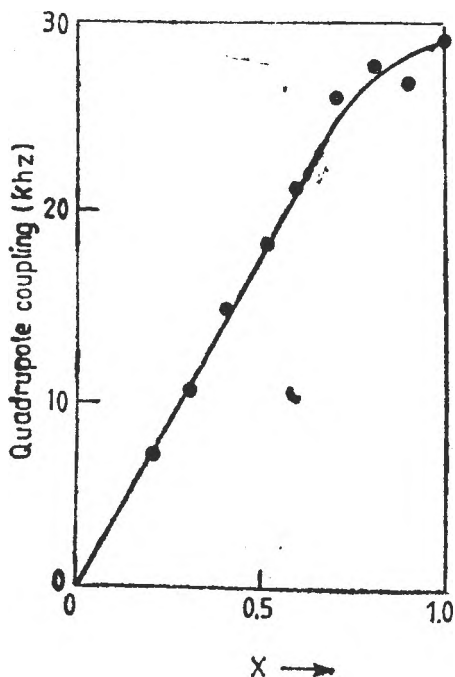


Fig. 13. Quadrupole coupling constant as a function of lithium content.

The NMR transitions of  ${}^7\text{Li}$  and diffractational measurements of the lattice expansion in the  $c$ -axis have revealed a total transition of  $2s$  lithium electron to the orbitals of the host material, with the forming of a single homogeneous phase with the general formula  $\text{Li}_x\text{TiS}_2$ , where  $0 < x < 1$ . The existence of a single phase increases the electrode stability and suggests its utilization as secondary, rechargeable cells.

**4. Conclusions.** The physical investigation methods, which were mentioned, can give the requisite information about the physico-chemical properties, and implicitly the electrochemical properties of the intercalation compounds.

Thus, by microscopy can set off the size of the component particles of the insertion products, as well as the structural details which are tied to lattice periodicity and by the existence of some defects, which allow the intercalation of lithium ions.

The quantitative informations about the crystalline structure can be much accurate obtained by diffractometrical measurements. By this way the symmetry

of the crystalline lattice, the lattice parameters can be determined and the position of the atoms in the unit cell. By the thermal neutron diffractometry the temperature at what appear transition metal ions can be established, which modify partially or even totally the crystal structure of the host material, and, implicitly of the intercalation compounds.

The radiospectroscopical methods give information about the kind of the interactions, type and characteristics of interatomic bonds. NMR measurements can pursue the diffusion phenomenon by which takes place the lithium intercalation. It has found exactly the lithium position in the lattice host material and the concentration of the lithium ions in the intercalation compounds.

## REFERENCES

1. G. Țarălunghă, L. Oniciu, Cs. Bolla, D. I. Boboș *this revue*, **37** (1-2), 115, 1992.
2. K. Tamura, T. Kahara, T. Horiba, N. Ebata, *US Pat.*, 4197366 (1980).
3. P. B. Hirsch, A. Howie R. B. Nicholson, D. W. Pashley, M. J. Whelen, *Electron Microscopy of Thin Crystals*, Butterwoods, London (1965).
4. H. W. Fuller, M. E. Halle, *J. Appl. Phys.*, **31**, 238 (1960).
5. I. Pop, M. Crișan, *Fizica corpului solid și a semiconductorilor*, Ed. did. și ped., București 1983.
6. E. Luca, M. Chiriac, M. Strat, V. Bărboiu, *Analiza structurală prin metode fizice*, vol. II, Ed. Acad., București, 1(1985).
7. S. Asbrink, J. Nerby, *Acta Cryst.*, **B 26**, 6, (1970).
8. R. Bates, Y. Jumel, *Lithium Batteries* (ed. J. P. Gabano), Academic Press, London (1983).
9. P. Podhajecky, Z. Zabrensky, P. Novak, *Electrochim. Acta*, **35**(1), 245 (1990)
10. G. A. Weigera, F. Jellinek, *J. Solid State Chem.*, **1**, 519 (1970).
11. S. Furuseth, L. Brattas, A. Kjekshus, *Acta Chem., Scand.*, **A 29**, 623 (1975).
12. R. R. Chianelli, *J. Crystal Growth*, **34**, 239 (1976).
13. Ch. Kittel, *Introducere în fizica corpului solid*, Ed. teh., București, (1972).
14. K. W. Andrews, *Interpretation of Electron Diffraction Patterns*, London, (1971).
15. B. E. P. Beeston, R. W. Horne, R. Markham, *Electron Diffraction and Optical Diffraction Techniques*, Ed. by Glauert, Amsterdam (1972).
16. I. D. Bursuc, N. D. Sulițanu, *Solidul - Fenomene, teorii, aplicații*, Ed. Științifică, București (1991).
17. G. E. Bacon, *Neutron Diffraction*, Clarendon Press, Oxford (1975).
18. H. Ikeda, M. Hane, S. Narukawa, S. Nakaido, *Manganese Dioxide Symposium*, **2**, 395 (1980).
19. H. Ikeda, S. Narukawa, S. Suenaga, *idem*, 414.
20. H. Ikeda, S. Narukawa, *J. Power Sources*, **9**, 329 (1983)
21. G. Pistoia, *J. Electrochem. Soc.*, **129**, 1861 (1982).
22. J. C. Nardi, *J. Electrochem. Soc.*, **132**, 1787 (1985).
23. R. G. Burns, *Manganese Dioxide Symposium*, **3**, 519 (1985).
24. T. Ohzuku, M. Kitagawa, T. Hirai, *J. Electrochem. Soc.*, **136**, 3168 (1989).
25. T. Ohzuku, M. Kitagawa, T. Hirai, *J. Electrochem. Soc.*, **137**, 40 (1990).
26. M. Voinov, *Electrochim. Acta*, **26**, 1373 (1981).
27. M. Voinov, *Electrochim. Acta*, **27**, 833 (1982).
28. F. Tedjar, *Contribution à l'étude physico-chimique de  $\gamma$ -MnO<sub>2</sub>*, Thèse, Grenoble, France (1988).
29. M. S. Whittingham, *Electrochim. Acta*, **20**, 575 (1975).
30. M. S. Whittingham, B. G. Silbenagel, *Solid Electrolytes*, Ed. Van Cool and P. Hagemmuller, Academic Press, New York (1977).
31. B. G. Silbenagel, M. S. Whittingham, *J. Chem Phys.*, **64**, 3670 (1976).
32. M. S. Whittingham, *Prog. Solid-St. Chem.*, **12**, 41 (1978).
33. E. J. Frazes, S. Phang, *J. Power Sources*, **6**, 307 (1981).



## CONSIDÉRATIONS CONCERNANT L'ÉCOULEMENT DES PHASES DANS LE ROTOR DES CENTRIFUGES DE SÉDIMENTATION. IMPLICATIONS FONCTIONNELLES

CĂLIN ANGHEL\* et VIOLETA ANGHEL\*\*

**RÉSUMÉ.** Ces considérations se constituent comme une corrélation directe entre les conditions de sédimentation (diamètre critique des particules, tracé limite, débit de suspension etc.) et les caractéristiques géométriques du tambour de sédimentation. Les déductions concernent seulement les centrifuges de sédimentation à flux intérieur de suspension. En acceptant l'idée de la circulation en couche mince marginale, on traite la sédimentation des particules solides d'une suspension, dans un tambour d'une forme quelconque, en présence du frottement de glissement entre la phase solide et le tambour. Les déductions théoriques seront particularisées pour deux types de tambours usuels.

**1. Généralités.** Dans la littérature de spécialité, l'analyse théorique et expérimentale de la sédimentation dans un champ centrifuge connaît une grande diversité de points de vue.

Pourtant, il y a des lignes communes dans l'analyse du phénomène, les différences provenant premièrement, du modèle physique choisit et des hypothèses de calcul. Indépendant de tous ces il y a deux conditions fondamentales bien distinctes dans l'analyse du processus :

a) Les particules solides de la suspension avec une distribution uniforme dans l'espace annulaire de liquide du tambour ont une trajectoire de sédimentation avec l'origine dans l'intérieur de cette zone.

b) Les particules solides de la suspension ont une trajectoire de sédimentation avec l'origine sur la surface intérieure de l'espace annulaire de liquide.

Les deux suppositions, généralement acceptées, conduisent à des résultats théoriques de fonctionnement bien supérieurs aux résultats constatés expérimental. Pour atténuer ces différences, beaucoup d'hommes de recherche ont introduit, à base des expériences effectués pour *typo*-dimensions, des facteurs de correction empiriques afférents aux relations théoriques. Parce que ces facteurs n'indiquent pas les causes générales d'incorrélation, en effectuant une correction globale, les hommes de recherche ont développé les études théoriques confirmés expérimental [3, 4, 5, 6, 7], par conséquent il y a une troisième condition fondamentale dans l'analyse de la sédimentation dans le champ centrifuge :

c) La sédimentation se produit en couche mince, dans la zone marginale du tambour.

Les théories élaborées en partant de cette condition conduisent à des résultats théoriques inférieures à ceux expérimentalement obtenus avec seule-

\* Univ. Cluj - Faculté de chimie.

\*\* Pharmec, S.A. - Cluj.

ment 10–15%, en assurant aussi une motivation palpable aux différentiations. Grace au caractère générale des résultats obtenus à base de cette troisième condition (la condition c), les considérations qui suivent sont basées sur cette condition fondamentale. Pour l'élaboration du modèle physique du processus qui sera analysé nous introduisons les hypothèses simplificatoires suivantes :

— la suspension est homogène, avec des concentrations volumétriques sous 5–10%, en état d'écoulement laminaire en régime stationnaire. ( $D\vec{w}/Dt = 0$ )

— la suspension est considérée comme un fluid de viscosité normale ( $\eta = \text{ct}$ ) et incompressible ( $\rho = \text{ct}$  et  $\text{div. } \vec{w} = 0$ )

— le gradient de pression dynamique est relativement négligable en comparaison avec le gradient de pression statique.

— les particules solides ont une forme sphérique et ils ne supportent pas des modifications de forme et des agglomérations.

— la sédimentation individuelle est considérée réalisée aussitôt que la particule touche la parois du tambour.

— on néglige l'action des forces Coriolis et d'inertie sur les particules.

Pour déterminer les conditions de sédimentation (diamètre limite, vitesse de sédimentation, trajet etc.) en corrélation directe avec la forme géométrique du tambour et des interdépendances de mouvement, dans le cas plus complexe d'un tambour entièrement occupé avec un flux de suspension, on analyse les implications dans un cas général d'un tambour matérialisé physique par une zone d'enveloppe de révolution pour laquelle on obtient la surface moyenne par la rotation d'une courbe quelconque  $C_i$ , autour de l'axe  $Oz$ .

A mentionner que l'analyse des écoulements, de la sédimentation etc., est considérée pour une seule section de passage, par rapport au système des coordonnées cartésien  $xOzy$  ou cylindrique,  $z, \theta, r$ .

En matérialisant la section de passage par deux génératrices  $C_1$  e  $C_2$  (fig. 1) et en considérant  $A_1, A_2$ , les points limite d'entrée de la suspension, respectivement,  $B_1, B_2$ , les points limite de sortie de la suspension, la distance  $h=h(\alpha)$  ou  $h=h(x, r)$  qui exprime la section de passage peut être écrit :

$$h = c \cos \alpha \quad (1)$$

**2. L'écoulement des phases dans le tambour.** Parce que l'analyse du processus à lieu dans les condition de l'écoulement en couche mince marginale on tient compte des précisions publiées en domaine. En ce cas, une particule aura théoriquement, trois possibilités de déplacement dans le tambour qui se trouve en mouvement de rotation : dans la direction radiale (la direction  $Ox$  ou  $Oy$  or  $r$ ), dans la direction tangentielle (la direction  $\theta$ ) et dans la direction axiale (la direction  $Oz$ ). Donc, on peut définir la vitesse absolue de cette particule :

$$\vec{w} = \vec{w}_r + \vec{w}_x + \vec{w}_\theta + \vec{w}_z \quad (2)$$

Parce que les recherches [5,6,7] ont montré que l'écoulement radiale est pratiquement nule, en s'atténuant rapidement au longue de 10–15% de la longueur du tracé de sédimentation, pour un mouvement relatif uniforme de la suspension de corp rigide, on peut introduir les simplifications :

$$w_r \simeq 0; \quad \omega = \frac{d\theta}{dt} = \text{const.}; \quad \frac{dz}{dt} = 0 \quad (3)$$

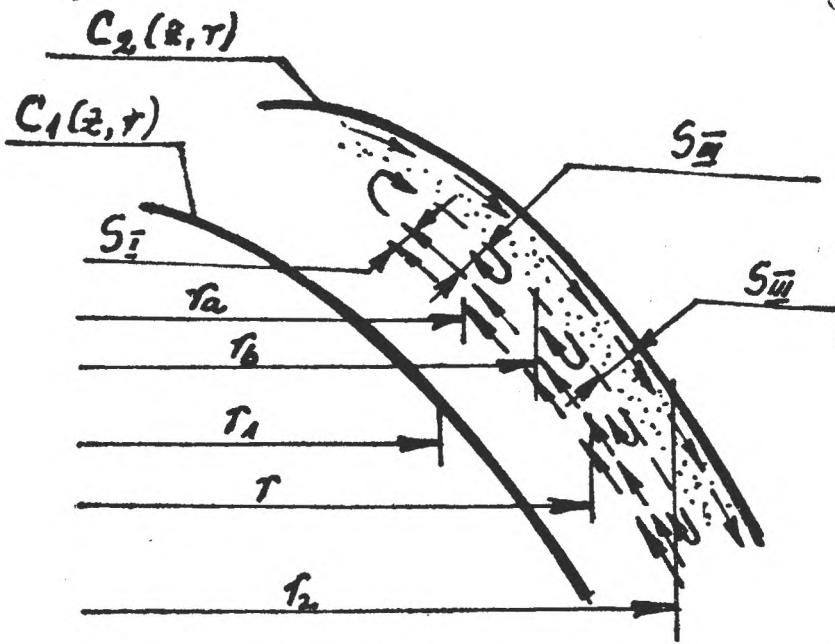


Fig. 1. La section théorique de passage

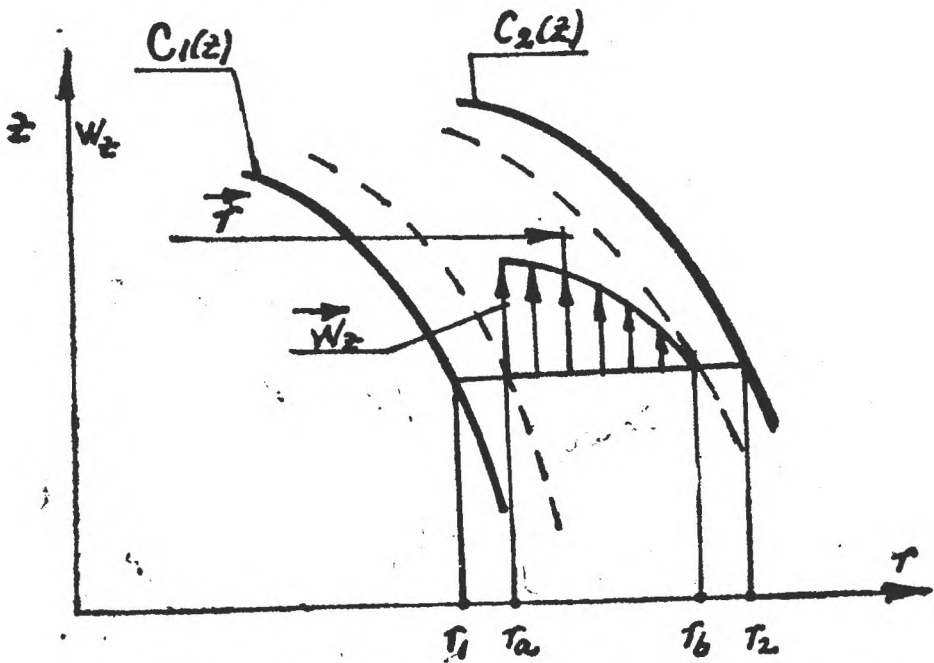


Fig. 2. La variation de la vitesse d'écoulement,  $W_z$ , sur la section de passage

Dans les conditions des hypothèses initiales et des celles précisées ultérieurement, les équations d'équilibre dynamique Navier-Stokes sont particularisées sous la forme :

$$\rho \vec{L} - \nabla p + \eta \nabla^2 \vec{w} = 0 \quad (4)$$

Parce que dans un champ de forces centrifuges, quand  $a_c = r\omega^2 \gg g$ , les forces de masse  $\vec{F}$  d'action sur la particule peuvent être approximées, sans introduire de grandes erreurs, à l'expression :

$$\vec{F} = \vec{F}_c$$

Le mouvement résultant du couche marginale de suspension à lieu pratiquement dans la direction de l'axe  $Oz$ , donc en projetant sur l'axe  $Oz$  l'équilibre exprimé par la relation (4) on obtient :

$$Z - \frac{1}{\rho} \frac{\partial p}{\partial z} + \nu \nabla^2 w_z = 0 \quad (5)$$

respectivement,

$$-\frac{\partial p}{\partial z} = \nu \nabla^2 w_z \quad (6)$$

relation qui permet à supposer que le gradient de pression statique de la couche marginale est la force motionnelle de l'écoulement.

Dans des coordonnées cylindriques, l'expression (6) est la suivante :

$$-\frac{\partial p}{\partial z} = 2\eta \frac{\partial^2 w_z}{\partial z^2} \quad (7)$$

Pour l'écoulement uniforme de la suspension, en généralisant la solution présentée dans la littérature [4,5] on obtient l'expression de la vitesse d'écoulement sur la couche marginale :

$$W_z = \frac{K}{12} (s^4 - r_*^4) \quad \begin{aligned} s &= r_b - r_a \\ r_* &= r - r_a \\ K &= \rho \omega^2 / 3\eta L \\ L &= z_2 - z_1 \end{aligned} \quad (8)$$

couche marginale délimitée par les rayons  $f_a$  et  $f_b$  (fig. 3).

De l'expression de la vitesse d'écoulement, résulte une variation parabolique sur la section de passage, variation confirmée par plusieurs sources bibliographiques [3,4,5,6]. Après l'interprétation des expressions au-dessus, le rapport des vitesses caractéristiques sera :

$$W_{zm} = 0,8 W_{z \max}$$

Parce que la vitesse moyenne d'écoulement par une section de passage quelconque  $A_1$  peut être exprimée :

$$W_{zm} = \frac{1}{A} \int_{A_1} W_z dA = \frac{Q_1}{A} \quad (9)$$

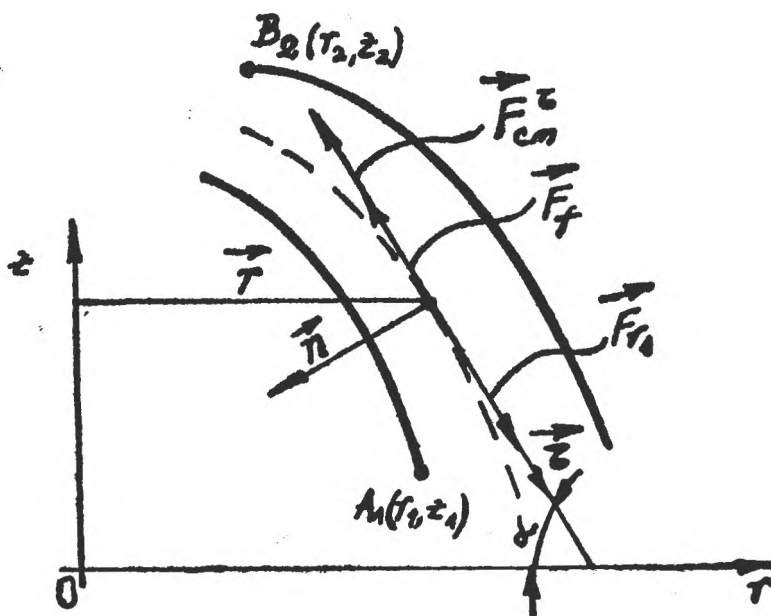


Fig. 3. La condition d'équilibre vectoriel des forces qui actionnent sur la particule e

on peut écrire pour une section d'un rayon quelconque, en rapportant à la superficie effective de passage (fig. 4) :

$$Q_1 = W_{zm} \cdot A \text{ ou } Q_1 = 0,42 Ks^4 r h \tag{10}$$

**3. La sédimentation des particules dans le champ centrifuge.** Plusieurs études traitent le problème de la centrifugation d'une manière restrictive, en isolant les particules solides de certaines interactions. Au-dessous, en partant des précisions antérieures, nous corrélons la sédimentation avec le profil du tambour, respectivement, le facteur de frottement  $\mu$ , de la particule solide sur la surface du tambour (fig. 4).

Théoriquement, le trajet limite de la particule solide peut se dérouler entre la marge inférieure du plateau, le point  $A_1(x_1, z_1)$  et la marge supérieure du plateau limitrophe, le point  $B(x_2, z_2)$ .

Les forces unitaires, rapportées à l'unité de volume qui agissent sur une particule quelconque,  $M$ , sont :

$F_{cm}$  — force de masse apparente,  $F$  — force de frottement de la particule,  $F_r$  — force de résistance hydraulique.

En considérant un flux laminaire avec la sédimentation dans le domaine Stokes, nous pouvons préciser :

$$Re = \frac{u \cdot d\rho}{\eta}, \quad A = \frac{\pi d^3}{4}, \quad \xi = \frac{24}{Re}, \quad u = \frac{dr}{dt}$$

respectivement, les composantes des forces unitaires, dans les directions caractéristiques :

$$\begin{aligned} F_{\text{cm}}^x &= \Delta\rho r \cdot \omega^2 \cdot \cos \alpha \\ F_{\text{cm}}^n &= \Delta\rho r \cdot \omega^2 \cdot \sin \alpha \\ F_f &= 3\pi\eta \cdot d \cdot u \\ F_f &= \eta\Delta\rho r \cdot \omega^2 \cdot \sin \alpha \end{aligned} \quad (11)$$

En acceptant pour l'évaluation quantitative du processus de sédimentation, le calcul avec la vitesse moyenne de sédimentation, considérée comme l'espace parcouru par la particule au milieu du trajet limite, rapporté à la durée de sédimentation et comparable avec la vitesse longitudinale de la couche écouillante,  $u_m \approx W_{zm}$ , la force de résistance hydraulique devient :

$$F_{r1} = \frac{9\eta Q_1}{\pi d^2 r h} \quad (12)$$

La condition d'équilibre des forces qui actionnent sur la particule au moment de la sédimentation (exprimée par vecteurs),

$$\vec{F}_{\text{cm}} + \vec{F}_f + \vec{F}_{r1} = 0 \quad (13)$$

projetée dans la direction  $\vec{\tau}$ , tangentielle au profilé générateur du tambour, devient :

$$F_{\text{cm}}^x = F_f + F_{r1} \quad (14)$$

En effectuant les substitutions correspondantes, on obtient :

$$r^2(\cos \alpha - \mu \sin \alpha) = \frac{9\eta Q_1}{\pi \Delta\rho \omega^2 h d^2} \quad (15)$$

ou :

$$r^2(\cos \alpha - \mu \sin \alpha) = B_1$$

ou :

$$B_1 = \frac{9\eta Q_1}{\pi \Delta\rho \omega^2 h d^2} \quad (16)$$

Si on exprime les fonctions trigonométriques,  $\sin \alpha$ , respectivement  $\cos \alpha$ , par des éléments différentiels on obtient la condition d'équilibre des forces sous la forme :

$$r^2(1 - \mu z') - B_1(1 + z'^2) = 0 \quad (17)$$

ou :

$$B_2 = \frac{9\eta Q_1}{\pi \Delta\rho \omega^2 c \cdot d^2} \quad (18)$$

L'interprétation des expressions (17) et (18) permet la précision des conditions de sédimentation : la vitesse de sédimentation, le diamètre limite, le trajet de sédimentation etc. L'interprétation peut être réalisée sur les expressions généralisées (17), (18), ce que conduit à des formes compliquées, ou en particulierisant pour des types concrètes de tambour, ce que représente la variante la plus convenable.

**4. Démonstration par la méthode de particulariser.** On analyse deux types usuels de tambour édifiateurs pour les extrêmes du cas généralisé.

#### 4.1. Le tambour cylindrique

L'équation de la ligne génératrice pour le profil cylindrique,

$$\frac{x}{a} + \frac{z}{b} = 1 \quad (19)$$

Si on impose que les génératrices soient parallèle avec l'axe Oz, on peut écrire :

- pour la courbe ( $C_1$ ) :  $x = R_1$
- pour la courbe ( $C_2$ ) :  $x = R_2$

Parce que :  $\alpha = 90^\circ$ ,  $z = H_T = \text{const.}$ , l'expression (17) devient :

$$\begin{aligned} r^2 - B_1 &= 0 \\ C &= (R_2 - R_1)^2 \end{aligned} \quad (20)$$

relations qui permettent d'expliciter rapidement les dimensions caractéristiques de sédimentation. Par conséquent le diamètre limite de sédimentation d'une particule qui se trouve au rayon courant "r", dans le flux de suspension sera :

$$d_{cr} = \sqrt{\frac{9\eta Q_1}{\pi \Delta \rho \omega^2 r^2 h}} \quad (21)$$

Concernant le trajet de la particule qui sédimente, il peut être établi en introduisant l'hypothèse de l'égalité entre la vitesse d'entraînement de la suspension et la vitesse d'écoulement axial (quand la particule commence à flotter) :

$$W_z \simeq U_s \quad (22)$$

ou :

$$W_z = \frac{dz}{dt}; \text{ respectivement, } U_s = \frac{dr}{dt}$$

En interprétant selon la méthodologie de la littérature on obtient le trajet :

$$Z_d = \frac{1}{24} \cdot \frac{\pi r \omega^2 \rho}{\eta_b \cdot Q_1} \left( (s^4 r_*^2 - \frac{r_*^2}{5}) \right) \quad (23)$$

4.2. *Le tambour conique.* L'équation des lignes génératrices du profil conique passant par deux points  $A_{11}, A_{12}$  ou  $A_{21}, A_{22}$ , aura l'expression :

$$\begin{vmatrix} x & z & 1 \\ x_1 & z_1 & 1 \\ x_2 & z_2 & 1 \end{vmatrix} = 0 \tag{24}$$

En notant :

$$k = \operatorname{tg} \alpha = \frac{z_2 - z_1}{x_2 - x_1}, \text{ le coefficient angulaire}$$

$$A_{11}A_{12} = L_T, \text{ la longueur du tambour}$$

et en supposant  $A_{11}$  sur l'origine  $Ox$  du système de référence, donc  $z_1 = 0$ , l'équation (24) devient :

$$z = (r - R_1) \frac{L_T \operatorname{tg} \alpha}{R_2 - R_1} \tag{25}$$

ou

$$z = (r - R_1) B_3 \tag{26}$$

ou

$$B_3 = \frac{L_T \operatorname{tg} \alpha}{R_2 - R_1} \simeq -\operatorname{tg} \alpha$$

En revenant dans la relation (17) on peut obtenir :

$$r^2 - \frac{(1 + B_3^2)^{\frac{1}{2}}}{(1 - \mu B_3)} \cdot B_1 = 0, \tag{27}$$

relation qui permet d'expliciter rapidement, dans le cas considéré des dimensions caractéristiques de sédimentation. Ainsi, le diamètre limite sera :

$$d_{cr} = \sqrt{\frac{9\eta\Omega_1}{\pi\Delta\rho\omega^2 r^2 h} \cdot \frac{(1 + B_3^2)^{\frac{1}{2}}}{(1 - \mu B_3)}} \tag{28}$$

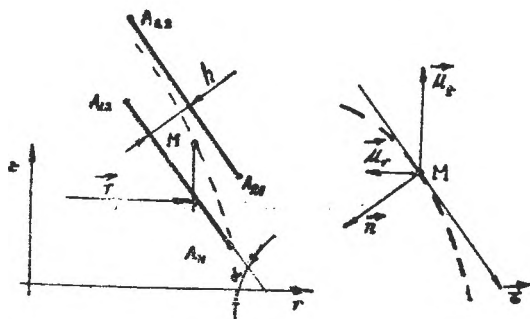


Fig. 4. La distribution de la vitesse d'écoulement, sur la section particulière du tambour conique

Relativement au trajet de la particule qui sédimente, par un raisonnement semblable à celui du cas antérieur, on obtient :

$$u_r = u_z,$$

ou :

$$u_r = \frac{dr}{dt} ; \quad u_z = \frac{dz}{dt} ; \quad z - \text{le trajet de la particule.}$$

L'équation différentielle du trajet de la particule dans le plan  $Z_x, Z_y$  :

$$\frac{dz}{u_z} = \frac{dr}{u_r} \quad (29)$$

Conformément avec et le sens des axes de coordonnées on peut écrire :

$$u_r = -W_r + \frac{\omega^2 \Delta \rho r}{k_1} \quad (30)$$

$$u_z = W_z$$

En substituant dans (30), on obtient :

$$dz = \frac{dr}{ar^2 - ctg \alpha}$$

ou

$$a = \frac{2\pi\omega^2\Delta\rho h}{k_1 \cdot Q_1 \sin \alpha} > 0 \quad (31)$$

En intégrant (31), on obtient :

$$Z = \frac{1}{2\sqrt{a \operatorname{ctg} \alpha}} \cdot \ln \frac{ar - \sqrt{a \operatorname{ctg} \alpha}}{ar + \sqrt{a \operatorname{ctg} \alpha}}, \quad (32)$$

L'expression (32) détermine pour la particule, un trajet logarithmique.

En réalisant l'intégrale définie entre les points  $A_{11}$  (d'entrée de la suspension), respectivement  $A_{22}$  (de sortie de la suspension), on obtient le trajet défini pour la particule qui a la dimension „d” :

$$Z_d = \frac{1}{2\sqrt{a \operatorname{ctg} \alpha}} \left[ \ln \frac{aR_2 - \sqrt{a \operatorname{ctg} \alpha}}{aR_2 + \sqrt{a \operatorname{ctg} \alpha}} - \ln \frac{aR_1 - \sqrt{a \operatorname{ctg} \alpha}}{aR_1 + \sqrt{a \operatorname{ctg} \alpha}} \right] \quad (33)$$

**Conclusions.** — En acceptant l'hypothèse de la circulation de la suspension en couche mince marginale on obtient, par l'analyse des relations (22), (24), (28), (32), la confirmation théorique mais seulement pour des angles  $\alpha \simeq 90^\circ$  — c'est le cas concret d'un tambour cylindrique. L'écoulement n'est pas dépendant du coefficient de frottement.

— Pour le tambour conique,  $\alpha < 90^\circ$ , l'écoulement marginal est perturbé. Dans la zone de turbulence  $S_{II}$  s'installe un contre-courant de sédimentation simultanément avec l'entrainement des particules déposées sur la paroi. La dépendance théorique entre l'écoulement et le coefficient de frottement (28), (32) a été constatée expérimentalement avec certitude. [1; 5,6]

— L'écart constaté [3,5,6] entre  $Q_{de}$  et  $Q_{e1}$ , oscille autour de 15%, est maintenu en outre à l'évaluation de la relation (10) et peut être expliqué, dans une première approximation, par l'interférence des écoulements radiaux et axiaux du tambour avec ceux tangentiels de vitesse,  $W_{er}$ . Ces interférences ont été négligé dans le calcul. L'écoulement est influencé fortement du mode d'alimentation de la suspension.

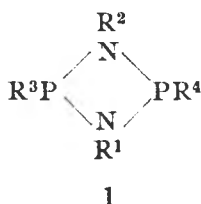
#### BIBLIOGRAPHIE

1. Sokolov, V. I., Semenov, E. V., *Him. promíslenost*, nr. 6, 1976, p. 478.
2. Semenov, E. V., *Jur. prikl. himii*, nr. 10, 1977 p. 2283.
3. Brunner, K. H., Molerus, O., *Chem Tch.*, **33**, nr. 5, 1981, p. 237–240.
4. Brunner K. H., Molerus, O., *Chem. Ing. Techn.*, **51**, nr. 3, 1979, p. 238–239.
5. Reuter, H., *Chem. Ing. Techn.*, **39**, nr. 5, 1967, p. 311–318.
6. Reuter, H., *Chem. Ing. Techn.*, **39**, nr. 10, 1967, p. 543–549.
7. Loke, H., Schürmmer, P., Werner, U., *Chem. Techn.*, **24**, nr. 12, 1972, p. 744–746.

NOTE DE CERCETAREON THE RING ANGLES IN THE FOUR-MEMBERED  
CYCLODIPHOSPHAZANES.

IOAN SILAGHI—DUMITRESCU\* and IONEL HAIDUC\*

In a recent study on the cis-trans isomerism in cyclodiphosphazanes [1] 7 we noted that the calculated PNP angle is always larger than  $90^\circ$  while the NPN angle is smaller than  $90^\circ$ . It seems that this is a common feature to all these rings and can not be changed by the substituents on phosphorus or nitrogen [2—17]



An earlier explanation of the small angle at phosphorus stated the repulsion between the phosphorus lone pairs [3a] and the PN bond electron pairs. Note however that in  $[\text{MoCp}^*(\text{CO})_2\text{PN}(t\text{-Bu})_2]_2$  where [17] the electron pairs of phosphorus are engaged in bonding with the organometallic moiety, the NPN angle is still smaller than the PNP angle and electron pair repulsion can hardly be advocated. Moreover, the angle at silicon in cyclodisilazanes [18] where no electron pairs at Si is also smaller than  $90^\circ$ .

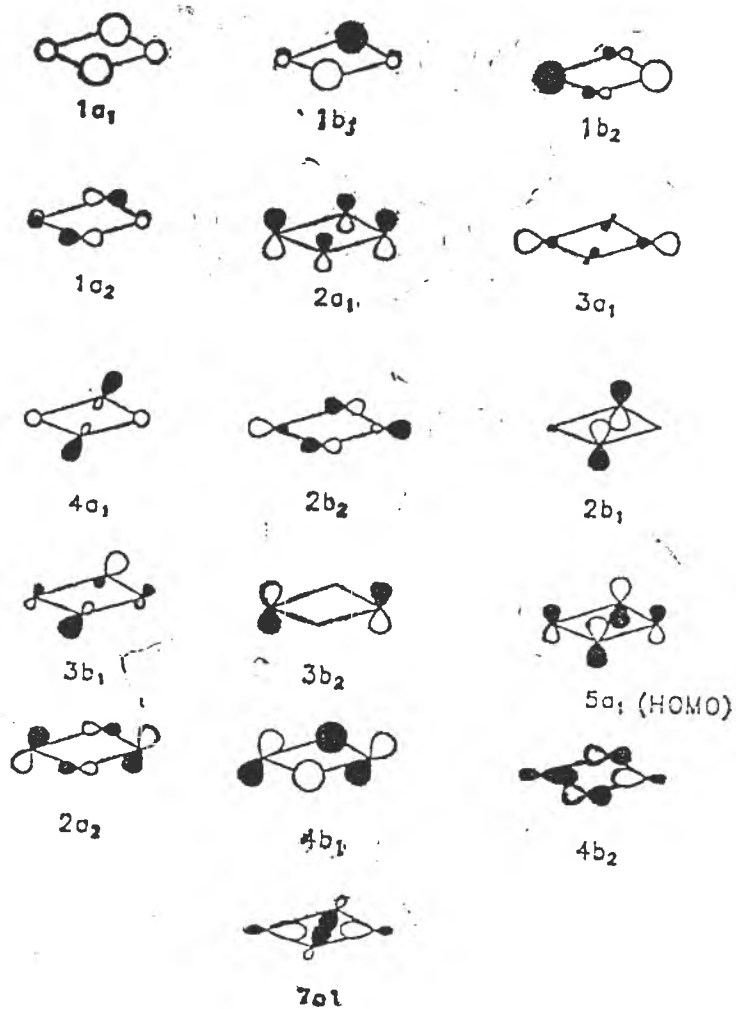
We propose here a simple explanation of the diamond shape of the  $\text{P}_2\text{N}_2$  emerging from MNDO [19] and EH [20] molecular orbital calculations.

We start from a naked  $\text{P}_2\text{N}_2^{4-}$ -ring with a perfect planar structure. The molecular orbitals of this system (shown in Figure 1) are just the heteroatomic relatives of the corresponding Walsh orbitals of cyclobutane [21, 22] and the highest occupied ones can be also related to the valence orbitals of cyclotetraphosphane [23].

Since the  $\pi$  system will mainly determine the shape of the actual ring, we discuss it in some detail. Also, the different weights of various atomic orbitals seems to be counterintuitive and it is notable that the HOMO of this system has a greater contribution from the nitrogen p orbitals (initially lower in energy than the corresponding phosphorus orbitals) than from the phosphorus orbitals.

First observe that the bare ring can be elongated along the P...P or the N...N axis (2);

\* Department of Chemistry, Babeș-Bolyai University, R-3100 Cluj-Napoca, Roumania.

Fig. 1. The molecular orbitals of  $P_2N_2^{4-}$ .

2a



2b

Smaller than  $90^\circ$  in (2a) and greater than  $90^\circ$  in (2b) angles at phosphorus are thus displayed. The  $\pi$  orbitals of these rings constructed from a P...P and N...N fragment (systems calculated for the same PN bond length 1.69 Å — by the Extended Huckel method) are given in figure 2.

The P...P distance of 2.53 Å (typical for the real systems) enables a quite good overlap across the ring ( $S = \text{cca } 0.1$ ) in 2a and the splitting of the (+) and (-) combinations of the phosphorus  $p_z$  orbitals is greater than 2 eV. Though the N...N distance is shorter than the P...P distance, it is still enough large to prevent an appreciable N...N  $\pi$  overlapping, so the splitting of the nitrogen p orbitals is only of the order of 0.2 eV. Consequently the phosphorus  $P^+$  combination falls at a lower position than the nitrogen  $N^+$  combination.

The interaction of  $P^+$  with  $N^+$  gives the bonding  $\pi$  mo which has a greater contribution from phosphorus (since it is closer to  $P^+$ ) and the antibonding  $\pi^*$  in which the weight of the nitrogen is higher (since it is closer to  $N^-$ ). As the P...P distance in 2b is smaller than in 2a, the P...P overlap is higher and the splitting of the phosphorus  $P^+$  and  $P^-$  combinations is larger than in 2a. This means that  $P^+$  of 2b falls at lower energy than  $P^+$  of 2a and  $P^-$  of 2b lies above  $P^-$  of 2a. When all orbitals are occupied as happens in the real compounds the  $P^-$  of 2b being higher than the  $P^-$  of 2a it is more destabilizing and the ring will open the angle at nitrogen by approaching 2a. In other words the transannular interaction between the orbitals on phosphorus is stronger than that between the nitrogen and this makes the NPN angle smaller than the PNP angle. A naked cyclodisilazane ring  $\text{Si}_2\text{N}_2$  has the pseudo  $\pi$  orbitals similar to those depicted in fig. 2. Considering that the substituents will not change too much the relative compositions of these orbitals, the shape of these rings can be traced also to the large separation on the  $P^+ - P^-$  combination of the more voluminous elements and consequently smaller NSiN than SiNSi angles are to be expected.

**Acknowledgement.** ISD is grateful to professor Rolf Gleiter for his hospitality in Heidelberg where the reported calculations have been carried out.

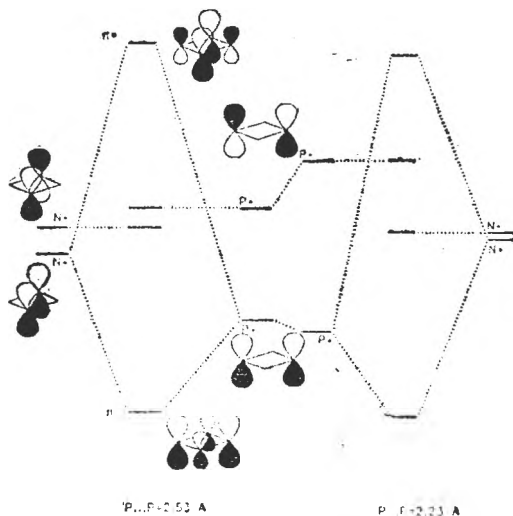


Fig. 2. The  $\pi$  orbitals of  $\text{P}_2\text{N}_2^+$  system.

#### REFERENCES

1. I. Silaghi-Dumitrescu, I. Haiduc, *Phosphorus Sulfur and Silicon and Related Elements*, in print.
2. K. W. Muir, J. P. Nixon *Chem. Commun.* 1971, 1405.

3. a) K. W. Muir, *J. Chem. Soc., Dalton Trans.*, 1975, 259; b) V. D. Romanenko, A. P. Drapailo, A. N. Chernega, I. N. Markovski, *Zh. Strukt. Khim.*, **61**, 2434 (1991).
4. a) R. Keat, A. N. Keith, A. MacPhee, K. W. Muir, D. G. Thompson, *J. Chem. Soc. Chem. Commun.*, 1978, 372; b) B. Ya. Antosyak, V. N. Biyushkin, *Zh. Struct. Khim.*, **31**, 122 (1990).
5. D. A. Harvey, R. Keat, A. N. Keith, K. W. Muir, D. S. Rycroft, *Inorg. Chim. Acta*, **34**, L201 (1979).
6. M. L. Thompson, A. Tarassoli, R. C. Haltiwanger, A. D. Norman, *J. Amer. Chem. Soc.*, **103**, 6771 (1981).
7. A. Tarassoli, M. L. Thompson, R. C. Haltiwanger, T. G. Hill, A. D. Norman, *Inorg. Chem.*, **27**, 3382 (1988).
8. W. Ahmad Kamil, M. R. Bond, J. M. Shreeve *Inorg. Chem.*, **26**, 2015 (1987).
9. M. L. Thompson, R. C. Haltiwanger, A. D. Norman, *J. Chem. Soc. Chem. Commun.* 1979, 647.
10. H. J. Chen, R. C. Haltiwanger, T. G. Hill, M. L. Thompson, D. E. Coons, A. D. Norman, *Inorg. Chem.*, **24**, 4725 (1985).
11. E. Niecke, W. Flick, S. Pohl, *Angew. Chem.*, **88**, 305 (1976); *Angew. Chem. Int. Ed. Engl.*, **15**, 309 (1976).
12. W. Schwarz, H. Hess, W. Zeiss, *Z. Naturforsch.*, **33b**, 723 (1987).
13. S. Pohl, *Z. Naturforsch.*, **34b**, 256 (1979).
14. H. Richter, E. Fluck, H. Riffel, H. Hess, *Z. anorg. allg. chem.*, **486**, 177 (1982).
15. S. S. Kumaravel, S. S. Khristinamurthy, B. R. Vincent, R. T. S. *Z. Naturforsch.*, **41b**, 1067 (1986).
16. A. Duborg, J. L. Delarbre, L. Maury, J. P. Declerq, *Acta Cryst.*, **C48**, 138(1992).
17. A. Dubois, N. F. Duesler, R. T. Paine, *Organometallics* **2**, 190, (1983).
18. I. Haiduc, D. B. Sowerby, *The Chemistry of Inorganic Homo- and Heterocycles*, Academic Press, London, 1987.
19. a) M. J. S. Dewar, W. Thiel, *J. Amer. Chem. Soc.*, **99**, 4899 (1977); b) M. J. S. Dewar, M. L. McKee, H. S. Rzepa, *J. Amer. Chem. Soc.*, **100**, 3607 (1978).
20. R. Hoffmann, *J. Chem. Phys.*, **39**, 1397 (1963).
21. R. Gleiter, *Top. Curr. Chem.*, **85**, 199 (1979) and references therein.
22. R. Gleiter, M. C. Böhm, M. Baudler, *Chem. Ber.*, **114**, (1981) 1004.

## CRONICĂ

### The 4<sup>th</sup> International East-Conference\*

The 4. International EAST-Conference will be held in Schwabisch Gmuend on November 18-19 1993 under the subject "New Materials and Technologies in Surface Finishing for Better Corrosion and Tribology Properties".

*The main topics of the conference will be:*

- ECD-Technologies, hard chrom incoatings, dispersion coatings
- PVD/CVD-Technologies for hard coatings
- Applications in industrial practice
  - motor and mechanical engineering
  - automobile industry
  - electronic industry
  - mining
- Model systems for material testing
- Surface interactions in medical application

Deadline dates for papers:

April 15, 1993 - Deadline for submission of abstracts (400-500 words)

May 15, 1993 - Notification of acceptance of papers

August 15, 1993 - Deadline for submission of final papers for publication in the EAST-Report.

**Cronica EAST.** 1. Since its foundation in autumn 1989, EAST cooperates closely with the American Electroplaters and Surface Finishers Society - AESF.

The American Electroplaters and Surface Finishers Society, Inc. is the largest international, professional society serving the surface finishing industry. With over 8,500 members and 86 branches, one of AESF's primary objectives is the transfer information about surface finishing technology throughout the world.

AESF sponsors two major conferences and exhibits each year, SUR/FIN and AESF Week the major winter event. Attended by thousands of industry professionals, SUR/FIN offers the latest technical developments as well as hundreds of exhibiting companies with the newest and best equipment and supplies on the market. It is the largest surface finishing conference and exhibit in the U.S.

**Plating & surface finishing**, the journal of the AESF, keeps readers up to date with the latest research, trends, and developments, the newest equipment, products and processes, and the better ways to do things in the widely diversified and rapidly changing surface finishing industry.

For more information contact the AESF at:

American Electroplaters and Surface Finishers Society

12644 Research Parkway, Orlando FL 32826, USA

Tel. ++1-407-2816441

Fax ++1-407-2816446

2. The Centre of Advanced Electroplating - CAG in collaboration with EAST will organize an "European Congress on in situ STM/AFM" in February 1994, in Copenhagen.

Main objectives dealt in this meeting will be: Electrochemical deposition of metals on ordered metal surfaces by underpotential and overpotential deposition, electrocrystallization participation of additives in the overlayer growth, deposition of metals by pulse plating, spectroscopy, deposition and identification of small organic molecules, deposition of large organic molecules and biological substances, equipment, hardware and software, as well as theoretical fundamentals.

\*) *European Academy of Surface Technology*

Interessents in further informations contact :

Dr. Per Moller  
CAG  
The Technical University of Denmark  
Building no. 425  
DK-2800 Lyngby  
Tel. ++45-45-931222

3. The 14<sup>th</sup> International Exhibition on Surface Treatments and Industrial Finishing (SIST 93) has been held in Paris from March 29 to 2 of April. In an area of 28,000 m<sup>2</sup>, 500 exhibitors coming from 13 countries have presented the last developments in the field of surface technology. The most important sectors concern the cleaning and the preparation of surfaces, then metal deposition and painting. The main theme of this exhibitions has been devoted to the protection of environment and the prevention against pollution. A special issue of "Galvano-Organo" concerns this event.
4. *News of DGO*. The DGO -- Deutsche Gesellschaft für Galvano- und Oberflächentechnik established a new branch for plasma technique. The major cooperation with the other DGO branches will deal with pretreatment (plasma etching, plasma activation) and combined processes (functional optimization of surface properties by combination of electrochemical and plasma processes).  
"Pretreatment -- Fundamentals for Successful Surface Finishing" was subject of the DGO spring meeting in Berlin. All aspects of environment protective pretreatment processes were discussed with special view to quality, materials, analysis and economics.  
The 15th „Ulmer Gespräch" took place on 6-7 May 1993, with subject "Metallisation of Plastics and Conductive Polymers". One of the primary objectives will be conductive polymers-materials used in interesting fields for application like electronics. In principle these materials can be of use to build up flexible thin layer substrates for metallisation as well as for intrinsic conductive electrodes.
5. *Corrosion Conference*. HUNKOR -- the Hungarian Corrosion Society will organize a congress on corrosion and corrosion protection in memoriam of Prof. Kurt Schwabe. The plenary and keynote lectures will be held by excellent scientists like O. M. Bockris, K. Lorenz, E. Heitz, J. Weber, F. Mansfield, W. Plieth and J. W. Schultze.  
The conference will take place in a small town called Tata, about 70 km southwest from Budapest, a nice place in a lake district.
6. Current informations about research activities statistics in Japan.

Table 1

Recent R &amp; D projects in surface technology in Japan

	A	B	C	D	AB	AD	CD	total
Fundamental	11	4	9	2	4	1	2	33 (16%)
Electronics	9	2	16	35	11	3	15	91 (45%)
Plating steel for automobile	4	--	5	11	1	3	1	25 (13%)
Composite plating	8	1	2	9	7	3	3	33 (16%)
Oxides & super conductive deposit	4	--	5	--	--	--	--	9 (5%)
Others	3	--	2	2	--	--	3	10 (5%)
	39	7	39	59	23	10	24	201
	19%	3%	19%	29%	11%	5%	12%	100%

The research objectives are:

- Fundamental — Properties of plating films, Depositing function, Depositing process
- Electronics — Under coating for hard disc memory, High density memory media, printed circuits board, EMI shielding
- Plating steel for automobile — Zn, Zn-Ni, Zn-Co, Zn-Al
- Composite plating — SiO<sub>2</sub>, SiC, TiC, ZrB<sub>2</sub>, Al<sub>2</sub>O<sub>3</sub>, WC, Diamond, Graphite as diversion agents
- Oxides & super conductive deposit — YBCO type deposit, Mo oxide, Co oxide for display, La chromite as high temperature electrode material.

Table 2

Recent R & D projects in plating processes in Japan

	A	B	C	D	AB	AD	CD	total
Electroplating	24	5	13	26	13	5	9	95 (47%)
Electroless	6	1	15	17	—	—	12	51 (25%)
Composite	6	1	2	7	8	2	3	29 (14%)
Fused salt bath	2	—	4	6	—	3	—	15 ( 7%)
Pulse plating	1	—	5	3	2	—	—	11 (5%)
	39	7	39	59	23	10	24	201
	19%	3%	19%	29%	11%	5%	12%	100%

The research objectives are:

- Electroplating — Single metal, Alloys, Oxides, Amorphous alloys such as Fe-W, Fe-Mo, Co-Ti, Ni-P, Ni-Fe-P, Ni-W-P/SiO<sub>2</sub>, Fe-Cr, Ni-Mo, Co-Mo, Ni-B, Ni-Ti, Pd-As
- Electroless — Cu, Ni-P, Ni-P/SiO<sub>2</sub>, Ni-Cu-P, Ni-Mo-P, Ni-W-P, Ni-Mo-B, Co-Ni-Re-P, Ni-P/SiC, Ni-Co-B, Pd-P, Pd-Ni-P, Au, Ag, Sn
- Composite plating — SiO<sub>2</sub>, SiC, TiC, ZrB<sub>2</sub>, Al<sub>2</sub>O<sub>3</sub>, WC, Diamond Graphite as dispersion agent
- Fused salt bath — Al, Al-Zn, Zn, Zn-Ni, Sn, MoS, Ag
- Pulse plating — Amorphous Pd, Ni-S

7. An international conference will be organized in October 1993, by the Electroplating Division of Russia Central House of Sciences & Technology in cooperation with the journal „Electroplating & Surface Treatment” and the Lami Ltd, Moscow. Under the subject „Electroplating '93 — Processes, Environment Protection, Equipment” main emphasis will be on the solution of environmental problems in metal finishing industries. Parallel to the conference an industrial fair will take place.

8. SYF — The Swedish Electroplaters and Surface Finishers Society was founded for companies engaged in electroplating. About 50 companies, job shop platers, in-house platers and suppliers, currently take part. SYF buys manpower from IVP, mainly Mr. Lars Clarin, to do the daily work. Activities going on includes following:  
 Environment, health and safety are today main objectives and SYF acts as a common industrial counterpart for the authorities in Sweden Common delivery terms for electroplating has been established. SYF Publishes a newsletter bi-monthly. Via lectures, visits etc. the know-how of the members are extended. Further activities are to be defined.  
 SYF develops an extensive international net of contacts.

*Trichlorethylene phase-out 1995.* The Swedish parliament has prohibited the use of some chlorinated solvents, among others trichlorethylene from 1 January 1996. An intensive work has now started to find alternatives in the numerous different types of application currently in

use. Many experiences are already achieved at a lot of companies by themselves or with assistance by vendors or consultants.

Now a cooperation starts which includes about 20 companies willing to share information and costs of necessary investigations.

Contact address:

Richard Berglind, IVF — Institut for Verkstadsteknik, Mölndalsvägen 85, S-41285 Göteborg, Sweden, Fax: ++46-31-407876

9. The Metal Finishing Association has published a survey of industrial prospects entitled "U.K. Coating Market up to 2005" commissioned from Dr. R. Artley and Prof. A. Matthews. It is available from the MFA offices at 10 Vyse Street, Birmingham B18 6LT, United Kingdom.  
The fifth International Conference on Adhesion will be held in York, 6-8 September 1993  
Details available from the Institute of Materials, 1 Carlton House Terrace, London SW1Y 5DB.

LIVIU ONICIU

RECENZII

"Oxford Chemistry Primers" Series editor, Stephen G. Davies, Oxford Science Publications, Oxford University Press, 8 vol., 1992.

This series of short texts (series editor Stephen G. Davies "The Dyson Perrins Laboratory", University of Oxford) provides accessible accounts of a range of essential topics in organic chemistry:

1. S.E. Thomas, Organic Synthesis: The Roles of Boron and Silicon
2. D.T. Davies, Aromatic Heterocyclic Chemistry
3. P.R. Jenkins, Organometallic Reagents in Synthesis
4. M. Sainsbury, Aromatic Chemistry
5. L.M. Harwood, Polar Rearrangements
6. I.E. Mark, Oxidations
7. J.H. Jones, Amino Acid and Peptide Synthesis
8. C.J. Moody and G.H. Witham Reactive Intermediates

All the basic principles and facts in a particular area are presented in a clear and straightforward style.

**Aromatic heterocyclic chemistry** David T Davies, ISBN 0-19-855660-8 1992, 88pp

The aim of this book is to present only the essential features of the more important ring systems. The emphasis of this short text, of prime importance to organic chemists working in the chemical industry, is on synthetic aspects rather than properties. It covers the essential details and basic principles with reference to all important classes of heterocyclic compounds

illustrating them with many examples of drug synthesis.

The book contains the following chapters: 1. Introduction 2. Pyrroles, thiophenes, and furans 3. Oxazoles, imidazoles and thiazoles 4. Isoxazoles, pyrazoles and isothiazoles 5. Pyridines 6. Quinolines and isoquinolines 7. Indoles 8. Five-membered ring heterocycles with three or four heteroatoms 9. Six-membered ring heterocycles containing one oxygen atom 10. Pyrimidines

David T. Davies, industrial scientist at The SmithKline Beecham Pharmaceuticals, Medicinal Research Centre, Harlow, Essex has produced an excellent introduction to aromatic heterocyclic chemistry.

**Aromatic chemistry**, Malcolm Sainsbury ISBN 019-855674-8, 1992, 92pp

The aim of this book is an introduction which deals with the fundamentals and provides the basis for deductive reasoning. In addition it emphasises and exemplifies the interrelationship of aromatic to aliphatic chemistry. It explains the concept of aromaticity and its wider implications to heterocyclic chemistry. The reactivity of polycyclic hydrocarbons and annulenes are introduced. Modern synthetic methods such as those involving the uses of organometallic reagents are included and the importance of arenes and carbenes in aromatic chemistry is discussed.

In a single volume Malcolm Sainsbury, Reader in Chemistry at the University of Bath, provides an excellent account of the fascinating topic of aromatic chemistry presented in an easy to read and student friendly style.

VASILE MICLĂUȘ

Michael Lederer, Alfred O. Kuhn  
**Adsorption on Cellulose, Collected Data on Chromatography on Cellulose with Aqueous Solvents**, Salle+Sauerländer, Aarau, Frankfurt am Main, Salzburg, 1990, 228 pag.

Although the stationary phases play a very important role in the Thin Layer Chromatography they haven't been specially treated till now. From the vast literature we had the general impression that the stationary phases were presented just as a practical application examples or in the best case in a separate chapter. In: "Adsorption on Cellulose, Collected Data on Chromatography on Cellulose with Aqueous Solvents", Lederer and Kuhn present in an original way one of the most important stationary phases: Cellulose. The book is in

fact a collection of data concerning the chromatography on cellulose with aqueous solvents. Those data are structured in nine chapters which are: amino acids and derivatives, alkaloids, dyes and pigments, antibiotics, compounds with heterocyclic oxygen, phenols, phenolic acids and related compounds, miscellaneous organic compounds and inorganic ions.

Thanks to the original and practical manner of presentation in tables, graphics and chromatograms, the book is very useful to the analytical chemists, researchers and students, who are interested in the application of Thin Layer Chromatography on Cellulose for the separation of different substances.

Dr. CONSTANTIN MĂRUȚOIU

În cel de al XXXVIII-lea an (1993) *Studia Universitatis Babeş-Bolyai* apare în următoarele serii :

matematică (trimestrial)  
fizică (semestrial)  
chimie (semestrial)  
geologie (semestrial)  
geografie (semestrial)  
biologie (semestrial)  
filosofie (semestrial)  
sociologie-politologie (semestrial)  
psihologie-pedagogie (semestrial)  
ştiinţe economice (semestrial)  
ştiinţe juridice (semestrial)  
istorie (semestrial)  
filologie (trimestrial)  
teologie ortodoxă (semestrial)  
educaţie fizică (semestrial)

In the XXXVIII-th year of its publication (1993) *Studia Universitatis Babeş-Bolyai* is issued in the following series :

mathematics (quarterly)  
physics (semesterily)  
chemistry (semesterily)  
geology (semesterily)  
geography (semesterily)  
biology (semesterily)  
philosophy (semesterily)  
sociology-politology (semesterily)  
psychology-pedagogy (semesterily)  
economic sciences (semesterily)  
juridical sciences (semesterily)  
history (semesterily)  
philology (quarterly)  
orthodox theology (semesterily)  
physical training (semesterily)

Dans sa XXXVIII-e anne (1993) *Studia Universitatis Babeş-Bolyai* parait dans les séries suivantes :

mathématique (trimestriellement)  
physique (semestriellement)  
chimie (semestriellement)  
géologie (semestriellement)  
géographie (semestriellement)  
biologie (semestriellement)  
philosophie (semestriellement)  
sociologie-politologie (semestriellement)  
psychologie-pédagogie (semestriellement)  
sciences économiques (semestriellement)  
sciences juridiques (semestriellement)  
histoire (semestriellement)  
philologie (trimestriellement)  
theologie orthodoxe (semestriellement)  
éducation physique (semestriellement)

43 870

Lei 1200